Studies on the Self-Assembly of Some Heterocycle Containing Star-Shaped and Polycatenar Mesogens

A Thesis Submitted in Partial Fulfillment of the

Requirements for the Degree of

Doctor of Philosophy

at

IIT Guwahati

by

Balaram Pradhan

Roll No. 136122026

Department of Chemistry

Indian Institute of Technology Guwahati

Guwahati-781039, Assam

India

May 2018

"Arise, Awake, and stop not till the goal is reached".

Swami Vivekananda

"Success is when your signature changes to autograph".

Dr. A. P. J. Abdul Kalam

Dedicated to

my beloved mother and brother……

DECLARATION

I do hereby declare that the research work embodied in this thesis entitled "***Studies on the self-assembly of some heterocycle containing star-shaped and polycatenar mesogens***" has been carried out by me under the supervision of **Dr. A. S. Achalkumar** in the Department of Chemistry, Indian Institute of Technology Guwahati, Assam - 781039, India.

In keeping with the general practice of reporting scientific observations, due acknowledgements have been made wherever the work described is based on the findings of other investigators.

IIT Guwahati
May, 2018

Balaram Pradhan
Roll No. 136122026

Dr. A. S. Achalkumar
Associate Professor
Department of Chemistry
Indian Institute of Technology Guwahati
Guwahati – 781039, Assam, India
Phone: +91-361-258-2329
Fax: +91-361-258-2349
E-mail: achalkumar@iitg.ernet.in
achalkumar78@gmail.com

CERTIFICATE

This is to certify that the research work presented in this thesis entitled "***Studies on the self-assembly of some heterocycle containing star-shaped and polycatenar mesogens***" is an authentic record of the results obtained from the research work carried out by **Mr. Balaram Pradhan (Roll No. 136122026)** under my supervision in the Department of Chemistry, Indian Institute of Technology Guwahati, India. This work is original and has not been submitted elsewhere for a degree or award.

IIT Guwahati
May, 2018

Dr. A. S. Achalkumar
Thesis Supervisor

ACKNOWLEDGEMENTS

The journey towards the completion of my thesis with the outcome of the years of experience, ideas generated in the form of knowledge, was full of hurdles paved way to the fruitful success. Over five years of my research career I have been supported and assisted by a large number of people, in regards to whom I want to convey my words of heartfelt thanks for their kindness, grace, attention, encouragement, and support.

At the very outset, with the deepest sense of gratitude, I wish to express my sincere thanks to my supervisor, Dr. Ammathnadu S. Achalkumar for his proficient guidance, inspiration, creative and scientific ideas which helped me to explore the domain of my work assembled in this thesis. He has given me an extraordinary amount of freedom to be creative and to work on the problems that have interested me. I have spent countless hours discussing research and ideas in science with him. Without his patience and guidance, I would not have finished this work. Of course, wherever I was standing in the shadow of fear of travel, he helped me to achieve the target by his constant encouragement with his true scientific spirit. It was one of the best choices I have ever made to choose him as my supervisor. Besides my supervisor, I would also like to express my deepest sense of gratitude and heartfelt thanks to my doctoral committee members, Dr. Bhubaneswar Mondal, Dr. Subhas Chandra Pan and Dr. Chandan Kumar Jana for their periodic evaluation of my work, valuable suggestions, constant support, and encouragement. I would like to express my sincere thanks to Dr. Chandan Mukherjee for providing me his electrochemical workstation for the analysis. I would like to acknowledge Mr. Joydip De, Dr. Monika Gupta and Dr. Santanu Kumar Pal, IISER Mohali, Mr. V. M. Vaisakh, Dr. G. G. Nair, Dr. D. S. Shankar Rao and Dr. S. K. Prasad, CeNS, Bangalore, for helping me with X-ray Diffraction analysis and rheological studies. I acknowledge them gratefully.

I would like to acknowledge Central Instruments Facility, IIT Guwahati for providing me the analytical facilities required during my research work. I wish to express my sincere gratitude to Indian Institute of Technology Guwahati for nurturing our research career and for all the facilities and financial support that was made available to me.

It would have been impossible for me to continue my five years stay of Ph. D research without the help and support of my batchmates; I am greatly indebted to them. I express my deep sense of gratitude to all my lab members (present and past) Dr. Nirmalangshu Chakraborthy, Dr. Suraj Kumar Pathak, Dr. Subrata Nath, Ms. Pratika Basumatary, Mr. Ravindra Kumar Gupta, Mr. Vinod Kumar Vishwakarma, Dr. Sachin Kumar Singh, Dr. Srikant Turlapati, Dr. Hemant Kumar Singh, Dr. Hidayath Ulla, Mr. Paresh Kumar Behera, Mr. Sibasankar Pradhan and Mr. Abhay Kumar Yadav for their help, scientific conversations and also maintaining a pleasant working environment throughout my Ph.D. tenure.

Of course, nothing would function properly without my beloved friends Yagna Prakash Bhoi, Biswajit Nayak, Prakash Ranjan Mohanta, Niranjan Meher, Tushar Kanta Sahu, Subhasish Behera, Bibhuti Bhusan Dash and Omkar Tripathy for being with me all the time starting from the beginning of my research career and for their help and guidance. My deep sense of gratitude to my friends especially Mr. Dillip Kumar Sahu and Miss Sukanya Gartia for being supportive all the time irrespective of situations.

Finally, my Ph.D. would not have been completed without the eternal love, care, bless, support, patience, non-refundable sacrifices and encouragement of my mother Mrs. Mamata Pradhan, my sweet younger brother Mr. Laxman Pradhan and my two wonderful uncles Mr. Mantu Pradhan and Mr. Mahadev Pradhan. They encouraged me to pay attention to the world around me and to wonder why and how things work. Of course, everything will go invalid if I forget the blessings of my beloved father late Satya Kumar Pradhan and finally almighty without whom nothing will function and I pray him for his blessings.

Balaram Pradhan

Some of the findings of this thesis have been communicated / published in international journals as given below;

1. Star-shaped fluorescent liquid crystals derived from *s*-triazine and 1,3,4-oxadiazole moieties, **B. Pradhan**, S. K. Pathak, R. K. Gupta, M. Gupta, S. K. Pal and A. S. Achalkumar, *J. Mater. Chem. C*, 2016, **4**, 6117-6130**.**

2. Effect of Atomic-Scale Differences on the Self-Assembly of Thiophene-based Polycatenars in Liquid Crystalline and Organogel States, **B. Pradhan**, V. M. Vaisakh, G. G. Nair, D. S. S. Rao, S. K. Prasad and A. S. Achalkumar, *Chem. Eur. J.*, 2016, **22**, 17843-17856.

3. Multifunctional hexacatenar mesogen exhibiting supergelation, AIEE and its ability as a potential volatile acid sensor, **B. Pradhan**, M. Gupta, S. K. Pal and A. S. Achalkumar, *J. Mater. Chem. C*, 2016, **4**, 9669-9673.

4. Columnar self-assembly of luminescent bent-shaped hexacatenars with a central pyridine core connected with substituted 1,3,4-oxadiazole and thiadiazoles, **B. Pradhan**, R. K. Gupta, S. K. Pathak, Joydip De, S. K. Pal and A. S. Achalkumar, *New J. Chem.*, 2018, **42**, 3781-3798.

Articles on results not included in this thesis;

1. Tuning the self-assembly and photophysical properties of bi-1,3,4-thiadiazole derivatives through electron donor-acceptor interactions and their application in OLEDs, A. K. Yadav, **B. Pradhan**, H. Ulla, S. Nath, Joydip De, S. K. Pal, M. N. Satyanarayan and A. S. Achalkumar, *J. Mater. Chem. C*, 2017, **5**, 9345-9358.

2. Nonsymmetrical cholesterol dimers constituting regioisomeric oxadiazole and thiadiazole cores: an investigation on structure-property correlation, **B. Pradhan**, N. Chakraborty, R. K. Gupta, G. Shanker and A. S. Achalkumar, *New J. Chem.*, 2017, **41**, 879-888.

3. Self-assembly of luminescent *N*-annulated perylene tetraesters into fluid columnar phases, R. K. Gupta, S. K. Pathak, **B. Pradhan**, D. S. Shankar Rao, S. K. Prasad and A. S. Achalkumar, *Soft Matter*, 2015, **11**, 3629-3636.

4. Perylo[1,12- b, c, d] Thiophene Tetraesters: A New Class of Luminescent Columnar Liquid Crystals, R. K. Gupta, **B. Pradhan**, S. K. Pathak, M. Gupta, S. K. Pal and A. S. Achalkumar, *Langmuir*, 2015, **31**, 8092-8100.

5. *Bay*-Annulated Perylene Tetraesters: A New Class of Discotic Liquid Crystals, R. K. Gupta, S. K. Pathak, **B. Pradhan**, M. Gupta, S. K. Pal and A. S. Achalkumar, *Chemphyschem*, 2016, **17**, 859-872.

6. Aromatic π-π driven supergelation, aggregation induced emission and columnar self-assembly of star-shaped 1,2,4-oxadiazole derivatives, S. K. Pathak, **B. Pradhan**, R. K. Gupta, M. Gupta, S. K. Pal and A. S. Achalkumar, *J. Mater. Chem. C*, 2016, **4**, 6546-6561.

7. Liquid Crystalline Star-shaped Supergelator Exhibiting Aggregation Induced Blue light Emission, S. K. Pathak, **B. Pradhan**, M. Gupta, S. K. Pal and A. S. Achalkumar, *Langmuir*, 2016, **32**, 9301-9312.

8. Tetrazole based supergelator as a sensitive and selective sensor for picric acid, with a fluorescence switching response, S. Nath, S. K. Pathak, **B. Pradhan**, R. K. Gupta, K. Anki Reddy, G. Krishnamoorthy and A. S. Achalkumar, *New J. Chem.*, 2018, **42**, 5382-5394.

9. Substituted Aroylhydrazone Based Polycatenars: Tuning of Liquid Crystalline Self-Assembly, H. K. Singh, B. Pradhan, S. K. Singh, R. Nandi, D. S. S. Rao, S. K. Prasad, A. S. Achalkumar and Bachcha Singh, *ChemistrySelect*, 2018, **3**, 4027- 4037.

List of Conferences/symposiums: (Oral/Poster);

1. Triazine based Star Shaped Molecules: Mesomorphic and Photophysical Behaviour, **B. Pradhan** and A. S. Achalkumar.
   Poster presented at RESEARCH CONCLAVE'16 held at IIT Guwahati 2016.

2. Mesomorphic and Photophysical Behaviour of Self assembled Triazine based Star shaped molecules, **B. Pradhan** and A. S. Achalkumar.
   Poster presented at National conference on Liquid Crystals (NCLC-22) held at DIT University, Dehradun, 21-23 Dec. 2015 (Awarded with Best Poster prize).

3. Pyridine based moldable supergelators demonstrate AIEE phenomena: A new class of blue light emitting polycatenar stabilizing columnar self-assembly
   B. Pradhan, A.K. Yadav and A. S. Achalkumar.
   Poster presented at REFLUX'16 held at IIT Guwahati, 25-27 March, 2016.

CONTENTS

List of abbreviations used in the text

anhyd	anhydrous
b s	broad singlet
Cr	crystal
Col	columnar
d	doublet
DCM	dichloro methane
dd	doublet of a doublet
DMF	*N, N'*-dimethylformamide
DMSO	dimethyl sulphoxide
equiv	equivalents
Et	ethyl
Et_3N	triethyl amine
EtOAc	ethyl acetate
Fig	figure
g	gram
h	hour
Hz	hertz
HRMS	high resolution mass spectrometry
I	isotropic
IR	infrared
J	joules
J	coupling constant
K	kelvin
LC	liquid crystal
m	multiplet
m	meta
MHz	megahertz
min	minutes
mmol	milli mole(s)

n	normal
N	nematic
N*	chiral nematic
NMR	Nuclear magnetic resonance
p	para
ppb	parts per billion
ppm	parts per million
q	quartet
R_f	retention factor
rt	room temperature
s	singlet
t	triplet
THF	tetrahydrofuran
TMS	tetramethyl silane
TLC	thin layer chromatography
UV	ultra violet
XRD	X-ray diffraction

GENERAL REMARKS

All commercially obtained chemicals were used as received. As required the solvents were dried as per the standard protocols. Silica gel or neutral alumina used as stationery phase for column chromatography. Alluminium sheets coated with silica gel were used for thin layer chromatography (TLC) to monitor the reactions and column purifications. Infrared spectra were measured on a Perkin Elmer IR spectrometer at room temperature by preparing the KBr pellet. ^{1}H and ^{13}C NMR spectra were recorded using Varian Mercury 400 MHz (at 298K) or Bruker 600 MHz NMR spectrometer. Mass spectrometry was carried out using MALDI-TOF mass spectrometer (Bruker Autoflex Speed MALDI TOF/TOF Mass Spectrometer) or High Resolution Mass Spectrometer. Polarizing optical microscope (POM) (Nikon Eclipse LV100POL) in conjunction with a controllable hot stage (Mettler Toledo FP90) was used for the characterization of mesogens. The phase transitions, associated enthalpy changes were obtained by differential scanning calorimeter (DSC) (Mettler Toledo DSC1). X-ray diffraction (XRD) studies were carried out using image plate and a detector. This setup had Cu Kα (λ = 0.15418 nm) radiation from a source (GeniX3D, Xenocs) operating at 50 kV and 0.6 mA in conjunction with a multilayer mirror was used to irradiate the sample. Glass capillaries containing the sample were used for the measurements. Thermogravimetric analysis (TGA) was accomplished with a thermogravimetric analyzer (Mettler Toledo, model TG/SDTA 851 e). Perkin-Elmer Lambda 750, UV/VIS/NIR spectrometer was used to obtain UV-Vis spectra, while Fluoromax-4 fluorescence spectrophotometer and Perkin Elmer LS 50B spectrometer were used to obtain emission spectra in solution state and solid thin film state respectively. Steady State anisotropy experiment was performed on Horiba Scientific Fluoromax spectrofluorometer 4. Time resolved lifetime measurements were done on time correlated single photon counter from Horiba Jobin Yvon (excitation by 440 nm laser diode). Cyclic Voltammetry (CV) studies were carried out using a Versa Stat 3 (Princeton Applied Research) instrument. Atomic Force microscopy (AFM) images were obtained for the spin-coated films using Agilent 5500-STM instrument. SEM images were obtained on a JEOL 7600F FESEM instrument. Rheological data is obtained using Rheometer MCR-302 Anton Paar.

PREFACE

Liquid crystals (LCs) are unique functional soft materials combining both order and mobility on molecular, supramolecular and macroscopic levels. The shape anisotropic molecules which exhibit this unique behavior are also known as mesogens. They can be organic (forming thermotropic and lyotropic phases), inorganic (metal oxides forming lyotropic phases) or organometallic (metallomesogens) in nature. Conventionally, the anisometric molecules employed to stabilize thermotropic LC phases are either rod-like (calamitic) or disc-like (discotic). Calamitics form the backbone of the well-established flat panel display industry. Discotic LCs also have made notable progress in recent years, both from scientific and application viewpoints and slowly they are finding a foothold in the main stream of organic electronics. It is also known that LC behavior is realizable with molecules differing in their shape from conventional LCs. The general feature of majority of such materials is the molecular structural contrast with in the molecule *i.e.*, these molecules are made up of chemically different molecular parts that are incompatible with each other. Some of the important examples of non-conventional systems are oligomers, polycatenars, bent-core molecules, polyhydroxy amphiphiles, octahedral complexes, star-shaped molecules, rod-coil molecules and dendrimers. In the case of non-conventional LCs, the main driving force for the self-assembly of these molecules to form liquid-crystalline (LC) phases is based on the nano-segregation of chemically or physically different building blocks and the tendency to efficiently fill the space in condensed state.

Polycatenars and star-shaped molecules belong to the class of non-conventional LCs, which display a remarkable mesophase behavior. Compared to the synthetic difficulty associated with discotics, these molecular designs are advantageous due to the inherent synthetic flexibility. Thus in the literature we find several structurally diverse polycatenar and star-shaped molecules stabilizing variety of mesophases and interesting properties. All the synthesized materials have been characterized by the requisite characterization techniques for their structural identity, thermal, photophysical and electrochemical behavior. This special state of matter is very sensitive to external perturbations like heat, pressure, electrical and magnetic fields. These materials are extremely sensitive to external stimuli and exhibit the self-healing of structural defects. These properties make such compounds fascinating and extremely appealing for the applications in material sciences as well as in life science. Important applications of

thermotropic LCs are liquid crystal displays, temperature sensors, privacy windows and selective reflecting pigments.

This thesis entitled *"Studies on the self-assembly of some heterocycle containing star-shaped and polycatenar mesogens"* have been divided into four chapters. Contents included in this thesis are based on the research output gained from my research program.

Chapter 1 This is an introductory chapter to LCs in general describing their classification and their important significance in material science. The chapter focuses in greater detail on the physical properties of non-conventional liquid crystals. Beginning with an overview of thermotropic LCs and their brief history, this chapter mainly focuses the major classes of columnar mesophases formed by non-conventional LCs, relevant mesomorphic and physical properties and finally, some applications and perspectives in material science and molecular electronics. Lastly a brief introduction on organic gelators and liquid crystalline physical gels along with their practical application has been described.

Chapter 2 This chapter deals with the synthesis and characterization of eight new star-shaped molecules with a central 2,4,6-triphenyl triazine core attached with three symmetrically substituted 1,3,4-oxadiazole arms with the variation in the number, length and pattern of peripheral chain substitution. Their thermal, electrochemical and photophysical properties with the help of various techniques were investigated. Compounds with three flexible chains at the periphery turned out to be crystalline irrespective of the chain length, whereas compounds with six and nine peripheral chains stabilized the Col_h phase over a wide thermal range. One of the compounds with peripheral *n*-hexadecyloxy substitution at 3 and 4 positions showed a technologically important room temperature Col_h phase. The mesophase range enhanced by lowering the chain length of these star shaped compounds from *n*-hexadecyloxy to *n*-dodecyloxy. The compound with three alkyl tails was crystalline, while the compound with six alkyl tails, where the alkoxy groups are in an adjacent position, exhibited the Col_h phase with a slight enhancement in the thermal range. A marked difference was visible in the case of compounds, where the alkyl tails were in alternate positions. These compounds exhibited high temperature Col_h and low temperature Col_r phases with an enhanced thermal range. A similar behavior was observed in the case of compounds with nine alkoxy tails. Overall, the lowering of chain length has increased the core-core interaction, leading to

the stabilization of the Col_r phase along with the Col_h phase and enhanced the thermal range. This demonstrated how a subtle change in the molecular structure through peripheral substitution alters the LC self-assembly. The photophysical properties of these star shaped molecules were extremely dependent on the number and pattern of peripheral chain substitution. They exhibited blue and green fluorescence in the solid/liquid crystal state. Preserved fluorescence in the solid state is explained due to the formation of aggregates, which do not quench the fluorescence. The aggregation quenching is not occurring here probably due to the columnar packing that includes several different diastereomeric conformations. Cyclic voltammetry studies revealed that these molecules possess lower LUMO levels and bandgaps compared to the 2,4,6-triphenyl triazine which is used in OLEDs, thus making them better candidates for electron transporting emissive layers.

Chapter 3 This chapter presents two series of polycatenar mesogens that contain a central thiophene moiety flanked with two substituted oxadiazole or thiadiazole moieties connected with alkoxyphenyl substituents. The number, length and position of substitution of the peripheral chains were varied. The oxadiazole-based polycatenars exhibited a columnar phase with rectangular and hexagonal or oblique symmetry, whereas thiadiazole-based polycatenars exhibited columnar phases with rectangular and/or hexagonal symmetry. All the compounds exhibited bright emission in the solution and thin-film states. Two oxadiazole-based molecules and one thiadiazole-based molecule exhibited good ability to undergo gelation in hydrocarbon solvents at very low concentrations, which qualifies them as supergelators. The supergelation is mainly supported by attractive π-π interactions, along with other secondary interactions. Of these gels, the oxadiazole- and thiadiazole-containing hexacatenars with *n*-hexadecyloxy chains were studied extensively. These gels showed aggregation-induced enhanced emission, which is of high technological importance for applications in solid-state emissive displays. X-ray diffraction studies showed that the fibers of the xerogels formed by the columnar organization of oxadiazole-based polycatenars with a rectangular lattice, whereas those of the thiadiazole-based polycatenars self-assembled with a hexagonal columnar arrangement. The number, length, and position of substitution of the peripheral tails and the type of the heterocycle moiety adjacent to the thiophene ring greatly affected the self-assembly of the molecules in the LC and gel states. Rheological measurements carried out on the samples confirmed the formation of gels quantitatively and showed that

these gels are mechanically robust. The impact of an atomic-scale difference (oxygen to sulfur, < 2% of the molecular weight) on the self-assembly and the macroscopic properties of these self-assembled compounds have been clearly visualized. This molecular design helps in the development of long molecular nanowires with a strong overlap of central conducting cores and an insulating peripheral sheath of flexible chains, which are promising fort the applications in organic electronic devices.

Chapter 4 In this chapter, we have synthesized and characterized several bent-shaped molecules with a central pyridine unit flanked by two unsymmetrically substituted 1,3,4-oxadiazole and thiadiazole moieties. The number and position of the terminal tails were varied. The type of the heterocycle and the number of peripheral tails had a significant impact on the stabilization of the liquid crystalline and organogel self-assembly as well as the photophysical properties. Thiadiazole based compounds exhibited higher mesophase stability in comparison to oxadiazole derivatives, while oxadiazole based compounds exhibited higher gelation tendency. In the case of oxadiazole derivatives, tetracatenar and hexacatenars exhibited gelation behavior, while in the case of thiadiazole derivatives only hexacatenars exhibited gelation. The number of peripheral tails also plays an important role in stabilizing the gelation in hydrocarbon solvents, which is evident from the fact that all the hexacatenars stabilized supergelation irrespective of the type of the heterocycle. The gelation is mainly promoted by attractive π-π interactions, which is in contrast to other supergelators that require strong intermolecular hydrogen bonding. The supergelators showed the capability to form self-standing, moldable gel at higher concentration. Thiadiazole based compounds exhibited bathochromically shifted absorption and emission in comparison to oxadiazole derivatives but with a lower quantum yield. In addition these compounds showed the ability to sense the acid with a quenching/shifting in the emission spectrum, which makes it possible to detect acids by naked eye at low concentration. Two of the hexacatenar supergelators investigated, exhibited aggregation induced enhanced emission with a several fold increase in luminescence intensity in the gel state. The variation in the gelation capability of these molecules shows that although the π-π interactions plays a major role in self-assembly, the nanoseggregation of incompatible molecular segments like peripheral flexible tails also contribute in organogelation and LC self-assembly. Scanning probe microscopic studies of the xerogels revealed a fibrillar network of several micrometers corroborating the long range supramolecular self-assembly. Extensive rheological studies proved the

viscoelastic and thixotropic nature of the gels. Similar AIEE effect was observed in the thin film state too. Stabilization of columnar self-assembly over a long range, along with AIEE behavior is significant from the perspective of emissive solid-state displays. In a nutshell, this study accounts the effect of molecular structural variations on the nature of supramolecular self-assembly and the resultant macroscopic properties, that is of substantial significance to the scientific community working in the broad area of supramolecular chemistry.

In conclusion the thesis presents a systematic study on the molecular structure and resulting self-assembly behavior of star-shaped and polycatenar molecules in liquid crystals and organogels. Again, it describes the effect of molecular structure in terms of the type of the heteroatom as well as the number and position of peripheral chains on the liquid crystalline and photophysical behavior of polycatenars. It is interesting to note that how an atomic-scale difference affects the self-assembly and the macroscopic properties of the mesogens studied in this thesis. The insights obtained from this work may provide new directions to the study of liquid crystalline organogelators and sensors.

Chapter 1

Introduction to liquid crystals and organogelators

Reproduced from *Angew. Chem. Int. Ed.*, 2018, **57**, 4355-4371, with the permission of Wiley VCH.

1.1. The liquid crystal state

Liquid crystals (LCs) are ordered fluids. In contrast to a solid crystal, where the molecules or atoms are situated on the points of a three-dimensional lattice, the molecules in a liquid crystal phase are distributed more or less at random directions along all three or at least two directions of space. Liquid crystal phases possess long-range orientational order. The degree of organization of liquid crystal is lesser than that of the solid crystalline state, but having more degree of organization than that in the liquid state. In other words, solids usually have both positional and orientational order, which implies that the center of mass of molecules is situated at a specific location and molecular axes point at certain directions. In case of a liquid, there is no specific location for the center of mass of molecules as it varies, since the molecules diffuse in all directions as shown in Fig. 1.1. Therefore, physical properties are not dependent on directions and hence this state is called isotropic state. The organization of the molecules in a well-defined way, provides anisotropic properties to the liquid crystals. The intermediate role between fully ordered and completely disordered systems has given the liquid crystalline state the name “mesomorphic state” and liquid crystal phases are sometimes referred to as “mesophases”. Likewise, a molecular structure generally suitable for the formation of liquid crystalline phases is called mesogenic and such molecules are called as mesogens. Overall, mesogens are anisotropic ordered fluids and sometimes described as "positionally disordered crystals" or "orientationally ordered liquids".[1] They have combined properties of crystal such as optical and electrical anisotropy and liquid-like molecular mobility and fluidity. This special state of matter is very sensitive to external perturbations like heat, pressure, electrical and magnetic fields. The molecular mobility and the tendency for self-organization stimulate the self-healing processes even after the material’s responses to these external stimuli. The self-healing and self-organizing properties make such compounds extremely attractive for applications in material sciences and biology.[2]

1.2. History of liquid crystals

In 1888, the botanical physiologist Friedrich Reinitzer[3a] was extracting cholesterol and their derivatives from carrots to establish its chemical formula. Again, he examined the physical and chemical properties of several derivatives of cholesterol and found that cholesteryl benzoate (**I**) (Fig. 1.2) had two different melting points. One is at 145 °C

where it liquefied to a cloudy liquid and the other one is at 179 °C where it went to a transparent liquid. The phenomenon was reversible. Similar behavior of cloudy liquid phenomenon observed from 116 ^{o}C to 134 ^{o}C in para-azoxy anisole (**II**) (Fig. 1.2) by Gattermann.[3b] Because of this preliminary work, Reinitzer is often recognized with the discovery of the new intermediate phase of matter - the liquid crystal phase.

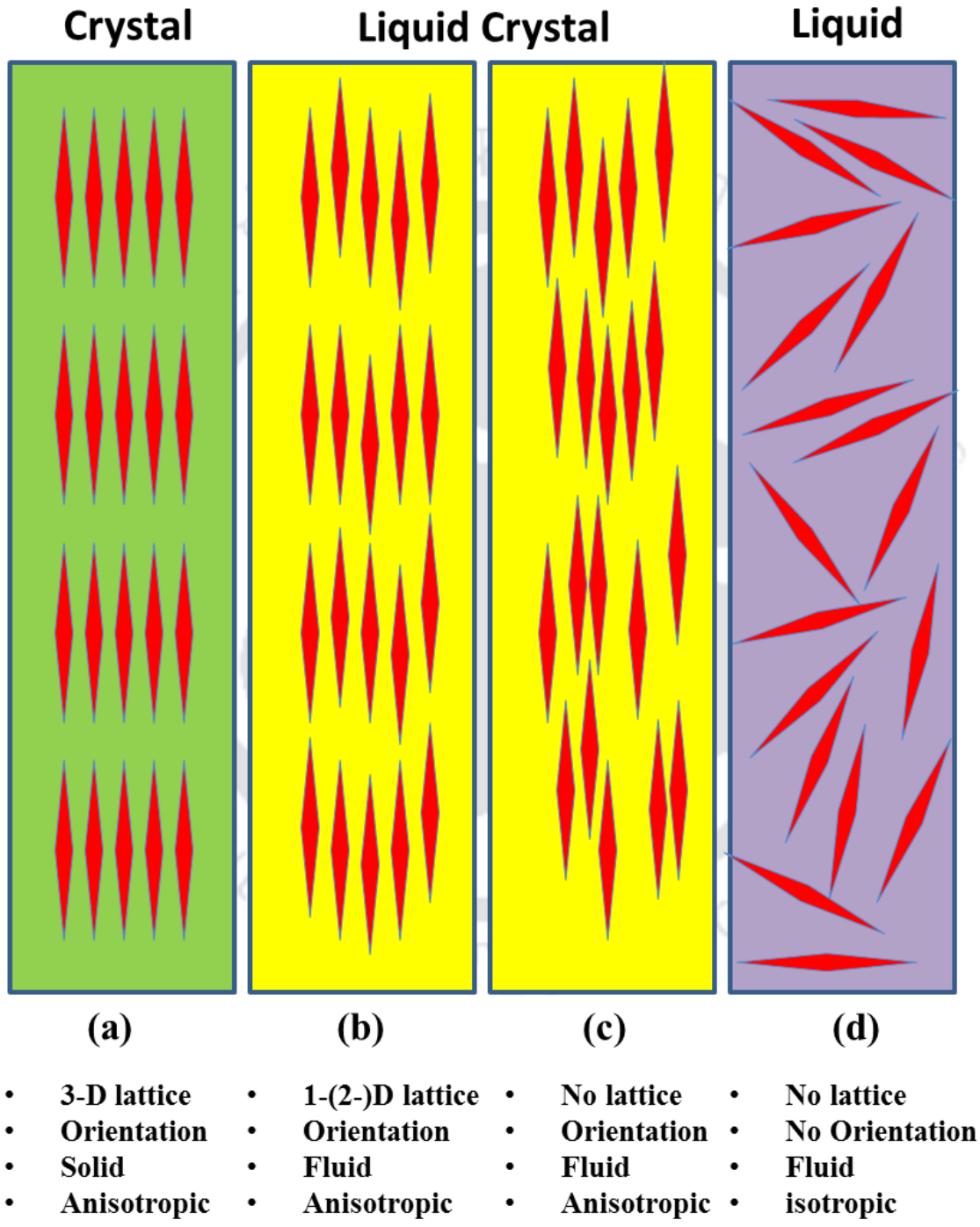

Figure 1.1. Basic structural difference among crystalline solid, liquid crystal and isotropic liquid.

Otto Lehmann[3c] was the first to observe combined properties of both the liquids in their mobility and crystals in their optical properties suggesting the name liquid crystals for these substances. He was also the first to use the term "fliessende krystalle" (flowing crystals) in 1889.[3d] In 1922, Friedel[4a] stressed that, although these states did exhibit some of the properties of crystalline matter and some of the properties of an isotropic liquid, these states are genuinely neither crystalline nor liquid. He suggested that it would be preferable to refer to the liquid crystalline state as mesophase. On the basis of optical studies, Friedel[4b] distinguished clearly three different types of mesophases namely smectic, nematic and cholesteric phases. During the first half of the twentieth century, Vorländer[4c] started systematic synthetic work in order to find out the molecular structure-property relationship. He remarked that the compounds having an elongated shape or rod-like shape exhibit mesophases.

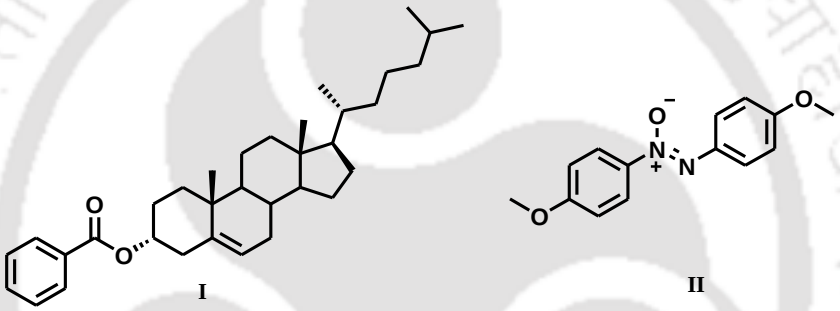

Figure 1.2. Structure of cholesteryl benzoate (**I**) and para-azoxy anisole (**II**).

Thus it was believed for a long time that only molecules, with a rod-like structure, could exhibit mesomorphism. In 1977, Chandrasekhar and his colleagues discovered that not only rod-like (calamitic) molecules but also compounds with disc-like (discotic) molecular shape are capable to form mesophases.[5] Generally discotic liquid crystals (DLCs) have flat or nearly flat, rigid aromatic cores surrounded by 3, 4 or 5 flexible peripheral aliphatic chains. Based on this general template, thousands of DLCs have been reported over the years. In 1996, a new addition to liquid crystal field was introduced, which are commonly known as banana-shaped (bent-shaped) molecules.[6] These molecules contain a central angular unit, two linear rigid cores and terminal flexible chains. The discovery of ferroelectricity in non-chiral banana-shaped molecules increased the research activity in this field of LCs. These and many other non-conventional structures exhibited interesting mesophase morphologies, which motivated scientists to attempt several non-conventional molecular structures that stabilize liquid crystallinity.

1.3. Classification of liquid crystals

Liquid crystals can be classified as shown in the Fig. 1.3. Broadly they can be classified into lyotropic and thermotropic LCs, depending on how the liquid crystalline phase has been obtained, whether by solvent addition on the amphiphilic system (lyotropic)[7] or by temperature variation (thermotropic).[7a] In thermotropic LCs the mesophase formation is temperature dependent, while in the case of lyotropic LCs the mesophase formation is solvent and concentration dependent. Besides, there are some molecules that exhibit LC phases under the influence of both heat and solvent; such systems have been referred as amphotropic LCs.[7c] Lyotropic LC phases are frequently encountered in everyday life and most importantly, life itself is critically based on such ordered fluids. Despite the significance of lyotropic LCs, thermotropic LCs have claimed a relatively greater attention, firstly because they are simple to realize and easy to handle and secondly, they serve as an important medium in the fabrication of low-power devices.

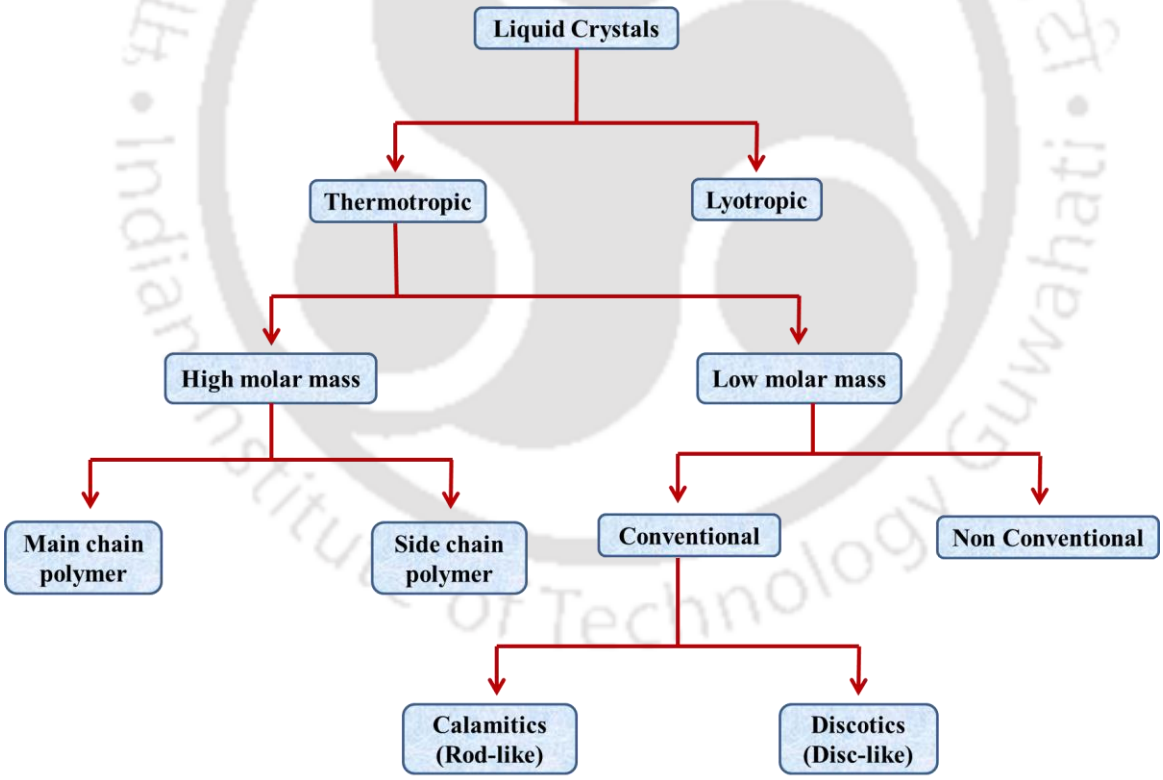

Figure 1.3. Schematic representation of general classification of liquid crystals.

The classification of mesophases is a complicated task as over the last few decades' varieties of mesophases have been discovered or synthesized through conventional, nonconventional or via new molecular architecture. There are different ways to classify these mesophases, in terms of shape (calamitic, discotic and banana-shaped mesogens

etc.), molecular size (as low and high molecular weight) and with respect to the type of mesophase formed (nematic, cholesteric, smectic and columnar etc.). The research work presented in this thesis focuses on thermotropic LCs and hence the discussion is restricted to this topic only.

1.4. Thermotropic liquid crystals

Most of the crystals on heating transform into the isotropic liquid phase by simultaneous loss of the long-range positional and orientational orders. If the molecules possess a certain amount of shape anisotropy, then the disappearance in one, two or three dimensions of long-range translational periodicity in the crystals may precede the collapse of the long-range orientational order. Such compounds may show a series of mesomorphic transitions into fluid states that exhibit varying degrees of the structural symmetries. The temperature at which the crystal transforms into mesophase is called melting point while that from the mesophase to isotropic state is called clearing point. Thermodynamically stable mesophases which appear both on heating and cooling are termed as enantiotropic, while the thermotropic mesophases that appear only on cooling are monotropic. Thermotropic LCs can be either high molar mass (polymeric) or low molar mass. Low molar mass thermotropic LCs can be classified further into conventional and non-conventional LCs.[8]

1.5. Conventional liquid crystals

Conventionally, rod-like and disc-shaped mesogens exhibit thermotropic mesomorphism; they are popularly known as calamitics and discotics respectively. For many years it was believed that the molecule has to be long or rod-shaped molecule[9] (Fig. 1.4b) such as 4-methoxybenzylidene-4'-*n*-butylaniline (MBBA) (**III**) and 4′-pentyl-4-cyanobiphenyl (5CB) (**IV**)[9l] could be mesogenic. However, in 1977 Chandrasekhar *et.al.* demonstrated that disc-like molecules (Fig. 1.4c) such as benzene-1,2,3,4,5,6-hexayl hexaoctanoate (**V**) also can display mesomorphism.[5b]

Rod-like or calamitic molecules have an elongated shape *i.e.* the molecular length (l) is notably greater than the molecular breadth (h) as depicted in Figure 1.4a. The shape anisotropy in combination with micro-segregation of incompatible parts in calamitic LCs results in a number of mesophase structures. Most of the rod-shaped mesogenic compounds contain two or more ring structures, linked together directly or through connecting groups. They frequently have terminal hydrocarbon chains and in some cases

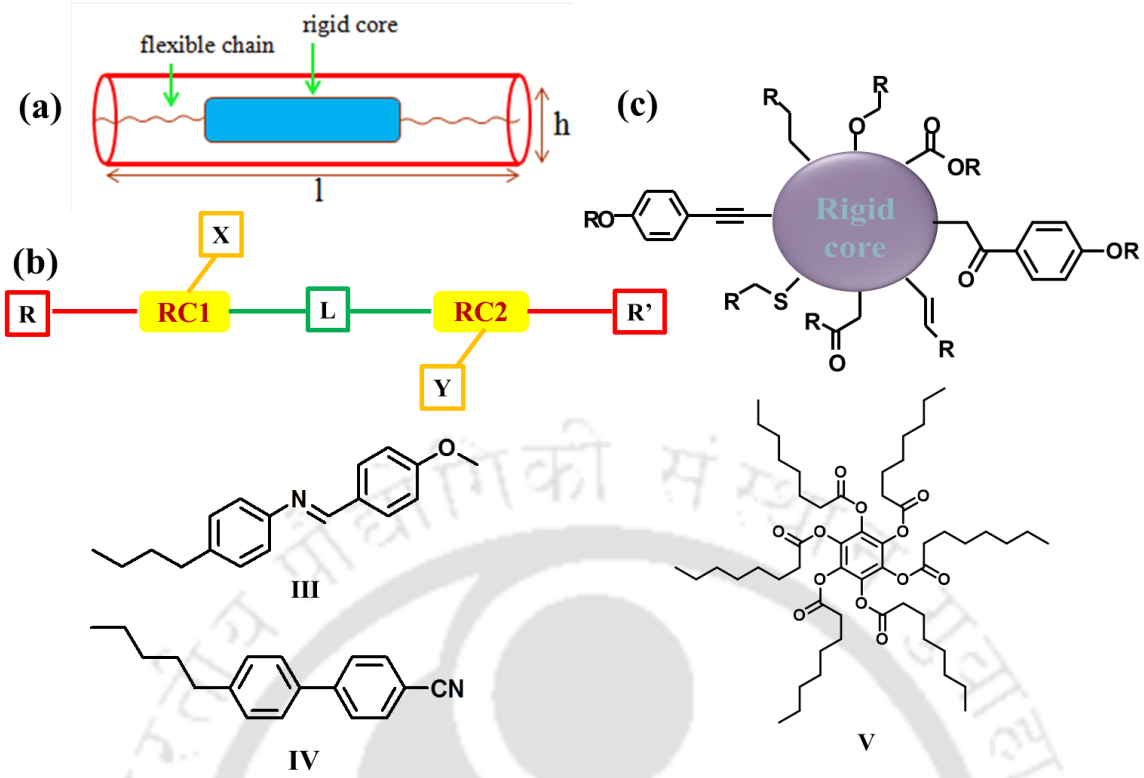

Figure 1.4. General templates for the rod-like (a), disc-mesogen (c) mesogens and representation of calamitic LCs where l >> h (b) and their respective representative examples **III**, **IV**, and **V**.

may contain lateral substituents as well. The representative chemical structure of these molecules can be demonstrated by the general template as shown in Figure 1.4b. RC1 and RC2 are the rigid cores that are often aromatic in nature (*e.g.* 1,4-phenyl, 2,5-pyrimidinyl, 2,6-naphthyl etc.) but can also be alicyclic (*e.g.* *trans*-4-cyclohexyl, cholesteryl etc.). In many examples, these two cores are connected via a covalent bond and in some cases, they are connected by linking unit L (*e.g.* -COO-, -CH_2-CH_2, -CH=N-, -N=N- etc.). The terminal substituents R and R' are usually either alkyl or alkoxy chains. In many cases, one of the terminal units is a polar substituent (*e.g.* CN, F, NCO, NCS, NO_2 etc.). In some special cases, lateral units X and Y (*e.g.* F, Cl, CN, CH_3 etc.) are also incorporated in the main molecular structure.

Discotic LCs are composed of a rigid core which is surrounded by three or more flexible aliphatic chains. Any type of change in the rigid core and peripheral flexible chains alter their self-assembly in bulk as well as in solution. These materials frequently have two, three, four or six-fold rotational symmetry. However, there are many exceptions and materials with low symmetry, a non-planar, non-aromatic core having a shorter number of chains are also documented to display discotic mesophase.[5c] The

mesomorphism is the result of the micro-segregation of the two constituents: the face on interactions between the conjugated rigid cores promote the crystalline character while the liquid character originates from the melting of the flexible peripheral alkyl chains in the mesophase. The search for such mesophase is mostly regulated by delicate changes in the number, size and nature of the lateral chains in addition to the central core. A general template for discotic mesogens is shown in Figure 1.4c. Most of the disc-shaped molecules display only one type of mesophase but few examples are known to exhibit polymorphism. Mesophases formed by discotic molecules are primarily classified as nematic (N), columnar (Col) and lamellar phases.[5] Most common phase in discotics is Col phase followed by nematic phase whereas the other phases are rarely observed. Since this thesis deals with non-conventional LCs, the discussion on conventional LCs is limited.

1.6. Non-conventional liquid crystals

In recent times a great deal of attention has been given to the formation of self-organized systems with multifarious mesophase morphologies. This is attained by modifying the shape of rigid parts by increasing the number of incompatible units in the molecules or by varying the volume-fractions of the incompatible fragments. These molecules with a shape deviating from the conventional rod or disc-shape are known as non-conventional LCs.[10] It is well known that anisotropic molecular shape and space filling play a vital role in self-assembly of mesogens. However, nanoscale segregation of incompatible molecular parts *i.e.* micro segregation has also been realized to play an important role in mesogenic self-assembly, resulting into new mesophase morphologies. The overall feature for the majority of such molecular systems is the molecular structural contrast within the molecule *i.e.* these molecules possess chemically different molecular units that are incompatible with one another. Some of the important examples of non-conventional systems (Fig. 1.5) are oligomers (**VI**)[11], polycatenars (**VII-IX**)[12], bent-core molecules (**X**)[13,10d], star-shaped molecules (**XI**)[14], polyhydroxy amphiphiles (**XII**)[15], dendrimers (**XIII**)[16] and octahedral complexes (**XIV**)[17]. Since this thesis deals with star-shaped and polycatenar LCs, we elaborate on these two classes in the next sections.

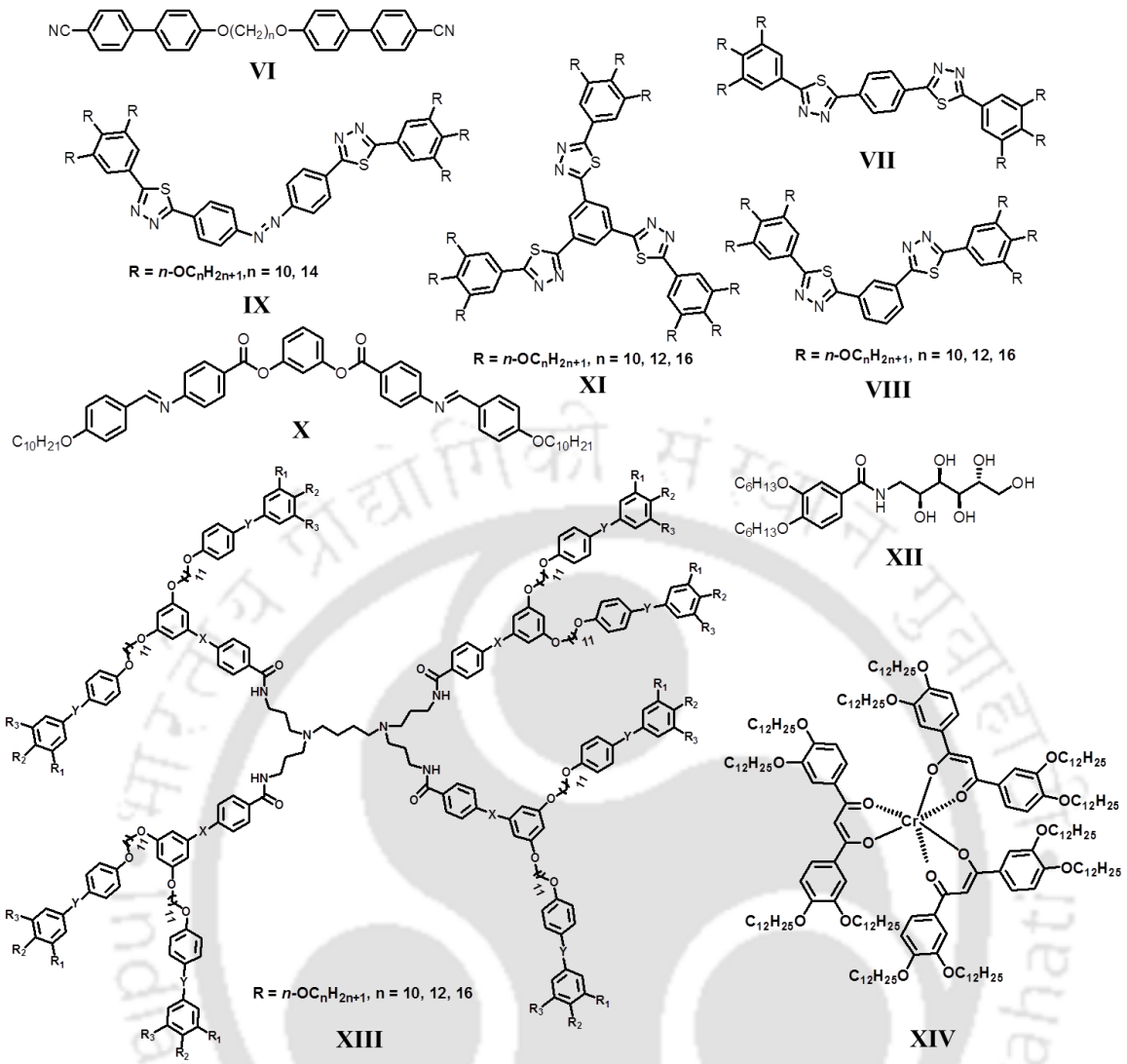

Figure 1.5. Molecular structures of different types of non-conventional LCs.

1.7. Star-shaped mesogens (Hekates)

Non-conventional LCs lack shape anisotropy in the core unit, but their lack of shape anisotropy to exhibit mesophases is compensated by the nanophase segregation of chemically or physically different molecular subunits and their tendency of efficient space filling. The simplest multiarm mesogens that do not fall in the category of rod-shaped mesogens, dimers or bananas are molecules with three arms symmetrically linked with core units, which possess *C*3 symmetry where all arms are identical. These are commonly known as star-shaped mesogens or hekates (Fig. 1.6). [18,19]

The star-shaped mesogens can be divided into three subgroups; stars with three mesogenic or promesogenic units linked to the central core with flexible spacers (subgroup I),[20] stars with a semi-flexible scaffold (subgroup II)[21] and shape-persistent

stars that are obtained by connecting the three rigid arms to central core through linkers (subgroup III)[22] as shown in Figure 1.7 and 1.8.

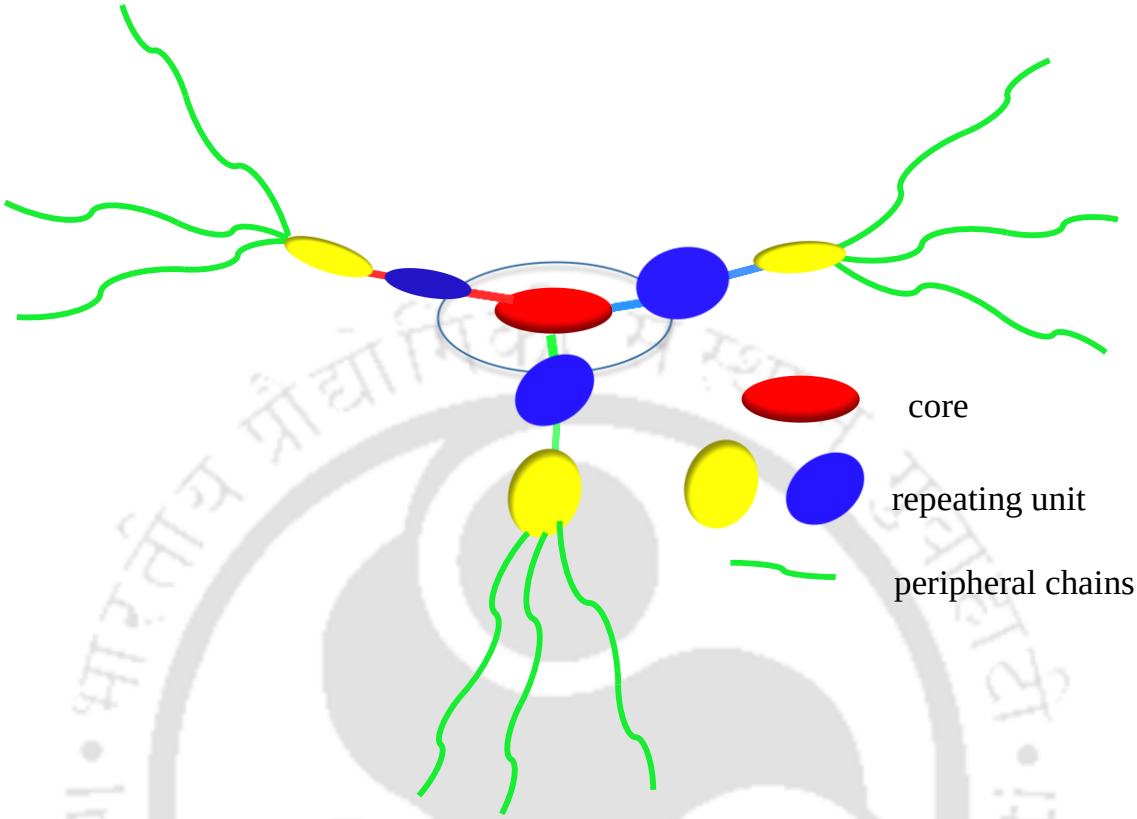

Figure 1.6. A general structure of star-shaped mesogens with three arms.

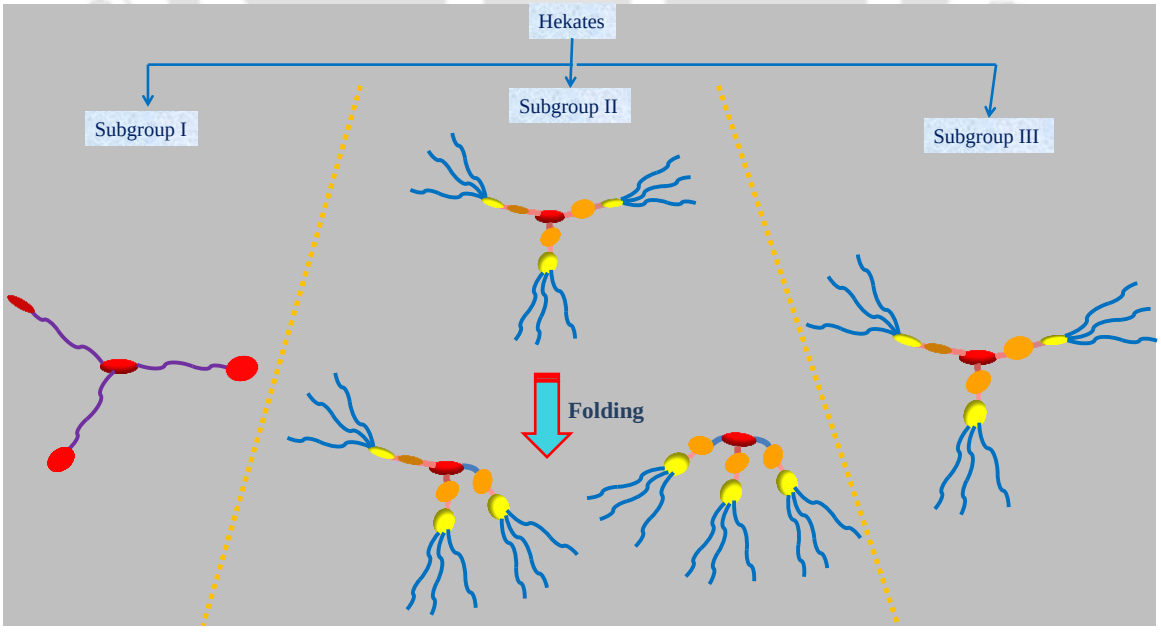

Figure 1.7. Schematic representation of general classification of star-shaped three-arm mesogens.

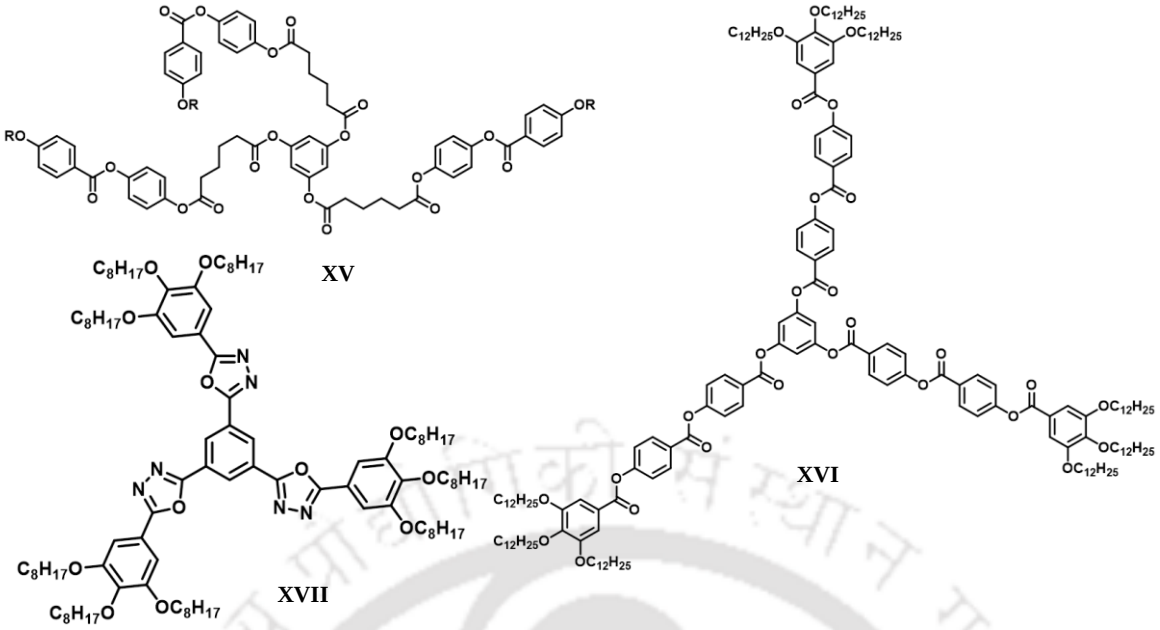

Figure 1.8. Flexible hekates (subgroup I) (**XV**); semi-flexible hekates (subgroup II) (**XVI**) and shape-persistent hekates (subgroup III) (**XVII**).

Inherent synthetic flexibility made these molecules advantageous over discotic molecules associated with synthetic difficulties. Thus the Col phases can be incorporated with other functional properties like hole or electron transport, nonlinear optical activity or fluorescence. The presence of the voids between the arms of the molecular structure helps to avoid the crystallization of mesophases and promote the glassy state. Col phases with glassy nature are important as they allow the movement of charge carriers through them with the simultaneous restriction of ionic impurities. There is a large void between the individual arms that have to be filled in condensed phases. Thus, one would not expect these molecules to form mesophases based on nanoseggregation of incompatible parts, due to the presence of large voids, which may promote the mixing of core and peripheral chains, especially in the subgroup of shape-persistent molecules (Subgroup III).

1.8. Polycatenars

Polycatenar mesogens or phasmids are regarded as the connecting link between conventional rod-like (calamitics) and disc-like (discotics) mesogens as they possess the structural features (Fig. 1.9) and exhibit rich mesomorphic behavior common to both classes of conventional LCs.[23] With regard to the stabilization of Col phase, this class of molecules are advantageous due to their lower melting/clearing point which helps in the

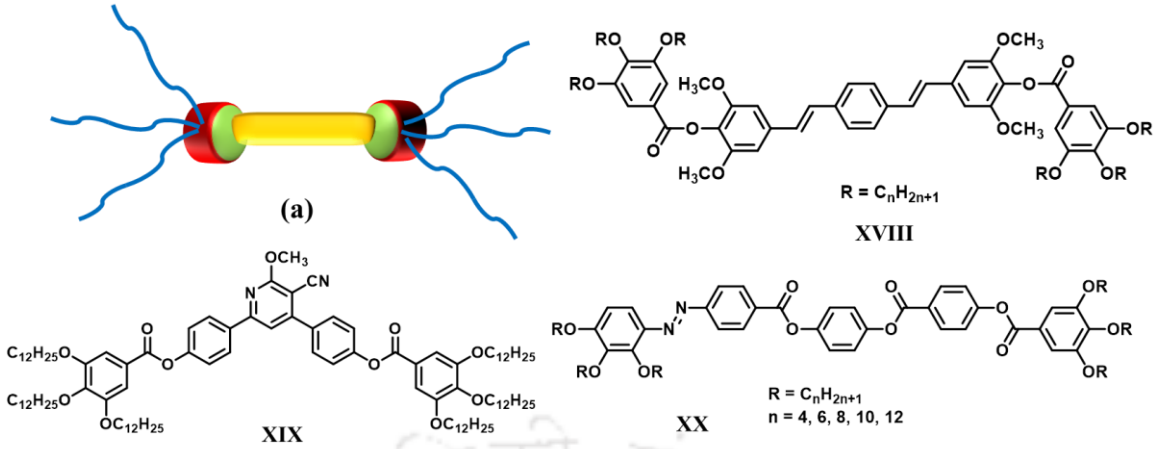

Figure 1.9. General templates for the polycatenar system and representative example.

alignment and the inherent synthetic flexibility to incorporate various functionalities, in comparison to calamitics and discotics. These molecules self-assemble into different LC phases due to the nanosegregation of aromatic units and flexible chains. Since polycatenars share the structural features of both calamitic and discotic LCs, they exhibit various LC phases like nematic, smectic (lamellar), cubic and Col phases, depending on the number of peripheral tails. Gin *et. al.* described a polycatenar structure (**XVIII**) with photophysical utilities.[24a] Prasad *et. al.* presented a polycatenar structure with a photoisomerizable azobenzene unit (**XX**).[24b] Gallardo *et. al.* described a bent-polycatenar with cyanopyridine as a central unit (**XIX**) which stabilized Col_h phase and also exhibit luminescence properties.[24c]

1.9. Mesophase morphologies of thermotropic columnar liquid crystals

On the basis of their chemical structure, shape of the constituent molecules and exterior factors such as temperature and pressure determine different types of LC phases. In this section, several types of columnar phases that exhibited by conventional and non-conventional LCs are discussed.

1.10. Types and structures of columnar phase

Depending on the degree of order in the molecular stacking, orientation of the molecules along the columnar axis, dynamics of the molecules within the columns and the two-dimensional lattice symmetry of the columnar packing, the Col phases may be classified in to seven classes as follows: (i) columnar hexagonal mesophase (Col_h), (ii) columnar square (tetragonal) phase (Col_{sq} or Col_{tet}), (iii) columnar rectangular mesophase (Col_r),

(iv) columnar oblique phase (Col_{ob}), (v) columnar plastic phase (Col_p), (vi) helical phase (H) and (vii) columnar lamellar phase (Col_L).

1.10.1. Columnar hexagonal phase (Col_h)

Hexagonal packing of the molecular columns is characteristics for columnar hexagonal mesophase as shown in table 1.1. The suggested abbreviation for columnar hexagonal phase is "Col_h" and the planar space group is *p*6*mm*. The X-ray scattering profiles of a Col_h phase consist of several peaks in small angle region whose spacings are in the ratio $1:1/\sqrt{3}:1/\sqrt{4}:1/\sqrt{7}:1/\sqrt{9}:1/\sqrt{12}:1/\sqrt{13}$: …$1/\sqrt{h^2+k^2+l^2}$ correspond to 100, 110, 200, 210, 300, 220, 310, …hkl planes respectively along with two broad peaks in the wide-angle region. These two peaks at wide-angle region correspond to the packing of flexible alkyl chains and intra columnar stacking of discotic cores respectively.[25]

1.10.2. Columnar tetragonal (square) phase (Col_t)

Tetragonal packing of the molecular columns is characteristics for columnar tetragonal mesophase as shown in table 1.1. The suggested abbreviation for columnar tetragonal phase is "Col_t" and the planar space group is *p*4*mm*. The X-ray scattering profiles of a columnar tetragonal phase consist of several peaks in small angle region whose spacings are in the ratio $1:1/\sqrt{2}:1/\sqrt{4}:1/\sqrt{5}:1/\sqrt{8}:1/\sqrt{9}:1/\sqrt{10}:1/\sqrt{13}:1/\sqrt{17}$: …$1/\sqrt{h^2+k^2}$ correspond to 100, 110, 200, 210, 220, 300, 310, 230,140 …hk0 planes respectively along with two broad peaks in the wide-angle region. In this mesophase the columns are vertical and they are self-organized in a quadrangular/square lattice. This phase is reported in few sugar molecules, phthalocyanines and supramolecular fluorinated LCs.[26]

1.10.3. Columnar rectangular phase (Col_r)

Here the columns are arranged in a rectangular pattern as shown in table 1.1 and is denoted by Col_r. The two dimensional space group of rectangular columnar phase are *p*2*mm, c*2*mm, p*2*gg* and *p*2*mg* which depends on the direction of the principle symmetry axis, that is the direction of columns. The molecules are elliptically placed in the plane which results in the deviation of symmetry of Col_r from a proper hexagonal arrangement. For that reason, strong core-core interactions are needed in the stabilization of the Col_r phase because the cores of one column must be tilted with respect to cores of neighboring columns. Therefore, with increasing of side-chain length, cross over from columnar rectangular to columnar hexagonal has been observed.[27]

1.10.4. Columnar oblique phase (Col_{ob})

In a columnar oblique (Col_{ob}) mesophase, columns are arranged in a parallelogram lattice and the molecules in each column are tilted as shown in table 1.1. The symmetry of this 2D lattice corresponds to the space group *p*1. Examples of Col_{ob} phases are rare because of the requirement of strong core-core interactions.[28b-d] Since *p*1 is a primitive planar space group, there are no reflection conditions as in the case of Col_h and Col_r phases and therefore all the reflections are allowed. Hence, the assignment of the oblique mesophase by X-ray diffraction study is not so straightforward. Fan-shaped textures and spiral textures are characteristic for Col_{ob} phase.[28]

1.10.5. Columnar plastic phase (Col_p)

Columnar plastic phase is characterized by 3D crystal-like order of the center of mass of the molecules, but the columns are organized in a 2D hexagonal lattice, while the discs within the columns are able to interchange about the column axis (Table 1.1). The suggested abbreviation for columnar plastic phase is "Col_p". In the case of Col_h phase, structural disorders such as nonparallel arrangement of the discs, longitudinal and lateral displacements, and rotation around the columnar axis take place, while the motional freedom of disks in the Col_p phase is limited. The X-ray diffraction pattern of Col_p phase exhibits low angle reflections that can be indexed to form a 2D hexagonal lattice. In addition, the profile for the plastic phase has reflections having mixed indices. The occurrence of the diffuse peaks in the wide-angle region which is due to the alkyl chains differentiates this phase from a crystalline phase. The wide-angle core-core reflection, which is usually diffuse in the Col phase, becomes very sharp and splits into two peaks.[29]

1.10.6. Columnar helical phase (H)

Columnar helical phase (H) is characterized by helically arranged columns with the hydrocarbon chains interdigitated in groups of three columns as shown in table 1.1. This exceptional mesophase structure with the helical order was observed in a triphenylene derivative namely hexahexylthiotriphenylene (HHTT).[30a,b] X-ray diffraction experiments have proved that the helical H phase is distinctive to HHTT and certain mixtures of compounds with an average chain length close to 6 carbons. [30c]

1.10.7. Columnar lamellar phase (Col_L)

Columnar lamellar mesophase is characterized by a layered structure with the columnar organization as shown in table 1.1 and exist in certain discotic compounds.[31,32] The suggested abbreviation for the columnar lamellar phase is "Col_L". The physical characteristics arrangements of molecules for this columnar lamellar phase are: firstly, the disc-shaped molecules arranged one above the other to form columns and secondly, these columns are assembled into different layers without any positional or translational correlation. The X-ray scattering profiles of a columnar lamellar phase consist of several peaks in the low angle region whose spacings are in the ratio 1:2:3 corresponding to the lamellar association of columns.

All the typical Col phases discussed in this thesis are summarized in table 1.1 with related schematics and structural parameters. The number of molecules in the unit cell can be calculated by using following equation:

$$Z = (\rho \times N_A \times S \times h_c)/M$$

Where ρ is the density of the liquid crystal phase, N_A is Avogadro's constant, S is the columnar cross-section area, h_c is the height of the columnar slice and M is the molecular weight of the constitutive molecule. S can be easily calculated from the cell parameters, keeping in mind that its expression depends on the geometry of the cell (Table 1.1). Therefore, a hypothesis on how mesogen molecules are eventually organized to form the discoidal shape can be formulated.

1.11. Identification of thermotropic mesophases

Since the discovery of LC molecules, till date a number of liquid crystalline phases have been observed. Precise characterization of LC phases generally requires the use of different techniques[1] as the structural differences between these phases are quite narrow. The most commonly used device to identify the LC phases is the polarizing optical microscope (POM) that reveals the characteristic optical texture of a mesophase.[1] The identification of mesophases through POM usually involves the magnified view of a thin sample of a mesogenic material sandwiched between a glass microscope slide and a glass coverslip. The textures are usually examined between crossed polarizers, in white light under orthoscopic illumination; the substrates are either chemically treated for homogeneous/homeotropic alignment or used without any pretreatment.

Table 1.1. Two-dimensional space groups of columnar liquid crystals with corresponding cross-section area and number of discoids (disc or ellipsoid) Z_{disc} in a cross section.

Type (notation)	**Space group**	**Extinction rules**	**Cross section**			**Three dimensional representation**
			Schematic	Area	Discoid number	
Columnar hexagonal (Col_h)	*p6mm*	No conditions	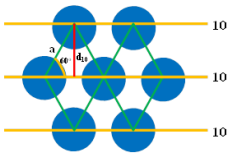	$S = a^2 sin60^o$	$Z_{disc} = 1$	
Columnar tetragonal (Col_{tet})	*p4mm*	No conditions	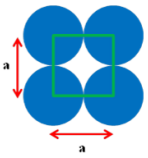	$S = a^2$	$Z_{disc} = 1$	
Columnar rectangular (Col_r)	*p2mm*	No conditions	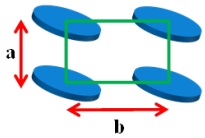	$S = ab$	$Z_{disc} = 1$	
	c2mm	*hk*: $h + k = 2n$, *h*0: $h = 2n$, 0*k*: $k = 2n$	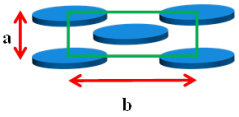		$Z_{disc} = 2$	
	p2gg	*hk*: no conditions, *h*0: $h = 2n$, 0*k*: $k = 2n$	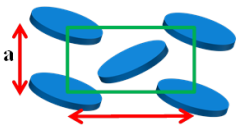		$Z_{disc} = 2$	
	p2mg	*hk*: no conditions, *h*0: no conditions, 0*k*: $k = 2n$	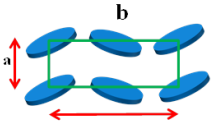		$Z_{disc} = 2$	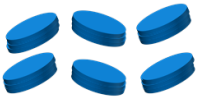
			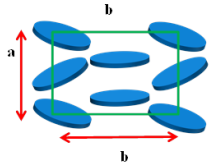		$Z_{disc} = 4$	
Columnar oblique (Col_o)	*p*1	No conditions	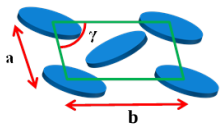	$S = absin\gamma$	$Z_{disc} = 2$	
Columnar plastic(Col_p)						
Columnar helical (H)						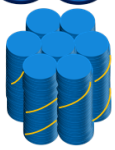
Columnar lamellar (Col_L)						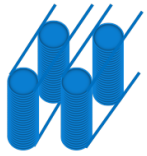

A calorimetric study using differential scanning calorimetry (DSC) is a complementary tool to microscopic studies to know the precise phase transition temperature and the enthalpy change associated with the transition. However, there are limitations in mesophase characterization by either of these methods as the optical textures of different smectic or Col phases are difficult to distinguish and the enthalpy values cannot be so characteristic for different phase transitions. Sometimes miscibility studies, in which a well-known liquid crystal phase is physically mixed with an unknown phase to ascertain the nature of the phase, are carried out based on the criterion of complete miscibility of identical phases. For unambiguous identification of mesophases, structural information such as relative molecular positions, the presence of long-range positional order, the quality of preferred molecular orientation etc. can be obtained from diffraction studies. X-ray, electron, and neutron radiations are suitable for diffraction studies. X-rays are probably the most convenient and widely used whereas electrons and neutrons have advantages in particular situations. Other experimental techniques such as electro-optic measurements and nuclear magnetic resonance (NMR) spectroscopy are also in use for the characterization of mesophases.

1.12. Applications of columnar phases

Numerous potential application of LCs and its technology has become the inseparable part of our daily life *viz.* wrist watches, pocket calculators, computer, laptop and televisions. LC displays were grown up rapidly due to their small size, ease of viewing, low power consumption and durability. Col phase offers a one-dimensional pathway for the charge migration where the central aromatic core acts as a conducting unit, while the external peripheral chains act as an insulating mantle. This LC phase is of great importance due to their inherent self-assembling and self-healing ability, which in turn enhances the physical properties (optical and conductive) due to the ordered organization. A careful molecular engineering can be employed to tailor these physical properties for enhancing the performance of Col phases as active materials in solar cells (good processability, large absorption coefficient, good charge carrier mobility), as they can be cheaper alternatives in comparison to inorganic counterparts. To meet all these objectives Col phases derived from electron rich/poor DLCs is the best choice, which mimic the single crystalline organic semiconductors. The “edge on” orientation of the Col phases can be translated into the active layers of field effect transistors (FET) which are the vital components of molecular electronic devices. The high mobility for photo-induced charge

carriers in the Col phases also makes them worthy of their application in fast and high resolution xerographic and laser printing as active charge transport layers.[33] Col LCs can be used as a sensitive sensors for both polar and nonpolar molecules because they have a unique conductive surface that can be altered due to the disturbance in the surface.[34] Recent years efforts are made to employ Col phases for construction of the organic light emitting diodes (OLEDs) as they can act as good emitting and conductive materials. Col phase with a combination of hole/electron transport and luminescence properties is an ideal material for the fabrication of OLEDs.[35]

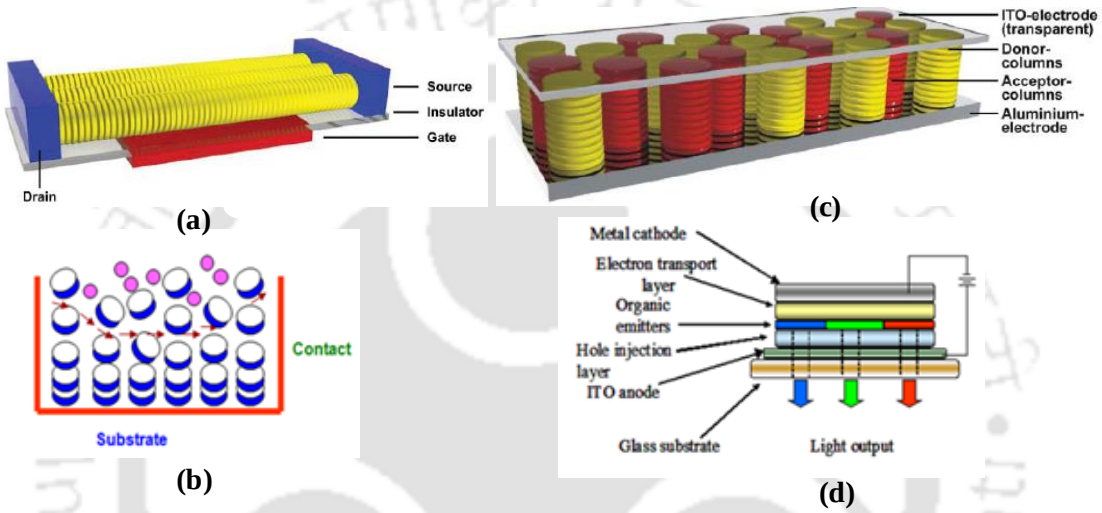

Figure 1.10. Schematic representations of molecular electronic devices from Col mesophases: (a) field effect transistor; (b) gas sensors; (c) photovoltaic or solar cells and (d) organic light emitting diodes, (Reproduced from reference [33a] with the permission from Royal Chemical Society)

1.13. The Gel state

In general, gels are viscoelastic solid-like materials comprised of an elastic cross-linked network and a solvent, which is the major component. Thus by weight, the gels are mostly liquid, but they behave like solids due to a three dimensional cross-linked network within the liquid. In other words, the gels are a dispersion of molecules of a liquid within a solid in which the solid is the continuous phase and the liquid is the discontinuous phase. Gels are defined as a substantially dilute cross-linked system, which exhibits no flow when in the steady-state. The three-dimensional cross-linked network within the liquid may result from physical bonds (physical gels) or chemical bonds (chemical gels). Gelation relies on a balance between solvent-gelator and gelator-gelator interactions.[36c,37b-g] The non-covalent interactions responsible for gelation are mainly the H-bonding, π-π stacking, donor-acceptor[36] interactions, metal coordination, solvophobic

forces (hydrophobic forces for gels in water) and van der waals interactions. Most of the naturally occurring gelators are macromolecular and they form gels by physical cross-linking (usually H-bonding[37]). Such macromolecules include gelatin, collagen, agar, starch etc. Gels derived from synthetic compounds can be subdivided on the basis of their constitution into macromolecular (polymer) and molecular. When the gels are formed by strong chemical bonds, they cannot be redissolved and are thermally irreversible (*e.g.* polyester, polyamide, poly(vinyl alcohol), polyethylene) whereas gels formed by weak noncovalent interactions (physical entanglements) are reversible (*e.g.* polyacrylate, polymethacrylate). Depending on the dispersion medium or the sol, gel can be classified as hydrogels, organogels and aerogels (Fig. 1.11). Since this thesis deals with organogels, our discussion is restricted to this topic only.

Organogels or organic gelators are non-crystalline, non-glassy, thermoplastic solid materials composed of a liquid organic phase entrapped in a three-dimensionally, cross-linked network. The liquid can be, for example, an organic solvent, mineral oil or vegetable oil. The solubility and particle dimensions of the structures are important characteristics for the elastic properties and firmness of the organogel. Organogels are frequently found in food processing, pharmaceuticals and cosmetics.

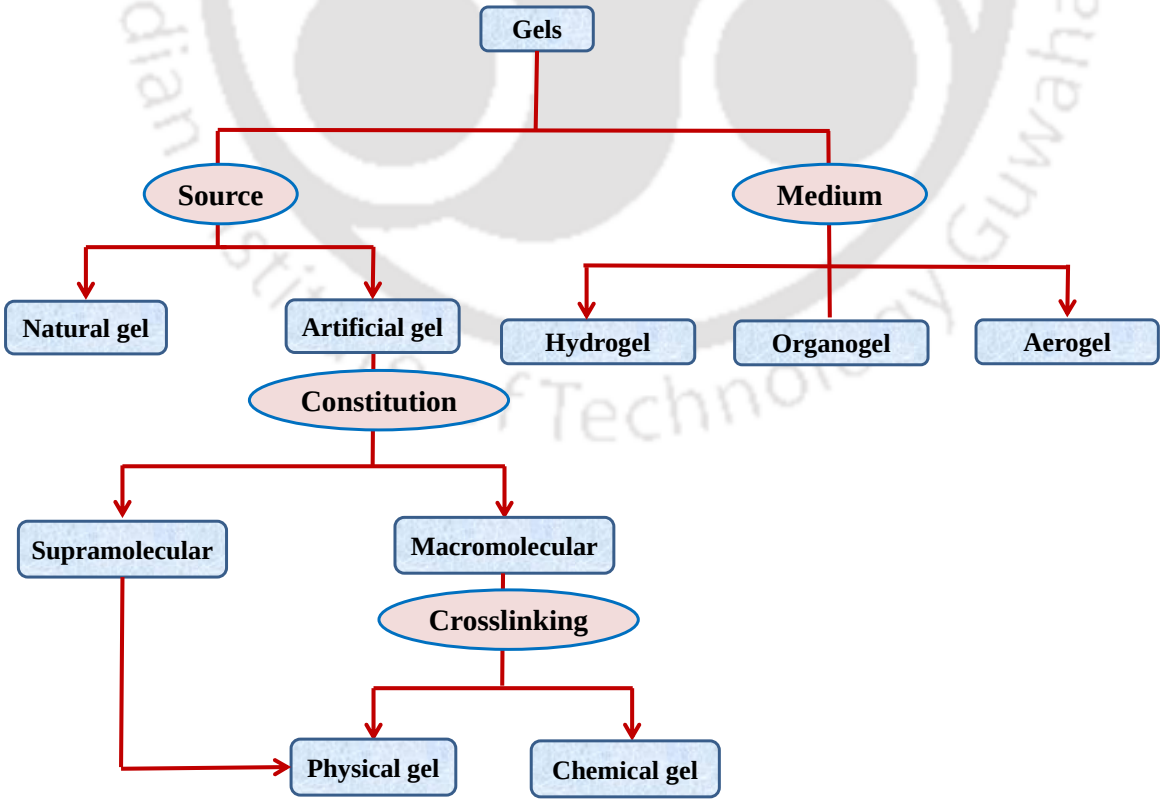

Figure 1.11. Schematic representation of general classification of gels.

Gels of a low molecular mass compound are usually prepared by heating the gelator in an appropriate solvent and cooling the resulting isotropic supersaturated solution to room temperature. When the hot solution is cooled, the molecules start to condense and three situations are possible: (i) a highly ordered aggregation giving rise to crystals, (ii) a random aggregation resulting in an amorphous precipitate or (iii) an aggregation process intermediate between these two, yielding a gel (Fig. 1.12). The process of gelation involves self-association of the gelator molecules to form long, polymer-like fibrous aggregates, which get entangled during the aggregation process forming a matrix that traps the solvent mainly by surface tension. This process prevents the flow of solvent under gravity and the mass appears like a solid. Determination of the sol-to-gel phase transition temperature (TSG or T_{gel}) is necessary.[38d] It is generally determined by a "dropping-ball method" where a small ball will be placed on top of the gel in a test tube and slowly heated in an oil bath at a fixed heating rate. T_g is defined as the temperature, when the ball had reached the bottom of the test tube.[38] Another important factor is critical gelation concentration (CGC) which means the minimum concentration is required to form a stable gel at room temperature[38b] and it is well known in literature that when the CGC is below or equal to 1 weight% it is called a supergelator.[39] Xerogels are solids formed from gels that do not suffer from shrinkage in the process. If the liquid system is almost entirely or wholly removed from the gel, then it will be called as a xerogel. Xerogels generally retain a high degree of porosity. Rubber and gelatin are examples of xerogels.

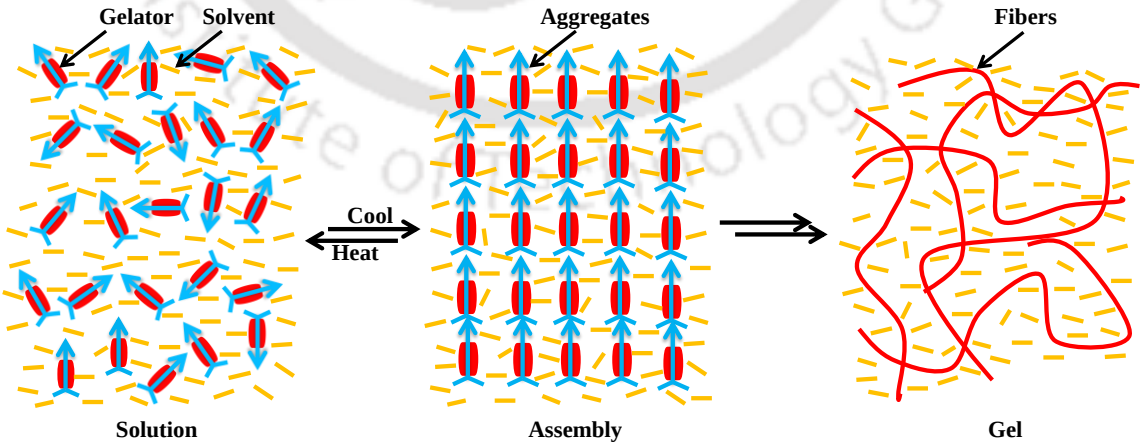

Figure 1.12. Schematic representation of the self-assembly of low molecular weight gelators into one dimensional aggregates and the subsequent formation of an entangled network.[43c]

LCs can be gelated with chemical or physical 3D network strucutures. The LC chemical gels[40] have been prepared by polymerisation of LC or non-LC monomers in liquid crystals. Liquid-crystalline physical gels are obtained by the self-assembly of fibrous solid networks of gelators in liquid crystals (Fig.1.13).[41] Liquid crystals become soft solids by gelation, keeping their stimuli-responsive properties. The formation of anisotropic phase-separated structures leads to the induction of new functions and the enhancement of the properties. The LC physical gels are normally formed by thermal processes, in which two independent transitions, the sol-gel transition of a gelator and the isotropic-anisotropic transition of a LC, are observed.

Due to the combination of two components which form phase separated anisotropic structures, LC physical gels exhibit enhanced or induced electronic, photochemical and electro-optical properties.[41] Furthermore, these gels can be exploited as a material for electro-optical memory,[41f] which can be attained by controlling reversible aggregation process under electric fields. The enhanced hole mobility[41g] was reported with the introduction of fibrous aggregates into triphenylene-based columnar liquid crystals. Similarly, the incorporation of photochromic azobenzenes or electroactive tetrathiafulvalenes into the chemical structures of gelators leads to the preparation of ordered functional materials.[41h]

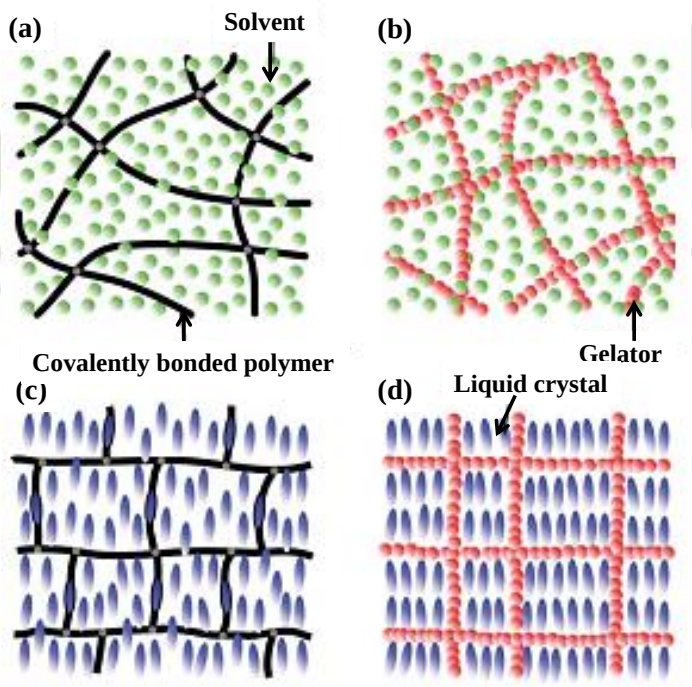

Figure 1.13. Schematic illustration of (a) chemical gels; (b) physical gels; (c) liquid-crystalline (LC) chemical gels and (d) LC physical gels (Reproduced from reference [46] with the permission from Royal Chemical Society).

An efficient methodology to elucidate the nature of an organogel is to begin with a characterization of its rheological and thermodynamic properties. Rheology is the study of the flow of matter, primarily in a liquid state, but also as 'soft solids' or solids under conditions in which they respond with plastic flow rather than deforming elastically in response to an applied force. Rheology offers a convenient method to measure the flow properties of gel like materials and facilitates the classification between “strong” and “weak” gel types.[42] Dynamic rheological measurements are done to establish the elastic nature of the gel samples that involved strain sweep, angular frequency sweep and step-strain measurements and it is characterized by $G^*(\omega) = G'(\omega) + iG''(\omega)$, where G’ is the storage modulus, G’’ is the loss modulus and ω is the angular frequency. At the microscopic level, the structures and morphologies of supramolecular gels have been investigated by conventional imaging techniques such as scanning electron microscope (SEM), transmission electron microscopy (TEM) and atomic force microscopy (AFM) while thermal and mechanical studies are used to understand the interactions between these structures. However, at the nanoscale, X-ray diffraction, small angle neutron scattering (SANS) and small angle X-ray scattering (SAXS) are required to elucidate the structures of supramolecular gels.

Application of organogels in drug delivery can be illustrated with the example of active enzymes and bacteria entrapped in apolar gels of gelatin. Highly concentrated oil-in-water (O/W) emulsions and various gels have been used as aviation fuels and in cosmetics while highly concentrated water-in-oil (W/O) emulsions are used in some explosives technologies.[43a] Many aqueous gels[43b] are employed for macromolecular separations, protein crystallization etc. While there are wide ranging applications for organogels in general, π-gels (formed due to π-π stacking interaction mainly) are of particular interest with respect to electronic and photonic applications.[44a,b] The special interests in π-gels are associated with their inherent electronic properties such as fluorescence,[45] charge carrier mobilities,[44d] electronic conductivities,[44d] etc. Therefore, in recent years, considerable effort has been put in by the scientific community to the design of π-gels for specific application in the field of advanced materials.[44,45] The present thesis also deals with the π-gels formed by some of the polycatenar mesogens.

1.14. References

1. (a) S. Chandrasekhar, in *Liquid Crystals*, 2nd Ed. Cambridge University Press: New York, 1994; (b) J. W. Goodby, P. J. Collings, T. Kato, C. Tschierske, H. Gleeson and P. Raynes, Eds. *Handbook of Liquid Crystals: Fundamentals*, Wiley-VCH: Weinheim, Germany, 2014, Vol. **1**; (c) T. Geelhaar, K. Griesar and B. Reckmann, *Angew. Chem. Int. Ed.*, 2013, **52**, 8798-8809; (d) P. J. Collings and M. Hird, *Introduction to Liquid Crystals Chemistry and Physics*, Taylor and Francis Ltd. London, 1997; (e) B. Bahadur, *Liquid Crystals: Application and Uses.* Vol. **1-3**, World Scientific, Singapore, 1990; (f) G. W. Gray, *Molecular structure and the properties of liquid crystals*, Academic Press, London and New York, 1962; (g) D. Demus and L. Richter, *Textures of liquid crystals*, 2nd Ed. Deutscher Verlag f. Grundstoffindustrie Leipzig, 1978; (h) G. W. Gray, *Handbook of liquid crystals*, Vol. **1**, Eds: D. Demus, J. W. Goodby, G. W. Gray, H. W. Spiess, and V. Vill, Wiley-VCH, Germany, 1998; (i) G. W. Gray and J. W. Goodby, *Smectic Liquid crystalline Textures and Structures*, Leonard Hill, Philadelphia, 1984; (j) P. G. de Gennes and J. Prost, *The Physics of Liquid Crystals*, Oxford Science Publication, Oxford, 1993; (k) S. Kumar, *Liquid Crystals: Experimental Study of Physical Properties and Phase Transitions*, Cambridge University Press, 1st Ed. 2001; (k) B. Wunderlich and J. Grebowicz, *Adv. Polym. Sci*., **2**, 60/61, 1-59, 1984.
2. (a) T. Kato, N. Mizoshita and K. Kishimoto, *Angew. Chem.*, 2006, **118**, 44-74; (b) T. Kato, N. Mizoshita and K. Kishimoto, *Angew. Chem. Int. Ed.*, 2006, **45**, 38-68.
3. (a) F. Reintzer, *Montash. Chem*., 1988, **9**, 421-441; (b) L. Gattermann, *Ber. Dtsch. Chem. Ges.*, 1890, **23**, 1218-1228; (c) O. Lehman, *Z. Krist.*,1890, **18**, 464-467; (d) O. Lehmann, *Z. Phys. Chem.*, 1889, **4**, 462-472.
4. (a) G. Friedel, *Ann. Phys.*,1922, **18**, 273-474; (b) G. Friedel and E. Friedel, *Z. Krist*., 1931, **79**, 1-60; (c) D. Vorländer, *Phys. Chem.*,1923, **105**, 211-254.
5. (a) S. Kumar, *Liquid Crystals Today*, 2009, **18**, 2-27; (b) S. Chandrasekhar, B. K. Sadashiva and K. A. Suresh, *Pramana*, 1977, **9**, 471-480; (c) S. Kumar, *Isr. J. Chem.*, 2012, **52**, 820-829.
6. (a) T. Niori, T. Sekine, J. Watanabe, T. Furukawa and H. Takazoe, *J. Mater. Chem*., 1996, **6**, 1231-1233; (b) G. Pelzi, S. Diele and W. Weissflog, *Adv. Mater*., 1999, **11**, 707-724; (c) C. Tschierske and G. Dantlgraber, *Pramana*, 2003, **61**, 455-481; (d) M. B. Ros, J. L. Serrano, M. R. De la Fuente and C. L. Folcia, *J. Mater. Chem.*, 2005, **15**, 5093-5098; (e) R. A. Reddy and C. Tschierske, *J. Mater. Chem.*,2006, **16**, 907-961; (f) H. Takezoe and Y. Takanishi, *Jpn. J. Appl. Phys*., 2006, **45**, L595- L597; (g) J. Etxebarria and M. B. Ros, *J. Mater. Chem*., 2008, **18**, 2919-2926.
7. (a) P. G. de Gennes and J. Prost, *The physics of Liquid Crystals*, 2nd Ed. (Oxford: Clarendon Press), 1993; (b) Y. Hendrikx, J. Charvolin, M. Rawiso and M. C. Holmes, *J. Phys. Chem.*, 1983, **87**, 3991-3999; (c) C. Tschierske, *C. Curr. Opin. Colloid Interface Sci.*, 2002, **7**, 355-370.
8. (a) D. Demus, *Liq. Cryst.*, 1989, **5**, 75-110; (b) C. Tschierske, *J. Mater. Chem*., 1998, **8**, 1485-1508; (c) C. Tschierske, *J. Mater. Chem*., 2001, **11**, 2647-2671; (d) C. Tschierske, *Annu. Rep. Prog. Chem. Sect. C*, 2001, **97**, 191-267; (e) C. Tschierske, *Curr. Opin. Colloid Interface Sci*., 2002, **7**, 69-80.
9. (a) H. Kelker and B. Scheurle, *Angew. Chem.*, 1969, **81**, 903-904; (b) C. T. Imrie and G. R. Luckhurst, in *Handbook of liquid crystals*, Vol-**2B**, Eds. D. Demus, J. W. Goodby, G. W. Gray and H. W. Spiess, V. Vill, Wiley-VCH, Germany, 1998, part – III, p.799; (c) C. T. Imrie and P. A. Henderson, *Curr. Opin. Colloid Interface Sci*., 2002, **7**, 298-311; (d) C. T. Imrie in *Structure and Bonding - Liquid crystals*, II, Ed:

D. M. P. Mingos, Springer-Verlag, 1999, p.149; (e) N. Tamaoki, *Adv. Mater*., 2001, **13**, 1135-1147; (f) C. V. Yelamaggad, G. Shanker, U. S. Hiremath and S. K. Prasad, *J. Mater. Chem.*, 2008, **18**, 2927-2949; (g) A. S. Achalkumar, U. S. Hiremath, D. S. Shankar Rao and C. V. Yelamaggad, *Liq. Cryst.*, 2011, **38**, 1563-1589; (h) E. Allard, F. Oswald, B. Donnio, D. Guillon, J. U. Delgado, F. Langa and R. Deschenaux, *Org. Lett*., 2005, **7**, 383-386; (i) C. V. Yelamaggad, S. A. Nagamani, U. S. Hiremath, D. S. S. Rao and S. K. Prasad, *Liq. Cryst*., 2002, **29**, 231-236; (j) C. T. Imrie, F. E. Karasz and G. S. Attard, *Macromolecules*, 1993, **26**, 545-550; (k) C. T. Imrie, P. A. Henderson and J. M. Seddon, *J. Mater. Chem.*, 2004, **14**, 2486-2488; (l) G. W. Gray, *Liquid Crystals*, 1998, **24**(1), 5-14.

10. (a) D. Demus, *Liq. Cryst.*, 1989, **5**, 75-110; (b) C. Tschierske, *J. Mater. Chem*., 1998, **8**, 1485-1508; (c) C. Tschierske, *J. Mater. Chem*., 2001, **11**, 2647-2671; (d) C. Tschierske, *Annu. Rep. Prog. Chem*., *Sect. C*, 2001, **97**, 191-267; (e) C. Tschierske, *Curr. Opin. Colloid Interface Sci*., 2002, **7**, 69-80.
11. (a) C. T. Imrie and P. A. Henderson, *Chem. Soc. Rev.*, 2007, **36**, 2096-2124; (b) C. T. Imrie, G. R. Luckhurst, in *Handbook of liquid crystals.*, Vol-**2B**, Eds.: D. Demus, J. W. Goodby, G. W. Gray, H. W. Spiess, V. Vill, WileyVCH, Germany, 1998, part – III, p. 799; (c) C. T. Imrie and P. A. Henderson, *Curr. Opin. Colloid Interface Sci*. 2002, **7**, 298-311; (d) C. T. Imrie in *Structure and Bonding-Liquid crystals, II*, Ed: D. Mingos, M. P. Springer-Verlag, 1999, p. 149; (e) N. Tamaoki, M. Moriyama and H. Matsuda, *Angew. Chem. Int. Ed*. 2000, **39**, 509-511; (f) N. Tamaoki, *Adv. Mater*. 2001, **13**, 1135-1147; (g) R. A. Reddy and C. Tschierske, *J. Mater. Chem*. 2006, **16**, 907-961; (h) H. Takezoe and Y. Takanishi, *J. App. Phys*., 2006, **45**, No. 2A, 597; (i) C. V. Yelamaggad, I. S. Shashikala, G. Liao, D. S. S. Rao, S. K. Prasad, Q. Li and A. Jakli, *Chem. Mater.*, 2006, **18**, 6100-6102; (j) V. A. Mallia and N. Tamaoki, *Chem. Soc. Rev*., 2004, **33**, 76-84; (k) C. V. Yelamaggad, A. S. Achalkumar, D. S. Shankar Rao and S. Krishna Prasad, *Org. Lett*., 2007, **9**, 2641-2644.
12. (a) S. K. Pathak, R. K. Gupta, S. Nath, D. S. S. Rao, S. K. Prasad and A. S Achalkumar, *J. Mater. Chem. C*, 2015, **3**, 2940-2952; (b) H. T. Nguyen, C. Destrade and J. Malthete, *Adv. Mater*., 1997, **9**, 375-388; (c) J. Malthete, H. T. Nguyen and C. Destrade, *Liq. Cryst.*, 1993, **13**, 171-187.
13. (a) T. Niori, T. Sekine, J. Watanabe, T. Furukawa and H. Takezoe, *J. Mater. Chem*., 1996, **6**, 1231-1233; (b) G. Pelzl, S. Diele and W. Weissflog, *Adv. Mater.*, 1999, **11**, 707-724; (c) K. Fodor-Csorba, A. Vajda, G. Galli, A. Jakli, D. Demus, S. Holly and E. Gacs-Batiz, *Macro. Chem. Phys*., 2002, **203**, 1556-1563.
14. (a) S. K. Pathak, S. Nath, R. K. Gupta, D. S. S. Rao, S. K. Prasad and A. S Achalkumar, *J. Mater. Chem. C*, 2015, **3**, 8166-8182; (b) A. Pegenau, P. Goring and C. Tschierske, *Chem. Commun.*, 1996, **27**, 2563-2564.
15. (a) K. Borisch, S. Diele, P. Goring, H. Muller and C. Tschierske, *Liq. Cryst.*, 1997, **22**, 427-443; (b) C. Tschierske, *Chem. Soc. Rev.*, 2007, **36**, 1930-1970.
16. (a) J. H. Cameron, A. Facher, G. Lattermann and S. Diele, *Adv. Mater*., 1997, **9**, 398-403; (b) A. Pegenau, T. Hegmann, C. Tschierske and S. Diele, *Chem. Eur. J*., 1999, **5**, 1643-1660; (c) S. I. Stupp, M. Keser and G. N. Tew, *Polymer*, 1998, **39**, 4505-4508; (d) H. Meier, M. Lehmann, and U. Kolb, *Chem. Eur. J*., 2000, **6**, 2462-2469; (e) V. Percec, A. E. Dulcey, V. S. K. Balagurusamy, Y. Miura, J. Smidrkal, M. Peterca, S. Nummelin, U. Edlund, S. D. Hudson, P. A. Heiney, H. Duan, S. N. Magonov and S. A. Vinogradov, *Nature*, 2004, **430**, 764-768; (f) M. Lehmann, C. Köhn, H. Meier, S. Renker and A. Oehlhof, *J. Mater. Chem.*, 2006, **16**, 441-451; (g) B. M. Rosen, C. J. Wilson, D. A. Wilson, M. Peterca, M. R. Imam and V. Percec, *Chem Rev.*, 2009, **109**,

6275-6540; (h) B. Donnio, *Inorganica Chimica Acta*, 2014, **409**, 53-67; (i) D. J. Pesak and J. S. Moore, *Angew. Chem. Int. Ed*., 1997, **36**, 1636-1639.

17. (a) H. Zeng and T. M. Swager, *J. Am. Chem. Soc*., 1994, **111**, 761-762; (b) T. M. Swager and H. Zeng, *Mol. Cryst. Liq. Cryst.*, 1995, **260**, 301-306.
18. (a) M. Lehmann, R. I. Gearba, M. H. J. Koch and D. A. Ivanov, *Chem. Mater.*, 2004, **16**, 374-376; (b) M. Lehmann and M. Jahr, *Chem. Mater*., 2008, **20**, 5453-5456; (c) H. Detert, M. Lehmann and H. Meier, *Materials*, 2010, **3**, 3218-3330; (d) M. Lehmann, *Chem. Eur. J.*, 2009, **15**, 3638-3651; (f) S. Varghese, N. S. S. Kumar, A. Krishna, D. S. S. Rao, S. K. Prasad and S. Das, *Adv. Funct. Mater*., 2009, **19**, 2064-2073.
19. (a) Colliers Encyclopedia, Vol. **12** (Eds.: W. D. Halsey, B. Johnston), Macmilllan, New York 1988; (b) W. Burkert, Greek Religion, Harvard University Press, Cambridge, 1985, p. 171.
20. (a) G. H. Mehl, A. J. Thornton and J. W. Goodby, *Mol. Cryst. Liq. Cryst.*, 1999, **332**, 455-461; b) S. Kumar and M. Manickam, *Liq. Cryst.*, 1999, **26**, 939-941; c) L. Wilson, *Liq. Cryst.*, 1994, **18**, 1005-1014.
21. (a) J. Barber, L. Puig, J. L. Serrano and T. Sierra, *Chem. Mater.*, 2004, **16**, 3308-3317; (b) D. Goldmann, D. Janietz, C. Schmidt and J. H. Wendorff, *Liq. Cryst.*, 1998, **25**, 711-719; (c) K. P. Van den Hout, R. Martín-Rapffln, J. A. J. M. Vekemans and E. W. Meijer, *Chem. Eur. J.*, 2007, **13**, 8111-8123; (d) J. J. van Gorp, J. A. J. M. Vekemans and E. W. Meijer, *Mol. Cryst. Liq. Cryst.*, 2003, **397**, 191-205.
22. (a) R. Christiano, D. M. Pereira de Oliveira Santos and H. Gallardo, *Liq. Cryst*., 2005, **32**, 7-14; (b) C. H. Lee and T. Yamamoto, *Mol. Cryst. Liq. Cryst.*, 2002, **378**, 13-21; (c) B. G. Kim, S. Kim and S. Y. Park, *Tetrahedron Lett*., 2001, **42**, 2697-2699; (d) J. C. Chang, J. R. Yeon, Y. S. Chin, M. J. Han and S. K. Hong, *Chem. Mater.*, 2000, **12**, 1076-1082; (e) J. C. Chang, J. H. Baik, C. B. Lee, M. J. Han and S. K. Hong, *J. Am. Chem. Soc.*, 1997, **119**, 3197-3198.
23. (a) J. W. Goodby, P. J. Collings, T. Kato, C. Tschierske, H. Gleeson and P. Raynes, Wiley-VCH, Weinheim, Germany 2014, **1**, *Handbook of Liquid Crystals: Fundamentals*, ed.; (b) C. Tschierske, *Angew. Chem. Int. Ed*., 2013, **52**, 8828-8878.
24. (a) B. P. Hoag and D. L. Gin, *Adv. Mater.*, 1998, **10**, 1546-1551; (b) N. G. Nagaveni, M. Gupta, A. Roy and V. Prasad, *J. Mater. Chem.*, 2010, **20**, 9089-9099; (c) R. L. Coelho, E. Westphal, D. Z. Mezalira and H. Gallardo, *Liquid Crystal*, 2017, **44**(2), 405-416.
25. (a) S. K. Prasad, D. S. S. Rao, S. Chandrasekhar and S. Kumar, *Mol. Cryst. Liq. Cryst*., 2003, **396**, 121-139; (b) R. L. Coelho, E. Westphal, D. Z. Mezalira and H. Gallardo, *Liquid Crystal*, 2017, **44**(2), 405-416.
26. (a) T. Vlad-Bubulak, J. Buchs, A. Kohlmeier, M. Bruma, and D. Janietz, *Chem. Mater.*, 2007**, 19**, 4460-4466; (b) K. Ohta, T. Watanabe, H. Hasebe, Y. Morizumi, T. Fujimoto and I. Yamamoto, *Mol. Cryst. Liq. Cryst*., 1991, **196**, 13-26; (c) K. Hatsusaka, K. Ohta, I. Yamamoto and H. Shirai, *J. Mater. Chem*., 2001, **11**, 423-433; (d) M. Ichihara, A. Suzuki, K. Hatsusaka and K. Ohta, *Liq. Cryst*., 2007, **34**, 555-567; (e) K. Praefcke, P. Marquard, B. Kohne, W. Stephan, A. M. Levelut and E. Watchtel, *Mol. Cryst. Liq. Cryst*., 1991, **203**, 149-158; (f) Md. A. Alam, J. Motoyanagi, Y. Yamamoto, T. Fukushima, J. Kim, K. Kato, M. Takata, A. Saeki, S. Seki, S. Tagawa and T. Aida, *J. Am. Chem. Soc.*, 2009, **131**, 17722-17723.
27. (a) A. M. Levelut, *J. Chem. Phys*., 1983, **80**, 149; (b) F. C. Frank and S. Chandrasekhar, *J. Phys*., 1980, **41**, 1285; (c) C. Destrade, P. Foucher, H. Gesparoux, H. T. Nguyen, A. M. Levelut and J. Malthete, *Mol. Cryst. Liq. Cryst*., 1984, **106**, 121.

28. (a) F. Morale, R. W. Date, D. Guillon, D. W. Bruce, R. L. Finn, C. Wilson, A. J. Black, M. Schroder and B. Donnio, *Chem. Eur. J*., 2003**, 9**, 2484; (b) C. Destrade, P. Foucher, H. Gasparoux, H. T. Nguyen, A. M. Levelut and Malthete, J. *Mol. Cryst. Liq.Cryst*., 1984, **106**, 121-146; (c) B. Donnio, B. Heinrich, H. Allouchi, J. Kain, S. Diele, D. Guillon and D. W. Bruce, *J. Am. Chem. Soc*., 2004, **126**, 15258-15268; (d) C. Destwde, N. H. Tinh, L. Mamlok and J. Malthete, *Mol. Cryst. Liq. Cryst*., 1984, **114**, 139-150.
29. B. Glusen, W. Heitz, A. Kettner and J. H. Wendorff, *Liq. Cryst*., 1996, **20**, 627-633.
30. (a) E. Fontes, P. A. Heiney and W. H. De Jeu, *Phys. Rev. Lett*., 1988, **61**, 1202; (b) P. A. Heiney, E. Fontes, W. H. De Jeu, A. Riera, P. Carroll and A. B. Smith III, *J. Phys. France*, 1989, **50**, 461-483; (c) S. H. J. Idziak, P. A. Heiney, J. P. McCauley, Jr. P. Carroll and A. B. Smith III, *Mol. Cryst. Liq. Cryst*., 1993, **237**, 271-275.
31. (a) K. Ohta, H. Muroki, A. Takagi, K. I. Hatada, H. Ema, I. Yamamoto and K. Matsuzaki, *Mol. Cryst. Liq. Cryst*., 1986, **140**, 131; (b) H. Sakashita, A. Nishitani, Y. Sumiya, H. Terauchi, K. Ohta and I. Yamamoto, *Mol. Cryst. Liq. Cryst*., 1988, **163**, 211.
32. (a) S. Mery, D. Haristoy, J. F. Nicoud, D. Guillon, S. Diele, H. Monobe and Y. Shimizu, *J. Mater. Chem*., 2002, **12**, 37-41; (b) P. Davidson, A. M. Levelut, H. Strzelecka and V. Gionis, *J. Phys. Lett*., 1983, **44**, 823-828.
33. (a) C. D. Simpson, J. Wu, M. D. Watson and K. Mullen, *J. Mater. Chem*., 2004, **14**, 494-504; (b) S. Laschat, A. Baro, N. Steinke, F. Giesselmann, C. Hägele, G. Scalia, R. Judele, E. Kapatsina, S. Sauer, A. Schreivogel and M. Tosoni, *Angew. Chem.Int. Ed*., 2007, **46**, 4832-4887.
34. N. Boden, R. Bissel, J. Clements and B. Movaghar, *Current science*, 1996, **71**, 599-601.
35. T. Christ, B. Glusen, A. Greiner, A. Kettner, R. Sander, V. Stumpflen, V. Tsukruk and J. H. Wendorff, *Adv. Mater*.,1997, **9**, 48-52.
36. (a) P. Terech and R. G. Weiss, *Chem. Rev.* 1997**, 97**, 3133-3159; (b) X. Y. Liu and J. L. Li, *Soft Fibrillar Materials: Fabrication and Applications*, 1st Edition. 2013 by Wiley-VCH Verlag GmbH & Co. KGaA; (c) Y. Lan and M. A. Rogers, *Cryst. Eng. Comm*., 2015, **17**, 8031-8038; (d) N. Yan, Z. Xu, K. K. Diehn, S. R. Raghavan, Y. Fang and R. G. Weiss, *J. Am. Chem. Soc*., 2013, **135**, 8989-8999; (e) X. Y. Liu and P. D. Sawant, *Adv. Mater*., 2002, **14,** 421-426; (f) R. Y. Wang, P. Wang, J. L. Li, B. Yuan, Y. Liu, L. Li and X. Y. Liu, *Phys. Chem. Chem. Phys*., 2013, **15**, 3313-3319; (g) D. Farbi, J. Guan and A. Cesaro, *Thermochim. Acta*, 1998, **321**, 3-16.
37. (a) S. Mukhopadhyay and U. Maitra, *Curr. Sci*., 2004, **87**, 1666-1683; (b) Y. Wu, S. Wu, G. Zou and Q. Zhang, *Soft Matter*, 2011, **7**, 9177-9183; (c) M. A. Rogers and A. G. Marangoni, *Langmuir*, 2009, **25**, 8556-8566; (d) A. R. Hirst, I. A. Coates, T. R. Boucheteau, J. F. Miravet, B. Escuder, V. Castelletto, I. W. Hamley and D. K. Smith, *J. Am. Chem. Soc*., 2008, **130**, 9113-9121; (e) J. Gao, S. Wu, T. J. Emge and M. A. Rogers, *Cryst. Eng. Comm.*, 2013, **15**, 4507-4515; (f) S. Wu, J. Gao, T. J. Emge and M. A. Rogers, *Soft Matter*, 2013, **9**, 5942-5950; (g) Y. Lan, M. G. Corradini, X. Liu, T. E. May, F. Borondics, R. G. Weiss and M. A. Rogers, *Langmuir*, 2014, **30**, 14128-14142; (h) Y. Lan, M. G. Corradini and M. A. Rogers, *Cryst. Growth Des*., 2014, **14**, 4811-4818.
38. (a) Z. Qi, N. L. Traulsen, P. M. de Molina, C. Schlaich, M. Gradzielski and C. A. Schalley, *Org. Biomol. Chem.*, 2014, **12**, 503-510; (b) R. G. Weiss, *J. Am. Chem. Soc.*, 2014, **136**, 7519-7530.; (c) A. R. Hirst, I. A. Coates, T. R. Boucheteau, J. F. Miravet, B. Escuder, V. Castelleto, I. W. Hamley and D. K. Smith, *J. Am. Chem. Soc*.,

2008, **130**, 9113-9121; (d) J. E. Eldridge and J. D. Ferry, *J. Phys. Chem.*, 1954, **58**, 992-995.

39. (a) S. K. Pathak, B. Pradhan, R. K. Gupta, M. Gupta, S. K. Pal and A. S. Achalkumar, *J. Mater. Chem. C*, 2016, **4**, 6546-6561; (b) T. Yamamoto and M. Yoshida, *Langmuir*, 2012, **28**, 8463-8469; (c) M. Zhang, D. Xu, X. Yan, J. Chen, S. Dong, B. Zheng and F. Huang, *Angew. Chem., Int. Ed.*, 2012, **51**, 7011-7015; (d) R. Yoshida, *Adv. Mater.*, 2010, **22**, 3463.
40. (a) R. A. M. Hikmet, *Adv. Mater.*, 1992, **4**, 679-683; (b) S. M. Kelly, *J. Mater. Chem.*, 1995, **5**, 2047-2061; (c) C. A. Guymon, E. N. Hoggan, N. A. Clark, T. P. Rieker, D. M. Walba and C. N. Bowman, *Science*, 1997, **275**, 57-59.
41. (a) N. Mizoshita, K. Hanabusa and T. Kato, *Adv. Funct. Mater.*, 2003, **13**, 313-317; (b) X. Tong and Y. Zhao, *J. Am. Chem. Soc.*, 2007, **129**, 6372-6373; (c) Y. Zao and X. Tong, *Adv. Mater.*, 2003, **15**, 1428-1431; (d) N. Mizoshita and T. Kato, *Adv. Funct. Mater.*, 2006, **16**, 2218-2224; (e) C. Tolksdorf and R. Zentel, *Adv. Mater.*, 2001, **13**, 1307-1310; (f) N. Mizoshita, Y. Suzuki, K. Hanabusa and T. Kato, *Adv. Mater.*, 2005, **17**, 692-696; (g) N. Mizoshita, H. Monobe, M. Inoue, M. Ukon, T. Watanabe, Y. Shimizu, K. Hanabusa and T. Kato, *Chem. Commun.*, 2002, 428-429; (h) M. Moriyama, N. Mizoshita, T. Yokota, K. Kishimoto and T. Kato, *Adv. Mater.*, 2003, **15**, 1335-1338.
42. P. Terech and R. G. Weiss, *Chem. Rev.*, 1997, **97**, 3133-3159.
43. (a) G. Haering and P. L. Luisi, *J. Phys. Chem.*, 1986, **90**, 5892-5895; (b) R. J. Phillips, W. M. Deen and J. F. Brady, *J. colloid and inter.sc.*, 1990, **139**, 363-373.
44. (a) A. R. Hirst, B. Escuder, J. F. Miravet and D. K. Smith, *Angew. Chem., Int. Ed.*, 2008, **47**, 8002-8018; (b) S. Banerjee, R. K. Das and U. Maitra, *J. Mater. Chem.*, 2009, **19**, 6649-6687; (c) A. Dawn, T. Shiraki, S. Haraguchi, S. I. Tamaru and S. Shinkai, *Chem. Asian J.*, 2011, **6**, 266-282; (d) S. S. Babu, S. Prasanthkumar and A. Ajayaghosh, *Angew. Chem., Int. Ed.*, 2012, **51**, 1766-1776.
45. (a) S. S. Babu, K. K. Kartha, A. Ajayaghosh, *J. Phys. Chem. Lett.*, 2010, **1**, 3413-3424; (b) A. Ajayaghosh, V. K. Praveen and C. Vijayakumar, *Chem. Soc. Rev.*, 2008, **37**, 109-122; (c) S. S. Babu, V. K. Praveen and A. Ajayaghosh, *Chem. Rev.*, 2014, **114**, 1973-2129.
46. T. Kato, Y. Hirai, S. Nakaso and M. Moriyama, *Chem. Soc. Rev.*, 2007, **36**, 1857-1867.

Chapter 2

Star-shaped fluorescent liquid crystals derived from *s*-triazine and 1,3,4-oxadiazole moieties

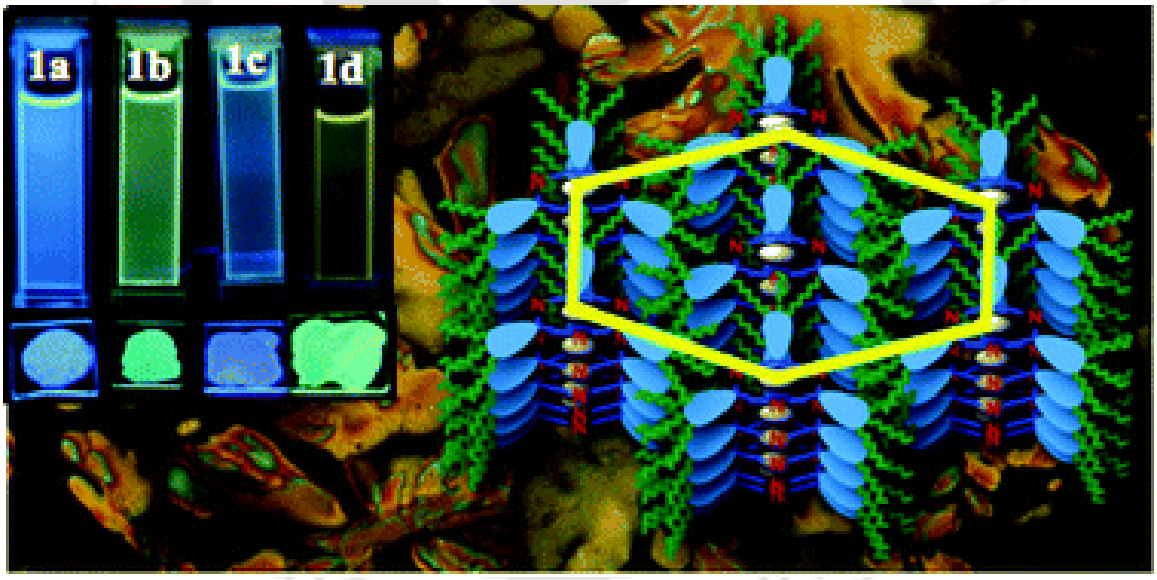

Results have been published in *J. Mater. Chem. C*, 2016, **4**, 6117-6130.

2.1. Introduction

The last four decades have witnessed tremendous research activities with respect to design and synthesis of various discotic liquid crystals.[1] Discotic liquid crystals are designed with the general structural template where a central disc-like core is substituted with three or more flexible chains. Discotic Liquid crystals mainly stabilize two mesophases *viz.* columnar (Col) phase and nematic (N) phase. Columnar phase formed by the one-dimensional stacking of discs to form columns. Based on the arrangement of these columns into different lattices they are classified into different columnar phases. Nematic phase is formed by the organization of discs with long-range orientational order but with no positional order. Over the years several innovative nonconventional molecular designs were shown to stabilize Col phases, which were initially observed for disc shaped molecules. These classes are polycatenars, dendrimers, metallomesogens, bent shaped molecules, oligomers, polymers and star shaped molecules.[2] Star shaped mesogens or 'hekates' are relatively a new class of nonconventional molecules that stabilize columnar liquid crystalline phases. These molecules are formed by the covalent linking of three arms symmetrically to a central core.[3] These arms may be linked to the central core through flexible or semi flexible or rigid linkers. Shape persistent star shaped mesogens are obtained, when the linkers connecting central core and three arms are rigid. These molecules lack the shape anisotropy of discotics required to exhibit mesophases, but their ability to form mesophases is solely driven by the nanophase segregation of chemically or physically different molecular subunits and their tendency to fill the space efficiently in bulk. Advantage of this molecular design with respect to discotics is, the synthetic flexibility provided to incorporate various functional units into the molecular structure. Hekates or star shaped mesogens can exhibit a variety of phases like nematic, columnar, cubic or soft crystal phases, because of the peculiar structure and the ease of tunability associated with this molecular design. The presence of the voids between the arms of the molecular structure helps the mesophases to freeze in glassy state. Several 1,3,5-substituted benzene based or heterocyclic cores have been utilized to prepare these star shaped mesogens. *s*-1,3,5-Triazine is a readily available C_3-symmetrical, trifunctional core to prepare star shaped mesogens.[4] Being a C_3-symmetric planar central core which helps in the self-assembly, it also acts as an *n*-type semiconductor owing to its electron poor nature. Triazine core can also be employed as an H-bonding acceptor, which stabilizes supramolecular liquid crystalline self-assembly.[5] Triazine based central core is

also used in the synthesis of oligomers[6] and dendrimers.[7] This core has also been utilized in the construction of octupolar materials[8] which show nonlinear optical activity with large first hyperpolarizability. 1,3,5-Triazine based star shaped mesogens have been prepared by one of the following methods, (i) the reaction of nucleophilic group functionalized aromatics with cyanuril chloride[9]; (ii) nucleophilic[9] or palladium catalyzed substitutions[10] with trihalo-1,3,5-triazines and (iii) cyclotrimerization of nitriles.[11, 12b, 17] Many fluorophores like styrene,[9,12] tolane,[13] carbazole[14] and triazole[15] and thiophenes[16] are connected to this central 1,3,5-triazine core to obtain luminescent mesogens. Marder *et.al.* prepared triazine derivatives where three trialkoxy phenyl substituted 1,3,4-oxadiazole moieties are directly connected to the central triazine cores.[18] Incorporation of 1,3,4-oxadiazoles in to the molecular structure has some advantages, as 1,3,4-oxadiazoles are well-known for their stability towards thermal, hydrolytic and oxidative degradation, intense fluorescence and good electron transporting properties. These compounds are widely used as electron carrier/hole blocking materials and also as electroluminescent layers in organic light emitting devices. Many other research groups have prepared star shaped molecules containing oxadiazole moieties connected to central benzene core at 1,3 and 5-positions.[18,19] In comparison to these benzene based hekates, reports on the triazine based hekates with 1,3,4-oxadiazole moieties are scarce. Probably the associated increase in the melting points with the incorporation of heterocycles discouraged the researchers.

In this chapter we present hitherto unreported fluorescent triazine based hekates with three unsymmetrically substituted 1,3,4-oxadiazole moieties, which stabilize wide range columnar hexagonal phases. The synthesized compounds vary from each other with respect to the number and length of the flexible chains. The number and length of the peripheral tails have a significant effect on the type and range of the Col phase. The lower chain length usually enhances the core-core interaction, which leads to the stabilization of the columnar rectangular (Col_r) phase, while the higher chain length usually promotes the columnar hexagonal (Col_h) phase.[1d] We attempt to shed light on the structure-property relationship in this class of star shaped molecules with respect to their thermal behavior and photophysical properties.

2.2. Results and discussion

2.2.1. Synthesis and Characterization

The synthetic strategy to obtain the target molecules and their precursors is illustrated in scheme 2.1. General procedures for the syntheses of ethyl gallate, 3,4-hexadecyloxy or

3,4-dodecyloxy ethyl benzoate, 3,5-hexadecyloxy ethyl benzoate, 3,5-dodecyloxy ethyl benzoate, 3,4,5-hexadecyloxy ethyl gallate,[20] 3,4,5-dodecyloxy ethyl gallate,[20] 4-hexadecyloxy ethyl benzoate[21] and 4-dodecyloxy ethyl benzoate[21] are reported earlier. Alkoxy esters (**3a-h**) were transformed to their respective hydrazides (**4a-h**) by treating with hydrazine hydrate in ethanol or *n*-butanol as solvent.[19,22] Hydrazides **4a-h** upon refluxing with 4,4',4''-(1,3,5-triazine-2,4,6-triyl)tribenzoic acid chloride in THF in presence of triethylamine yielded tri-N-benzoylbenzohydrazides.[19] These compounds were heated with $POCl_3$ to obtain the target molecules **TZ1-8.**[19,22] The key intermediate 4,4',4''-(1,3,5-triazine-2,4,6-triyl)tribenzoic acid (**2**) was prepared by chromic oxide mediated oxidation of 2,4,6-tri-p-tolyl-1,3,5-triazine (**1**) in good yield.[23] Compound **1** was in turn obtained by the triflic acid catalyzed trimerization of p-tolunitrile.[24] The structures of all the intermediates and target molecules were confirmed using ^{1}H NMR, ^{13}C NMR, IR spectroscopy and HRMS or MALDI-TOF mass spectra. (See experimental part presented in section 2.4 for the details).

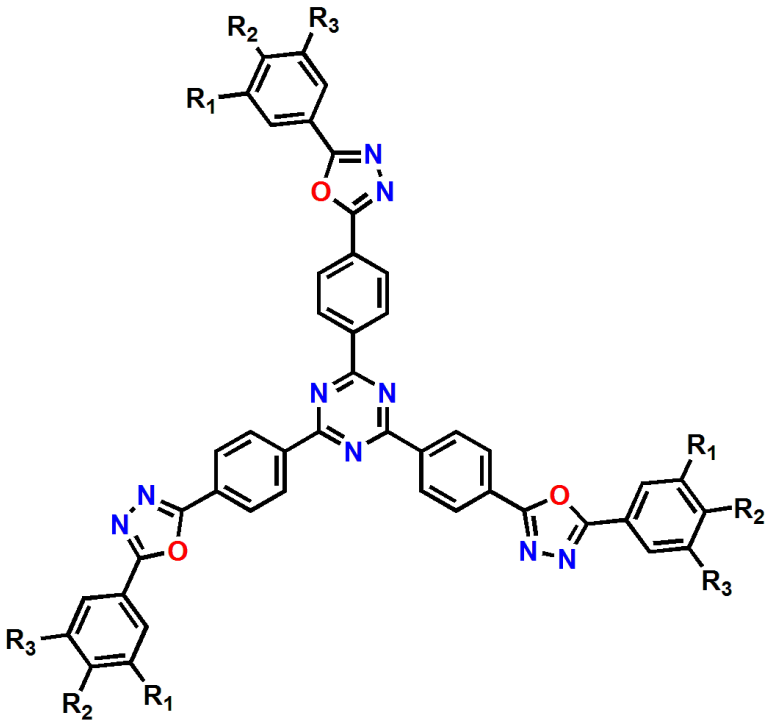

TZ1: $R_1 = R_3 = H$, $R_2 = n\text{-}OC_{16}H_{33}$
TZ2: $R_1 = H$, $R_2 = R_3 = n\text{-}OC_{16}H_{33}$
TZ3: $R_1 = R_3 = n\text{-}OC_{16}H_{33}$, $R_2 = H$
TZ4: $R_1 = R_2 = R_3 = n\text{-}OC_{16}H_{33}$

TZ5: $R_1 = R_3 = H$, $R_2 = n\text{-}OC_{12}H_{25}$
TZ6: $R_1 = H$, $R_2 = R_3 = n\text{-}OC_{12}H_{25}$
TZ7: $R_1 = R_3 = n\text{-}OC_{12}H_{25}$, $R_2 = H$
TZ8: $R_1 = R_2 = R_3 = n\text{-}OC_{12}H_{25}$

Figure 2.1. The molecular structures of star-shaped LCs derived from *s*-triazine and 1,3,4-oxadiazoles.

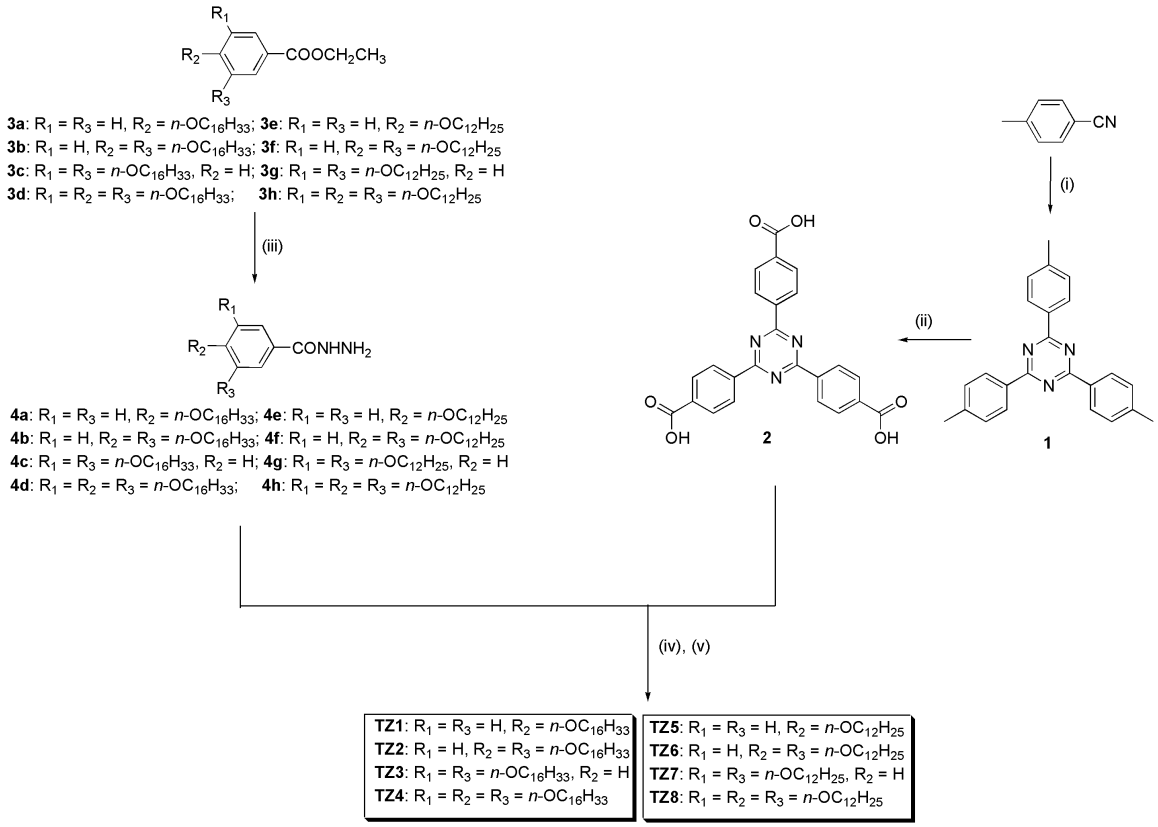

Scheme 2.1. Synthesis of star- shaped LCs. (i) CF_3SO_3H, dry DCM, 0 ^{O}C - rt, 12 h, 90%; (ii) CH_3COOH, H_2SO_4, CrO_3, Ac_2O, 0 ^{O}C - rt, 24 h, 85%; (iii) $NH_2NH_2.H_2O$, ethanol, reflux, 48 h (65–75%); (iv) 4,4',4''-*s*-triazine-2,4,6-triyl-tribenzoic acid chloride, THF, triethylamine, 6 h, reflux; (v) $POCl_3$, reflux, 17 h (45-50%).

2.2.2. Thermal behavior

All the compounds were investigated with the help of Polarizing Optical Microscopy (POM) and Differential Scanning Calorimetry (DSC). Mesomorphic behavior, phase transition temperatures and associated enthalpy changes are presented in table 2.1. Figure 2.2 graphically represents the thermal behavior of compounds **TZ1-8** in the first cooling cycle. Compound **TZ1** with three hexadecyloxy tails did not show any mesophase and showed a crystal to isotropic transition at 173 ^{o}C. It did not show any mesophase on cooling cycle, instead an isotropic to crystal transition at 172 ^{o}C. This shows that three flexible tails are not enough to induce the nanophase segregation of molecular subunits in this class of star shaped molecules.[25] POM images of this compound at different temperatures indicated the crystalline nature of the sample (Fig. 2.4a-b). This was surprising considering a small enthalpy change (2-3 kJ/mol) observed in DSC studies.

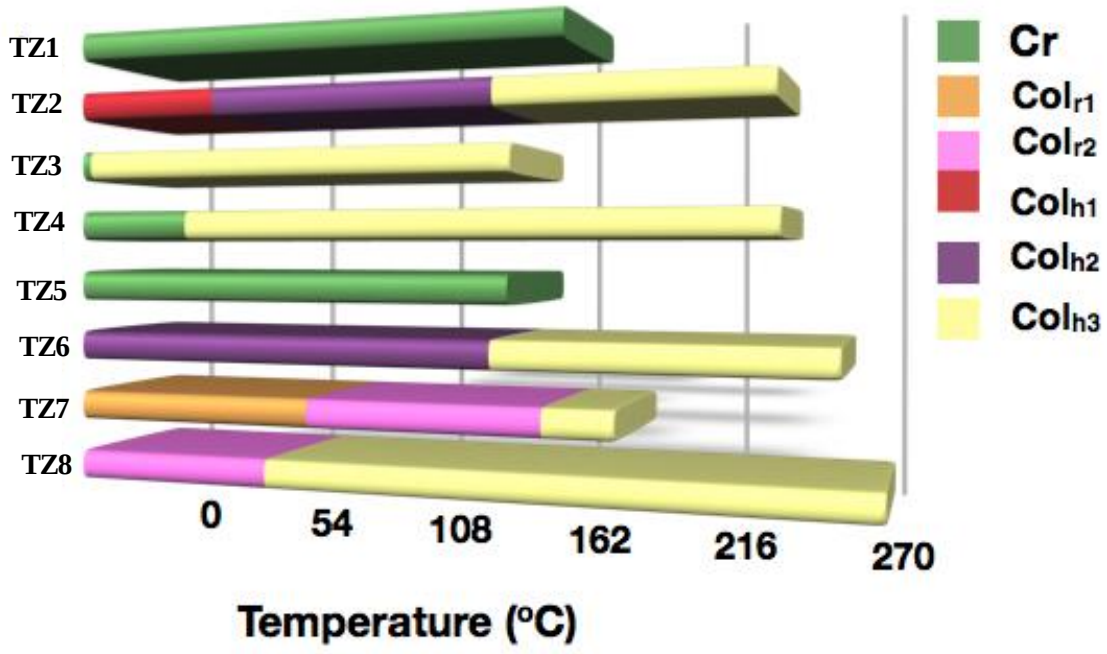

Figure 2.2. Bargraph summarizing the thermal behavior of compounds **TZ1-8** (first cooling cycle).

Compound **TZ2** with six hexadecyloxy tails exhibited enantiotropic mesomorphic behavior. In the heating cycle the compound showed a crystal to mesophase transition (ΔH = 104.2 kJ/mol) at a temperature of ≈52 ^{o}C. This birefringent liquid undergoes further transition at ≈153 ^{o}C as observed in DSC scans before going to an isotropic liquid state at 239 ^{o}C. Upon cooling the isotropic liquid a dendritic growth was appeared which soon coalesces in to a mosaic pattern interspersed with homeotropic regions (Fig. 2.3a). At 149 ^{o}C a transition was observed in the mesophase, where the texture remains same, but the color of the mosaic pattern gets changed (Fig. 2.3b-c). On further cooling a broad exothermic peak (ΔH = 207.1 kJ/mol) corresponding to crystallization was observed in the DSC scan at ≈50 ^{o}C, while the texture remains unchanged with a concurrent loss of fluidity (Fig. 2.3d & 2.5a). In the next heating scan a transition appeared at a temperature of ≈53 ^{o}C (ΔH = 106.3 kJ/mol) showing that this transition is not due to glass forming. In order to assign the symmetry of the columnar phase powder X-ray diffraction of the sample was carried out at different temperature intervals. X-ray diffraction of the sample carried out at 200 ^{o}C showed a sharp peak centered at 43.2 Å at the low-angle region, followed by two diffused peaks at 5.18 and 3.76 Å respectively (Fig. 2.5b, Table 2.2).

Table 2.1. Phase transition temperatures [a] (^{o}C) and corresponding enthalpies (kJ/mol) of star shaped LCs.

Entry	Phase sequence	
	2nd Heating	**1st Cooling**
TZ1	Cr 175.4 (3) I	I 172.4 (2.4) Cr
TZ2	Col_{h1} 53.4 (106.3) Col_{h2} 152.5 (80.6) Col_{h3} 238.5(18.4) I	I 237.1 (17.2) Col_{h3} 149 (80.2) Col_{h2} 50.37 (207.1) Col_{h1}
TZ3	Cr 5.4 (127.4) Col_h 156.8 (9.9) I	I 154.6 (11.1) Col_h 3 (173.7) Cr
TZ4	Cr 47.4 (163.8) Col_h 240 (34.1) I	I 238.1 (31.7) Col_h 39.9 (526.8) Cr
TZ5	Cr_1 53.6 (17.2) Cr_2 157.7 (126.1) I	I 154.1 (9.5) Cr_2 41.4 (20.8) Cr_1
TZ6	Cr 48.8 (225.03) Col_{h2} 161.1 (69.1) Col_{h1} 251.2 (14.7) I	I 255.3 (14.0) Col_{h1} 148.1 (59.9) Col_{h2} [b]
TZ7	Cr 48.9 (382.04) Col_{r2} [c] 90 Col_{r1} 170 Col_h 190.1 (22.3) I	I 188.1 (20.9) Col_h [c]165 Col_{r1} 84.9 (25.3) Col_{r2} [b]
TZ8	Col_r 86.6 (135.2) Col_h 276.38 (24.8) I	I 267.9 (429.0) Col_h 69.7 (26.32) Col_r [b]

[a]Peak temperatures in the DSC thermograms obtained during the first heating and cooling cycles at 5 ^{o}C/min. Col_h = Columnar hexagonal phase; [b]Mesophase freezing in the glassy state; [c]Transition detected in polarizing optical microscope but not observed in DSC.

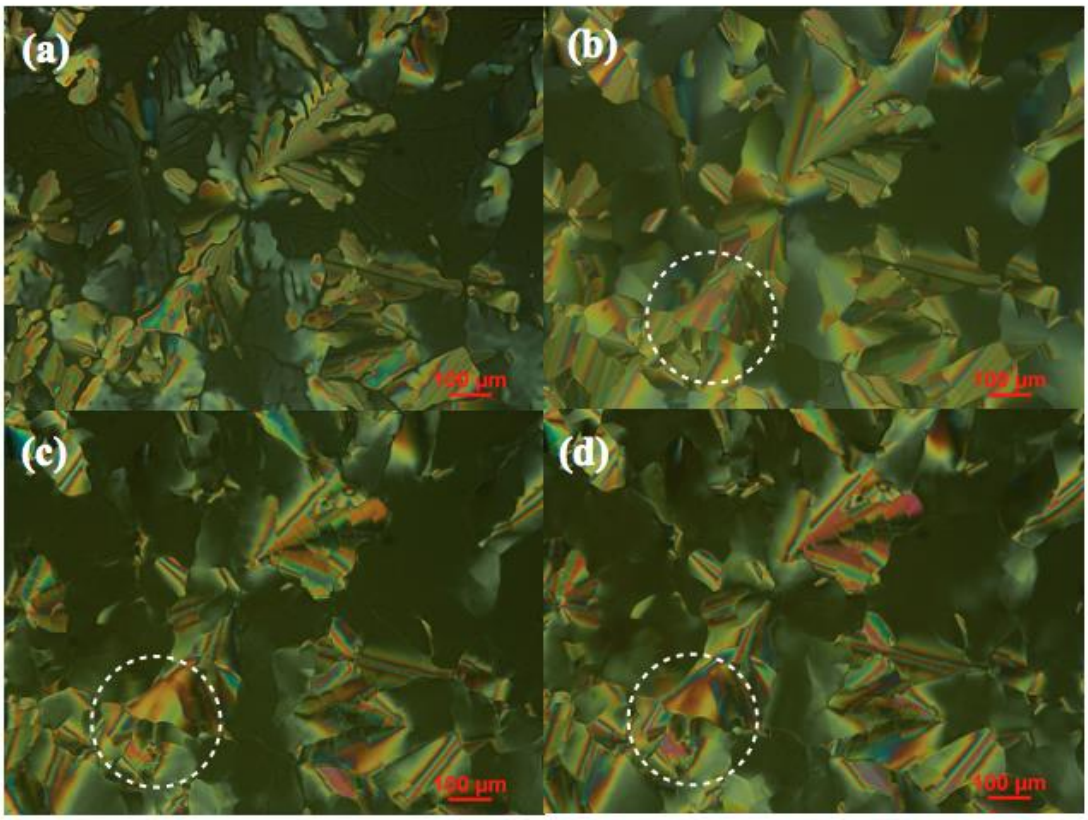

Figure 2.3. Photomicrographs of textures as seen by POM for the Col_{h3} phase of compound **TZ2** (a) at 230 °C; (b) Col_{h3} phase at 155 ^{o}C; (c) Col_{h2} phase at 134 ^{o}C; (d) Col_{h1} phase at 28 ^{o}C.

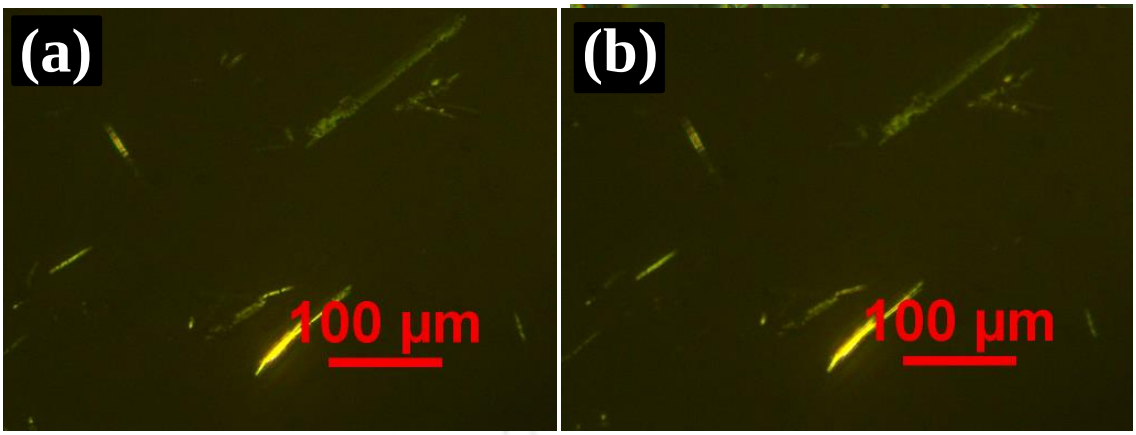

Figure 2.4. Photomicrographs of textures as seen by POM of Compound **TZ1** at (a) 140 ^{o}C and (b) 40 ^{o}C.

Though the observation of a single peak at low angle does not confirm the Col_h phase, textural evidence strongly suggests that it is Col_h phase. The absence of other peaks in low angle is ascribed to a minimum in the form factor.[22,26] The sharp peak at the low angle specifies the distance between the adjacent (100) planes, *i.e.* d_{10}, from which lattice parameter '*a*' can be calculated. Lattice parameter '*a'* gives the intercolumnar distance, which was found to be 49.9 Å. This is significantly lesser (25 %) than the molecular diameter, *i.e.* 65.78 Å, which may be due to the intercalation of peripheral flexible chains. This is understandable considering the large voids present between the arms of the star shaped molecule, where there is a possibility of alkyl chains filling up the voids (Fig. 2.6). The first diffused peak at 5.18 Å in wide-angle region corresponds to the packing of peripheral flexible tails, while the second diffused peak at 3.76 Å corresponds to the stacking of molecules in the individual columns (Fig. 2.5b). Similar intracolumnar distances are found in triindole-based discotics (3.9-4.4 Å), where the authors ascribed this due to the presence of phenyl linkers between the central core and peripheral flexible chains.[27] It is possible that with the increase in the length of the arms in hekates, the arms are twisted in conformation with respect to the central planar core and this leads to an increase in the core-core stacking distance. Additionally these three different arms may have different diastereomeric conformations too. The small textural change observed at 149 ^{o}C along with the exothermic peak (ΔH = 80.2 kJ/mol) in DSC prompted us to carry out XRD studies well below this transition temperature, *i.e.* at 100 ^{o}C. The XRD pattern showed two peaks at low angle centered at 45.37 and 22.30 Å, along with the two diffused peaks at 4.96 and 3.74 Å. This diffraction pattern is similar to the high temperature Col_h phase observed for compound **TZ2**.

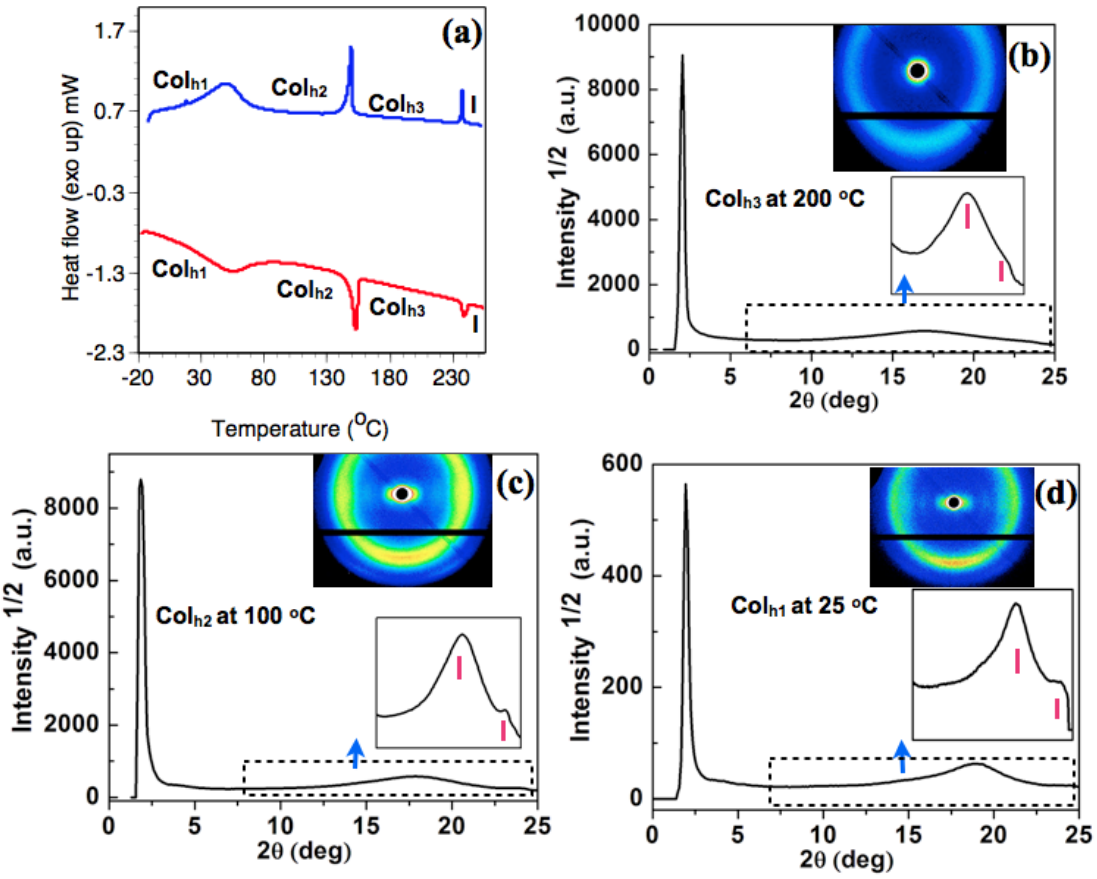

Figure 2.5. DSC traces obtained for first cooling (blue trace) and second heating (red trace) cycles of compound **TZ2** at a rate of 5 ^{o}C/min (a); XRD profiles depicting the intensity against the 2θ obtained for the Col$_{h3}$ phase of compound **TZ2** at 200 °C (b); Col$_{h2}$ phase of compound **TZ2** at 100 °C (c) and Col$_{h1}$ phase of compound **TZ2** at 25 °C (d); inset shows the image pattern obtained.

The intercolumnar distance was found to be 52.4 Å. The intercolumnar distance '*a*' is more than the observed intercolumnar distance at 200 ^{o}C (20 % lesser than molecular diameter). Thus the transition at 153 ^{o}C points to a transition between two Col$_{h}$ phases. Such transition between two Col$_{h}$ phases is not very common, but has been reported in literature.[26c] As the intracolumnar distance remains constant at both temperatures, we observe only an increase in the intercolumnar distance by 5 Å. This may be due to the stretching of peripheral alkyl tails. Considering the transition at 50 ^{o}C with the unchanged texture we measured the XRD well below this temperature, *i.e.* at room temperature. The XRD pattern was almost similar to the measurement carried out at 100 ^{o}C, with the comparable intercolumnar distance. The only difference was the decrease in alkyl chain stacking and core-core stacking distance. Thus compound **TZ2** exhibited a transition between three columnar hexagonal phases (designated as Col$_{h1}$, Col$_{h2}$ and Col$_{h3}$), as evidenced from POM, DSC and XRD studies. The difference between these three Col$_{h}$ phases is very subtle as seen from XRD studies.

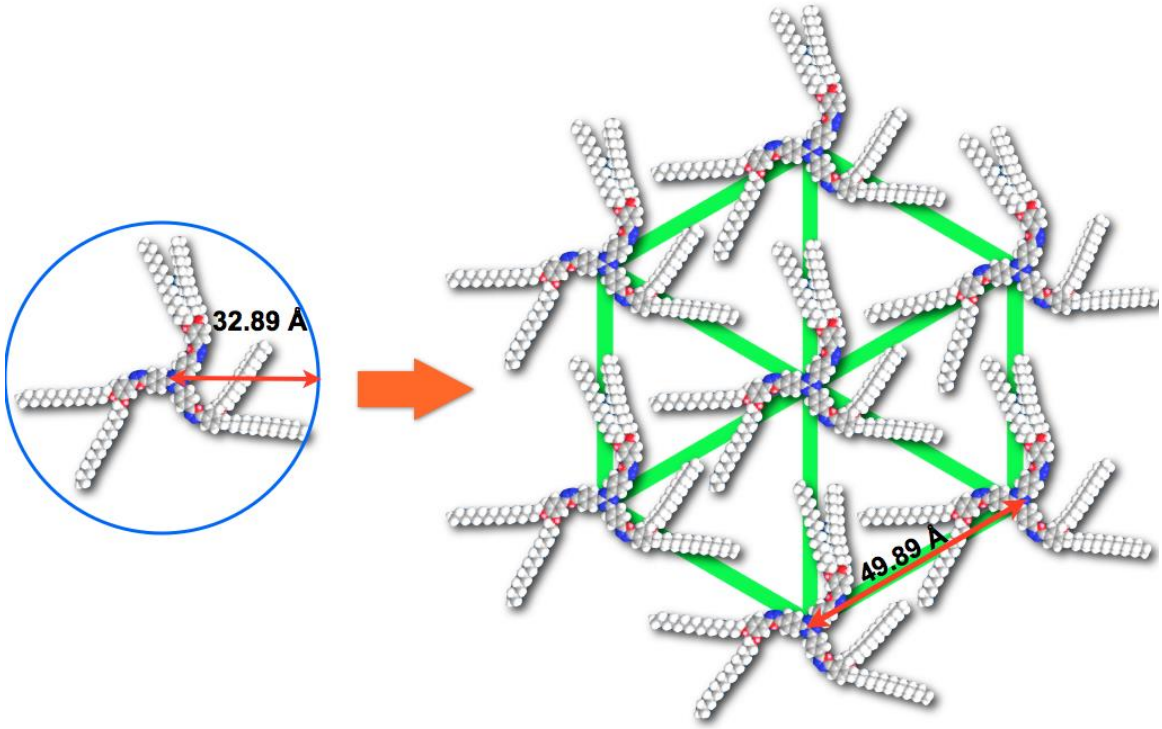

Figure 2.6. Schematic showing the self-assembly of compound **TZ2** into Col_h phase at 200 ^oC.

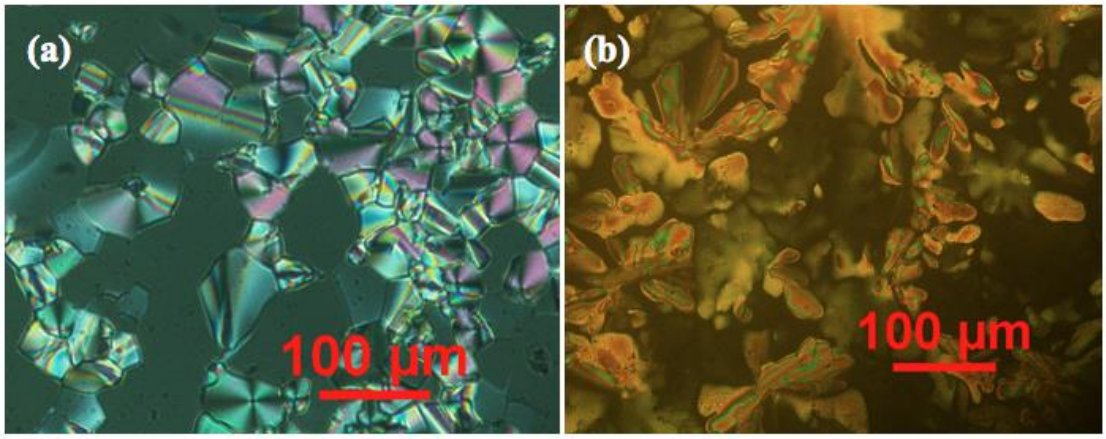

Figure 2.7. Photomicrographs of textures as seen by POM for the Col_h phase of compound **TZ3** at 30 °C (a) and compound **TZ4** at 237 ^oC (b).

As shown in the table 2.2, for other compounds (**TZ3-4**), there was no significant change in intercolumnar distance with respect to temperature, which is very hard to explain. However, we can infer from the data obtained that, compound **TZ2** with peripheral chains substituted at 3 and 4 positions of the benzene ring self-assembles with more intercalation at higher temperature Col_{h3} phase than in low temperature Col_{h2} and Col_{h1} phase.

Table 2.2. Results of the (*hkl*) indexation of the XRD profiles of the compounds **TZ2-4** at a given temperature (T) of the mesophases[a].

Compounds (*D*/Å)	Phase (T/°C)	d_{obs}(Å)[b]	d_{cal}(Å)[b]	Miller indices *hkl*	Lattice parameter (Å)
TZ2 (65.78)	Col_{h3} (200)	43.20 5.18 (h_a) 3.76 (h_c)	43.20	100 001	a = 49.89
	Col_{h2} (100)	45.37 22.30 4.96 (h_a) 3.74 (h_c)	47.63 23.81	100 200 001	a = 52.36
	Col_{h1} (25)	45.34 21.21 4.68 (h_a) 3.63 (h_c)	45.33 22.66	100 200 001	a = 52.35
TZ3 (64.31)	Col_h (140)	39.54 5.11 (h_a) 3.77 (h_c)	39.51	100 001	a = 45.63
	Col_h (100)	39.56 14.59 5.07 (h_a) 3.76 (h_c)	39.53 14.94	100 210 001	a = 45.65
	Col_h (25)	39.59 15.09 4.88 (h_a) 3.78 (h_c)	39.56 14.95	100 210 001	a = 45.69
TZ4 (66.46)	Col_h (200)	41.33 23.04 16.06 5.20 (h_a) 3.82 (h_c)	41.32 23.86 15.62	100 110 210 001	a = 47.72
	Col_h (150)	41.32 23.51 15.89 5.12 (h_a) 3.76 (h_c)	41.29 23.84 15.60	100 110 210 001	a = 47.68

[a]The diameter (D) of the disc (estimated from Chem 3D Pro 8.0 molecular model software from Cambridge Soft). [b]d_{obs}: spacing observed; d_{cal}: spacing calculated (deduced from the lattice parameters; a for Col_h). Spacings marked h_a and h_c correspond to diffuse reflections in the wide-angle region that arise from correlations between the alkyl chains and core regions, respectively.

There is also a possibility that it can achieve various conformations due to its unsymmetrical peripheral substitution, which may be a reason for this observation. The decrease in the *d*-spacing values at wide-angle region with the decrease in temperature follows the usual trend. This difference between compound **TZ2** and **TZ3-4** is again due to the peripheral substitution.

Compound **TZ3**, which is a regioisomer of compound **TZ2** with six hexadecyloxy tails, exhibited a wide range enantiotropic columnar mesophase over 150 degrees including room temperature. This is quite interesting to see how a small change in the substitution pattern, *i.e.* transition from peripheral 3,4- to 3,5-alkoxyl group substitution improves the mesophase stability of the star shaped molecules.

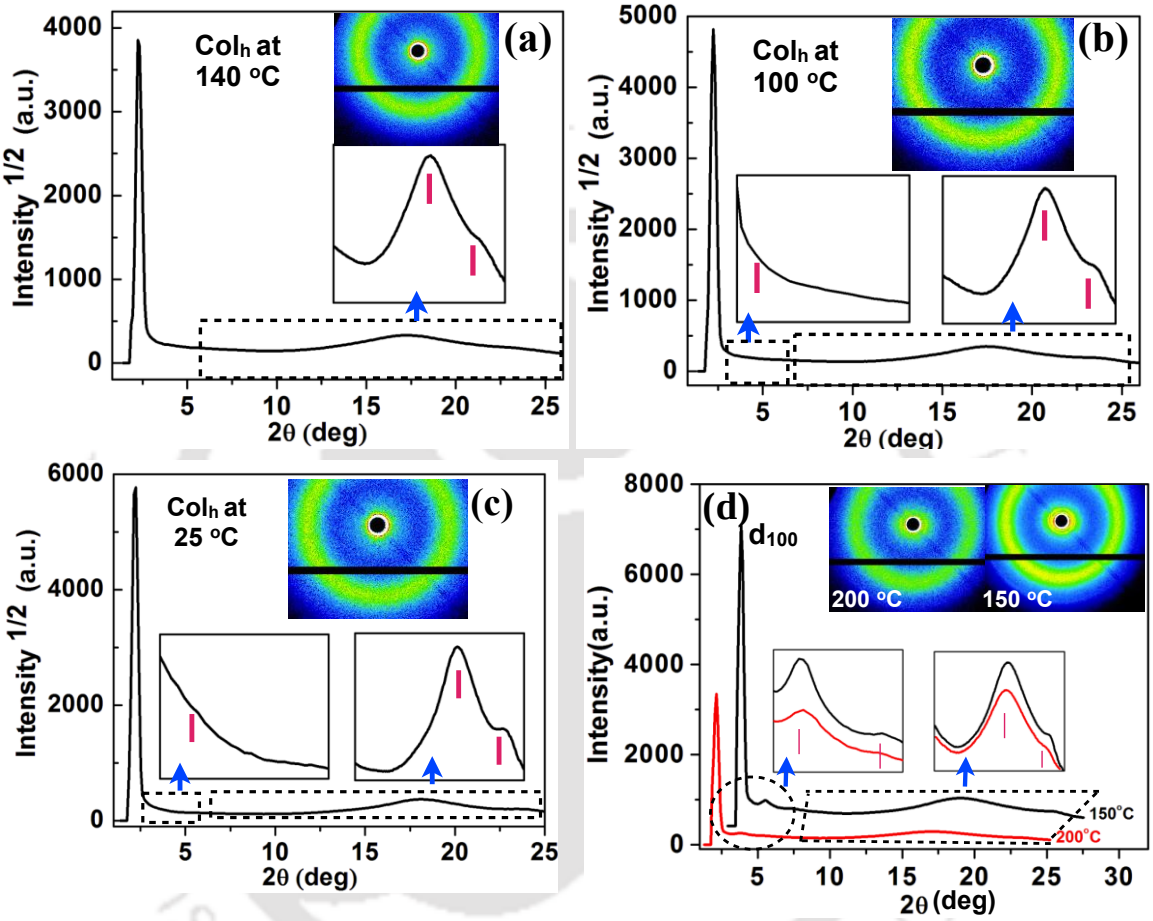

Figure 2.8. XRD profiles depicting the intensity against the 2θ obtained for the Col$_h$ phase of compound **TZ3** at 140 °C (a); Col$_h$ phase of compound **TZ3** at 100 °C (b); Col$_h$ phase of compound **TZ3** at 25 °C (c); Col$_h$ phase of compound **TZ4** at 200 °C (red trace) and at 150 °C (black trace) (d); inset shows the image pattern obtained.

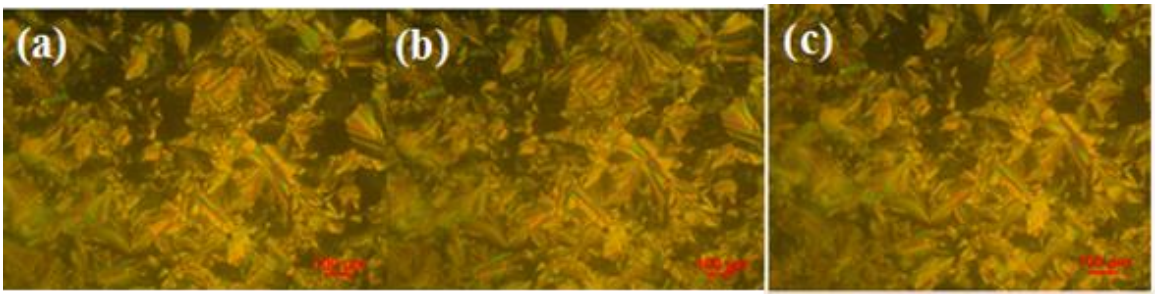

Figure 2.9. POM images of Col$_h$ phase of compound **TZ4** on a cooling process from isotropic melt at (a) 200^{o}C; (b) 100^{o}C and (c) 50^{o}C.

The texture was a combination of mosaics, small focal conics and homeotropic regions and it remained unchanged at room temperature (Fig. 2.7a). Compound **TZ3**, in the cooling cycle DSC traces showed a peak centered at 3 ^{o}C (ΔH = 173.7 kJ/mol) (Table 2.1). Powder XRD studies conducted at different temperature intervals suggested that the phase under investigation is Col_h as explained below. The powder XRD patterns at different temperatures showed a single reflection corresponding to Miller indices 100 (Fig. 2.8a-c). The intercolumnar distance with the decrease in temperature showed little variation in contrast to the Col_h phase exhibited by compound **TZ2**, but higher interdigitation of peripheral alkyl tails. Compound **TZ4**, with nine peripheral hexadecyloxy tails also exhibited a wide range columnar hexagonal mesophase (table 2.1) of almost 200 degrees, with higher melting and isotropic temperatures in comparison to compound **TZ3**, which is confirmed by POM (Fig. 2.9), DSC and XRD investigations. We were curious to know the impact of shortening the length of peripheral alkyl chain on the thermal behavior of the star shaped molecules as in **TZ5-8** in comparison to compounds **TZ1-4.** Compounds **TZ5-8** are the lower homologues of compounds **TZ1-4** with *n*-dodecyloxy chains at the periphery, prepared by maintaining the same substitution pattern.

Compound **TZ5** with three *n*-dodecyloxy chains was crystalline, but with a lower isotropic temperature than its higher homologue **TZ1**. Compound **TZ6** with six *n*-dodecyloxy chains exhibited an enantiotropic behavior with a higher isotropic temperature than compound **TZ2** and hence showing a larger mesophase width. The compound **TZ6** on cooling from the isotropic liquid state showed a birefringent pattern of mosaic texture (Fig. 2.10a), which is frequently observed for Col_h phases. DSC scans in cooling cycle showed a transition at ≈148 ^{o}C (ΔH = 60 kJ/mol) (Table 2.1), while texture did not show much variation except the change in color of the mosaic pattern, which remained unchanged till room temperature (Fig. 2.10b). The texture is not shearable, thus confirming the freezing of Col_h phase in glassy state. But the second heating showed a crystallization peak at ≈49 ^{o}C (ΔH = 225 kJ/mol), before converting to form a birefringent fluidic pattern. XRD studies have been carried out at 220, 130 and 25 ^{o}C. The XRD patterns were characteristic of Col_h phase (Table 2.3 & Fig. 2.13). The peaks at low angle can be indexed into Miller indices 100 and 200. These values are in the ratio of 1:1/√4 conforming the hexagonal lattice (except the missing 1/√3 reflection), which is similar to the XRD pattern observed for compound **TZ2**.

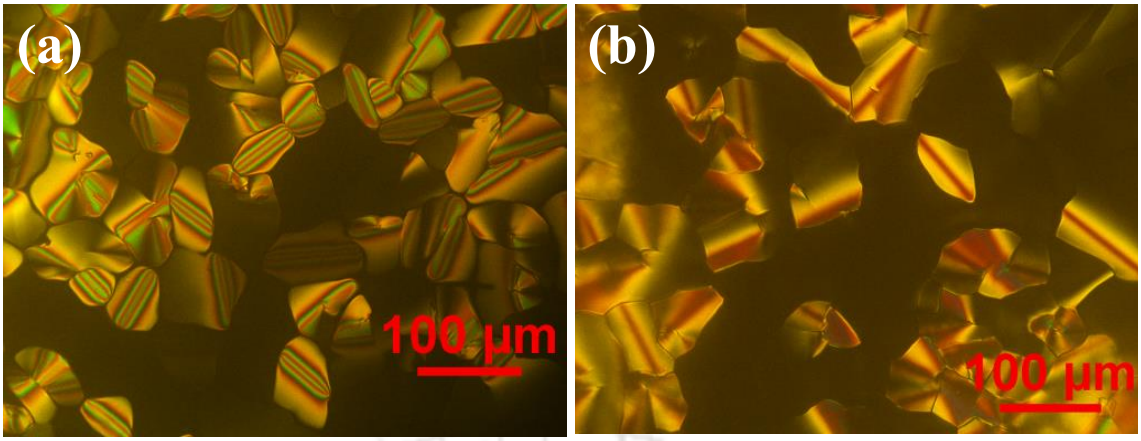

Figure 2.10. POM images obtained for the Col_h phase of compound **TZ6** at 238 °C (a) and RT (b).

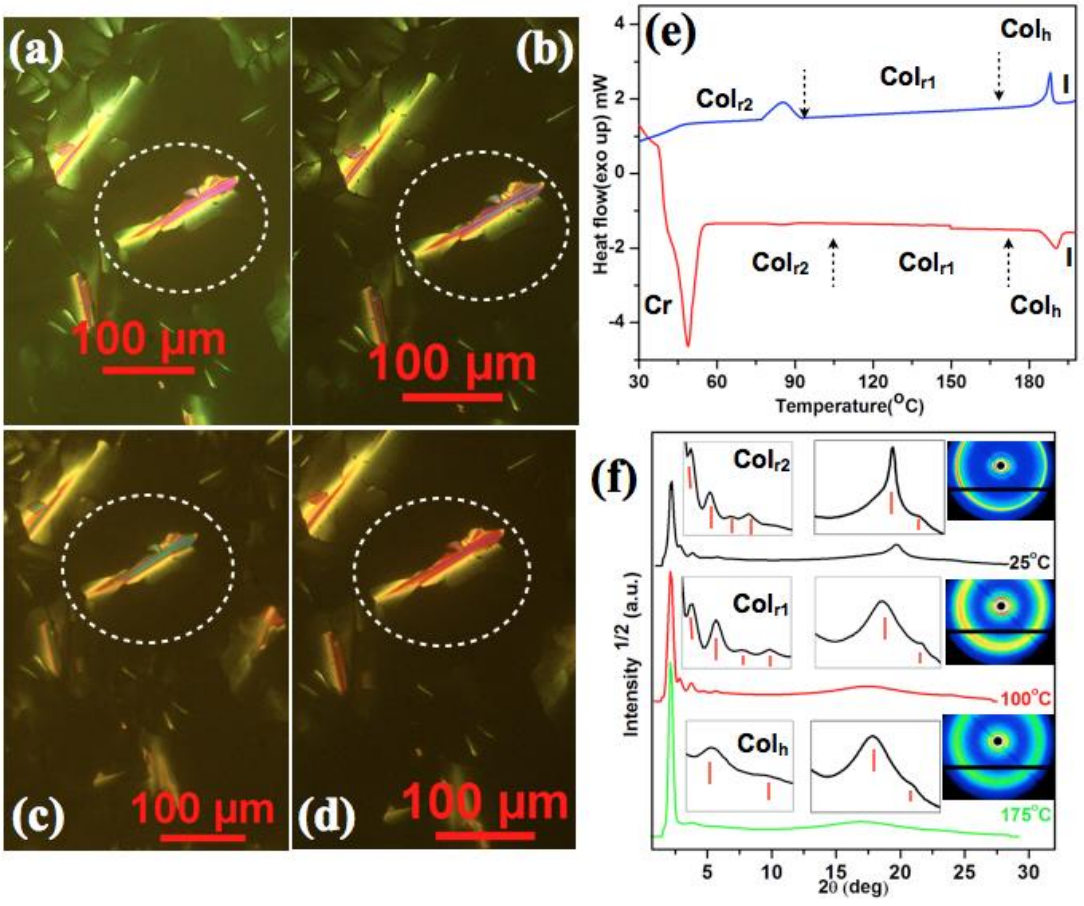

Figure 2.11. POM images of compound **TZ7** in Col_h phase at 175 °C(a); Col_h to Col_{r1} transition at 165 °C (b); Col_{r1} phase at 100 °C (c); Col_{r2} phase at 25 °C (d); DSC scans for the first cooling (blue trace) and second heating (red trace) cycles (e); XRD profiles depicting the intensity against the 2θ obtained for the Col_h phase of compound **TZ7** at 175 °C, Col_{r1} phase at 100 °C and Col_{r2} phase at 25 °C (f).

Table 2.3. Results of the (*hkl*) indexation of the XRD profiles of the compounds **TZ6-8** at a given temperature (T) of the mesophases[a].

Compounds (*D*/Å)	Phase (T/°C)	d_{obs}(Å)[b]	d_{cal}(Å)[b]	Miller indices *hkl*	Lattice parameter (Å)
TZ6 (54.89)	Col_{h1} (220)	42.97	42.94	100	*a* = 49.59
		5.22(h_a)		001	
		3.75(h_c)			
	Col_{h2} (130)	45.67	45.64	100	*a* = 52.70
		22.53	22.82	200	
		5.01(h_a)			
		3.76(h_c)		001	
	Col_{h2} (25)	46.78	46.75	100	*a* = 53.98
		23.27	23.38	200	
		16.64	17.67	210	
		9.11			
		4.65(h_a)			
		3.72(h_c)		001	
TZ7 (53.94)	Col_h(175)	41.48	41.46	100	*a* = 47.87
		23.29	23.94	110	
		15.79	15.67	210	
		5.25(h_a)		001	
		3.76(h_c)			
	Col_{r1}(100)	41.47	37.54	110	*a* = 61.62
		30.81	30.81	200	*b* = 47.34
		23.67	23.67	020	
		18.88	18.77	220	
		15.47	15.41	300	
		5.10(h_a)		001	
		3.73(h_c)			
	Col_{r2}(25)	39.73	36.90	110	*a* = 61.5
		30.75	30.75	200	*b* = 46.12
		23.06	23.06	020	
		18.13	18.45	220	
		15.21	15.38	300	
		12.26	11.53	030	
		4.50(h_a)			
		3.71(h_c)		001	
TZ8 (56.24)	Col_h (230)	41.50	41.47	100	*a* = 47.89
		22.81	23.94	110	
		15.61	15.68	210	
		5.31(h_a)			
		3.83(h_c)		001	
	Col_r (25)	41.47	37.41	110	*a* = 63.54
		31.77	31.77	200	*b* = 46.28
		23.14	23.14	020	
		18.33	19.26	310	
		15.64	15.88	300	
		12.45	11.57	030	
		4.54(h_a)			
		3.71(h_c)		001	

[a]The diameter (D) of the disc (estimated from Chem 3D Pro 8.0 molecular model software from Cambridge Soft). [b]d_{obs}: spacing observed; d_{cal}: spacing calculated (deduced from the lattice parameters; *a* and *b* for Col_h and Col_r). Spacings marked h_a and h_c correspond to diffuse reflections in the wide-angle region that arise from correlations between the alkyl chains and core regions, respectively.

Compound **TZ7** exhibited higher melting and isotropic temperatures than compound **TZ3**, which may be due to the increased core-core interaction and decreased fluidity of the molecular structure. On cooling from the isotropic liquid the compound exhibited a mosaic texture interspersed with homeotropic domains. This optical texture showed a small change in the color and brightness at a temperature of 165 ^{o}C (Fig. 2.11a-b), while there was no corresponding signature in DSC scans (Fig. 2.11e). Further cooling showed a transition at ≈85 ^{o}C (ΔH = 25.3 kJ/mol), but the change in texture was minimal. Powder XRD studies carried out at 175 ^{o}C, 100 ^{o}C and at room temperature to investigate these observations (Fig. 2.11f & Table 2.3). The XRD pattern obtained at 175 ^{o}C was reminiscent of Col_h phase. The pattern consisted of three reflections at low angle corresponding to the *d* spacings of 41.48, 23.29 and 15.79 Å, which can be indexed to 100, 110 and 210 reflections with a reciprocal spacing ratio of 1:1/√3:1/√7. This was accompanied with the two diffused peaks at the wide-angle region at *d* spacings of 5.25 and 3.76 Å, which correspond to the packing of flexible tails and the rigid cores in the Col_h phase. The diffraction pattern observed at 100 ^{o}C showed many peaks at low angle region. The five *d* spacings in the low angle region can be assigned to (110), (200), (220), (030) and (400) reflections from a rectangular lattice. The lattice constants were found to be a = 61.62 Å and b = 56.06 Å. Formation of Col_r phase requires higher core-core interaction as the first column should know how the neighboring column will organize. It is often found that in a series of compounds the compounds with shorter chains exhibit Col_r phase.[1b,d,26g] In the case of a columnar hexagonal to rectangular transition the (100) splits into two peaks mainly (110) and (200).This is because as soon as the lattice deviates from the hexagonal symmetry the d_{110} and d_{200} spacing no longer remains degenerate and two separate reflections are observed in the small angle region.[1b] The diffused peaks at wide-angle region with the *d* spacings 5.1 and 3.73 Å correspond to the packing of alkyl tails and the stacking of the aromatic cores. The room temperature XRD pattern also showed a similar diffraction pattern that can be assigned to Col_r phase. Since there was an enthalpy change detected in DSC along with textural variation we have denoted these phases as Col_{r1} and Col_{r2}. Compound **TZ8** exhibited an improved thermal behavior in comparison to compound **TZ4**, but exhibited a transition between wide range Col_h phase and Col_r phase. Again the optical texture did not show much variation during this transition (Fig. 2.12), but DSC scans showed the enthalpy change corresponding to this phase transition, which was further corroborated by XRD studies carried out at different temperatures (Table 2.3 & Fig. 2.13).

Thus the effect of lowering of chain length in these star shaped compounds from *n*-hexadecyloxy to *n*-dodecyloxy can be summarized as follows. The thermal behavior of the compounds with three alkyl tails (**TZ1** and **TZ5**) was similar as they turned out to be crystalline irrespective of the chain length. The compounds with six alkyl tails (**TZ2** and **TZ6**), where the alkoxy groups are in the adjacent position, exhibited the Col_h phase. The lower chain analogue **TZ6** exhibited a slightly enhanced thermal range. These two compounds show transitions between three Col_h phases, where the decrease in temperature led to the Col_h phase with a shorter core-core distance and a longer intercolumnar distance. The transition between different Col_h phases may be due to the possibilities of attaining various conformations with respect to temperature, due to the unsymmetric peripheral substitution. This observation is limited to the type of peripheral substitution, which is not seen in the other compounds of the respective series. A marked difference was visible in the case of compounds **TZ3** and **TZ7**, where the alkyl tails are in alternate positions. Compound **TZ3** exclusively stabilized the Col_h phase, while **TZ7** was bimesomorphic exhibiting high temperature Col_h and low temperature Col_r phases with an enhanced thermal range. A similar behavior was observed in the case of compounds with nine alkoxy tails, *i.e.* compounds **TZ4** and **TZ8**. Overall, the lowering of chain length has increased the core-core interaction, leading to the stabilization of the Col_r phase along with the Col_h phase and enhanced the thermal range. This demonstrated how a subtle change in the molecular structure through peripheral substitution alters the liquid crystal self-assembly. Overall, these star shaped compounds showed enhanced mesophase stability in comparison to the earlier reported triazine based polyether derivatives, which showed the Col phase only upon complexation with trinitroflurenone (TNF).[29]

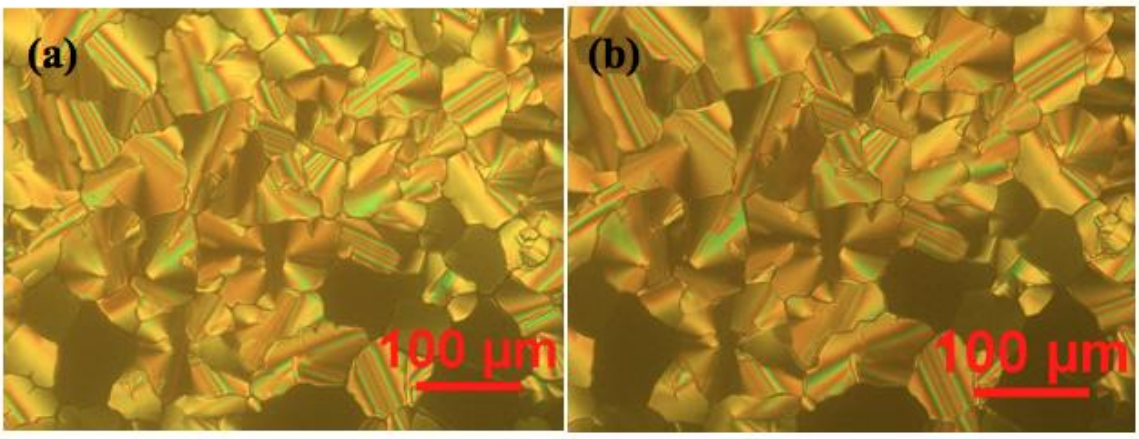

Figure 2.12. POM images of compound **TZ8** in Col_h phase at 130 ^oC (a) and Col_r phase at RT (b).

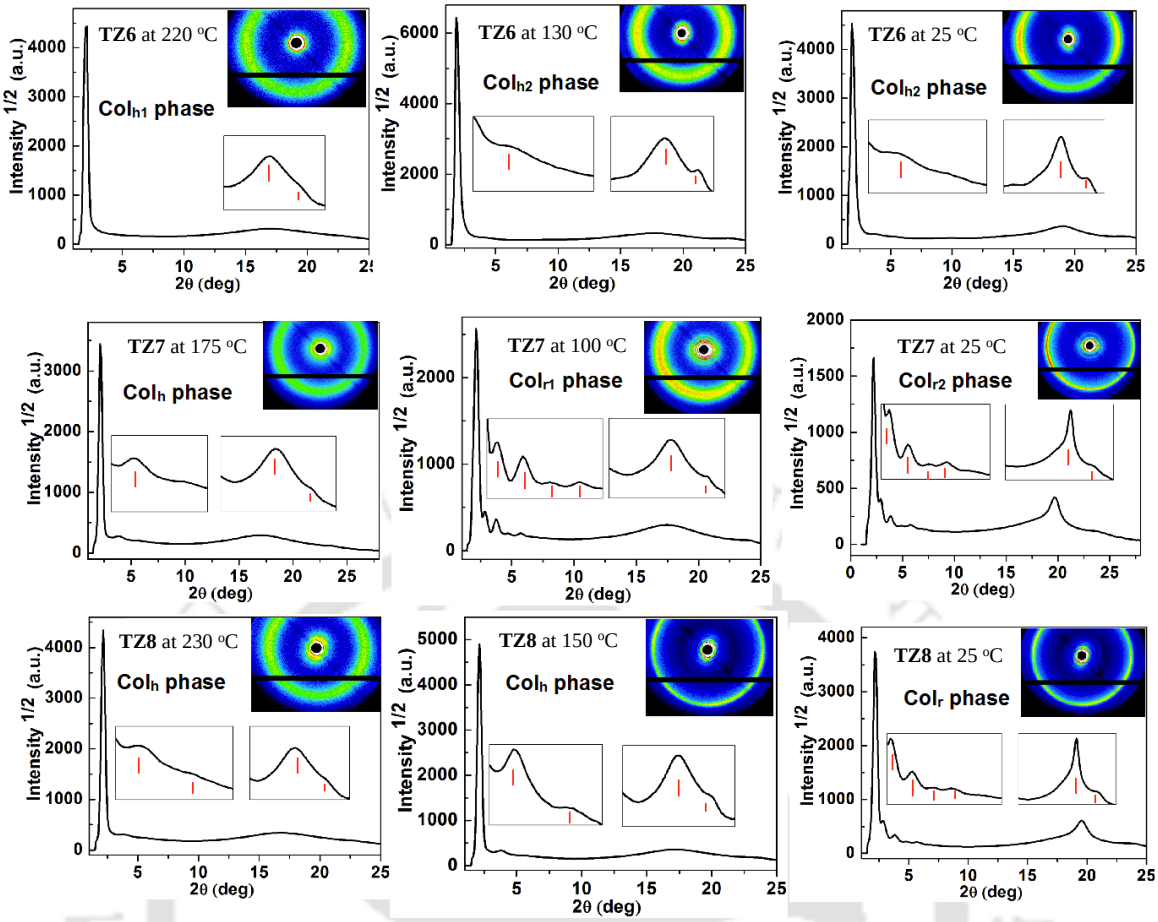

Figure 2.13. XRD profiles depicting the intensity against the 2θ obtained for compounds **TZ6-8** (Inset shows the expanded regions and image patterns obtained).

When compared to the similar star shaped mesogens containing tolane moieties which exhibit short range disordered Col_h phases, the present series of compounds exhibit an ordered Col_h phase over a wide thermal range, which may be due to the enhanced core–core interaction caused by the polar oxadiazole units.[13]

2.2.3. Photophysical properties

We expected an influence on photophysical properties based on the substitution pattern but not on the length of the peripheral chain.[26h] The photophysical properties of the star shaped molecules **TZ1-8** were studied in detail, *i.e.* in solution and thin film (Table 2.4). Absorption and fluorescence spectra of compounds **TZ1-8** were taken in micromolar THF solution (Fig. 2.14 and Fig. 2.15). As can be seen, the absorption spectra for the solutions of compounds **TZ1-4** showed two absorption maxima in the range of 275-343 nm, while that of compounds **TZ5-8** showed two absorption maxima in the range of 279-349 nm. These compounds showed large values of molar extinction coefficients

(ε = 16610-28490 $M^{-1}cm^{-1}$). The absorption bands are corresponding to π-π* and n-π* transitions of this molecular system. The first band at a lower wavelength originates from the 1,3,5-triazine system according to the previous reports.[13] Optical bandgaps of these systems were calculated from the long edge of the absorption spectrum and found to fall in the range of 3.12-3.36 eV. Emission spectra of compounds **TZ1-8** exhibited a single emission maximum centered around 453-540 nm with a large Stokes shift of 123-197 nm. Emission spectra changed with respect to the substitution pattern at the periphery but not on the length of the peripheral tails. Compounds **TZ1** and **TZ3** showed emission maxima centered at 458 and 453 nm with a blue emission in solution (at 365 nm UV light, Fig. 2.14e). Compounds **TZ2** and **TZ4** showed emission maxima centered at 506 and 540 nm with a green and yellow-green emission (at 365 nm UV light, Fig. 2.14e). A similar emission behavior was observed for compounds **TZ5-8** (Fig. 2.15). Relative quantum yield for compounds **TZ1-8** were measured with respect to quinine sulphate solution (0.1 M H_2SO_4 with a quantum yield of 0.54) and found to be in the range of 0.28-0.31 (Table 2.4, 2.5 and Fig. 2.16).

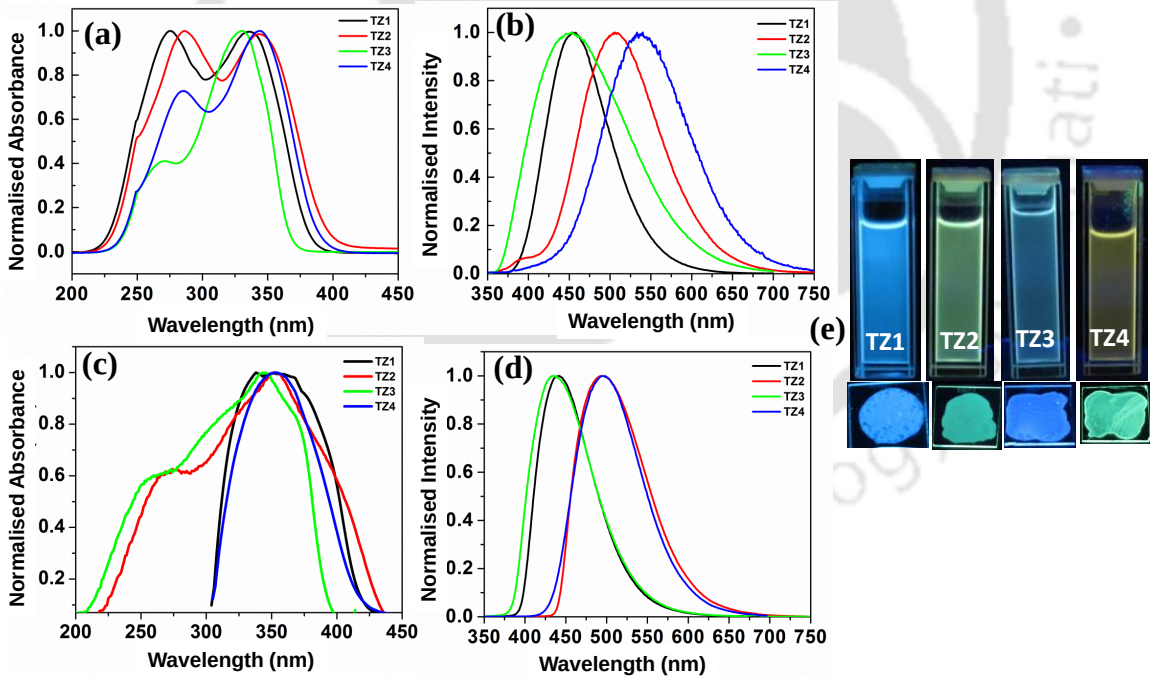

Figure 2.14. Normalized absorption (a) and emission spectra (b) in THF solution (20 μM) obtained for **TZ1-4**; normalized absorption (c) and emission spectra (d) in thin film state; Pictures of solutions of compounds **TZ1-4** in THF and in thin film state (drop casted from 2 mM solutions in toluene) as seen with 365 nm UV light (e).

Table 2.4. Photophysical properties of compounds **TZ1-8** in solution[a] and film state.

Entry	Solution State						Thin film State		
	Absorption(nm)	**Emission[b](nm)**	**Stokes shift(nm)**	**λ_{onset} (nm)**	**$\Delta E^{c,d}_{opt}$**	**Relative Q. Y.**	**Absorption (nm)**	**Emission[b](nm)**	**Stokes shift(nm)**
TZ1	275,335	458	123	386	3.21	0.28	356	442	86
TZ2	286,343	506	163	397	3.12	0.31	276, 352	495	143
TZ3	285,331	453	122	369	3.36	0.29	262, 345	435	90
TZ4	271,343	540	197	395	3.14	0.31	352	495	143
TZ5	279, 340	456	116	387	3.21	0.25	349	455	107
TZ6	279, 349	501	152	394	3.15	0.33	263, 354	487	133
TZ7	270, 329	451	122	366	3.39	0.27	267, 346	449	105
TZ8	283, 344	537	193	385	3.23	0.31	357	504	147

[a]micromolar solutions in THF; [b]excited at the respective absorption maxima; [c]Band gap determined from the red edge of the longest wave length (λ_{onset}) in the UV-vis absorption spectra; [d] In volts (eV).

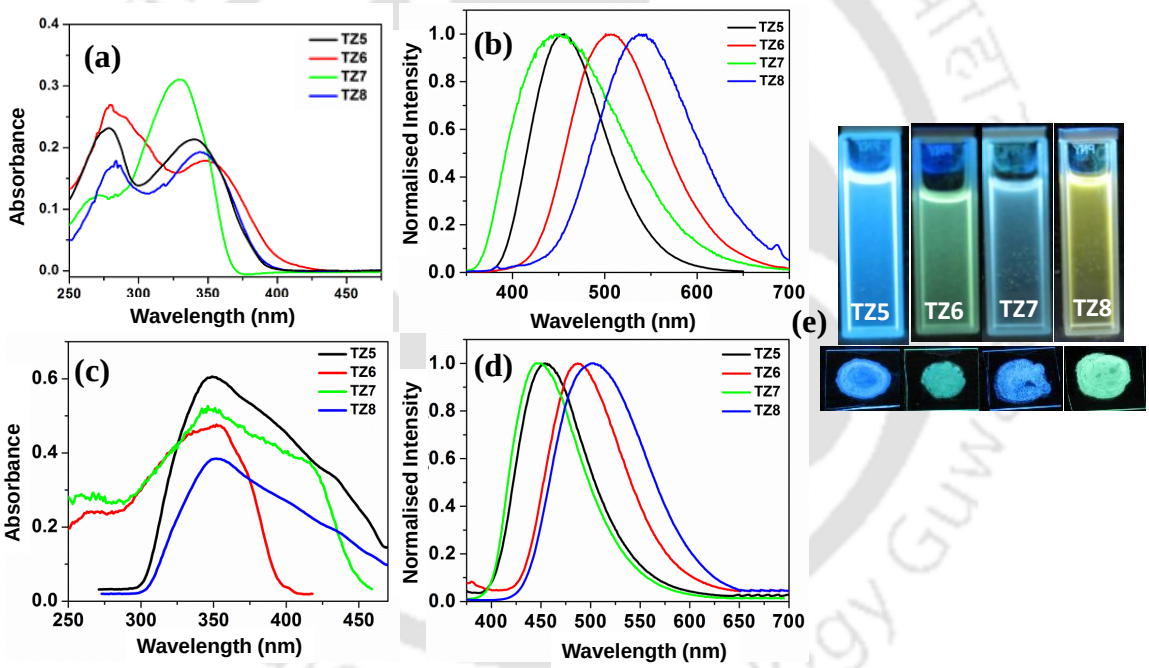

Figure 2.15. Absorption (a) and normalized emission spectra (b) in THF solution (20 μM) obtained for **TZ5-8**; absorption (c) and normalized emission spectra (d) in thin film state; Pictures of solutions of compounds **TZ5-8** in THF and in thin film state (drop casted from 2 mM solutions in toluene) as seen with 365 nm UV light (e).

Quantum yield was measured according to established procedure by using quinine sulfate in 0.1 M H_2SO_4 solution as the standard. Absolute values were calculated according to the following equation: $Q_S = Q_R \times (m_S / m_R) \times (n_S / n_R)^2$ Where, Q: Quantum yield, m: Slope of the plot of integrated fluorescence intensity *vs* absorbance; n: refractive index (1.407 for THF and 1.33 for distilled water); the subscript R refers to the reference fluorophore *i.e.* quinine sulphate solution in 0.1 M H_2SO_4 and subscript S refers to the

sample under investigation. In order to minimize re-absorption effects, absorbance was kept below 0.15 at the excitation wavelength of 347 nm. Quantum Yield of quinine sulphate is 0.54. Simplified equation for the calculation after substituting the appropriate values is given as: $Q_S = 0.54 \times (m_S/2.71) \times (1.407/1.33)^2 = 0.223 \times m_S$ and values obtained are given in the table 2.5.

Thin films of the samples were produced by drop casting the 2 milimolar solutions of compounds in toluene on glass slides. The absorption spectra of these films were found to be broad, comprising single or two bands with a small red shift (Table 2.4, Fig. 2.14c & 2.15c), while the emission spectra did not vary much from the solution spectra, but they showed a blue shift. In the case of compounds **TZ1** and **TZ2** the observed blue shift was 16 and 11 nm respectively, while in the case of compounds **TZ3** and **TZ4** the blue shift was found to be 18 and 45 nm respectively. A similar behavior was observed in the case of compounds **TZ5-8** (Fig. 2.15). Further if we look closely at the absorption spectra of these compounds in the thin film state, we see that there is a band at a lower wavelength observed only for compounds **TZ2**, **TZ3**, **TZ6** and **TZ7**. This is observed specifically for these compounds, which contain six alkyl tails, confirming that this arises because of the solid-state packing that is different from compounds **TZ1**, **TZ4**, **TZ5** and **TZ8**. The emission colors observed under the long wavelength UV light was almost similar to that obtained in solutions (Fig. 2.14e). Red shifted absorption bands in the solid state is usually observed with the formation of J-aggregates; where the molecules are stacked in a head to tail fashion,[11] but we cannot rule out this observation due to the organization of the star shaped molecules in different diastereomeric conformations within the column. In order to get a clear view of the aggregation phenomena we have measured the UV and fluorescence spectra of these compounds as a function of increasing concentration starting from micromolar solution in THF.

Table 2.5. Results of the quantum yield of the compounds **TZ1-8** in THF solution.

Entry	m_S	m_R	$Q_s^{a,b,c}$	Entry	m_S	m_R	$Q_s^{a,b,c}$
TZ1	1.26	2.71	0.28	**TZ5**	1.13	2.71	0.25
TZ2	1.40	2.71	0.31	**TZ6**	1.45	2.71	0.33
TZ3	1.29	2.71	0.29	**TZ7**	1.22	2.71	0.27
TZ4	1.39	2.71	0.31	**TZ8**	1.36	2.71	0.31

[a] Measured in THF; [b]Excited at absorption maxima; [c]Standard quinine sulphate ($Q_f = 0.54$) in 0.1M H_2SO_4.

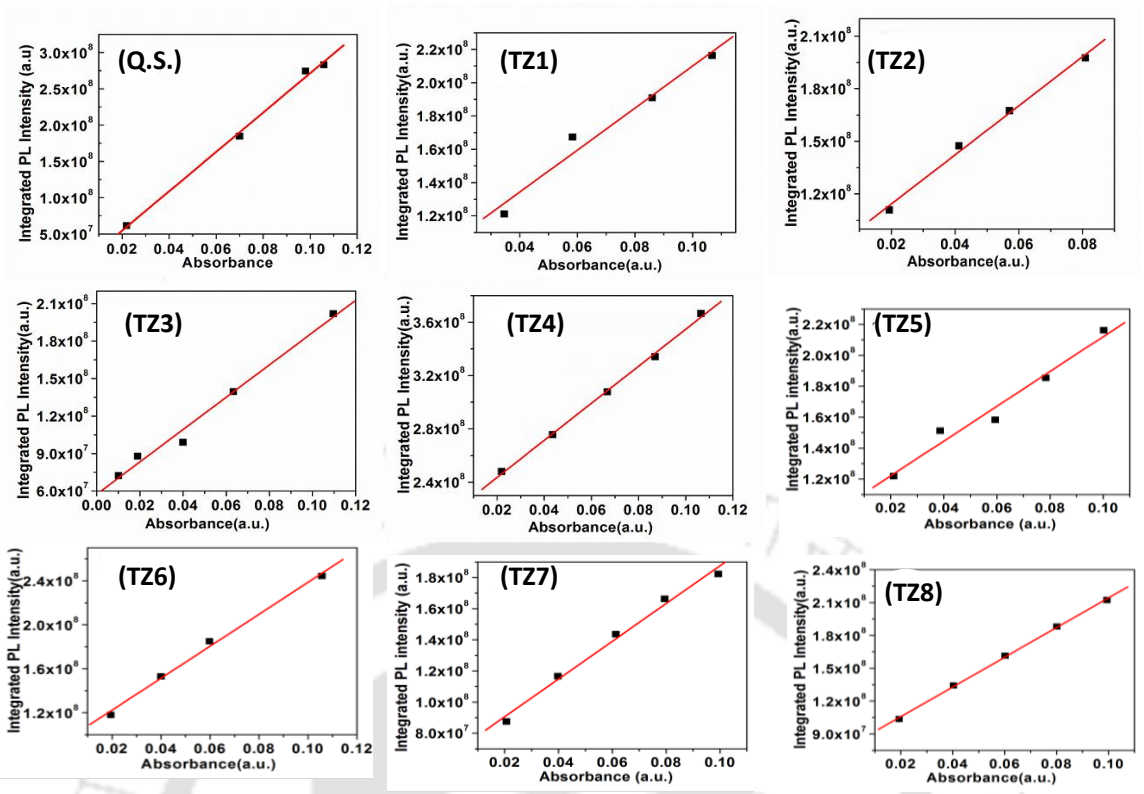

Figure 2.16. Plots of integrated photoluminescence intensity *vs* absorbance of Quinine sulphate (0.1M H_2SO_4 solution) and compounds **TZ1-8** (micromolar THF solution).

At a particular concentration (6.25×10^5 M for compounds **TZ1-3**, 3.12×10^5 M for compound **TZ4**) the luminescence intensity was found to be high (Fig. 2.17a). A further increase in concentration reduced the luminescence intensity, which may be due to the aggregation induced quenching. We have measured the fluorescence lifetime at three different concentrations to understand this observation. Fluorescence lifetime measurements at micromolar concentrations revealed the existence of one species, which is a solvated monomer. At a concentration where the luminescence intensity was high, we observed two species, one with a lower lifetime and the other with a higher lifetime. This biexponential decay is due to the presence of aggregated species and solvated monomers. The presence of two species is due to the high solubility of these compounds in THF. Some of the molecules may prefer to remain as solvated monomers even at the highest concentration (Fig. 2.18, Table 2.6). The absorption spectra showed two maxima where the first one at a lower wavelength was found with reduced intensity in comparison to the absorption spectra obtained for micromolar solution (Fig. 2.17b). All the compounds except compound **TZ3** showed a small red shift in their absorption maximum, while the absorption maximum of **TZ3** did not change much (Tables 2.4 and 2.6). Similarly the luminescence spectra showed a blue shifted emission maximum for all the compounds

except compound **TZ2**, which showed a small red shift. Thus as we see from Tables 2.4 and 2.6, absorption and emission spectra follow a similar trend (either a gradual decrease or increase in the wavelength) as they move from low to high concentration or to the thin film state. The fluorescence lifetime measurements carried out for the thin films showed two lifetimes, one is of a higher lifetime corresponding to aggregates, while the lower one is corresponding to monomer species. The data are comparable to the properties of these compounds in the solution state (Table 2.7).

We were particularly interested to examine the photophysical properties of compounds **TZ3** and **TZ7**, which exhibit room temperature Col_h and Col_r phases respectively. A thin film of compound **TZ3** was prepared by heating the sample sandwiched between two glass slides to the isotropic state and annealing it to room temperature. Similarly, a thin film of compound **TZ7** was prepared by annealing it in the Col_r phase. The liquid crystal film of compound **TZ3** showed an absorption maximum of 347 nm, which is red shifted by 16 nm in comparison to solution spectra. The emission spectrum was blue shifted with an emission maximum of 435 nm (stoke's shift of 90 nm) (Fig. 2.19a). This observation was in line with the data obtained for the drop casted samples. In the literature, observation of a red-shifted absorption maximum in comparison with that in the solution state is attributed to the formation of J-type aggregates.[28] But considering the possibilities of various diastereomeric conformations that can be attained by these molecules; we cannot specify this observation for the formation of J-type aggregates.

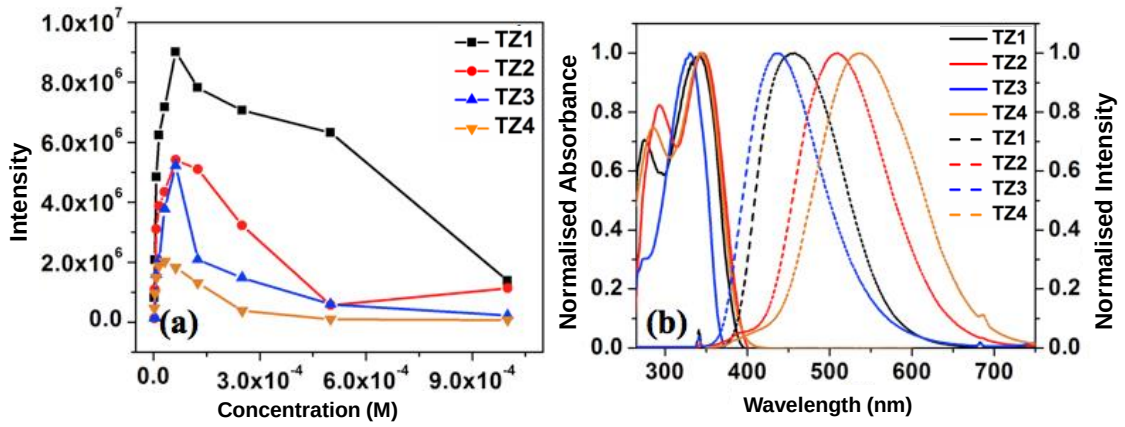

Figure 2.17. Emission intensity *vs* concentration plots of compounds **TZ1-4** in THF solution (a); Absorption and emission spectra at the concentration where highest emission intensity was observed (b).

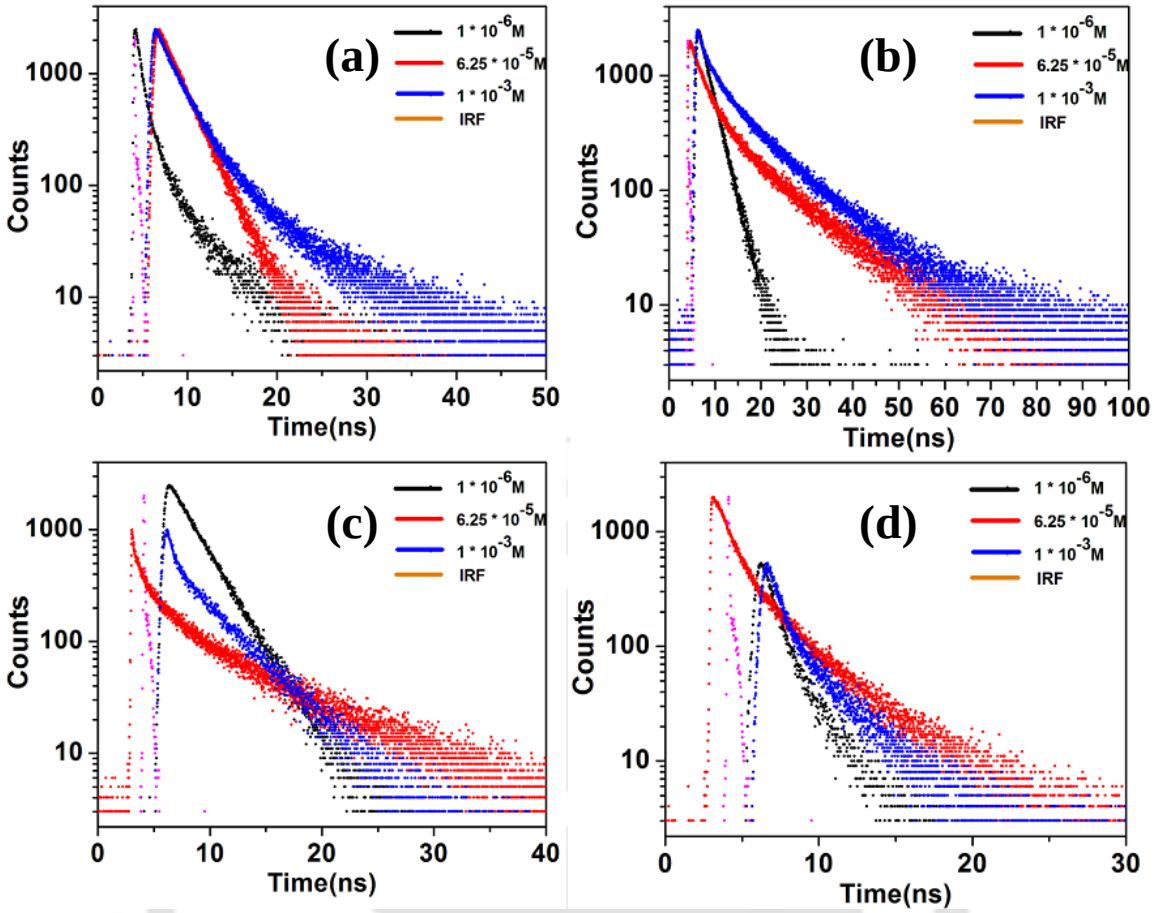

Figure.2.18. The fluorescence decay profiles of compounds **TZ1-4** in THF at high dilution (black trace), at a concentration where the emission intensity is high (red trace) and at high concentration where the emission intensity is less (blue trace). (Orange trace is instrument response function: IRF; λ_{exc} = 336 nm).

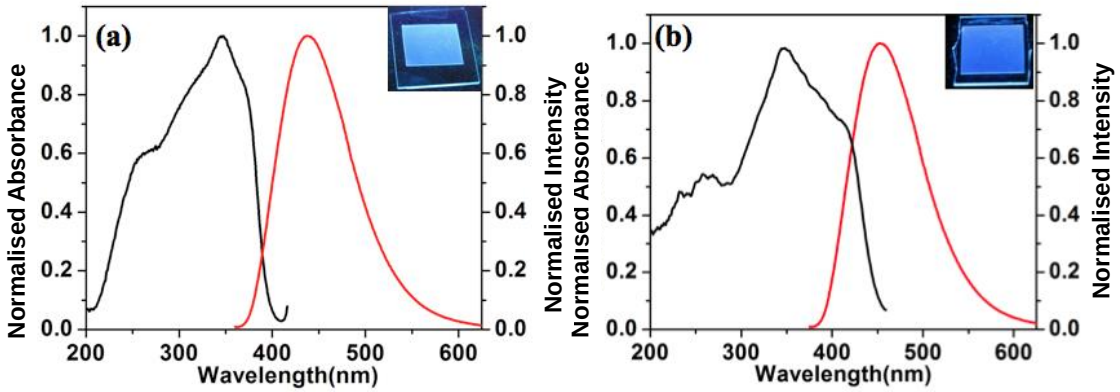

Figure 2.19. (a) Normalized absorption (black trace) and emission spectra (red trace) of LC thin film of compound **TZ3** (inset shows the thin film under UV light); (b) Normalized absorption (black trace) and emission spectra (red trace) of LC thin film of compound **TZ7** (inset shows the thin film under UV light).

Table 2.6. Photophysical properties of compounds **TZ1-4** in 6.25×10^{-5} M THF solution and in thin film drop casted from 2 mM solutions in toluene.

Entry	Absorption (nm)	Emission (nm)	Fraction of molecules	Life time (ns)	Absorption (nm)	Emission (nm)	Fraction of molecules	Life time (ns)
TZ1	275, 338	452	65%	3.50	356	442	86%	3.64
			35%	1.67			14%	0.72
TZ2	293, 346	510	53%	13.40	276, 352	495	50%	10.19
			47%	3.01			50%	2.55
TZ3	274, 331	435	53%	6.24	262, 345	435	51%	10.83
			47%	0.82			49%	2.11
TZ4	286, 344	535	49%	3.79	352	495	74%	8.65
			51%	0.93			26%	2.81

Table 2.7. Fluorescence life time data obtained for compounds **TZ1-4** at different concentrations.

Entry	Absorption (nm)	Emission (nm)	Concentration(M)	Fraction of molecules (%)	Life time (ns)
TZ1	275, 338	452	1×10^{-6}	100%	2.41
			6.25×10^{-5}	65%, 35%	3.50, 1.67
			1×10^{-3}	26%, 74%	7.24, 2.25
TZ2	293, 346	510	1×10^{-6}	100%	2.52
			6.25×10^{-5}	53%, 47%	13.40, 3.01
			1×10^{-3}	65%, 35%	12.14, 2.77
TZ3	274, 331	435	1×10^{-6}	100%	4.14
			6.25×10^{-5}	53%, 47%	6.24, 0.82
			1×10^{-3}	65%, 35%	5.04, 0.70
TZ4	286, 344	535	1×10^{-6}	100%	1.23
			3.12×10^{-5}	49%, 51%	3.79, 0.93
			1×10^{-3}	60%, 40%	3.41, 0.78

The absorption spectra of compound **TZ7** were also red-shifted in comparison to the solution spectra by 16 nm (absorption maximum: 349 nm), while there was no much difference with respect to the emission spectra (emission maximum: 452 nm). This behavior is similar to that of compound **TZ3** irrespective of the chain length and type of columnar packing. Similar star shaped compounds reported by others, where a central triazine core connected with *trans*-stilbene chromophores showed a blue shifted emission,[12b] while the molecules with tolane moieties showed red shifted emission.[13a] Preservation of solid-state/liquid crystal state emission along with good thermal stability makes these compounds promising for organic dye lasers and OLEDs.

2.2.4. Electrochemical behavior

Energy levels of frontier molecular orbitals (HOMO and LUMO) and the energy gap of these levels in star shaped molecules **TZ1-4** were obtained by cyclic voltammetry (CV) and the data are tabulated in table 2.8. All the compounds exhibited irreversible oxidation and reduction waves (Fig. 2.20). The optical band gap E_{opt} was estimated from the red edge of the absorption spectra. Energy levels of LUMO and HOMO were determined by using the formulae E_{LUMO} = - (4.8 - $E_{1/2,\ Fc,\ Fc^+}$ + $E_{red,\ onset}$) eV and E_{HOMO} = - (4.8 - $E_{1/2,\ Fc,\ Fc^+}$ + $E_{ox,\ onset}$) eV. There was no much impact on the energy levels of frontier molecular orbitals with respect to substitution, and the bandgaps were found to be in the range of 2.53-2.62 eV. These values are slightly smaller than their corresponding optical band gap values (Table 2.4). These values can be compared with 2,4,6-triphenyl-1,3,5-triazine, which is one of the oldest materials used in OLED fabrication as a hole-blocking material.[29]

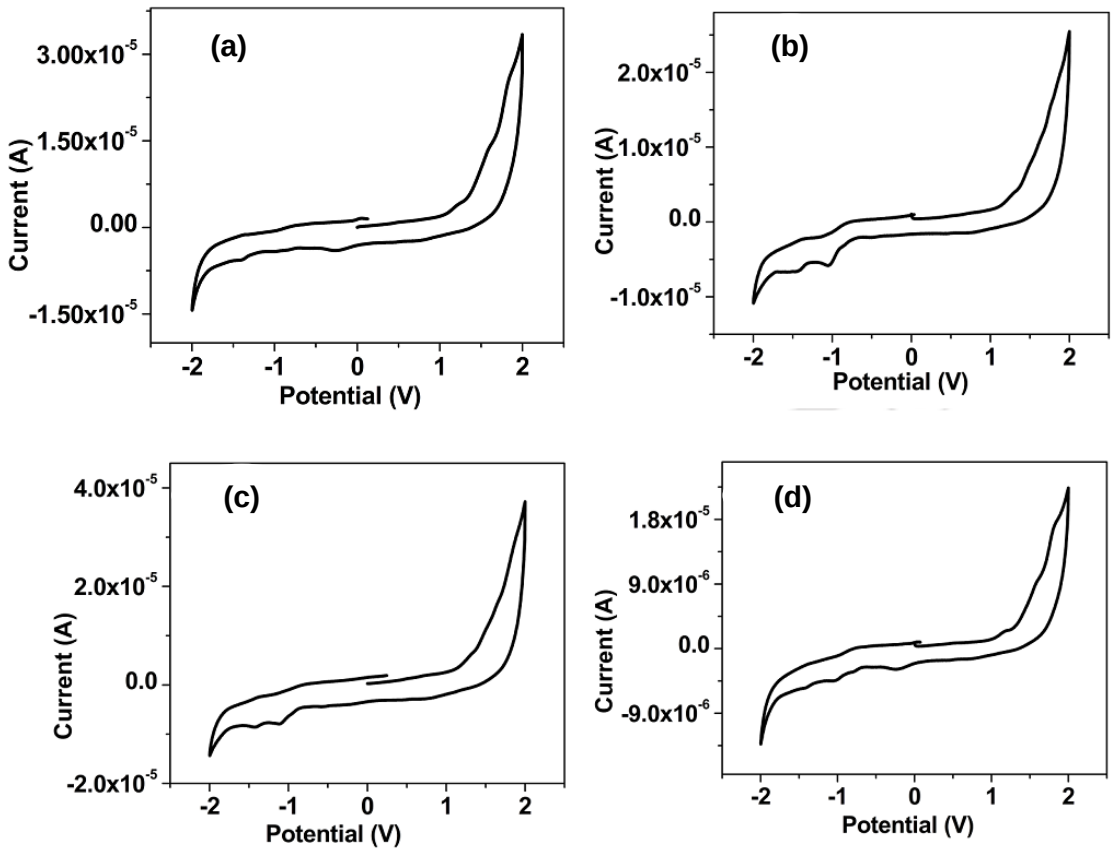

Figure 2.20. Cyclic voltammograms of the compounds **TZ1-4** (a-d) in anhydrous dichloromethane solution of tetra-*n*-butyl ammonium perchlorate (0.1 M) at a scanning rate 0.5mV/s; the half wave potential of Fc/Fc^+ was found to be 0.517 V relative to Ag/Ag^+ reference electrode**.**

Table 2.8. Electrochemical properties of compounds **TZ1-4** in micromolar DCM solutions.

Entry [a]	E_{1red} (V) [c]	E_{1oxd} (V)	E_{HOMO} (eV)[b]	E_{LUMO} (eV)[c]	ΔE_{CV} (eV)[d]	$\Delta E_{g, opt}$ (eV)[e]
TZ1	-1.02	1.57	-5.91	-3.32	2.59	3.21
TZ2	-1.05	1.48	-5.82	-3.29	2.53	3.12
TZ3	-1.11	1.48	-5.82	-3.23	2.59	3.36
TZ4	-1.03	1.59	-5.93	-3.31	2.62	3.14

[a]Experimental conditions: $Ag/AgNO_3$ as the reference electrode, glassy carbon as the working electrode, platinum rod as the counter electrode, TBAP (0.1M) as the supporting electrolyte, RT, scanning rate 0.05 mV s^{-1}; [b]Estimated from the onset oxidation peak values by using the formula E_{HOMO}= -(4.8-$E_{1/2, Fc, Fc+}$ + $E_{ox, onset}$); [c]Estimated from the onset reduction peak values by using E_{LUMO}= -(4.8-$E_{1/2, Fc, Fc+}$ + $E_{red, onset}$), $E_{1/2, Fc, Fc+}$ = 0.46 V; [d]Estimated from the formula ΔE_{CV}= E_{LUMO}-E_{HOMO}; [e]Bandgap determined from the red edge of the longest wavelength in the UV/Vis absorption spectrum.

This compound exhibits a LUMO and HOMO levels of -2.8 eV and -6.5 eV respectively. The optical band gap was found to be 3.71 eV[30], which is higher than the present series where three symmetrically substituted 1,3,4-oxadiazoles are connected to the central ring (3.2-3.4 eV) (Table 2.8). The LUMO levels of the compounds **TZ1-4** were lower than 2,4,6-triphenyl-1,3,5-triazine (-3.23 to -3.32 eV), while the HOMO levels higher and were in the range of -5.8 to -5.9 eV. Thus the substitution with alkoxyphenyl oxadiazole moiety on the 2,4,6-triphenyl-1,3,5-triazine lowers the LUMO; increases the HOMO level and thus a resultant lowering of the band gap. The lower LUMO level and bandgaps of these star-shaped molecules may reduce the barriers for electrons, with the simultaneous blocking of the hole movement. Thus the extensive π-conjugation and the introduction of the electron donating groups to the electron deficient central triazine ring is a simple method to modify the frontier molecular orbital energy levels and band gap. Additionally, the 1,3,4-oxadiazole units bring about the higher thermal stability and emissive nature that is very vital for the solid-state display devices. Similar comparable values were observed when the central triazine unit was connected to fluorene through different linkers.[30-32]

2.3. Conclusion

In summary, we have synthesized eight new star-shaped molecules with a central 2,4,6-triphenyl triazine core attached with three symmetrically substituted 1,3,4-oxadiazole arms with the variation in the number, length and pattern of peripheral chain substitution. These compounds were investigated for their thermal, electrochemical and photophysical properties with the help of various techniques. Compounds with three flexible chains at

the periphery turned out to be crystalline irrespective of the chain length, whereas compounds with six and nine peripheral chains stabilized the Col_h phase over a wide thermal range. One of the compounds with peripheral *n*-hexadecyloxy substitution at 3 and 4 positions showed a technologically important room temperature Col_h phase. Lowering the chain length of these star shaped compounds from *n*-hexadecyloxy to *n*-dodecyloxy enhanced the mesophase range. The compound with three alkyl tails was crystalline, while the compound with six alkyl tails, where the alkoxy groups are in an adjacent position, exhibited the Col_h phase with a slight enhancement in the thermal range. A marked difference was visible in the case of compounds, where the alkyl tails were in alternate positions. This compound exhibited high temperature Col_h and low temperature Col_r phases with an enhanced thermal range. A similar behavior was observed in the case of compounds with nine alkoxy tails. Overall, the lowering of chain length has increased the core-core interaction, leading to the stabilization of the Col_r phase along with the Col_h phase and enhanced the thermal range. This demonstrated how a subtle change in the molecular structure through peripheral substitution alters the liquid crystal self-assembly. The photophysical properties of these star shaped molecules were extremely dependent on the number and pattern of peripheral chain substitution. They exhibited blue and green fluorescence in the solid/liquid crystal state. Preserved fluorescence in the solid state is explained due to the formation of aggregates, which do not quench the fluorescence. The aggregation quenching is not occurring here probably due to the columnar packing that includes several different diastereomeric conformations. Cyclic voltammetry studies revealed that these molecules possess lower LUMO levels and bandgaps compared to the 2,4,6-triphenyl triazine which is used in OLEDs, thus making them better candidates for electron transporting emissive layers. The ability to overcome the aggregation induced quenching of fluorescence; higher thermal stability and beneficial band gap are the properties which make these molecules promising from the viewpoint of emissive displays and organic lasers.

2.4. Experimental Section

In this section the detailed synthetic procedures and the molecular structural characterization data have been presented for the intermediates and target compounds mentioned in the scheme.

Synthesis of 2,4,6-tri (*p*-tolyl)-1,3,5-triazine (**1**):

p-Tolunitrile (17.07 mmol, 1 equiv.) was dissolved in dry dichloromethane (15 mL). At 0 ^{o}C, trifluoromethanesulfonic acid (51.22 mmol, 3 equiv.) was slowly added to this solution. The mixture was stirred at room temperature for 12 h, then poured into ice water and neutralized with ammonium hydroxide. The precipitate was filtered out and then washed with water and acetone several times. Then the compound was recrystallized from toluene.

R_f = 0.4 (20% EtOAc-hexane); white solid; yield: 90%; IR (KBr pellet): ν_{max} in cm^{-1} 2981, 2928, 2856, 1715, 1579, 1511, 1468, 1436, 1366, 1313, 1254, 1167, 1103, 770, 647; ^{1}H NMR ($CDCl_3$, 400 MHz, 298 K): δ 8.65 (d, 6H, *J* = 8Hz, H_{Ar}), 7.36 (d, 6H, *J* = 7.6Hz, H_{Ar}), 2.48 (s, 9H, 3 × CH_3); ^{13}C NMR ($CDCl_3$, 100 MHz, 298 K): δ 171.62, 143.09, 133.97, 129.55, 129.13, 21.95; HRMS (+ESI) exact mass calculated for $C_{24}H_{22}N_3$ ($M+H^+$): 352.1814, Found: 352.1814.

Synthesis of 4,4′,4″-*s*-triazine-2,4,6-triyl-tribenzoic acid (**2**):

2,4,6-tri(*p*-tolyl)-1,3,5-triazine (5.69 mmol, 1 equiv.) was taken in a round bottom flask with acetic acid (20 mL). Then, 4.4 mL of H_2SO_4, chromium oxide (34.14 mmol, 6 equiv.) and 4.8 mL of acetic anhydride were added to the flask with stirring under ice bath. The resulting black slurry was stirred overnight and then poured into cold water. Then the precipitate was filtered out and the solid was washed with water. This solid was dissolved in aqueous NaOH solution. Again the solution was filtered out to remove undissolved starting material and then, the solution was acidified with HCl to give white precipitate. Then, the precipitate was filtered out and recrystallized from DMF.

R_f = 0.4 (EtOAc); white solid; yield: 85%; IR (KBr pellet): ν_{max} in cm^{-1} 2781, 2664, 1720, 1627, 1516, 1432, 1283, 1207, 878, 665; ^{1}H NMR (DMSO-d_6, 600 MHz, 298 K): δ 8.78 (d, 6H, *J* = 8.4Hz, H_{Ar}), 8.16 (d, 6H, *J* = 8.4Hz, H_{Ar}), 3.37 (b s, 3H, 3 × COOH); ^{13}C NMR (DMSO-d_6, 150 MHz, 298 K): δ 170.44, 166.81, 138.64, 134.68, 129.73, 128.76;

HRMS (-APCI) exact mass calculated for $C_{24}H_{14}N_3O_6$ ($M\text{-}H^+$): 440.0883, Found: 440.0434.

Synthesis of ethyl 4-(*n*-hexadecyloxy)benzoate (**3a**):

A mixture of ethyl 4-hydroxybenzoate (18.1 mmol, 1 equiv.), anhydrous K_2CO_3 (39.82 mmol, 2.2 equiv.), *n*-bromohexadecane (19.91 mmol, 1.1 equiv.) were taken in dry DMF (15 mL) and heated at 80 ^oC for 24 h under nitrogen atmosphere. After the reaction time was over, the reaction mixture was poured into ice water and extracted with ethyl acetate. The extract was washed with brine, dried over anhydrous Na_2SO_4 and then concentrated. The crude product was purified by column chromatography on silica gel. Elution with hexane followed by 2-5% ethyl acetate-hexane yielded the desired product.

R_f = 0.4 (5% EtOAc-hexane); white solid; yield: 85%; IR (KBr pellet): ν_{max} in cm^{-1} 2921, 2847, 1714, 1606, 1511, 1470, 1367, 1287, 1243, 1105, 695; ^1H NMR ($CDCl_3$, 400 MHz, 298 K): δ 7.98 (d, 2H, *J* = 9.2Hz, H_{Ar}), 6.89 (d, 2H, *J* = 8.4Hz, H_{Ar}), 4.34 (q, 2H, *J* = 7.2Hz, $COOCH_2$), 3.99 (t, 2H, *J* = 6.4Hz, OCH_2), 1.75-1.83 (m, 2H, CH_2), 1.39-1.47 (m, 2H, CH_2), 1.36 (t, 3H, CH_3), 1.25-1.32 (m, 24H, 12 × CH_2), 0.88 (t, 3H, CH_3); ^{13}C NMR ($CDCl_3$, 100 MHz, 298 K): δ 166.65, 163.09, 131.70, 122.87, 114.21, 68.40, 60.78, 32.14, 29.91, 29.88, 29.80, 29.77, 29.58, 29.34, 26.20, 22.91, 14.60, 14.33; HRMS (+APCI) exact mass calculated for $C_{25}H_{43}O_3$ ($M+H^+$): 391.3207, Found: 391.3100.

Synthesis of ethyl 3,4-bis(hexadecyloxy)benzoate (**3b**):

A mixture of ethyl 3, 4-dihydroxybenzoate (16.5 mmol, 1 equiv.), anhydrous K_2CO_3 (72.6 mmol, 4.4 equiv.), *n*-bromohexadecane (36.3 mmol, 2.2 equiv.) were taken in dry DMF (15 mL) and heated at 80 ^oC for 24 h under nitrogen atmosphere. Then the reaction mixture was poured into ice water and extracted with ethyl acetate. The extract was washed with brine, dried over anhydrous Na_2SO_4 and then concentrated. The crude product was purified by column chromatography on silica gel. Elution with hexane followed by 2-5% ethyl acetate-hexane yielded the desired product.

R_f = 0.45 (5% EtOAc-hexane); white solid; yield: 80%; IR (KBr pellet): ν_{max} in cm^{-1} 3419, 2919, 2849, 1710, 1598, 1518, 1277, 1211, 1129, 761; ^1H NMR ($CDCl_3$, 400 MHz, 298 K): δ 7.63 (d, 1H, *J* = 8Hz, H_{Ar}), 7.54 (s, 1H, H_{Ar}), 6.86 (d, 1H, *J* = 8Hz, H_{Ar}), 4.34 (q, 2H, *J* = 8Hz, $COOCH_2$), 4.02-4.05 (m, 4H, 2 × OCH_2), 1.78-1.87 (m, 4H, 2 × CH_2), 1.43-1.49 (m, 4H, 2 × CH_2), 1.38 (t, 3H, CH_3), 1.25-1.36 (m, 48H, 24 × CH_2), 0.88 (t, 6H, 2 ×

CH_3); ^{13}C NMR ($CDCl_3$, 100 MHz, 298 K): δ 166.75, 153.35, 148.70, 123.66, 122.99, 114.56, 112.14, 69.52, 69.21, 60.90, 32.15, 29.93, 29.89, 29.85, 29.83, 29.64, 29.61, 29.59, 29.42, 29.30, 26.24, 26.20, 22.91, 14.62, 14.33; HRMS (+ESI) exact mass calculated for $C_{41}H_{75}O_4$ ($M+H^+$): 631.5665, Found: 631.5665.

Synthesis of ethyl 3,5-bis(hexadecyloxy)benzoate (**3c**):

A mixture of ethyl 3,5-dihydroxybenzoate (16.5 mmol, 1 equiv.), anhydrous K_2CO_3 (72.6 mmol, 4.4 equiv.), *n*-bromohexadecane (36.3 mmol, 2.2 equiv.) were taken in dry DMF (15 mL) and heated at 80 ^oC for 24 h under nitrogen atmosphere. Then the reaction mixture was poured into ice water and extracted with ethyl acetate. The extract was washed with brine, dried over anhydrous Na_2SO_4 and then concentrated. The crude product was purified by column chromatography on silica gel. Elution with hexane followed by 2-5% ethyl acetate-hexane yielded the desired product.

R_f = 0.45 (5% EtOAc-hexane); white solid; yield: 80%; IR (KBr pellet): ν_{max} in cm^{-1} 3434, 1703, 1596, 1452, 1399, 1164, 1029, 1001, 851, 771; ^1H NMR ($CDCl_3$, 600 MHz, 298 K): δ 7.16 (s, 2H, H_{Ar}), 6.63 (s, 1H, H_{Ar}), 4.36 (q, 2H, *J* = 6Hz, $COOCH_2$), 3.97(t, 4H, 2 × OCH_2), 1.75-1.80 (m, 4H, 2 × CH_2), 1.39-1.47 (m, 4H, 2 × CH_2), 1.37 (t, 3H, CH_3), 1.26-1.34 (m, 48H, 24 × CH_2), 0.88 (t, 6H, 2 × CH_3); ^{13}C NMR ($CDCl_3$, 150 MHz, 298 K): δ 166.73, 160.34, 132.41, 107.85, 106.51, 68.52, 61.25, 32.15, 29.92, 29.88, 29.82, 29.80, 29.59, 29.41, 26.24, 22.91, 14.54, 14.33; HRMS (+ESI) exact mass calculated for $C_{41}H_{75}O_4$ ($M+H^+$): 631.5665, Found: 631.5651.

Synthesis of ethyl 3,4,5-trihexadecyloxy benzoate (**3d**):

A mixture of ethyl gallate (15.1 mmol, 1 equiv.), anhydrous K_2CO_3 (99.9 mmol, 6.6 equiv.), *n*-bromohexadecane (49.83 mmol, 3.3 equiv.) were taken in dry DMF (15 mL) and heated at 80 ^oC for 24 h under nitrogen atmosphere. Then the reaction mixture was poured into ice water and extracted with ethyl acetate. The extract was washed with water, dried over anhydrous Na_2SO_4 and then concentrated. The crude product was purified by column chromatography on silica gel. Elution with hexane followed by 2-5% ethyl acetate-hexane yielded the desired product.

R_f = 0.5 (5% EtOAc-hexane); white solid; yield: 75%; IR (KBr pellet): ν_{max} in cm^{-1} 2922, 2850, 1716, 1583, 1468, 1426, 1331, 1218, 1110, 1041; ^1H NMR ($CDCl_3$, 400 MHz, 298 K): δ 7.25 (s, 2H, H_{Ar}), 4.35 (q, 2H, *J* = 7.2Hz, $COOCH_2$), 4.01 (t, 6H, 3 × OCH_2), 1.25-

1.82 (m, 84H, 42 × CH_2), 0.87(m, 12H, 4 × CH_3); ^{13}C NMR ($CDCl_3$, 100 MHz, 298 K): δ 166.70, 153.04, 142.61, 125.28, 108.29, 73.72, 69.44, 61.17, 33.05, 32.16, 30.56, 29.94, 29.89, 29.87, 29.80, 29.63, 29.60, 29.57, 26.32, 26.29, 22.92, 14.63, 14.33; HRMS (+ESI) exact mass calculated for $C_{57}H_{107}O_5$ ($M+H^+$): 871.8113, Found: 871.8031.

Synthesis of ethyl 4-(*n*-dodecyloxy)benzoate (**3e**):

A mixture of ethyl 4-hydroxybenzoate (18.1 mmol, 1 equiv.), anhydrous K_2CO_3 (39.82 mmol, 2.2 equiv.), *n*-bromododecane (19.91 mmol, 1.1 equiv.) were taken in dry DMF (15 mL) and heated at 80 ^oC for 24 h under nitrogen atmosphere. After the reaction time was over, the reaction mixture was poured into ice water and extracted with ethyl acetate. The extract was washed with brine, dried over anhydrous Na_2SO_4 and then concentrated. The crude product was purified by column chromatography on silica gel. Elution with hexane followed by 2-5% ethyl acetate-hexane yielded the desired product.

R_f = 0.35 (5% EtOAc-hexane); white solid; yield: 90%; IR (KBr pellet): ν_{max} in cm^{-1} 2921, 2847, 1714, 1606, 1511, 1470, 1367, 1287, 1243, 1105, 695; ^{1}H NMR ($CDCl_3$, 600 MHz, 298 K): δ 7.98 (d, 2H, *J* = 8.4Hz, H_{Ar}), 6.89 (d, 2H, *J* = 9Hz, H_{Ar}), 4.34 (q, 2H, *J* =6Hz, $COOCH_2$), 3.99 (t, 2H, *J* = 6Hz, OCH_2), 1.79 (m, 2H, CH_2), 1.42-1.46 (m, 2H, CH_2), 1.37 (t, 3H, CH_3), 1.26-1.35 (m, 16H, 8 × CH_2), 0.88 (t, 3H, CH_3); ^{13}C NMR ($CDCl_3$, 150 MHz, 298 K): δ 166.66, 163.06, 131.69, 122.80, 114.17, 68.34, 60.78, 32.12, 29.83, 29.79, 29.76, 29.56, 29.31, 26.81, 22.90, 14.58, 14.33; HRMS (+APCI) exact mass calculated for $C_{21}H_{35}O_3$ ($M+H^+$):335.2586, Found: 335.2586.

Synthesis of ethyl 3,4-bis (dodecyloxy)benzoate (**3f**):

A mixture of ethyl 3, 4-dihydroxybenzoate (16.5 mmol, 1 equiv.), anhydrous K_2CO_3 (72.6 mmol, 4.4 equiv.), *n*-bromododecane (36.3 mmol, 2.2 equiv.) were taken in dry DMF (15 mL) and heated at 80 ^oC for 24 h under nitrogen atmosphere. Then the reaction mixture was poured into ice water and extracted with ethyl acetate. The extract was washed with brine, dried over anhydrous Na_2SO_4 and then concentrated. The crude product was purified by column chromatography on silica gel. Elution with hexane followed by 2-5% ethyl acetate-hexane yielded the desired product.

R_f = 0.40 (5% EtOAc-hexane); white solid; yield: 84%; IR (KBr pellet): ν_{max} in cm^{-1} 3419, 2919, 2849, 1710, 1598, 1518, 1277, 1211, 1129, 761; ^{1}H NMR ($CDCl_3$, 600 MHz, 298 K): δ 7.64 (d, 1H, *J* = 6Hz, H_{Ar}), 7.54 (s, 1H, H_{Ar}), 6.86 (d, 1H, *J* = 6Hz, H_{Ar}), 4.34 (q,

2H, *J* = 6Hz, $COOCH_2$), 4.04 (t, 4H, 2 × OCH_2), 1.83-1.84 (m, 4H, 2 × CH_2), 1.47 (m, 4H, 2 × CH_2), 1.38 (t, 3H, CH_3), 1.26-1.35 (m, 32H, 16 × CH_2), 0.88 (t, 6H, 2 × CH_3); ^{13}C NMR ($CDCl_3$, 150 MHz, 298 K): δ 166.67, 153.32, 148.68, 123.65, 122.96, 114.46, 112.08, 69.47, 69.20, 60.90, 32.14, 29.90, 29.86, 29.82, 29.62, 29.58, 29.40, 29.28, 26.21, 26.18, 22.90, 14.61, 14.32; HRMS (+ESI) exact mass calculated for $C_{33}H_{59}O_4$ ($M+H^+$): 519.4413, Found: 519.4412.

Synthesis of ethyl 3, 5-bis(dodecyloxy)benzoate (**3g**):

A mixture of ethyl 3,5-dihydroxybenzoate (16.5 mmol, 1 equiv.), anhydrous K_2CO_3 (72.6 mmol, 4.4 equiv.), *n*-bromododecane (36.3 mmol, 2.2 equiv.) were taken in dry DMF (15 mL) and heated at 80 ^oC for 24 h under nitrogen atmosphere. Then the reaction mixture was poured into ice water and extracted with ethyl acetate. The extract was washed with brine, dried over anhydrous Na_2SO_4 and then concentrated. The crude product was purified by column chromatography on silica. Elution with hexane followed by 2-5% ethyl acetate-hexane yielded the desired product.

R_f = 0.40 (5% EtOAc-hexane); white solid; yield: 87%; IR (KBr pellet): ν_{max} in cm^{-1} 3434, 1703, 1596, 1452, 1399, 1164, 1029, 1001, 851, 771; ^{1}H NMR ($CDCl_3$, 600 MHz, 298 K): δ 7.16 (d, 2H, *J* = 6Hz, H_{Ar}), 6.62 (t, 1H, H_{Ar}), 4.35 (q, 2H, *J* = 6Hz, $COOCH_2$), 3.96 (t, 4H, 2 × OCH_2), 1.73-1.81 (m, 4H, 2 × CH_2), 1.40-1.46 (m, 4H, 2 × CH_2), 1.38 (t, 3H, CH_3), 1.26-1.36 (m, 32H, 16 × CH_2), 0.88 (t, 6H, 2 × CH_3); ^{13}C NMR ($CDCl_3$, 150 MHz, 298 K): δ 166.73, 160.29, 132.35, 107.78, 106.44, 68.48, 61.28, 32.14, 30.04, 29.99, 29.98, 29.88, 29.86, 29.82, 29.79, 29.59, 29.57, 29.39, 26.22, 22.91, 14.54, 14.35; HRMS (+ESI) exact mass calculated for $C_{33}H_{59}O_4$ ($M+H^+$): 519.4413, Found: 519.4412.

Synthesis of ethyl 3,4,5-tridodecyloxy benzoate (**3h**):

A mixture of ethyl gallate (15.1 mmol, 1 equiv.), anhydrous K_2CO_3 (99.9 mmol, 6.6 equiv.), *n*-bromododecane (49.83 mmol, 3.3 equiv.) were taken in dry DMF (15 mL) and heated at 80 ^oC for 24 h under nitrogen atmosphere. Then the reaction mixture was poured into ice water and extracted with ethyl acetate. The extract was washed with water, dried over anhydrous Na_2SO_4 and then concentrated. The crude product was purified by column chromatography on silica gel. Elution with hexane followed by 2-5% ethyl acetate-hexane yielded the desired product.

R_f = 0.45 (5% EtOAc-hexane); white solid; yield: 82%; IR (KBr pellet): ν_{max} in cm^{-1} 2922, 2850, 1716, 1583, 1468, 1426, 1331, 1218, 1110, 1029, 985, 820; ^{1}H NMR ($CDCl_3$, 600 MHz, 298 K): δ 7.25 (s, 2H, H_{Ar}), 4.35 (q, 2H, *J* = 7.2Hz, $COOCH_2$), 4.01 (t, 6H, 3 × OCH_2), 1.79-1.83 (m, 4H, 2 × CH_2), 1.72-1.75 (m, 2H, 1 × CH_2), 1.44-1.49 (m, 6H, 3 × CH_2), 1.30 (t, 3H, CH_3), 1.26-1.35 (m, 48H, 24 × CH_2), 0.88 (m, 9H, 3 × CH_3); ^{13}C NMR ($CDCl_3$, 150 MHz, 298 K): δ 166.67, 152.98, 142.45, 125.23, 108.17, 108.12, 73.68, 69.34, 61.16, 32.16, 32.14, 30.53, 30.08, 30.05, 29.97, 29.95, 29.94, 29.92, 29.88, 29.85, 29.79, 29.61, 29.59, 29.52, 26.30, 26.71, 22.91, 14.61, 14.33; HRMS (+ESI) exact mass calculated for $C_{45}H_{83}O_5$($M+H^+$): 703.6241, Found: 703.6240.

Synthesis of ethyl 4-(hexadecyloxy)benzhydrazide (**4a**):

A mixture of ethyl 4-(hexadecyloxy)benzoate (19 mmol, 1 equiv.), excess hydrazine hydrate (20 equiv.) in ethanol were refluxed for 48 h. Excess solvent was removed and water (100 mL) was added to it. Resulting precipitate was collected by filtration, washed with excess water, dried under vacuum and recrystallization from ethanol gave white solid product.

R_f = 0.25 (30% EtOAc-hexane); white solid; yield: 75%; IR (KBr pellet): ν_{max} in cm^{-1} 3429, 2919, 2850, 1648, 1617, 1508, 1472, 1252, 1180, 836; ^{1}H NMR ($CDCl_3$, 400 MHz, 298 K): δ 7.69 (d, 2H, *J* = 8Hz, H_{Ar}), 7.33 (b s, 1H, CONH), 6.91 (d, 2H, *J* = 8Hz, H_{Ar}), 4.07 (b s, 2H, NH_2), 3.98 (s, 2H, OCH_2), 1.75-1.82 (m, 2H, CH_2), 1.41-1.45 (m, 2H, CH_2), 1.25-1.31 (m, 24H, 12 × CH_2), 0.87 (m, 3H, CH_3); ^{13}C NMR ($CDCl_3$, 100 MHz, 298 K): δ 168.61, 162.31, 128.81, 124.77, 114.62, 68.43, 32.12, 29.88, 29.85, 29.78, 29.75, 29.56, 29.31, 29.18, 22.88, 14.31; HRMS (+APCI) exact mass calculated for $C_{23}H_{41}N_2O_2$ ($M+H^+$): 377.3168, Found: 377.3082.

Synthesis of ethyl 3,4-bis(hexadecyloxy)benzhydrazide (**4b**):

A mixture of ethyl 3,4-bis(hexadecyloxy)benzoate (10.2 mmol, 1 equiv.), excess hydrazine hydrate (20 equiv.) in ethanol were refluxed for 48 h. Excess solvent was removed and water (100 mL) was added to it. Resulting precipitate was collected by filtration, washed with excess water, dried under vacuum and recrystallization from ethanol gave white solid product.

R_f = 0.25 (20% EtOAc-hexane); white solid; yield: 70%; IR (KBr pellet): ν_{max} in cm^{-1} 3248, 2919, 2848, 1711, 1514, 1467, 1278, 1212, 1150, 761; ^{1}H NMR ($CDCl_3$, 400 MHz,

298 K): δ 7.34 (d, 1H, *J* = 8Hz, H_{Ar}), 7.26 (b s, 1H, CONH), 7.22 (dd, 1H, *J* = 4Hz, *J* = 8Hz, H_{Ar}), 6.85 (d, 1H, *J* = 8Hz, H_{Ar}), 4.08 (b s, 2H, NH_2), 4.00-4.05 (m, 4H, 2 × OCH_2), 1.79-1.86 (m, 4H, 2 × CH_2), 1.38-1.50 (m, 4H, 2 × CH_2), 1.25-1.36 (m, 48H, 24 × CH_2), 0.88 (m, 6H, 2 × CH_3); ^{13}C NMR ($CDCl_3$, 150 MHz, 298 K): δ 168.77, 152.55, 149.33, 125.21, 119.70, 112.76, 112.65, 69.62, 69.37, 32.15, 29.94, 29.89, 29.85, 29.63, 29.59, 29.43, 29.34, 26.23, 22.90, 14.33; HRMS (+ESI) exact mass calculated for $C_{39}H_{73}N_2O_3$ ($M+H^+$): 617.5621, Found: 617.5726.

Synthesis of ethyl 3,5-bis(hexadecyloxy)benzhydrazide (**4c**):

A mixture of ethyl 3,5-bis(hexadecyloxy)benzoate (10.2 mmol, 1 equiv.), excess hydrazine hydrate (20 equiv.) in ethanol were refluxed for 48 h. Excess solvent was removed and water (100 mL) was added to it. Resulting precipitate was collected by filtration, washed with excess water, dried under vacuum and recrystallization from ethanol gave white solid product.

R_f = 0.25 (20% EtOAc-hexane); white solid; yield: 70%; IR (KBr pellet): ν_{max} in cm^{-1} 3446, 2920, 2849, 1597, 1469, 1332, 1170, 1064, 913, 721; ^{1}H NMR ($CDCl_3$, 400 MHz, 298 K): δ 7.38 (b s, 1H, CONH), 6.83 (s, 2H, H_{Ar}), 6.58 (s, 1H, H_{Ar}), 4.08 (b s, 2H, NH_2), 3.95 (t, 4H, 2 × OCH_2), 1.74-1.79 (m, 4H, 2 × CH_2), 1.42-1.46 (m, 4H, 2 × CH_2), 1.26-1.41 (m, 48H, 24 × CH_2), 0.88 (m, 6H, 2 × CH_3); ^{13}C NMR ($CDCl_3$, 100 MHz, 298 K): δ 168.91, 160.71, 134.76, 105.34, 105.02, 68.57, 32.14, 29.92, 29.88, 29.82, 29.79, 29.58, 29.38, 26.22, 22.91, 14.34; HRMS (+ESI) exact mass calculated for $C_{39}H_{73}N_2O_3$ ($M+H^+$): 617.5621, Found: 617.5600.

Synthesis of ethyl 3,4,5-tris(hexadecyloxy)benzhydrazide (**4d**):

A mixture of ethyl 3,4,5-tri-*n*-hexadecyloxybenzoate (10 mmol, 1 equiv.), excess hydrazine hydrate (20 equiv.) in ethanol were refluxed for 48 h. Excess solvent was removed and water (100 mL)was added to it. Resulting precipitate was collected by filtration, washed with excess water, dried under vacuum. The solid was recrystallized from ethanol to yield a white solid product.

R_f = 0.52 (20% EtOAc-hexane); white solid; yield: 75%; IR (KBr pellet): ν_{max} in cm^{-1} 3448, 3248, 2921, 2850, 1635, 1579, 1466, 1427, 1238, 1122; ^{1}H NMR ($CDCl_3$, 400 MHz, 298 K): δ 7.22 (b s, 1H, CONH), 6.92 (s, 2H, H_{Ar}), 4.07 (s, 2H, NH_2), 3.99 (m, 6H, 3 × OCH_2), 1.26-1.80 (m, 84H, 42 × CH_2), 0.88 (m, 9H, 3 × CH_3); ^{13}C NMR ($CDCl_3$,

150 MHz, 298 K): δ 168.70, 153.54, 141.92, 127.68, 105.74, 69.60, 30.53, 29.97, 29.95, 29.88, 29.60, 26.30, 22.92, 14.33; HRMS (+ESI) exact mass calculated for $C_{55}H_{105}N_2O_4$ ($M+H^+$): 857.8074, Found: 857.8151.

Synthesis of ethyl 4-(dodecyloxy)benzhydrazide (**4e**):

A mixture of ethyl 4-(dodecyloxy)benzoate (19 mmol, 1 equiv.), excess hydrazine hydrate (20 equiv.) in ethanol were refluxed for 48 h. Excess solvent was removed and water (100 mL) was added to it. Resulting precipitate was collected by filtration, washed with excess water, dried under vacuum and recrystallization from ethanol gave white solid product.

R_f = 0.30 (40% EtOAc-hexane); white solid; yield: 85%; IR (KBr pellet): ν_{max} in cm^{-1} 3429, 2919, 2850, 1648, 1617, 1508, 1472, 1252, 1180, 836; ^1H NMR ($CDCl_3$, 600 MHz, 298 K): δ 7.69 (d, 2H, *J* = 9Hz, H_{Ar}), 7.31 (b s, 1H, CONH), 6.92 (d, 2H, *J* = 6Hz, H_{Ar}), 4.07 (b s, 2H, NH_2), 3.98 (t, 2H, OCH_2), 1.76-1.80 (m, 2H, CH_2), 1.43-1.46 (m, 2H, CH_2), 1.26-1.36 (m, 16H, 8 × CH_2), 0.88 (m, 3H, CH_3); ^{13}C NMR ($CDCl_3$, 150 MHz, 298 K): δ 168.64, 162.36, 128.80, 124.77, 114.67, 68.45, 32.09, 29.76, 29.57, 29.51, 29.32, 26.19, 22.88, 14.32; HRMS (+APCI) exact mass calculated for $C_{19}H_{33}N_2O_2$ ($M+H^+$): 321.2542, Found: 321.2522.

Synthesis of ethyl 3, 4-bis (dodecyloxy)benzhydrazide (**4f**):

A mixture of ethyl 3,4-bis(dodecyloxy)benzoate (10.2 mmol, 1 equiv.), excess hydrazine hydrate (20 equiv.) in ethanol were refluxed for 48 h. Excess solvent was removed and water(100 mL) was added to it. Resulting precipitate was collected by filtration, washed with excess water, dried under vacuum and recrystallization from ethanol gave white solid product.

R_f = 0.3 (30% EtOAc-hexane); white solid; yield: 78%; IR (KBr pellet): ν_{max} in cm^{-1} 3248, 2919, 2848, 1711, 1514, 1467, 1278, 1212, 1150, 761; ^1H NMR ($CDCl_3$, 600 MHz, 298 K): δ 7.34 (d, 1H, *J* = 6Hz, H_{Ar}), 7.26 (b s, 1H, CONH), 7.22 (dd, 1H, *J* = 4Hz, *J* = 8Hz, H_{Ar}), 6.85 (d, 1H, *J* = 9Hz, H_{Ar}), 4.04 (b s, 2H, NH_2), 4.00-4.03 (m, 4H, 2 × OCH_2), 1.79-1.86 (m, 4H, 2 × CH_2), 1.33-1.46 (m, 4H, 2 × CH_2), 1.25-1.29 (m, 32H, 16 × CH_2), 0.88 (m, 6H, 2 × CH_3); ^{13}C NMR ($CDCl_3$, 150 MHz, 298 K): δ 168.77, 152.55, 149.33, 125.21, 119.70, 112.76, 112.65, 69.62, 69.37, 32.15, 29.94, 29.89, 29.85, 29.63, 29.59,

29.43, 29.34, 26.23, 22.90, 14.33; HRMS (+ESI) exact mass calculated for $C_{31}H_{57}N_2O_3$ ($M+H^+$): 505.4364, Found: 505.4258.

Synthesis of ethyl 3, 5-bis (dodecyloxy)benzhydrazide (**4g**):

A mixture of ethyl 3,5-bis(dodecyloxy)benzoate (10.2 mmol, 1 equiv.), excess hydrazine hydrate (20 equiv.) in ethanol were refluxed for 48 h. Excess solvent was removed and water (100 mL) was added to it. Resulting precipitate was collected by filtration, washed with excess water, dried under vacuum and recrystallization from ethanol gave white solid product.

R_f = 0.35 (30% EtOAc-hexane); white solid; yield: 80%; IR (KBr pellet): ν_{max} in cm^{-1} 3446, 2920, 2849, 1597, 1469, 1332, 1170, 1064, 913, 721; ^{1}H NMR ($CDCl_3$, 600 MHz, 298 K): δ 7.44 (b s, 1H, CONH), 6.83 (s, 2H, H_{Ar}), 6.57 (s, 1H, H_{Ar}), 4.88 (br s, 2H, NH_2), 3.94 (t, 4H, 2 × OCH_2), 1.73-1.78 (m, 4H, 2 × CH_2), 1.33-1.43 (m, 4H, 2 × CH_2), 1.25-1.32 (m, 32H, 16 × CH_2), 0.87 (m, 6H, 2 × CH_3); ^{13}C NMR ($CDCl_3$, 150 MHz, 298 K): δ 168.94, 160.40, 134.71, 105.34, 105.03, 68.56, 32.13, 29.87, 29.83, 29.79, 29.56, 29.36, 26.20, 22.89, 14.32; HRMS (+ESI) exact mass calculated for $C_{31}H_{57}N_2O_3$ ($M+H^+$): 505.4364, Found: 505.4258.

Synthesis of ethyl 3, 4, 5-tris (dodecyloxy)benzhydrazide (**4h**):

A mixture of ethyl 3,4,5-tri-*n*-dodecyloxybenzoate (10 mmol, 1 equiv.), excess hydrazine hydrate (20 equiv.) in ethanol were refluxed for 48 h. Excess solvent was removed and water (100 mL) was added to it. Resulting precipitate was collected by filtration, washed with excess water, dried under vacuum. The solid was recrystallized from ethanol to yield a white solid product.

R_f = 0.4 (20% EtOAc-hexane); white solid; yield: 80%; IR (KBr pellet): ν_{max} in cm^{-1} 3448, 3248, 2921, 2850, 1635, 1579, 1466, 1427, 1238, 1122; ^{1}H NMR ($CDCl_3$, 600 MHz, 298 K): δ 7.31 (b s, 1H, CONH), 6.92 (s, 2H, H_{Ar}), 4.98 (s, 2H, NH_2), 3.99 (t, 6H, 3 × OCH_2), 1.79-1.82 (m, 4H, 2 × CH_2), 1.70-1.75 (m, 2H, 2 × CH_2), 1.44-1.45 (m, 6H, 3 × CH_2), 1.25 (m, 48H, 24 × CH_2), 0.87 (m, 9H, 3 × CH_3); ^{13}C NMR ($CDCl_3$, 150 MHz, 298 K): δ 168.95, 153.38, 141.52, 127.63, 106.61, 73.71, 69.47, 32.13, 30.49, 29.90, 29.84, 29.59, 29.57, 29.51, 26.27, 22.89, 14.31; HRMS (+ESI) exact mass calculated for $C_{43}H_{81}N_2O_4$ ($M+H^+$): 689.6196, Found: 689.5764.

Synthesis of **TZ1**:

A suspension of 4,4′,4″-*s*-triazine-2,4,6-triyl-tribenzoic acid (2.5 mmol), thionyl chloride (6 mL) and one drop of DMF (catalytic amount) was refluxed for 24 h. The excess of thionyl chloride was removed by distillation and then the crude product was dried in vacuo and used for the next reaction without further purification and characterization. A solution of 4,4′,4″-*s*-triazine-2,4,6-triyl-tribenzoic acid chloride (2.2 mmol, 1 equiv.) in THF was added dropwise into a solution of ethyl 4-(hexadecyloxy)benzohydrazide (6.8 mmol, 3.05 equiv.) and triethylamine (6.6 mmol, 3 equiv.) in THF under argon atmosphere. The reaction mixture was refluxed for 18 h. After cooling to room temperature, THF was evaporated in rotavapor and the residue was extracted with ethyl acetate and concentrated. The resulting crude product was directly used for next reaction. The crude product (0.3 mmol, 1 equiv.) was dissolved in $POCl_3$ (20 equiv.) and refluxed for about 16 h. The whole solution was slowly added to ice water and extracted with chloroform. The extract was washed with brine, dried over anhydrous Na_2SO_4 and then concentrated. Then, the crude product was further purified through column chromatography on neutral alumina. Elution with 20-30% chloroform-hexane yielded the desired product.

R_f = 0.35 (20% chloroform-hexane); off white solid; yield: 45%; IR (KBr pellet): ν_{max} in cm^{-1} 3444, 2923, 2851, 1610, 1581, 1518, 1495, 1367, 1256, 1176, 1016, 800, 745, 657, 516; ^1H NMR ($CDCl_3$, 600 MHz, 298 K): δ 8.69 (d, 6H, *J* = 7.8Hz, H_{Ar}), 8.15 (d, 6H, *J* = 7.8Hz, H_{Ar}), 7.99 (d, 6H, *J* = 8.4Hz, H_{Ar}), 6.98 (d, 6H, *J* = 9Hz, H_{Ar}), 4.00 (t, 6H, 3 × OCH_2), 1.80-1.85 (m, 6H, 3 × CH_2), 1.42-1.50 (m, 6H, 3 × CH_2), 1.25-1.39 (m, 72H, 36 × CH_2), 0.89 (t, 9H, 3 × CH_3); ^{13}C NMR ($CDCl_3$, 150 MHz, 298 K): δ 170.74, 165.12, 163.93, 160.86, 138.45, 138.41, 129.67, 127.69, 127.15, 125.04, 105.33, 68.64, 32.15, 29.95, 29.90, 29.72, 29.59, 29.49, 26.31, 22.91, 14.32; MALDI TOF MS: *m/z* for $C_{93}H_{124}N_9O_6[M+H^+]$, calculated: 1463.9708, Found: 1464.1720.

Synthesis of **TZ2**:

4,4′,4″-*s*-triazine-2,4,6-triyl-tribenzoic acid (2.5 mmol) in 6 mL of thionyl chloride and one drop of DMF (catalytic amount) was refluxed for 24 h. The excess of thionyl chloride was removed by distillation and then the crude product was dried in vacuo and used for the next reaction without further purification and characterization. A solution of 4,4′,4″-*s*-triazine-2,4,6-triyl-tribenzoic acid chloride (2.2 mmol, 1 equiv.) in THF was added drop

wise into a solution of 3,4,-bis(hexadecyloxy) benzhydrazide (6.8 mmol, 3.05 equiv.) and triethylamine (6.6 mmol, 3 equiv.) in THF under argon atmosphere. The reaction mixture was refluxed for 18 h. After cooling to room temperature, THF was evaporated in rotavapor and the residue was extracted with ethyl acetate and concentrated. The resulting crude product was directly used for next reaction. The crude product (0.3 mmol, 1 equiv.) was dissolved in $POCl_3$ (20 equiv.) and refluxed for about 16 h. The whole solution was slowly added to ice water and extracted with chloroform. The extract was washed with brine, dried over anhydrous Na_2SO_4 and then concentrated. Then, the crude product was further purified through column chromatography on neutral alumina. Elution with 50-60% chloroform-hexane yielded the desired product.

R_f = 0.25 (60% chloroform-hexane); yellow solid; yield: 45%; IR (KBr pellet): ν_{max} in cm^{-1} 3447, 2920, 2850, 1607, 1558, 1515, 1465, 1370, 1275, 1215, 1014, 816, 738, 697, 520; ^1H NMR ($CDCl_3$, 600 MHz, 298 K): δ 8.75 (d, 6H, *J* = 6.6Hz, H_{Ar}), 8.20 (d, 6H, *J* = 6.6Hz, H_{Ar}), 7.56 (d, 6H, *J* = 9Hz, H_{Ar}), 6.94 (d, 3H, *J* = 8.4Hz, H_{Ar}), 4.06 (m, 12H, 6 × OCH_2), 1.85-1.89 (m, 12H, 6 × CH_2), 1.48-1.55 (m, 12H, 6 × CH_2), 1.26-1.42 (m, 144H, 72 × CH_2), 0.87 (t, 18H, 6 × CH_3); ^{13}C NMR ($CDCl_3$, 150 MHz, 298 K): δ 171.15, 165.34, 163.79, 152.71, 149.61, 138.52, 129.82, 128.01, 127.24, 120.75, 116.17, 113.09, 111.90, 69.67, 69.37, 32.17, 29.97, 29.91, 29.72, 29.69, 29.60, 29.49, 29.39, 26.30, 26.26, 22.92, 14.35; MALDI TOF MS: *m/z* for $C_{141}H_{220}N_9O_9[M+H^+]$, Calculated: 2184.7068, Found: 2184.3430.

Synthesis of **TZ3**:

4,4′,4″-*s*-triazine-2,4,6-triyl-tribenzoic acid (2.5 mmol) in 6 mL of thionyl chloride and one drop of DMF (catalytic amount) was refluxed for 24 h. The excess of thionyl chloride was removed by distillation and then the crude product was dried in vacuo and used for the next reaction without further purification and characterization. A solution of 4,4′,4″-*s*-triazine-2,4,6-triyl-tribenzoic acid chloride (2.2 mmol, 1 equiv.) in THF was added dropwise into a solution of 3,5,-bis(hexadecyloxy)benzhydrazide (6.8 mmol, 3.05 equiv.) and triethylamine (6.6 mmol, 3 equiv.) in THF under argon atmosphere. The reaction mixture was refluxed for 18 h. After cooling to room temperature, THF was evaporated in rotavapor and the residue was extracted with ethyl acetate and concentrated. The resulting crude product was directly used for next reaction. The crude product (0.3 mmol, 1 equiv.) was dissolved in $POCl_3$ (20 equiv.) and refluxed for about 16 h. The whole solution was

slowly added to ice water and extracted with chloroform. The extract was washed with brine, dried over anhydrous Na_2SO_4 and then concentrated. Then, the crude product was further purified through column chromatography on neutral alumina. Elution with 30-40% chloroform-hexane yielded the desired product.

R_f = 0.35 (60% chloroform-hexane); yellow solid; yield: 45%; IR (KBr pellet): ν_{max} in cm^{-1} 3444, 2922, 2852, 1601, 1554, 1518, 1463, 1373, 1232, 1170, 1015, 819, 741, 677, 517; ^{1}H NMR ($CDCl_3$, 600 MHz, 298 K): δ 8.74 (d, 6H, *J* = 8.4Hz, H_{Ar}), 8.20 (d, 6H, *J* = 8.4Hz, H_{Ar}), 7.16 (s, 6H, H_{Ar}), 6.55 (s, 3H, H_{Ar}), 3.97 (t, 12H, 6 × OCH_2), 1.79-1.84 (m, 12H, 6 × CH_2), 1.46-1.51 (m, 12H, 6 × CH_2), 1.34-1.42 (m, 144H, 72 × CH_2), 0.87 (t, 18H, 6 × CH_3); ^{13}C NMR ($CDCl_3$, 150 MHz, 298 K): δ 170.74, 165.12, 163.96, 163.93, 160.86, 138.41, 129.65, 127.69, 127.16, 125.04, 105.33, 68.64, 32.15, 29.95, 29.90, 29.72, 29.59, 29.49, 26.31, 22.91, 14.32; MALDI TOF MS: *m/z* for $C_{141}H_{220}N_9O_9[M+H^+]$, calculated: 2184.7068, Found: 2184.1720.

Synthesis of **TZ4**:

4,4′,4″-*s*-triazine-2,4,6-triyl-tribenzoic acid (2.5 mmol) in 6 mL of thionyl chloride and one drop of DMF (catalytic amount) was refluxed for 24 h. The excess of thionyl chloride was removed by distillation and then the crude product was dried in vacuo and used for the next reaction without further purification and characterization. A solution of 4,4′,4″-*s*-triazine-2,4,6-triyl-tribenzoic acid chloride (2.2 mmol, 1 equiv.) in THF was added dropwise into a solution of 3,4,5-tris(hexadecyloxy)benzhydrazide (6.8 mmol, 3.05 equiv.) and triethylamine (6.6 mmol, 3 equiv.) in THF under argon atmosphere. The reaction mixture was refluxed for 18 h. After cooling to room temperature, THF was evaporated in rotavapor and the residue was extracted with ethyl acetate and concentrated. The resulting crude product was directly used for next reaction. The crude product (0.3 mmol, 1 equiv.) was dissolved in $POCl_3$ (20 equiv.) and refluxed for about 16 h. The whole solution was slowly added to ice water and extracted with chloroform. The extract was washed with brine, dried over anhydrous Na_2SO_4 and then concentrated. Then, the crude product was further purified through column chromatography on neutral alumina. Elution with 20-30% chloroform-hexane yielded the desired product.

R_f = 0.45 (60% chloroform-hexane); off white solid; yield: 50%; IR (KBr pellet): ν_{max} in cm^{-1} 3444, 2919, 2850, 1592, 1556, 1521, 1493, 1375, 1238, 1121, 1015, 843, 794, 696, 519; ^{1}H NMR ($CDCl_3$, 600 MHz, 298 K): δ 8.96 (d, 6H, *J* = 8.4Hz, H_{Ar}), 8.38 (d, 6H, *J* =

8.4Hz, H_{Ar}), 7.37 (s, 6H, H_{Ar}), 4.11 (t, 12H, 6 × OCH_2), 4.07 (t, 6H, 3 × OCH_2), 1.85-1.90 (m, 12H, 6 × CH_2),1.76-1.81 (m, 6H, 3 × CH_2), 1.48-1.55 (m, 18H, 9 × CH_2), 1.33-1.41 (m, 216H, 108 × CH_2), 0.87 (t, 27H, 9 × CH_3); ^{13}C NMR ($CDCl_3$, 150 MHz, 298 K): δ 171.19, 165.40, 164.02, 153.87, 141.89, 138.63, 129.83, 127.92, 127.33, 118.39, 105.78, 73.87, 69.65, 32.15, 30.62, 29.96, 29.91, 29.85, 29.70, 29.60, 26.36, 22.91, 14.33; MALDI TOF MS: *m/z* for $C_{189}H_{316}N_9O_{12}[M+H^+]$, calculated: 2906.4461, Found: 2906.1250.

Synthesis of **TZ5**:

A suspension of 4,4′,4″-*s*-triazine-2,4,6-triyl-tribenzoic acid (1.5 mmol), thionyl chloride (6 mL) and one drop of DMF (catalytic amount) was refluxed for 24 h. The excess of thionyl chloride was removed by distillation and then the crude product was dried *in vacuo* and used for the next reaction without further purification and characterization. A solution of 4,4′,4″-*s*-triazine-2,4,6-triyl-tribenzoic acid chloride (1.2 mmol, 1 equiv.) in THF was added dropwise into a solution of ethyl 4-(dodecyloxy)benzohydrazide(3.96 mmol, 3.3 equiv.) and triethylamine (3.6 mmol, 3 equiv.) in THF under argon atmosphere. The reaction mixture was refluxed for 18 h. After cooling to room temperature, THF was evaporated in rotavapor and the residue was extracted with ethyl acetate and concentrated. The resulting crude product was directly used for next reaction. The crude product (0.2 mmol, 1 equiv.) was dissolved in $POCl_3$ (20 equiv.) and refluxed for about 16 h. The whole solution was slowly added to ice water and extracted with chloroform. The extract was washed with brine, dried over anhydrous Na_2SO_4 and then concentrated. Then, the crude product was further purified through column chromatography on neutral alumina. Elution with 60-70% DCM-hexane yielded the desired product.

R_f = 0.25 (40% DCM-hexane); off white solid; yield: 43%; IR (KBr pellet): ν_{max} in cm^{-1} 3444, 2919, 2850, 1592, 1556, 1521, 1493, 1375, 1238, 1121, 1015, 843, 794, 696, 519; ^{1}H NMR ($CDCl_3$, 600 MHz, 298 K): δ 8.69 (d, 6H, *J* = 6Hz, H_{Ar}), 8.15 (d, 6H, *J* = 6Hz, H_{Ar}), 7.99 (d, 6H, *J* = 8.4Hz, H_{Ar}), 6.98 (d, 6H, *J* = 6Hz, H_{Ar}), 4.00 (t, 6H, *J* = 6Hz, 3 × OCH_2), 1.82-1.83 (m, 6H, 3 × CH_2), 1.47-1.51 (m, 6H, 3 × CH_2), 1.15-1.44 (m, 48H, 24 × CH_2), 0.88 (t, 9H, 3 × CH_3); ^{13}C NMR ($CDCl_3$, 150 MHz, 298 K): δ 170.77, 165.16, 163.96, 160.90, 138.49, 138.45, 129.71, 127.73, 127.20, 125.08, 105.37, 68.68, 32.19,

29.99, 29.94, 29.76, 29.63, 29.53, 26.34, 22.95, 14.36; MALDI TOF MS: *m/z* for $C_{81}H_{100}N_9O_6[M+H^+]$, calculated: 1294.7797, Found: 1294.6316.

Synthesis of **TZ6**:

4,4′,4″-*s*-triazine-2,4,6-triyl-tribenzoic acid (1.5 mmol) in 6 mL of thionyl chloride and one drop of DMF (catalytic amount) was refluxed for 24 h. The excess of thionyl chloride was removed by distillation and then the crude product was dried in vacuo and used for the next reaction without further purification and characterization. A solution of 4,4′,4″-*s*-triazine-2,4,6-triyl-tribenzoic acid chloride (1.2 mmol, 1 equiv.) in THF was added drop wise into a solution of 3,4,-bis(dodecyloxy) benzhydrazide (3.96 mmol, 3.3 equiv.) and triethylamine (3.6 mmol, 3 equiv.) in THF under argon atmosphere. The reaction mixture was refluxed for 18 h. After cooling to room temperature, THF was evaporated in rotavapor and the residue was extracted with ethyl acetate and concentrated. The resulting crude product was directly used for next reaction. The crude product (0.2 mmol, 1 equiv.) was dissolved in $POCl_3$ (20 equiv.) and refluxed for about 16 h. The whole solution was slowly added to ice water and extracted with chloroform. The extract was washed with brine, dried over anhydrous Na_2SO_4 and then concentrated. Then, the crude product was further purified through column chromatography on neutral alumina. Elution with 40-50% DCM-hexane yielded the desired product.

R_f = 0.4 (30% DCM-hexane); pale yellow solid; yield: 52%; IR (KBr pellet): ν_{max} in cm^{-1} 3444, 2922, 2852, 1601, 1554, 1518, 1463, 1373, 1232, 1170, 1015, 819, 741, 677, 517; ^{1}H NMR ($CDCl_3$, 600 MHz, 298 K): δ 8.75 (d, 6H, *J* = 6.6Hz, H_{Ar}), 8.20 (d, 6H, *J* = 6.6Hz, H_{Ar}), 7.58 (d, 6H, *J* = 6Hz, H_{Ar}), 6.93 (d, 3H, *J* = 6Hz, H_{Ar}), 4.04-4.07 (m, 12H, 6 × OCH_2), 1.84-1.89 (m, 12H, 6 × CH_2), 1.48-1.54 (m, 12H, 6 × CH_2), 1.25-1.42 (m, 96H, 48 × CH_2), 0.87 (t, 18H, *J* = 6Hz, 6 × CH_3); ^{13}C NMR ($CDCl_3$, 150 MHz, 298 K): δ 171.15, 165.34, 163.79, 152.71, 149.61, 138.52, 129.82, 128.01, 127.24, 120.75, 116.17, 113.09, 111.90, 69.67, 69.37, 32.17, 29.97, 29.91, 29.72, 29.69, 29.60, 29.49, 29.39, 26.30, 26.26, 22.92, 14.35; MALDI TOF MS: *m/z* for $C_{117}H_{172}N_9O_9[M+H^+]$, calculated: 1848.3312, Found: 1848.3049.

Synthesis of **TZ7**:

4,4′,4″-*s*-triazine-2,4,6-triyl-tribenzoic acid (1.5 mmol) in 6 mL of thionyl chloride and one drop of DMF (catalytic amount) was refluxed for 24 h. The excess of thionyl chloride

was removed by distillation and then the crude product was dried in vacuo and used for the next reaction without further purification and characterization. A solution of 4,4′,4″-*s*-triazine-2,4,6-triyl-tribenzoic acid chloride (1.2 mmol, 1 equiv.) in THF was added dropwise into a solution of 3,5,-bis(dodecyloxy)benzhydrazide (3.96 mmol, 3.3 equiv.) and triethylamine (3.6 mmol, 3 equiv.) in THF under argon atmosphere. The reaction mixture was refluxed for 18 h. After cooling to room temperature, THF was evaporated in rotavapor and the residue was extracted with ethyl acetate and concentrated. The resulting crude product was directly used for next reaction. The crude product (0.2 mmol, 1 equiv.) was dissolved in $POCl_3$ (20 equiv.) and refluxed for about 16 h. The whole solution was slowly added to ice water and extracted with chloroform. The extract was washed with brine, dried over anhydrous Na_2SO_4 and then concentrated. Then, the crude product was further purified through column chromatography on neutral alumina. Elution with 40-50% DCM-hexane yielded the desired product.

R_f = 0.3 (30% DCM-hexane); white sticky solid; yield: 46%; IR (KBr pellet): ν_{max} in cm^{-1} 3447, 2920, 2850, 1607, 1558, 1515, 1465, 1370, 1275, 1215, 1014, 816, 738, 697, 520; ^{1}H NMR ($CDCl_3$, 600 MHz, 298 K): δ 8.74 (d, 6H, *J* = 8.4Hz, H_{Ar}), 8.20 (d, 6H, *J* = 8.4Hz, H_{Ar}), 7.15 (s, 6H, H_{Ar}), 6.54 (s, 3H, H_{Ar}), 3.96 (t, 12H, *J* = 6Hz, 6 × OCH_2), 1.79-1.82 (m, 12H, 6 × CH_2), 1.42-1.49 (m, 12H, 6 × CH_2), 1.26-1.39 (m, 96H, 48 × CH_2), 0.87 (t, 18H, *J* = 6Hz, 6 × CH_3); ^{13}C NMR ($CDCl_3$, 150 MHz, 298 K): δ 170.76, 165.15, 163.99, 163.95, 160.89, 138.44, 129.68, 127.72, 127.19, 125.07, 105.36, 68.67, 32.18, 29.98, 29.93, 29.75, 29.62, 29.52, 26.33, 22.94, 14.35; MALDI TOF MS: *m/z* for $C_{117}H_{172}N_9O_9[M+H^+]$, calculated: 1848.3312, Found: 1848.4331.

Synthesis of **TZ8**:

4,4′,4″-*s*-triazine-2,4,6-triyl-tribenzoic acid (1.5 mmol) in 6 mL of thionyl chloride and one drop of DMF (catalytic amount) was refluxed for 24 h. The excess of thionyl chloride was removed by distillation and then the crude product was dried in vacuo and used for the next reaction without further purification and characterization. A solution of 4,4′,4″-*s*-triazine-2,4,6-triyl-tribenzoic acid chloride (1.2 mmol, 1 equiv.) in THF was added dropwise into a solution of 3,4,5-tris(dodecyloxy)benzhydrazide (3.96 mmol, 3.3 equiv.) and triethylamine (3.6 mmol, 3 equiv.) in THF under argon atmosphere. The reaction mixture was refluxed for 18 h. After cooling to room temperature, THF was evaporated in rotavapor and the residue was extracted with ethyl acetate and concentrated. The resulting

crude product was directly used for next reaction. The crude product (0.2 mmol, 1 equiv.) was dissolved in $POCl_3$ (20 equiv.) and refluxed for about 16 h. The whole solution was slowly added to ice water and extracted with chloroform. The extract was washed with brine, dried over anhydrous Na_2SO_4 and then concentrated. Then, the crude product was further purified through column chromatography on neutral alumina. Elution with 20-30% DCM-hexane yielded the desired product.

R_f = 0.35 (40% DCM-hexane); off white solid; yield: 52%; IR (KBr pellet): ν_{max} in cm^{-1} 3444, 2923, 2851, 1610, 1581, 1518, 1495, 1367, 1256, 1176, 1016, 800, 745, 657, 516; ^{1}H NMR ($CDCl_3$, 600 MHz, 298 K): δ 8.96 (d, 6H, *J* = 6Hz, H_{Ar}), 8.38 (d, 6H, *J* = 6Hz, H_{Ar}), 7.23 (s, 6H, H_{Ar}), 4.11 (t, 12H, *J* = 6Hz, 6 × OCH_2), 4.06 (t, 6H, *J* = 6Hz, 3 × OCH_2), 1.86-1.89 (m, 12H, 6 × CH_2),1.51-1.57 (m, 6H, 3 × CH_2), 1.37-1.39 (m, 18H, 9 × CH_2), 1.25-1.34 (m, 144H, 72 × CH_2), 0.86 (t, 27H, *J* = 6Hz, 9 × CH_3); ^{13}C NMR ($CDCl_3$, 150 MHz, 298 K): δ 171.21, 165.43, 164.05, 153.89, 141.92, 138.66, 129.86, 127.95, 127.36, 118.42, 105.81, 73.90, 69.68, 32.18, 30.65, 29.99, 29.94, 29.88, 29.73, 29.63, 26.39, 22.94, 14.36; MALDI TOF MS: *m/z* for $C_{153}H_{244}N_9O_{12}[M+H^+]$, calculated: 2400.8793, Found: 2400.6810.

2.5. References

1. (a) R. J. Bushby and O. R. Lozman, *Current Opinion in Colloid & Interface Science,* 2002, **7**, 343-354; (b) S. Laschat, A. Baro, N. Steinke, F. Giesselmann, C. Hägele, G. Scalia, R. Judele, E. Kapatsina, S. Sauer, A. Schreivogel and M. Tosoni, *Angew. Chem. Int. Ed.*, 2007, **46**, 4832-4887; (c) S. Kumar, *Isr. J. Chem.*, 2012, **52**, 820-829; (d) T. Wöhrle, I. Wurzbach, J. Kirres, A. Kostidou, N. Kapernaum, J. Litterscheidt, J. C. Haenle, P. Staffeld, A. Baro, F. Giesselmann and S. Laschat, *Chem. Rev.,* 2016, **116**, 1139-1241.
2. J. W. Goodby, P. J. Collings, T. Kato, C. Tschierske, H. Gleeson and P. Raynes, *Handbook of Liquid Crystals: Fundamentals* ed., Wiley-VCH, Weinheim, Germany, 2014, **1**.
3. M. Lehmann, *Chem. Eur. J.*, 2009, **15**, 3638-3651.
4. (a) H. Detert, M. Lehmann and H. Meier, *Materials*, 2010, **3**, 3218-3330; (b) B. Roy, N. De and K. C. Majumdar, *Chem. Eur. J.*, 2012, **18**, 14560-14588.
5. (a) G. H. Mehl, A. J. Thornton and J. W. Goodby, *Mol. Cryst. Liq. Cryst.*, 1999, **332**, 455-461; (b) D. Goldmann, D. Janietz, C. Schmidt and J. H. Wendorff, *Liq. Cryst.*, 1998, **25**, 711-719; (c) J. Barberá, L. Puig, P. Romero, J. L. Serrano and T. Sierra, *J. Am. Chem. Soc.*, 2005, **127**, 458-464.
6. F. Yang, J. Xie, H. Guo, B. Xu and C. Li, *Liq. Cryst.*, 2012, **39**, 1368-1374.
7. (a) M. B. Steffensen, E. Hollink, F. Kuschel, M. Bauer and E. E. Simanek, *J. Polym. Sci., Part A: Polym. Chem.*, 2006, **44**, 3411; (b) L. L. Lai, C. H. Lee, L. Y. Wang, K. L. Cheng and H. F. Hsu, *J. Org. Chem.*, 2008, **73**, 485-490.
8. H. C. Jeong, M. J. Piao, S. H. Lee, M. Y. Jeong, K. M. Kang, G. Park, S. J. Jeon and B. R. Cho, *Adv. Funct. Mater.*, 2004, **14**, 64-70.
9. K. C. Majumdar, N. De, B. Roy and A. Bhaumik, *Liq. Cryst.*, 2010, **37**, 1459-1464.
10. (a) W. Shu and S. Valiyaveettil, *Chem. Commun*., 2002, 1350-1351; (b) H. Lee, D. Kim, H. K. Lee, W. Qiu, N. K. Oh, W. C. Zin and K. Kim, *Tetrahedron Lett.*, 2004, **45**, 1019-1022.
11. S. Kotha, D. Kashinath and S. Kumar, *Tetrahedron Lett*., 2008, **49**, 5419-5423.
12. (a) H. C. Holst, T. Pakula and H. Meier, *Tetrahedron*, 2004, **60**, 6765-6775; (b) H. K. Dambal and C. V. Yelamaggad, *Tetrahedron Lett*., 2012, **53**, 186-190.
13. (a) C. H. Lee and T. Yamamoto, *Tetrahedron Lett.*, 2001, **42**, 3993-3996; (b) C. H. Lee and T. Yamamoto, *Bull. Chem. Soc. Jpn.*, 2002, **75**, 615-618.
14. R. Bai, S. Li, Y. Zou, C. Pan, P. Xie, B. Kong, X. Zhou and R. Zhang, *Liq. Cryst.*, 2001, **28**, 1873-1876.
15. (a) E. Beltran, J. L. Serrano, T. Sierra and R. Gimenez, *Org. Lett*., 2010, **12**, 1404-1407; (b) E. Beltran, J. L. Serrano, T. Sierra and R. Gimenez, *J. Mater. Chem.*, 2012, **22**, 7797-7805.
16. T. Yasuda, T. Shimizu, F. Liu, G. Ungar and T. Kato, *J. Am. Chem. Soc.*, 2011, **133**, 13437-13444.
17. H. W. Gibson, D. L. Dotson, H. Marand and T. M. Swager, *Mol. Cry. Liq. Cry.*, 2006, **326**, 113-138.
18. Y. D. Zhang, K. G. Jespersen, M. Kempe, J. A. Kornfield, S. Barlow, B. Kippelen and S. R. Marder, *Langmuir*, 2003, **19**, 6534-6536.
19. (a) R. Cristiano, D. M. P. D. O. Santos and H. Gallardo, *Liq. Cryst.*, 2005, **32**, 7-14; (b) S. K. Pathak, R. K. Gupta, S. Nath, D. S. Shankar Rao, S. K. Prasad and A. S. Achalkumar, *J. Mater. Chem. C*, 2015, **3**, 2940-2952.
20. H. Yu, B. Liu, Y. Wang, J. Wang and Q. Hao, *SoftMatter*, 2011, **7**, 5113-5115.

21. H. Dai, X. Yang, X. Tan, F. Su, X. Cheng, F. Liu and C. Tschierske, *Chem. Commun.*, 2013, **49**, 10617-10619.
22. S. K. Pathak, R. K. Gupta, S. Nath, D. S. Shankar Rao, S. K. Prasad and A. S. Achalkumar, *J. Mater. Chem. C*, 2015, **3**, 8166-8182.
23. D. Sun, S. Ma, Y. Ke, D. J. Collins and H. C. Zhou, *J. Am. Chem. Soc.*, 2006, **128**, 3896-3897.
24. Z. Lin, T. J. Emge and R. Warmuth, *Chem. Eur. J.*, 2011, **17**, 9395-9405.
25. J. Barbera, M. A. Godoy, P. I. Hidalgo, M. L. Parra, J. A. Ulloa and J. M. Vergara, *Liq. Cryst*., 2007, **34**, 1249-1267.
26. (a) J. Barbera, R. Gimenez and J. L. Serrano, *Chem. Mater*., 2000, **12**, 481-489; (b) J. L. Serrano and T. Sierra, *Chem. Eur. J.*, 2000, **6**, 759-766; (c) S. Ito, M. Ando, A. Nomura, N. Morita, C. Kabuto, H. Mukai, K. Ohta, J. Kawakami, A. Yoshizawa and A. Tajiri, *J. Org. Chem*., 2005, **70**, 3939-3949; (d) A. Hayer, V. de Halleux, A. Kohler, A. El-Garoughy, E. W. Meijer, J. Barbera, J. Tant, J. Levin, M. Lehmann, J. Gierschner, J. Cornil and Y. H. Geerts, *J. Phys. Chem. B*, 2006, **110**, 7653-7659; (e) L. Alavarez, J. Barbera, L. Puig, P. Romero, J. L. Serrano and T. Sierra, *J. Mater. Chem.*, 2006, **16**, 3768-3773; (f) C. V. Yelamaggad, A. S. Achalkumar, D. S. S. Rao and S. K. Prasad, *J. Mater. Chem.*, 2007, **17**, 4521-4529; (g) C. V. Yelamaggad, A. S. Achalkumar, D. S. S. Rao and S. K. Prasad, *J. Org. Chem*., 2007, **72**, 8308-8318; (h) C. V. Yelamaggad, A. S. Achalkumar, D. S. S. Rao, M. Nobusawa, H. Akutsu, J. Yamada and S. Nakatsuji, *J. Mater. Chem.*, 2008, **18**, 3433-3437; (i) A. S. Achalkumar, U. S. Hiremath, D. S. Shankar Rao, S. Krishna Prasad and C. V. Yelamaggad, *J. Org. Chem.*, 2013, **78**, 527-544.
27. E. M. Garcia-Frutos, U. K. Pandey, R. Termine, A. Omenat, J. Barbera, J. L. Serrano, A. Golemme and B. GomezLor, *Angew. Chem. Int. Ed.*, 2011, **50**, 7399-7402.
28. F. Würthner, T. E. Kaiser and C. R. SahaMöller, *Angew. Chem. Int. Ed.*, 2011, **50**, 3376-3410.
29. D. D. Prabhu, N. S. S. Kumar, A. P. Sivadas, S. Varghese and S. Das, *J. Phys. Chem. B*, 2012, **116**, 13071-13080.
30. R. Fink, C. Frenz, M. Thelakkat and H. W. Schmidt, *Macromolecules*, 1997, **30**, 8177-8181.
31. H. Zhong, H. Lai and Q. Fang, *J. Phys. Chem. C*, 2011, **115**, 2423-2427.
32. N. A. Kukhta, J. Simokaitiene, D. Volyniuk, J. Ostrauskaite, J. V. Grazulevicius, G. Juska and V. Jankauskas, *Synthetic Metals*, 2014, **195**, 266-275.

Chapter 3

Effect of atomic-scale differences on the self-assembly of thiophene-based polycatenars in liquid crystalline and organogel states

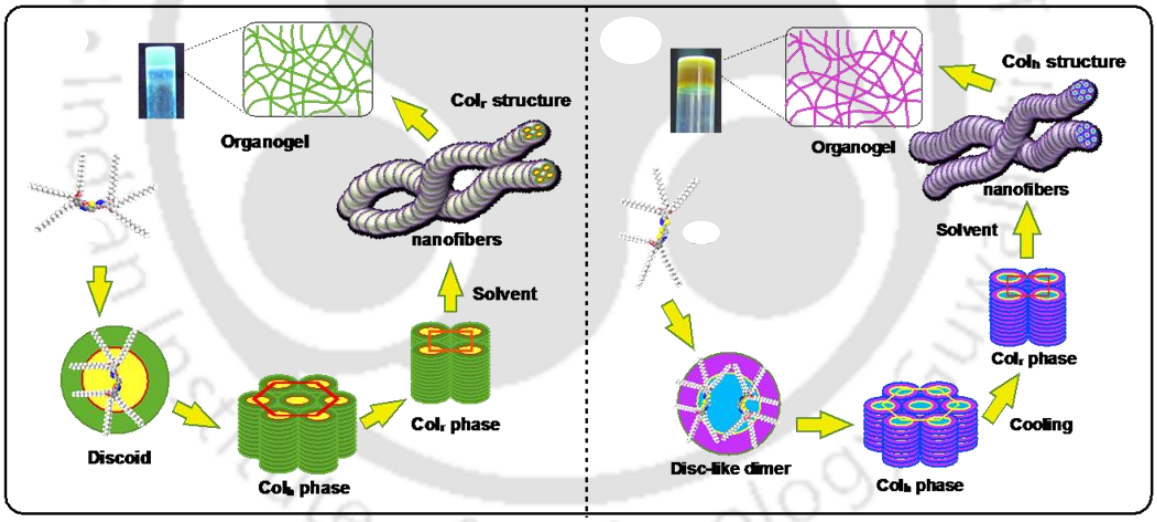

Results have been published in *Chem. Eur. J.*, 2016, **22**, 17843-17856.

3.1. Introduction

Thiophene-based molecular materials are an extensively studied type of heterocyclic materials because of their synthetic flexibility and applications as n-type (electron-rich) semiconductor systems.[1] Thiophene-based oligomers and polymers are known for their unique optoelectronic properties and have found utility in the fabrication of field-effect transistors,[2] light emitting diodes,[3] and photovoltaic cells.[4] Most oligothiophenes must be purified by vacuum-sublimation techniques due to their poor solubility. Thus, liquid-crystalline (LC) thiophene derivatives seem to be good alternatives due to their good solubility because of which they can be easily purified. Furthermore, good-quality thin films can be obtained by simple solution-processing techniques and further molecular alignment can be addressed through annealing. Most of the thiophene-based liquid crystals reported stabilize nematic and smectic phases.[5] A few oligomers with a higher number of flexible terminal tails were reported to stabilize columnar (Col) phases.[6] Stabilization of Col phases in this class of materials is beneficial because the stacking of molecules one above the other to form columns of indefinite length provides a pathway for one-dimensional charge migration. As mentioned earlier, the ease of processability makes the Col phase an ideal substitute for conjugated polymers or organic single crystals from the viewpoint of optoelectronic devices.[7] π-Conjugated molecules that contain strong donor (D) and acceptor(A) systems show intramolecular charge transfer and low bandgap properties, which make them attractive.[8] Kato *et. al.* reported star shaped molecules containing three donor thiophene moieties connected to a central electron-accepting triazine moiety, which exhibited a Col phase with ambipolar conductivity.[6b] 1,3,4-Oxadiazole derivatives, which are known for their electron-deficient and fluorescence nature, are finding applications in OLEDs as electron transport and electroluminescent layers.[9] These have been integrated into the liquid-crystal design to obtain conductive smectic or columnar mesophases.[10] 1,3,4-Thiadiazole derivatives are less often reported, but they also exhibit promising thermal and photophysical behavior.[11] The self-assembly of thiophene-based molecules into organogels has been studied extensively because of the enhanced charge transport behavior and optoelectronic properties due to molecular packing in the self-assembled systems.[3a,12] In most cases, such self-assembled systems are assisted by intermolecular hydrogen bonding augmented by peptide or amide units. Recently, a few liquid crystalline polycatenars with 1,3,4-oxadiazole units have exhibited gelation, which is exclusively supported by π-π

interactions.[13] However, there are no reports on thiophene-containing organogels, which are stabilized mainly by π-π interactions. Tailoring the molecular structure to obtain these long-range-ordered self-assembled structures is important, given their potential applications in optoelectronic devices.

Considering all these aspects, we aspired to design a new polycatenar system that contains a central electron-rich thiophene unit connected to two electron-deficient fluorophores, such as substituted 1,3,4-oxadiazole or 1,3,4-thiadiazole units. We expected that these compounds would show good luminescence, thermal behavior, and ability to undergo organogelation. The alternate arrangement of donor and acceptor moieties may modulate the bandgap of these molecules. We envisaged that the presence of oxadiazole and thiadiazole could result in a drastic difference in the self-assembly and related macroscopic properties. The number of flexible chains, their positions and their length were modified to understand the impact on the self-assembly and photophysical properties of these polycatenar systems.

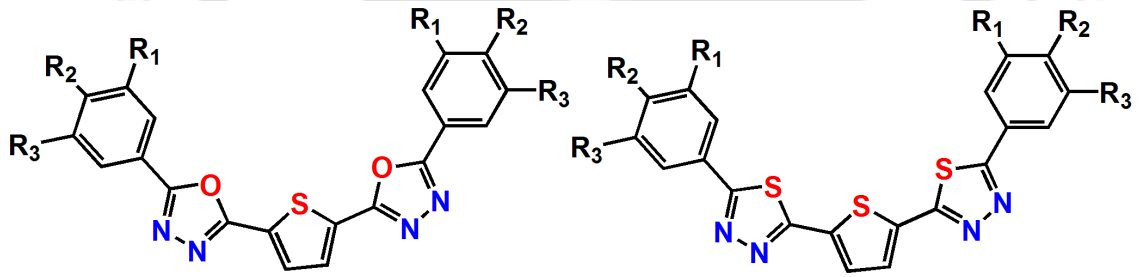

TO1: R_1 = H, R_2 = R_3 = *n*-$OC_{16}H_{33}$
TO2: R_1 = R_3 = *n*-$OC_{16}H_{33}$, R_2 = H
TO3: R_1 = R_2 = R_3 = *n*-$OC_{16}H_{33}$
TO4: R_1 = R_2 = R_3 = *n*-$OC_{10}H_{21}$

TT1: R_1 = H, R_2 = R_3 = *n*-$OC_{16}H_{33}$
TT2: R_1 = R_3 = *n*-$OC_{16}H_{33}$, R_2 = H
TT3: R_1 = R_2 = R_3 = *n*-$OC_{16}H_{33}$
TT4: R_1 = R_2 = R_3 = *n*-$OC_{10}H_{21}$

Figure 3.1. The molecular structures of thiophene based 1,3,4-oxadiazole and 1,3,4-thiadiazole derivatives.

3.2. Results and discussion

3.2.1. Synthesis and Characterization

The synthetic route is elucidated in scheme 3.1. Common methodologies for the synthesis were same as reported elsewhere.[11] Alkoxyethyl benzoates **3b-d, 5d** were prepared by using the williamson's ether synthesis. Alkylation of ethyl-3,4-dihydroxy benzoate gave compound **3b**. Ethyl-3,5-dihydroxy benzoate was O-alkylated to give compound **3c**, whereas alkylation of ethyl-3,4,5-trihydroxy benzoate gave compounds **3d** and **5d**. On treatment with hydrazine hydrate, these esters gave respective hydrazides **4b-d, 6d**, which

were treated with thiophene-2,5-diacid chloride under basic conditions to give the corresponding hydrazides (**7a–d**). These hydrazides were treated with phosphoryl chloride to give the corresponding dioxadiazoles (**TO1-4**) or with Lawesson's reagent to give the thiadiazole derivatives (**TT1-4**). The electron-withdrawing nature of the oxadiazole units compared with the thiadiazole units is reflected by the low-field ^{1}H NMR signals obtained for compounds **TO1-4** with respect to compounds **TT1-4** (see the section 3.4). For example, the ^{1}H NMR spectrum of compound **TO3** with two oxadiazole units showed low-field signals for protons H_a and H_b compared with those of compound **TT3** with two thiadiazole units (Fig. 3.2). The structures of all the intermediates and target molecules were confirmed using ^{1}H NMR, ^{13}C NMR, IR spectroscopy, HRMS and MALDI-TOF mass spectra. (See experimental part presented in section 3.4 for the details).

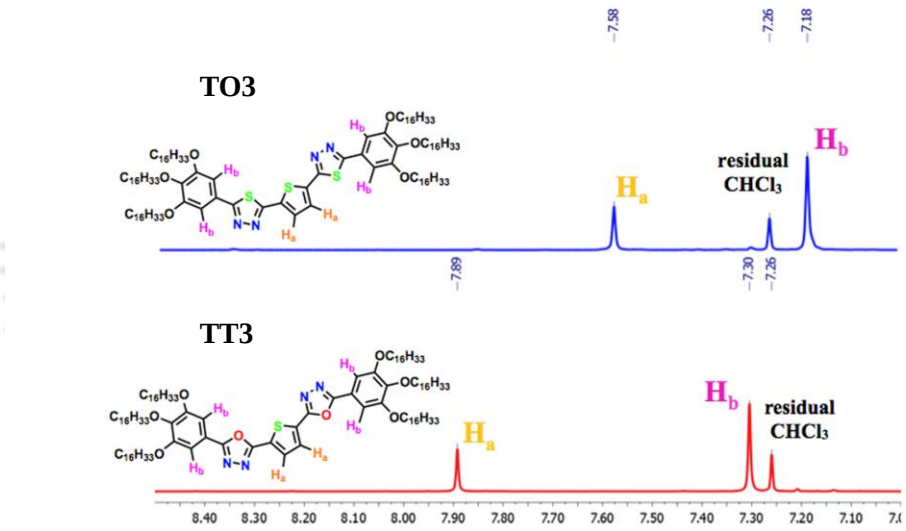

Figure 3.2. Overlay of the expanded portion of the ^{1}H NMR spectra ($CDCl_3$, 600 MHz) of **TO3** and **TT3**.

3.2.2. Thermal behavior

All the compounds were investigated by using thermogravimetric analysis (TGA), polarizing optical microscopy (POM) and differential scanning calorimetry (DSC). Polycatenars were stable up to at least 315 ^{o}C, except for compounds **TO2** and **TT2**. These compounds, which have alkoxy groups at the 3,5-positions, were stable only up to approximately 230 ^{o}C, as shown by the TGA results (Fig. 3.4). The mesophase-type, phase-transition temperatures and associated enthalpy changes are presented in Table 3.1. Fig. 3.3 graphically represents the thermal behavior of compounds in the second heating scans.

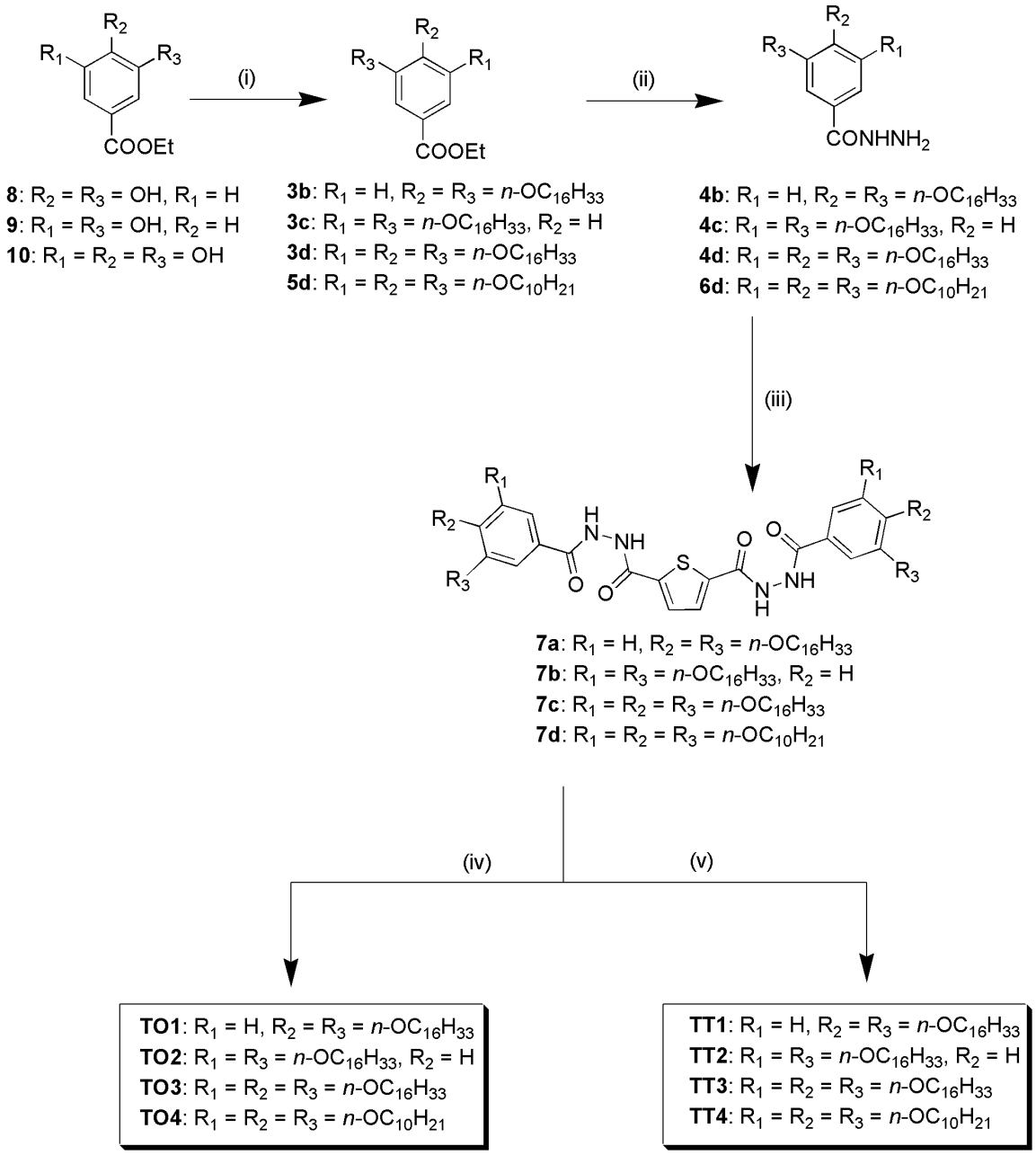

Scheme 3.1. Synthesis of thiophene based 1,3,4-oxadiazole and 1,3,4-thiadiazole derivatives. i) *n*-bromoalkane, anhydrous K_2CO_3, DMF, 80 ^oC, 24h (70-80%); ii) $NH_2NH_2{\cdot}H_2O$, ethanol or butanol, reflux, 48h (70-80%); iii) thiophene-2,5-acidchloride, THF, Et_3N, 12h, reflux (70-80%); iv) $POCl_3$, reflux, 17h (60-70%); v) Lawesson's reagent, toluene, reflux, 17h (40-50%).

A crystalline sample of oxadiazole-based polycatenar **TO1**, with four hexadecyloxy tails connected to the terminal benzene rings at the 3,4-positions, exhibited enantiotropic mesomorphism; on heating, the crystalline sample showed a transition to a birefringent fluid at a temperature of approximately 113 ^oC, after passing through a few crystal-to-crystal transitions as observed in the DSC scans. The birefringent fluid was shearable and converted to an isotropic liquid at a temperature of about 138 ^oC. On

cooling (5 ^{o}C min^{-1}), the isotropic liquid showed a transition to a birefringent texture comprised of a mosaic pattern interspersed with homeotropic domains (Fig. 3.5a). The mesophase existed up to 129 ^{o}C over a temperature range of 9 ^{o}C and then transformed into another mesophase, as shown by a sudden change in the birefringence accompanied by an enthalpy change in the DSC (Fig. 3.5b, c). This mesophase existed up to around 88 ^{o}C, and then crystallized as observed with a loss of shearability and change in the textural pattern. The XRD studies were carried out at two different temperatures, that is, 136 and 122 ^{o}C (Table 3.2). The XRD pattern obtained at 136 ^{o}C showed several peaks in the low angle region with *d*-spacings of 44.41, 42.34, 41.28, 40.36, and 36.12 Å, along with a diffuse peak at a wide angle with a *d*-spacing of 4.61 Å. The wide-angle diffuse peak corresponds to the packing of flexible tails.

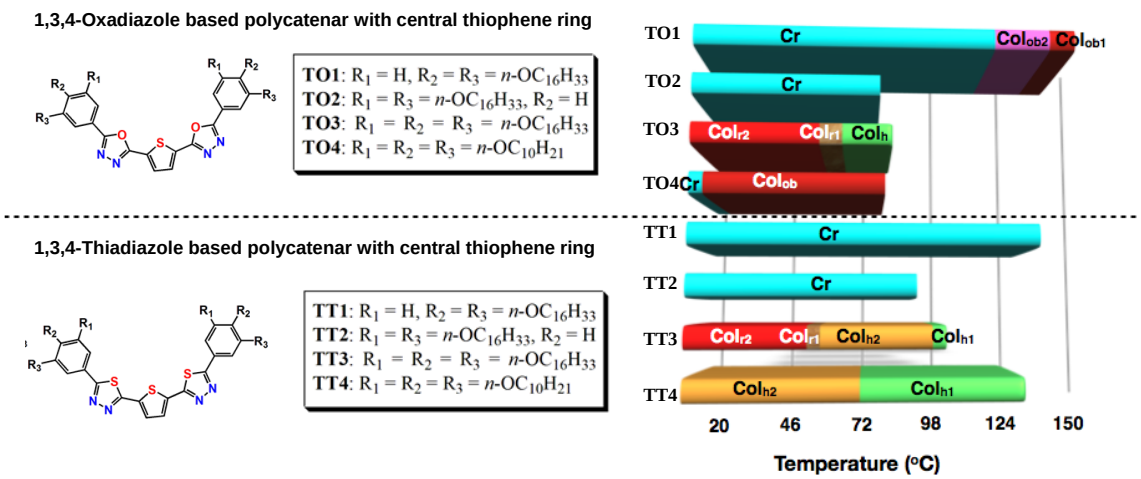

Figure 3.3. Bar graph summarizing the thermal behavior of **TO1-4** and **TT1-4** (second heating cycle); Col_{ob} = Columnar oblique phase, Col_r = Columnar rectangular phase, Col_h = Columnar hexagonal phase, Cr = Crystalline phase.

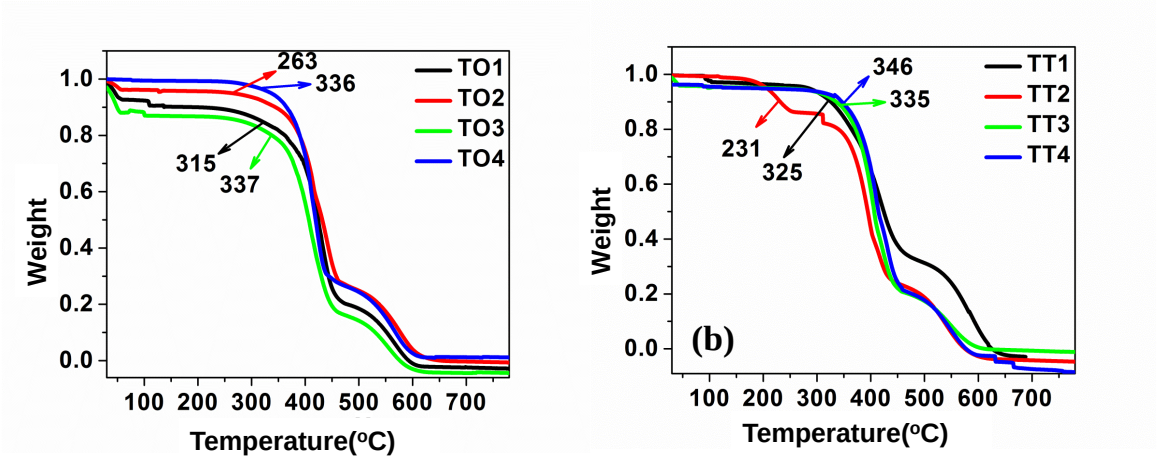

Figure 3.4. TGA curves of compounds **TO1-4** (a); compounds **TT1-4** (b) carried out at a rate of 10 ^{o}C/min under nitrogen atmosphere.

Table 3.1. Phase transition temperatures [a] (^{o}C) and corresponding enthalpies (kJ/mol) of polycatenar LCs.

Entry	Phase sequence	
	2nd Heating	**1st Cooling**
TO1	Cr 113.0 (138.1) Col_{ob2} 130.2 (28.4) Col_{ob1}138.1 (25.4) I	I 138.2 (24.8) Col_{ob1} 129.3 (27.3) Col_{ob2} 87.9 (125.7) Cr
TO2	Cr_1 29.1 (203.1) Cr_2 73.5 (124.1) Cr_3 77.3 (129.4) I	I 20.6 (142.38) Cr
TO3	Col_{r2} 58.8 (56.1) Col_{r1} 65.7 (127.07) Col_h 81.1(2.8) I	I 77 (3.9) Col_h 53.5 (127.5) Col_{r1} 48.7 (71.7) Col_{r2} [b]
TO4	Cr 24.24 (28.7) Col_{ob} 78.8 (10.5) I	I 75.4 (10.3) Col_{ob} 16.3 (16) Cr
TT1	Cr_1 64.2 (10.4) Cr_2 101.3 (19.8) Cr_3 105.8 (7.1) $Cr_4$125.8 (17.9) I	I 100.6 (33.2) Cr_3 91.2 (99.3) Cr_2 55.4 (10.6) Cr_1
TT2	Cr 88.3 (277.6) I	I 65.5 (278.5) Cr
TT3	Col_{r2} 55.8 (11.3) Col_{r1} 59.7 (65.4) Col_{h2} 93 (26.7) Col_{h1} 97.2 (20.2) I	I 96.1 (20.9) Col_{h1} 90.9 (25.4) Col_{h2} 55.1 (75.2) Col_{r1} 48.1 (10.9) Col_{r2} [b]
TT4	Col_{h2} 71.5 (16.0) Col_{h1} 120.5 (71.6) I	I 116.6 (69.5) Col_{h1} 67.4 (15.8) Col_{h2} [b]

[a]Peak temperatures in the DSC thermograms obtained during the first heating and cooling cycles at 5 ^{o}C/min. Col_h = Columnar hexagonal phase; [b]Mesophase freezes in glassy state and does not crystallize upto -20^{0}C. Col_{ob} = Columnar oblique phase, Col_r = Columnar rectangular phase, Col_h = Columnar hexagonal phase, Cr = Crystalline, I=Isotropic.

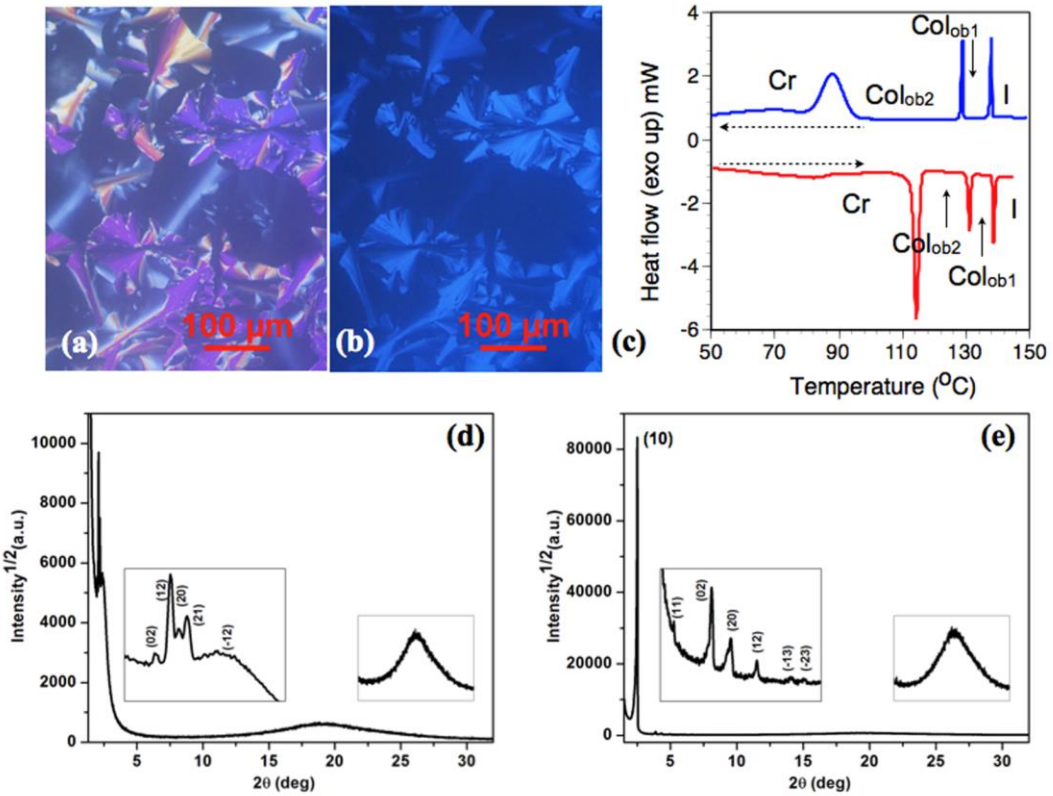

Figure 3.5. POM images of **TO1** a) at 132 (Col_{ob1} phase) and b) 122 ^{o}C (Col_{ob2} phase); c) DSC thermograms of **TO1** showing the first cooling (upper trace) and second heating (lower trace); XRD patterns obtained for **TO1** at d) 136 (Col_{ob1} phase) and e) 122 ^{o}C (Col_{ob2} phase).

The low-angle *d* spacings ($0 < 2\theta < 5^{o}$) correspond to the miller indices (02), (12), (20), (21) and (-12) of a columnar oblique (Col_{ob}) lattice. The lattice parameters derived from these reflections were found to be a = 83.9 and b = 90.2 Å with at tilt angle of $\gamma = 79.9^{o}$. The XRD pattern obtained at 122 ^{o}C showed a complex diffraction pattern with many peaks at low angles, but they could be assigned to another Col_{ob} phase with at tilt angle of $\gamma = 68^{o}$, and the lattice parameters a and b were reduced to almost half compared with the high-temperature Col_{ob} phase. The number of molecules in a unit cell (Z) was found to be 1.3. These two Col_{ob} phases are denoted as Col_{ob1} andCol_{ob2}.

Compound **TO2**, with four alkoxy tails connected to the terminal benzene rings at the 3- and 5-positions, proved to be crystalline, which shows the delicate balance involved in the LC self-assembly. Compound **TO3**, with six hexadecyloxy tails connected to the terminal benzene rings at the 3,4,5-positions, showed a mixture of pseudo-focal conic fans with mosaic patterns (Fig. 3.6a) on slow cooling of the isotropic liquid at a rate of 5 ^{o}C min^{-1}. DSC scans during cooling showed transitions at approximately 54 (ΔH = 127.5 kJ mol^{-1}) and 49 ^{o}C (ΔH = 71.7 kJmol^{-1}; Fig. 3.6d). The first transition did not show a major difference in the optical texture, except for a decrease in the birefringence (Fig. 3.6b), whereas the next transition showed the growth of a needle-like texture on the existing mosaic pattern (Fig. 3.6c). This pattern remained unchanged up to room temperature. We carried out XRD studies at 65 and 40 ^{o}C and room temperature (Table 3.2). The diffraction pattern at 65 ^{o}C exhibited two sharp reflections at low angles with *d* spacings of 35.47 and 20.53 Å, along with a diffuse peak at wide angle with a *d* spacing of 4.48 Å. The first two d spacings in the low-angle region correspond to Miller indices (10) and (11) of a columnar hexagonal (Col_{h}) lattice. The lattice parameters were found to be a = 41 Å. The spacing ratio is 1:0.578, which corresponds to a Col_{h} phase. The number of molecules derived from this lattice parameter in the unit hexagonal cell was found to be approximately 2. On cooling, this phase passed through a transition that spanned 5 ^{o}C, as seen in the DSC scans (Fig. 3.6d), with a slight change in the color of the textural pattern. We could not carry out XRD studies in this short interval. The XRD studies carried out at 40 and 25 ^{o}C were almost identical. For example, the XRD pattern at 25 ^{o}C exhibited several peaks in the low-to-mid angle region with d spacings of 37.52, 21.02, 18.27, and 13.68 Å that corresponded to Miller indices (01), (10), (11), and (12) of a rectangular lattice. The spacing ratios were 1:0.56:0.49:0.36, which vary slightly from the spacing ratio in the higher-temperature

XRD pattern obtained for Col_h phase. This could indicate the continuation of a higher-temperature Col_h phase. However, in view of the signatures from the DSC scans and a better agreement between the measured and calculated spacing values, we suggest that the lattices could be rectangular in nature. The wide angle region showed two diffuse peaks at 4.15 and 4.17 Å. Here, the first peak corresponds to the packing of flexible alkyl tails, whereas the second diffuse peak originates from the stacking of the cores. There was not much change in the lattice parameters and the number of molecules within the rectangular unit cell. The number of molecules in a unit cell was found to be one irrespective of temperature. We denote this phase as Col_{r2}, whereas the phase present between Col_h and Col_{r2} that spans a thermal range of 5 ^oC is denoted as the Col_{r1} phase because of the high enthalpy change associated with the phase transition from the high-temperature Col_h phase (Fig. 3.6a-c). Compound **TO4** with six *n*-decyloxy chains showed a mosaic texture on cooling from the isotropic liquid state, and the texture remained unchanged to room temperature (Fig. 3.7a, b). This compound showed crystallization at 16 ^oC, as determined from the DSC cooling scan (ΔH = 16 kJmol^{-1}; Fig. 3.7c). From the XRD studies, it was found that the Col_{ob} phase was stabilized throughout the thermal range (Fig. 3.7d, e). Thus polycatenars with shorter alkyl chains stabilized the Col_{ob} phase, whereas polycatenars with longer alkyl chains (**TO3**) stabilized the Col_h and Col_r phases.

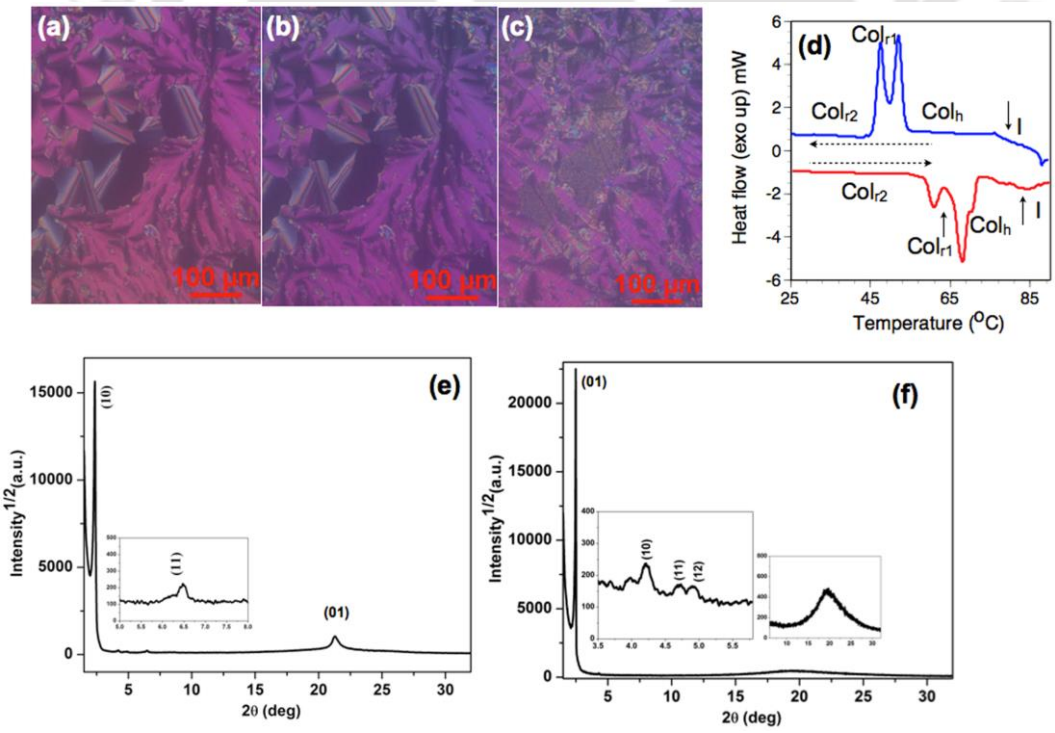

Figure 3.6. POM images of **TO3** at a) 65 (Col_h phase); b) 50 (Col_{r1} phase) and c) 28 ^oC (Col_{r2} phase); d) DSC thermograms of compound **TO3** showing first cooling (upper trace) and second heating (lower trace); XRD patterns obtained for **TO3** at e) 65 (Col_h phase) and f) 25 ^oC (Col_{r2} phase).

Table 3.2. Results of indexation of XRD profiles of compounds **TO1, TO3 & TO4**, at a given temperature (T) of the mesophases[a].

Compounds (*D*/Å)	Phase, Symmetry (T/°C)	d_{obs}(Å)[b]	d_{cal}(Å)[b]	Miller indices *hkl*	Lattice parameter[c]
TO1 (56.24)	Col_{ob1}, *p*1 (136)	44.41	44.41	02	*a* = 83.9 Å
		42.34	42.34	12	*b* = 90.2 Å
		41.28	41.28	20	*γ* = 79.9°
		40.36	40.24	21	
		36.12	36.53	-12	
		4.61(h_a)[d]			
	Col_{ob2}, *p*1 (122)	35.24	35.24	10	*a* = 38.0 Å
		22.80	22.80	-11	*b* = 44.1 Å
		20.44	20.44	02	*γ* = 68.0°
		17.83	17.62	20	
		15.29	15.36	-12	
		14.53	14.70	13	
		13.38	13.50	23	
		4.50 (h_a)[d]			
TO3 (60.30)	Col_h, *p6mm* (65)	35.47	35.47	10	*a* = 41 Å
		20.53	20.53	11	
		4.48 (h_a)[d]			
	Col_{r2}, *p2mm* (40)	37.63	37.63	01	*a* = 21.0 Å
		21.00	21.00	10	*b* = 37.6 Å
		18.28	18.33	11	
		13.64	14.01	12	
		4.20 (h_a)[d]			
		4.19 (h_c)[d]			
	Col_{r2}, p2mm (25)	37.52	37.52	01	*a* = 21.0 Å
		21.02	21.02	10	*b* = 37.5 Å
		18.27	18.34	11	
		13.68	13.99	12	
		4.15 (h_a)[d]			
		4.17 (h_c)[d]			
TO4 (45.35)	Col_{ob}, *p*1 (72)	33.78	33.78 33.01	01	*a* = 35.2 Å
		33.01	29.24	11	*b* = 40.7 Å
		29.24		10	*γ* = 56.1°
		4.50 (h_a)[d]			
		3.61 (h_c)[d]			
	Col_{ob}, *p*1 (50)	32.59	32.59	01	*a* = 34.4 Å
		30.71	30.71	11	*b* = 37.2 Å
		30.05	30.05	10	*γ* = 61.0°
		4.48 (h_a)[d]			
		3.59 (h_c)[d]			
	Col_{ob}, *p*1 (25)	32.09	32.09	11	*a* = 33.06 Å
		31.18	31.18	01	*b* = 32.12 Å
		15.57	15.57	12	*γ* = 76.1°
		4.41 (h_a)[d]			
		3.52 (h_c)[d]			

[a]The diameter (D) of the disc (estimated from Chem 3D Pro 8.0 molecular model software from Cambridge Soft). [b]d_{obs}: spacing observed; d_{cal}: spacing calculated (deduced from the lattice parameters; *a* and *b* for Col_{ob} and Col_r). [c] ***γ*** is the column tilt angle. [d]Spacings marked h_a and h_c correspond to diffuse reflections in the wide-angle region that arise from correlations between the alkyl chains and core regions, respectively.

The thermal behavior of the next series of polycatenars, in which the central thiophene ring was connected to two symmetrically substituted 1,3,4-thiadiazole rings, is discussed below. Compounds **TT1** and **TT2**, with four *n*-hexadecyloxy tails connected to the terminal benzene rings at the 3,4- and 3,5- positions, proved to be crystalline.

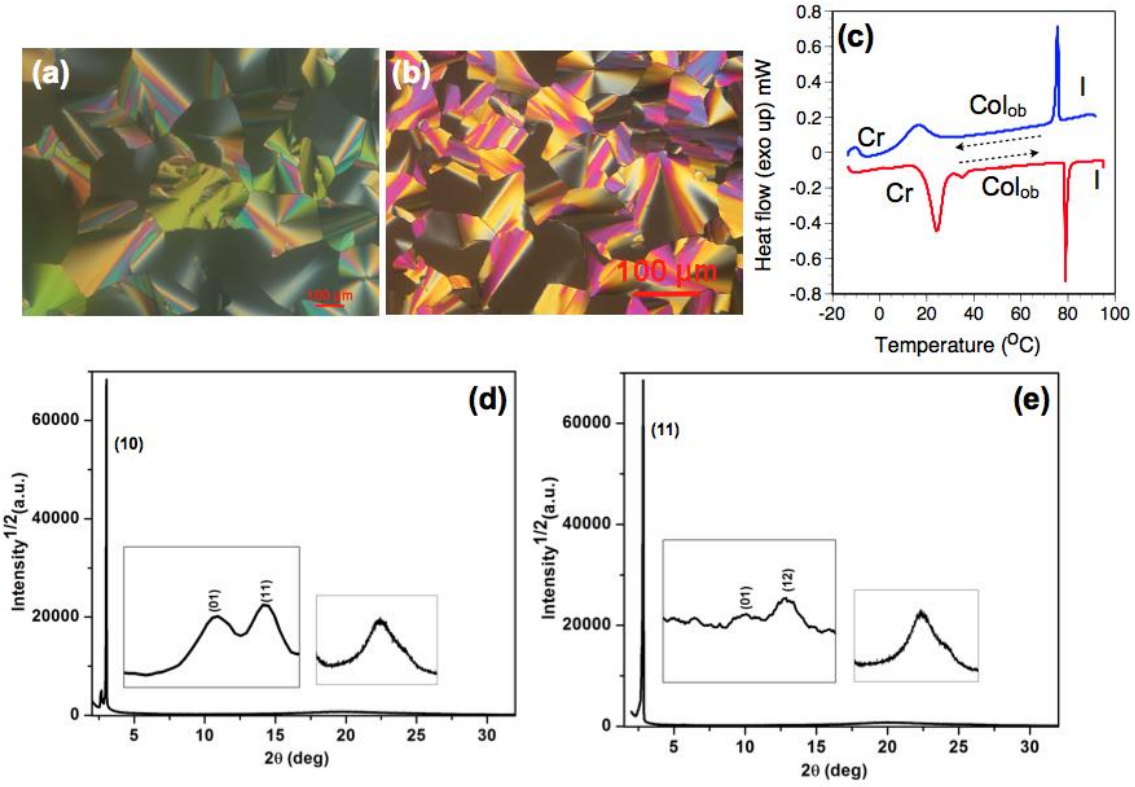

Figure 3.7. POM Images of compound **TO4** at a) 75 (Col$_{ob}$ phase) and b) 30 ^{o}C (Col$_{ob}$ phase); c) DSC thermograms of compound **TO4** showing first cooling (blue trace) and second heating (red trace); XRD patterns obtained for compound **TO4** at d) 72 (Col$_{ob}$ phase) and e) 25 ^{o}C (Col$_{ob}$ phase).

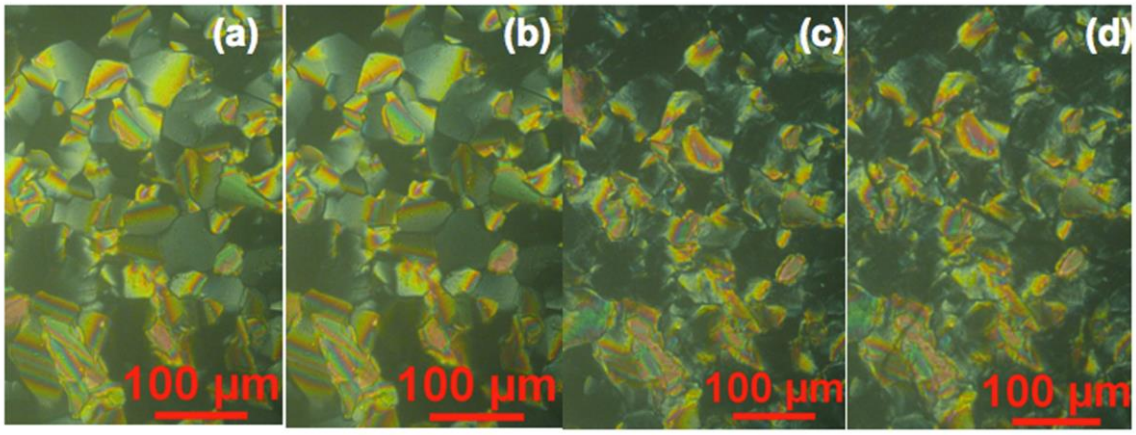

Figure 3.8. POM images of **TT3** at a) 95 (Col$_{h1}$ phase); b) 88 (Col$_{h2}$ phase); c) 50 (Col$_{r1}$ phase) and d) 25 ^{o}C (Col$_{r2}$ phase).

On cooling from the isotropic temperature, hexacatenar **TT3**, with six *n*-hexadecyloxy tails, showed a mosaic pattern interspersed with homeotropic domains, which is characteristic of a uniaxial phase (Fig. 3.8a). At approximately 91 ^{o}C (ΔH = 25.4 kJ mol^{-1}), a transition was observed in the DSC scan, whereas this change was very hard to detect in the POM (Fig. 3.9a and 3.8b). The XRD pattern obtained at 90 ^{o}C shows two peaks at low angle with d spacings of 35.51 and 20.49 Å, along with two diffuse peaks at wide angle with d spacings of 4.58 and 3.7 Å (Table 3.3, Fig. 3.9b). The first two low-angle peaks can be indexed to (10) and (11) reflections from a hexagonal lattice. The wide-angle spacing corresponds to the packing of alkyl tails and the distance between the cores. The calculated lattice parameter *a* was 41 Å, which is 30% less than the molecular length (60.4 Å) of the polycatenar in the all-*trans* conformation. This difference indicates an intercalation of the peripheral tails of neighboring molecules in the Col_h phase. We denote this columnar phase as Col_{h2}, whereas the one at higher temperature (>91 ^{o}C) is denoted as the Col_{h1} phase, based on the textural similarity. The number of molecules in the unit hexagonal cell was found to be two. This columnar phase spanned a thermal range of 36 ^{o}C before showing a textural change at approximately 48 ^{o}C, coupled with an enthalpy change of 104.9 kJmol^{-1}. The XRD pattern obtained at 50 ^{o}C showed *d* spacings of 42.01, 25.63, 10.31, 5.77, 4.27, and 4.22 Å (Fig. 3.9c). The relatively diffuse peak at 4.27 Å can be assigned to the packing of alkyl tails, whereas the other peaks correspond to Miller indices (01), (11), (31), and (45) of a rectangular lattice. The lattice parameters of the rectangular cell are *a* = 32.3 and *b* = 42 Å, with approximately two molecules (*Z* = 1.9) in the unit cell. We denoted this phase as Col_{r1}. The DSC scan showed a further transition at approximately 48 ^{o}C (ΔH = 38.5 kJ mol^{-1}), whereas the texture remained same without showing signs of crystallization to room temperature. The XRD pattern obtained at room temperature (Fig. 3.9d) exhibited additional reflections in the mid-angle region, but these reflections fit to a rectangular lattice and we denoted this phase as Col_{r2}.The two phases differ from each other with respect to the value of a. The Col_{r2} phase shows a reduced value of *a*, whereas the value of *b* remains almost same.

On cooling, the isotropic liquid of compound **TT4**, which is the lower homologue of compound **TT3** (with six *n*-decyloxy chains), showed the growth of spherulites that originated from the dark field of view (Fig. 3.10a). Further cooling resulted in a transformation of these spherulites into a mosaic pattern at around 67 ^{o}C (Fig. 3.10b), which remained unchanged to room temperature (Fig. 3.10c).

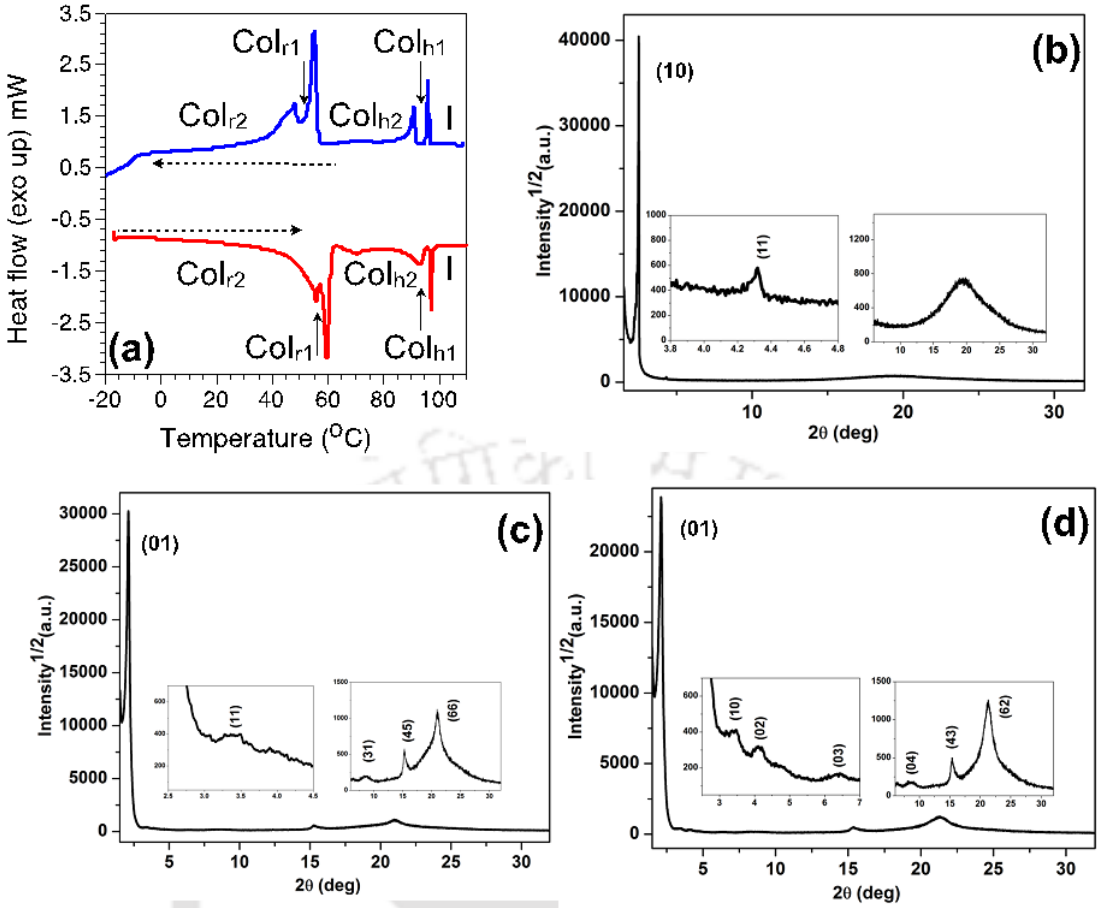

Figure 3.9. a) DSC thermograms of **TT3** showing first cooling (upper trace) and second heating (lower trace); XRD patterns obtained for **TT3** at b) 90 (Col$_{h2}$ phase); c) 50 (Col$_{r1}$ phase); and d) 25 °C (Col$_{r2}$ phase).

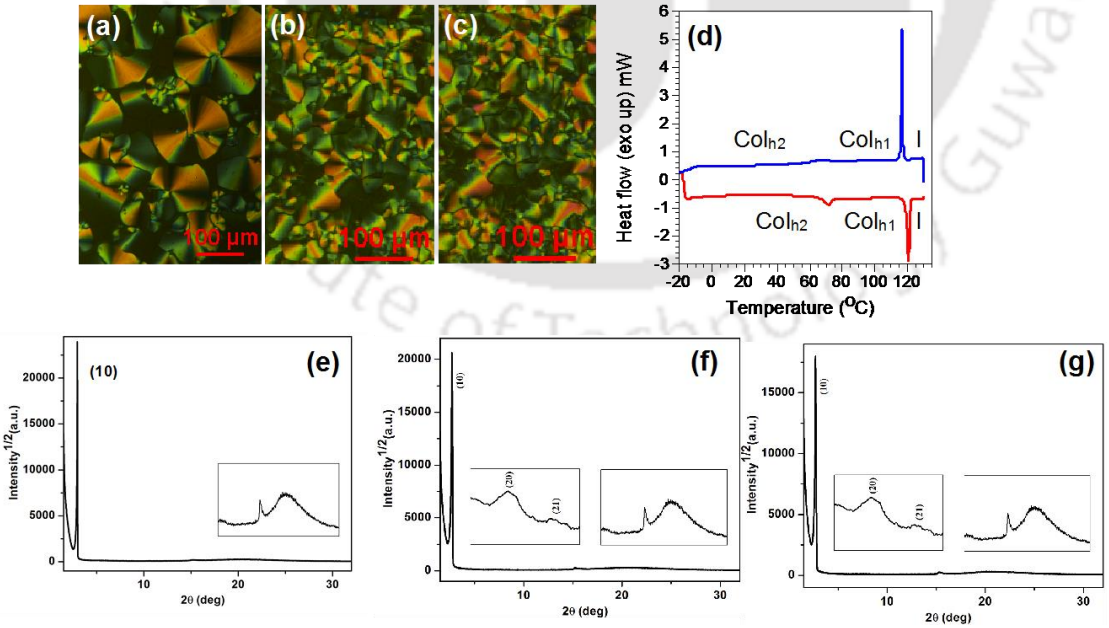

Figure 3.10. POM Images of compound **TT4** at a) 110 (Col$_{h1}$ phase); b) 65 (Col$_{h2}$ phase) and c) 28 °C (Col$_{h2}$ phase); d) DSC thermograms of compound **TT4** showing first cooling (blue trace) and second heating (red trace); XRD patterns obtained for compound **TT4** at e) 110 (Col$_{h1}$ phase); f) 60 (Col$_{h2}$ phase) and g) 25 °C (Col$_{h2}$ phase).

Table 3.3. Results of the (*hkl*) indexation of the XRD profiles of the compounds **TT3-4** at a given temperature (T) of the mesophases[a].

Compounds (*D*/Å)	Phase, Symmetry (T/°C)	d_{obs}(Å)[b]	d_{cal}(Å)[b]	Miller indices *hkl*	Lattice parameter (Å)
TT3 (60.40)	Col_{h2}, *p6mm* (90)	35.51	35.51	10	a = 41.0
		20.49	20.43	11	
		4.58 (h_a)[c]			
		3.70 (h_c)[c]			
	Col_{r1}, *p2mm* (50)	42.01	42.01	01	a = 32.3
		25.63	25.63	11	b = 42.0
		10.31	10.44	31	
		5.77	5.83	45	
		4.27 (h_a)[c]			
		4.22 (h_c)[c]			
	Col_{r2}, *p2mm* (25)	41.76	41.76	01	a = 25.6
		25.60	25.60	10	b = 41.8
		21.06	20.88	02	
		13.83	13.92	03	
		10.32	10.44	04	
		5.74	5.81	43	
		4.19 (h_a)[c]			
		4.17 (h_c)[c]			
TT4 (46.49)	Col_{h1}, *p6mm* (110)	29.82	29.82	10	a = 34.4
		5.77 (h_a)			
		4.34 (h_c)			
	Col_{h2}, *p6mm* (60)	32.68	32.68	10	a = 37.7
		16.38	16.34	20	
		11.74	12.35	21	
		5.78 (h_a)[c]			
		4.26 (h_c)[c]			
	Col_{h2}, *p6mm* (25)	35.52	35.52	10	a = 37.6
		16.27	16.26	20	
		12.19	12.29	21	
		5.74 (h_a)[c]			
		4.18 (h_c)[c]			

[a]The average diameter (D) of the polycatenars (estimated from Chem 3D Pro 8.0 molecular model software from Cambridge Soft). [b]d_{obs}: spacing observed; d_{cal}: spacing calculated (deduced from the lattice parameters; a and b for Col_h and Col_r phase; [c]spacings marked h_a and h_c correspond to diffuse reflections in the wide-angle region arising from correlations between the alkyl chains and core regions, respectively.

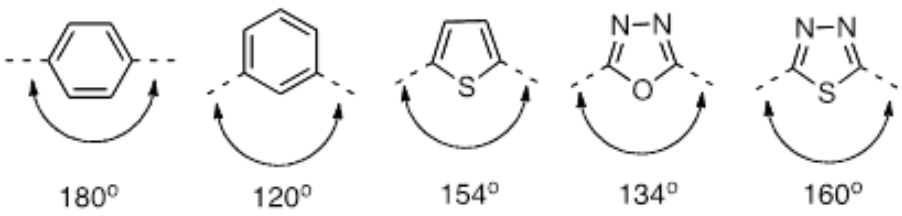

Figure 3.11. Comparison of the bent angles of different central and side rings of the polycatenars. [23]

This transition was confirmed by the DSC scans, which showed an enthalpy change of 15.8 kJmol^{-1} (Fig. 3.10d, table 3.1). There was no sign of crystallization up to -20 ^{o}C, as revealed by the DSC results. The XRD patterns obtained at 110, 60, and 25 ^{o}C confirmed a Col_h phase (Fig. 3.10e-g, Table 3.3). The DSC scans showed that there is a transition between two Col_h phases, which we denoted as Col_{h1}, and Col_{h2}. It is surprising that the lower homologue exhibited a Col_h phase in contrast to the oxadiazole analogue (**TT4**), which exhibited a Col_{ob} phase.

Looking at the thermal behavior, we can conclude that the length of the peripheral chain and pattern of substitution matters in determining the thermal range of the mesophase. Oxadiazole derivative **TO2** and thiadiazole-based polycatenar compound **TT2** were crystalline in nature and showed that peripheral chain substitution at the 3,5-positions is not conducive for mesophase stabilization. This may be due to the lack of space filling and nano segregation. Compound **TO1**, with four peripheral alkyl chains substituted at the 3- and 4-positions of the terminal benzene ring, was liquid crystalline, whereas corresponding thiadiazole compound **TT1** was crystalline, which indicated the effect of the thiadiazole ring on the self-assembly. Compounds **TO3** and **TT3** showed an enhanced mesophase range with respect to **TO1-2** and **TT1-2**, which showed that substitution at the 3, 4 and 5-positions stabilized the columnar packing. Furthermore, a reduction in the length of the peripheral chain from *n*-hexadecyloxy to *n*-decyloxy (for compounds **TO4** and **TT4**) led to the broadest thermal range in the respective series. Oxadiazole derivatives **TO1**, **TO3** and **TO4** showed stabilized Col_r, Col_h or Col_{ob} phases, whereas thiadiazole derivatives **TT3-4** exhibited Col_r and Col_h phases. Liquid crystallinity and the width of the mesophase exhibited by compounds **TO1, TO3, TO4** and **TT3**, **TT4** is a summation of bent-angle, dipole moment, and space-filling effects and nanophase segregation. It is difficult to pinpoint a certain factor that establishes a relationship between the structure and the thermal behavior. This shows that a delicate ratio of incompatible subunits in a shape-anisotropic molecule is required to affect the nanophase segregation, which results in LC self-assembly. A general comparison of oxadiazole- and thiadiazole-based polycatenars based on a central thiophene leads to the following generalizations: Compounds with thiadiazole linkage show a rich phase sequence compared with oxadiazole derivatives. More importantly, the longer the chain length, the richer the phase sequence for both linking groups (oxadiazole or thiadiazole). For example, the higher (C16) homologue of the thiadiazole linking group (**TT3**) shows a Iso–Col_{h1}–Col_{h2}–Col_{r1}–Col_{r2} phase sequence, whereas the lower (C10) homologue (**TT4**)

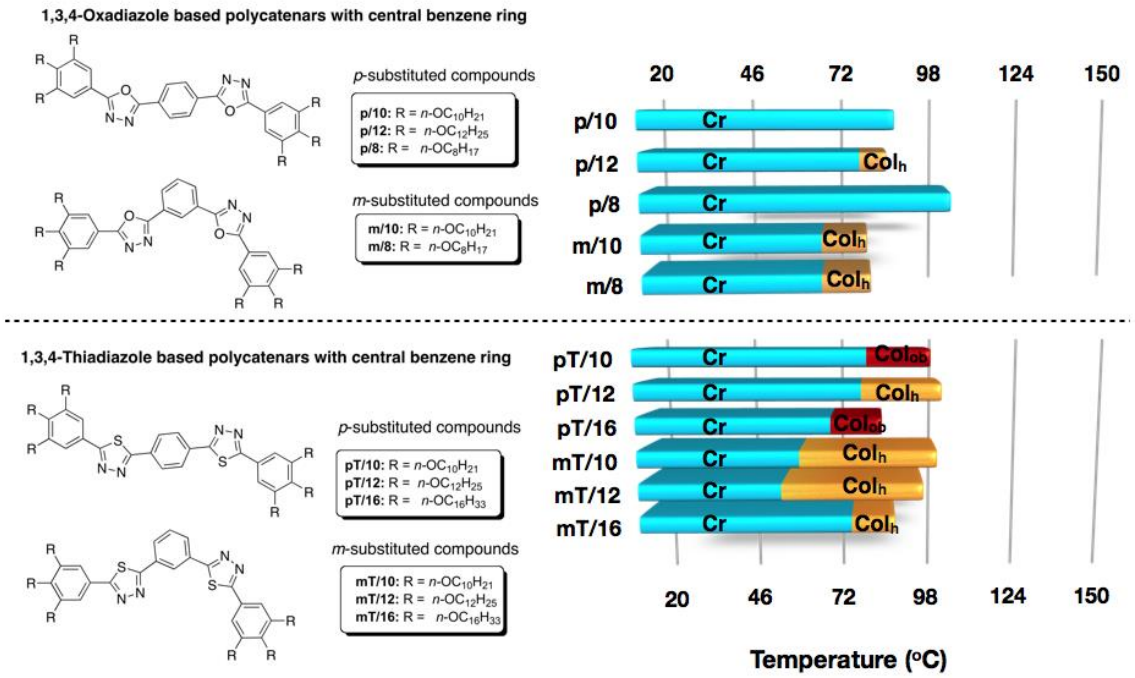

Figure 3.12. Bar graph summarizing the thermal behavior of 1,3,4-oxadiazole based polycatenars[10c,d] with a central benzene ring substituted at *p*- and *m*- position and 1,3,4-thiadiazole based polycatenars[11b] with a central benzene ring substituted at *p*- and *m*- position (second heating cycle) (Col_{ob} = Columnar oblique phase; Col_h = Columnar hexagonal phase.)

has only two mesophases. Similarly, the C16 homologue of the oxadiazole linking group (**TO3**) exhibits a Col_h phase and two rectangular columnar phases, whereas the C10 homologue (**TO4**) shows only the oblique columnar mesophase. A possible reason for this difference could be better isolation of the central cores in a columnar structure, provided by the longer peripheral chains.

Another point to be noted is that replacing a benzene ring with a thiophene ring leads to a richer mesophase scenario. We can compare the thermal behavior of these polycatenars (Fig. 3.3) with previously reported polycatenars with a central benzene ring and substituted 1,3,4-oxadiazole[10c, d] or 1,3,4-thiadiazole[11b] as side rings. Figure 3.12 shows the phase-transition temperatures and mesophase widths of these polycatenars. To make a clear comparison, we chose the hexacatenar with *n*-decyloxy tails from each series. The bent angles of the central cores and other heterocycles help us to understand their impact on the self-assembly (Fig. 3.11). The bent angle of polycatenars with a central benzene ring can be either 180 (for **p/ 10** and **pT/10**, *p*-substituted compounds) or 120^o (for **m/10** and **mT/10**, *m*-substituted compounds). Here, for both series of oxadiazole- and thiadiazole-based polycatenars, *m*-substituted compounds show higher mesophase stabilization. Note that oxadiazole derivative **p/10** was crystalline, whereas

m/10 exhibited a Col_h phase. For the thiadiazole-based polycatenars, again the *m*-substituted compound **mT/10** showed a wider thermal range than *p*-substituted compound **pT/10**.Compared with polycatenars with oxadiazole side rings (bent angle ≈134^o), polycatenars based on thiadiazole side rings (bent angle ≈160^o) show higher mesophase stability. Therefore, an increase in the bent angle of the side rings helps to enhance the mesophase width.

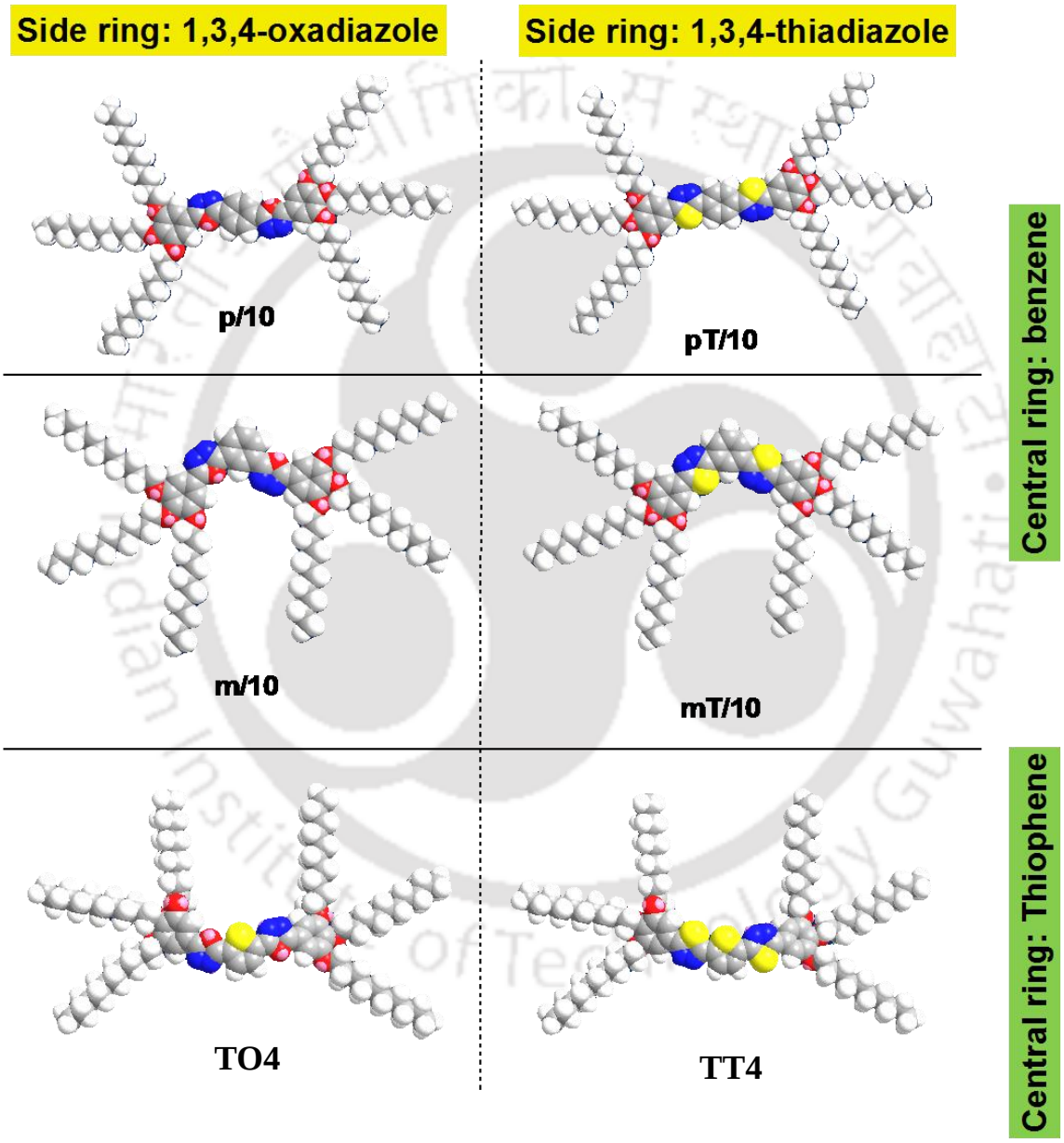

Figure 3.13. Space filling energy minimized (all-*trans*) molecular models obtained for polycatenars with a central benzene ring and for polycatenars with a central thiophene ring (estimated from Chem 3D Pro 8.0 molecular model software from Cambridge Soft).

Herein, the bent angle of the central thiophene ring is around 150°.[23] This is an intermediate angle compared with *p* or *m*-substituted benzene. In this case, polycatenars with oxadiazole and thiadiazole side rings exhibited liquid crystallinity. The mesophase width is larger than *m*- and *p*-substituted polycatenars (both oxadiazole and thiadiazole) with a central benzene ring. It should be noted that, as in the case of benzene-centered polycatenars, thiadiazole-based polycatenar **TT4** showed a wider thermal range than its oxadiazole counterpart (**TO4**). Molecular models of hexacatenars with *n*-decyloxy chains are provided in figure 3.13. This study confirms that this very small deviation in the bent angle (which is the effect of the hetero atom of the constituent rings in the polycatenar) leads to a huge difference in the self-assembly in the bulk. Smaller bent angles lead to a higher dipole moment, as in the case of oxadiazole derivatives, whereas larger bent angles reduce the overall dipole moment, as in the case of thiadiazole or thiophene derivatives. This also has a direct consequence on the mesophase stability. Another important factor is the bent angle provided by the central thiophene unit, which is very favorable for mesophase stabilization compared with previously reported benzene-centered polycatenars.

3.2.3. Photophysical properties

Photophysical properties of the polycatenars **TO1-4** and **TT1-4** were investigated in the solution and thin film states (Table 3.4). Absorption and emission spectra of these compounds were recorded for micromolar solution in THF (Fig. 3.14). As can be seen, the absorption spectra for the solutions of oxadiazole based compounds **TO1-4** showed absorption maxima in a range of λ = 362 to 365 nm (Fig. 3.14a), whereas the thiadiazole based compounds **TT1-4** showed slightly red-shifted absorption spectra λ = 368 to 394 nm (Fig. 3.14b). Oxadiazole derivatives **TO1-4** showed higher bandgaps (3.07-3.2 eV) than thiadiazole derivatives **TT1-4** (2.73-2.92 eV). Similarly, the emission maxima of compounds **TO1-4** were in the range of λ = 442 to 476 nm, whereas the emission maxima of compounds **TT1-4** were in the range of λ = 476 to 490 nm. The molar extinction coefficients of oxadiazole derivatives **TO1-4** (ε = 28,800-31,150 M^{-1} cm^{-1}) were found to be more than thiophene derivatives **TT1-4** (ε = 20,650-22,900 M^{-1} cm^{-1}). The absorption bands mainly correspond to π-π* transition of this molecular system. Thin films of these compounds showed small shifts in their absorption and emission spectra due to aggregation. Oxadiazole-based compounds **TO1-4** showed higher quantum yields of 0.56

Table 3.4. Photophysical properties of compounds **TO1-4** and **TT1-4** in solution[a] and film state.

Entry	Solution State						Thin film State		
	Absorption(nm)	**Emission[b](nm)**	**Stokes shift(nm)**	**λ_{onset} (nm)**	**$\Delta E^{c,d}_{opt}$**	**Relative Q. Y.**	**Absorption (nm)**	**Emission[b](nm)**	**Stokes shift(nm)**
TO1	365	442	77	405	3.07	0.72	365	473	108
TO2	353	476	123	388	3.20	0.65	368	453	85
TO3	362	472	110	405	3.07	0.57	367	478	111
TO4	362	472	110	405	3.07	0.56	367	501	134
TT1	368	476	108	455	2.73	0.50	373	486	113
TT2	374	476	102	425	2.92	0.50	371	473	102
TT3	383	487	104	455	2.73	0.54	365	512	147
TT4	394	490	96	441	2.82	0.61	369	507	138

[a]micromolar solutions in THF; [b]excited at the respective absorption maxima; [c]Band gap determined from the red edge of the longest wave length (λ_{onset}) in the UV-vis absorption spectra; [d] In volts (eV).

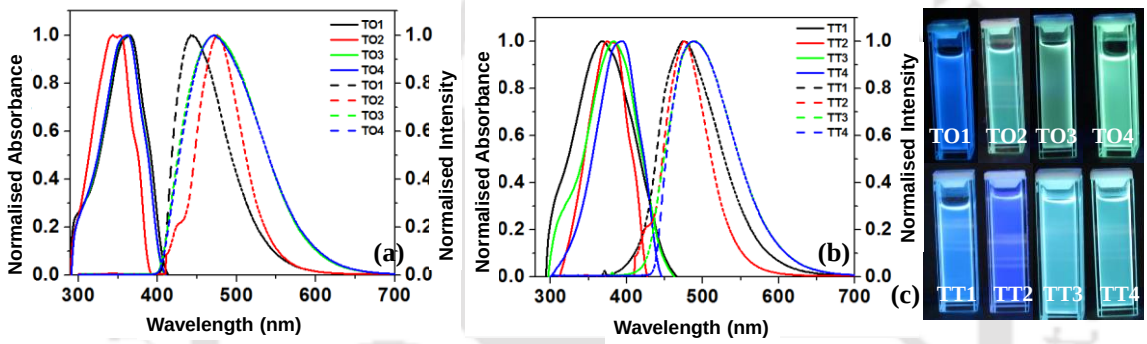

Figure 3.14. Absorption (solid trace) and emission (dotted trace) spectra of compounds a) **TO1-4** and b) **TT1-4**; c) photographs taken under the UV light (λ_{ex} = 365 nm; micromolar solution in THF.

to 0.72, whereas thiadiazole-based compounds **TT1-4** exhibited slightly lower quantum yields in the range of 0.5 to 0.61 (Fig. 3.15, Table 3.5). The observed quantum yields are higher in comparison to polycatenars with a central benzene ring instead of thiophene.[11b] Quantum yield was measured according to established procedure by using quinine sulfate in 0.1 M H_2SO_4 solution as the standard. Absolute values were calculated according to the following equation: $Q_S = Q_R \times (m_S / m_R) \times (n_S / n_R)^2$ Where, Q: Quantum yield, m: Slope of the plot of integrated fluorescence intensity *vs* absorbance; n: refractive index (1.407 for THF and 1.33 for distilled water); the subscript R refers to the reference fluorophore *i.e.* quinine sulphate solution in 0.1 M H_2SO_4 and subscript S refers to the sample under investigation. In order to minimize re-absorption effects, absorbance was kept below 0.15 at the excitation wavelength of 347 nm. Quantum Yield of quinine sulphate is 0.54. Simplified equation for the calculation after substituting the appropriate values is given as: $Q_S = 0.54 \times (m_S/2.71) \times (1.407/1.33)^2 = 0.223 \times m_S$ and values obtained are given in the table 3.5.

Table 3.5. Results of the quantum yield of the compounds **TO1-4** and **TT1-4** in THF solution.

Entry	m_S	m_R	$Q_s^{a,b,c}$	Entry	m_S	m_R	$Q_s^{a,b,c}$
TO1	3.21	2.71	0.72	**TT1**	2.25	2.71	0.50
TO2	2.91	2.71	0.65	**TT2**	2.22	2.71	0.50
TO3	2.55	2.71	0.57	**TT3**	2.43	2.71	0.54
TO4	2.49	2.71	0.56	**TT4**	2.72	2.71	0.61

[a] Measured in THF; [b]Excited at absorption maxima; [c]Standard quinine sulphate (Q_f = 0.54) in 0.1M H_2SO_4.

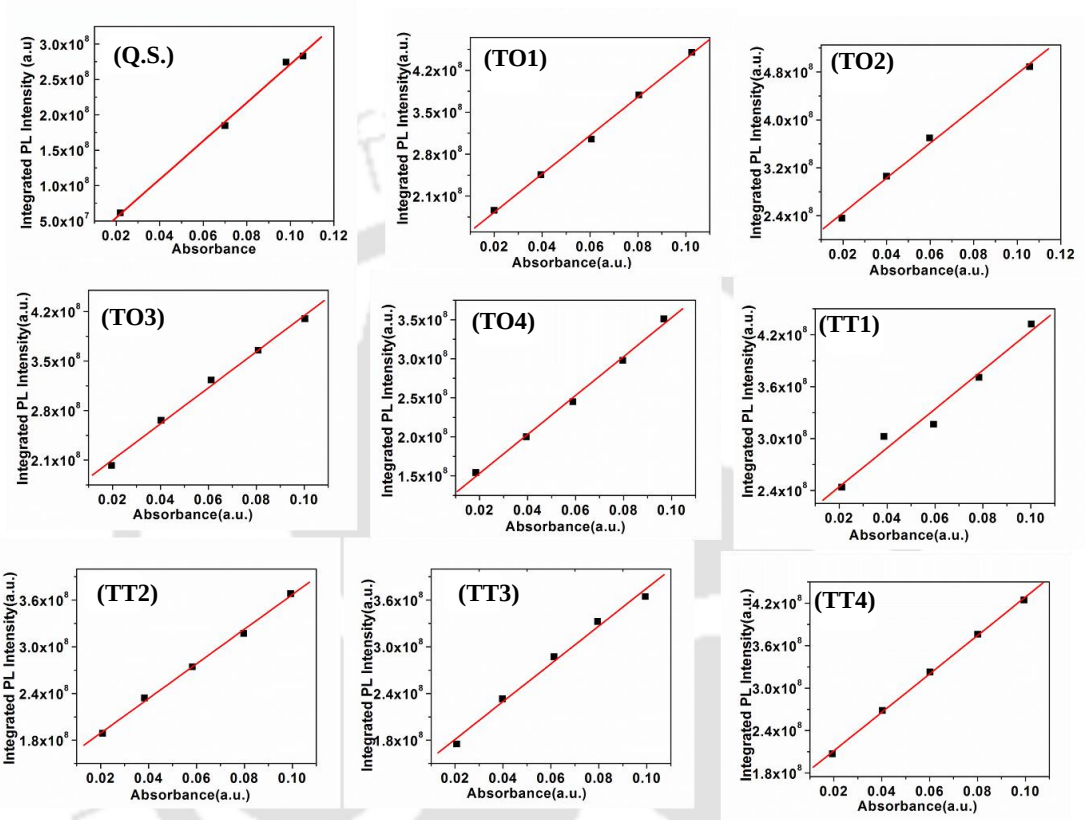

Figure 3.15. Plots of integrated photoluminescence intensity vs absorbance of Quinine sulphate (0.1M H_2SO_4 solution), compounds **TO1-4** and **TT1-4** (micromolar THF solution).

The thin films of these compounds were prepared by drop casting the micromolar solutions of these compounds in toluene onto glass slides. The absorption spectra and emission spectra of these compounds were found to be broad compared with their solution spectra (Fig. 3.16). The absorption spectra of the thin films of oxadiazole-based compounds **TO1-4** show a red-shift compared with the solution spectra; even though the absorption maximum of compound **TO1** in the thin film state shows the same value as in solution, the difference spectra shows the red-shift (Fig. 3.17, 3.16a). Other than compound **TO2**, the emission spectra of **TO1**, **TO3** and **TO4** showed a red-shift (Fig. 3.16b). In the case of thiadiazole-based compounds, all the compounds exhibited blue-shifted absorption spectra except for compound **TT1** (Fig. 3.16d). The emission spectra

of the films of thiadiazole derivatives **TT1** and **TT3-4** showed a red-shift, while that of the compound **TT2** was blue-shifted (Fig. 3.16e). All the compounds showed a visually perceivable bright emission in the thin-film state on irradiation with long-wavelength UV light (Fig. 3.16c and f). It is evident from previous reports that the red-shifted absorption spectra in the aggregated state points to the formation of J-type aggregates,[14] in which the molecules are arranged in a slipped-stack position, whereas the blue shifted absorption spectra indicates the formation of H-type aggregates, in which the molecules are arranged in a cofacial manner. J-aggregates are supposed to be highly luminescent compared with H-aggregates, in which luminescence is quenched. However, there are a few reports of fluorescent H-type aggregates.[15] Here we cannot provide conclusive proof of the formation of a particular type of aggregate in the thin films because of the possibility of several diastereomeric conformations for these polycatenars.

Photophysical properties of representative compounds **TO3** and **TT3** in solution were studied with respect to different solvents to examine their behavior with solvent polarities (Fig. 3.18, Table 3.6). The absorption spectra did not vary much with respect to solvent polarity, which indicates the nonpolarity of the molecules in the ground state. In contrast to the absorption spectra the emission spectra showed a red-shift, which indicates

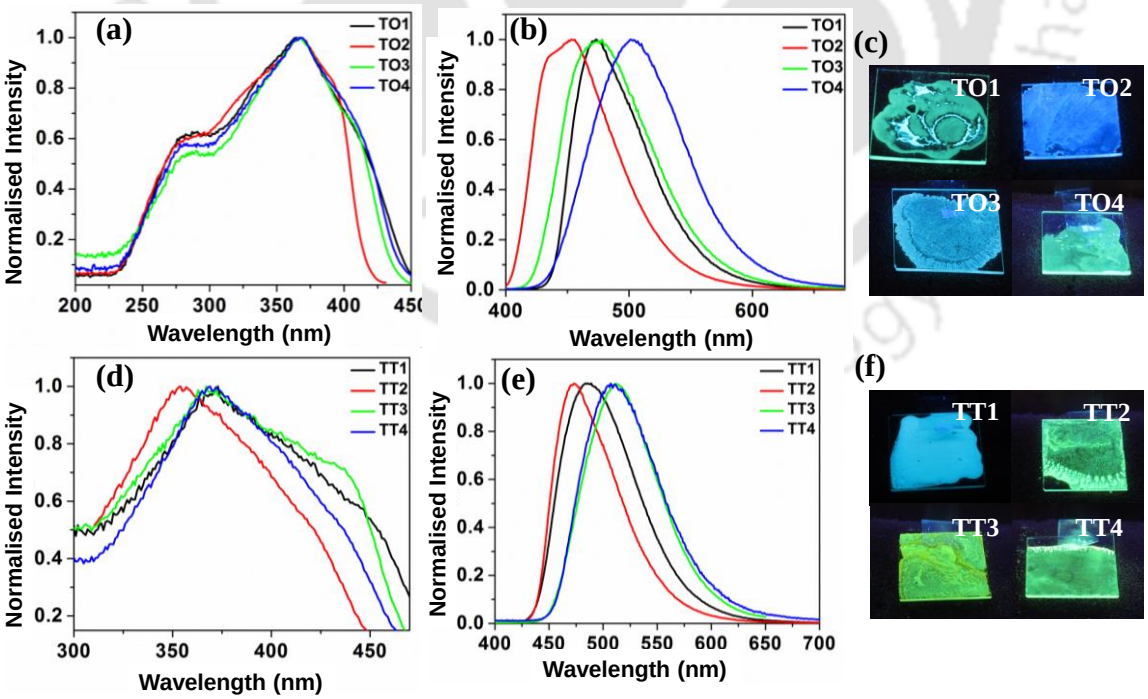

Figure 3.16. a) Normalized Absorption and b) emission spectra of **TO1-4** and d) Normalized Absorption and e) emission spectra of compounds **TT1-4**; c, f) Photographs of thin films of **TO1-4** and **TT1-4** taken under the UV light (λ_{ex} = 365 nm).

the polar nature of the excited state. The presence of donor and acceptor moieties in conjugation leads to the localization of π-electrons towards the acceptor unit in polar solvents. This leads to an internal charge-transfer state in addition to the locally excited state. The internal charge transfer state is affected by solvent polarity. Thus the energy gap between the ground and excited state is reduced in polar solvents, which leads to a red-shifted emission.

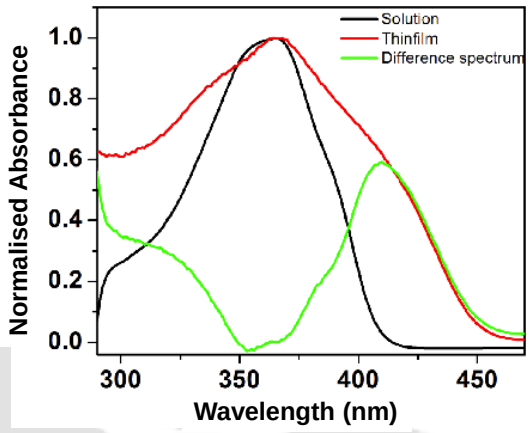

Figure 3.17. Absorption spectra of compound **TO1** in THF solution and thin film state, Difference spectrum shows a red shift.

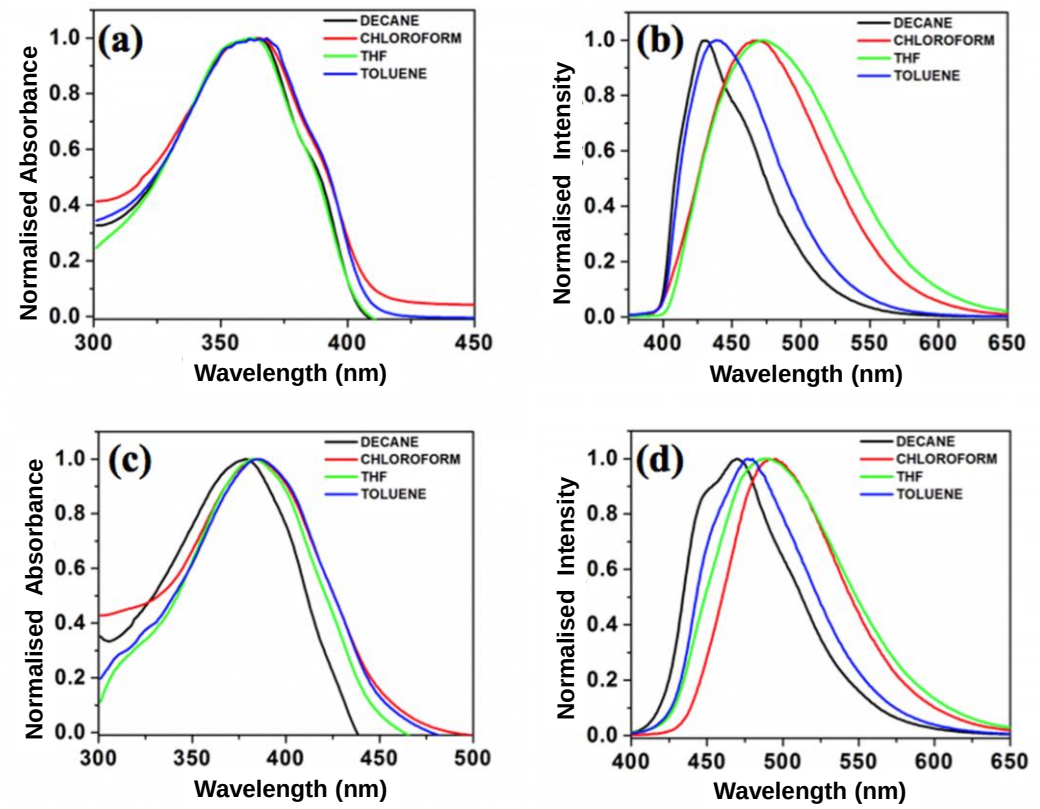

Figure 3.18. a) Normalized absorption and b) emission spectra of **TO3** (20 µmol) in different solvents and c) Normalized absorption and d) emission spectra of **TT3** (20 µmol) in different solvents.

Table 3.6. Photophysical properties in different solvents[a].

Entry	Solvent	Absorption (nm)	Emission[b] (nm)	Stokes shift (nm)
TO3	Decane	362	431	69
	Toluene	362	438	76
	Chloroform	362	468	106
	THF	362	472	110
TT3	Decane	379	470	91
	Toluene	386	477	91
	Chloroform	386	495	101
	THF	383	487	112

[a] micromolar solutions in Decane, Toluene, Chloroform, THF; [b] excited at the respective absorption maxima.

3.2.4. Electrochemical behavior

Energy levels of frontier molecular orbitals (HOMO and LUMO) of the polycatenars were obtained by using cyclic voltammetry (CV) and the data are tabulated in table 3.7. All the compounds exhibited irreversible oxidation and reduction waves (Fig. 3.19).

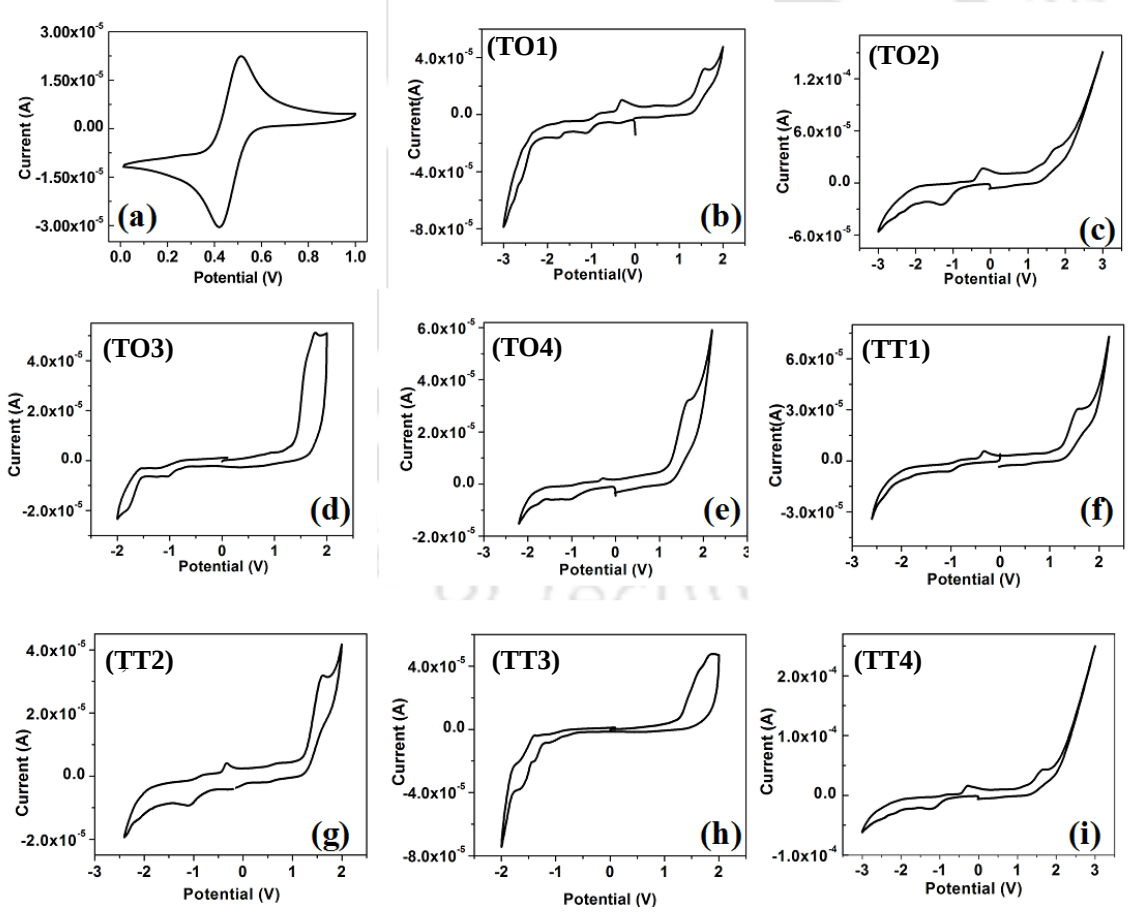

Figure 3.19. Cyclic voltammograms of (a) ferrocene; (b-e) **TO1-4** and (f-i) **TT1-4** in anhydrous DCM solution of tetra-*n*-butyl ammonium perchlorate (0.1 M) at a scanning rate 0.5mV/s; the half wave potential of Fc/Fc^+ was found to be 0.46 V relative to Ag/Ag^+ reference electrode.

Table 3.7. Electrochemical properties of compounds **TO1-4** and **TT1-4** in micromolar DCM solutions.

Entry [a]	E_{1red} (V) [c]	E_{1oxd} (V)	E_{HOMO} (eV)[b]	E_{LUMO} (eV)[c]	ΔE_{CV} (eV)[d]	$\Delta E_{g, opt}$ (eV)[e]
TO1	-1.16	1.61	-5.95	-3.18	2.77	3.07
TO2	-1.30	1.74	-6.08	-3.04	3.04	3.20
TO3	-1.06	1.77	-6.11	-3.28	2.83	3.07
TO4	-1.13	1.66	-6.00	-3.21	2.79	3.07
TT1	-1.04	1.60	-5.94	-3.30	2.64	2.73
TT2	-1.13	1.61	-5.95	-3.21	2.74	2.92
TT3	-1.03	1.56	-5.90	-3.31	2.59	2.73
TT4	-1.17	1.62	-5.96	-3.17	2.79	2.82

[a]Experimental conditions: $Ag/AgNO_3$ as the reference electrode, glassy carbon as the working electrode, platinum rod as the counter electrode, TBAP (0.1M) as the supporting electrolyte, RT, scanning rate 0.05 mV s^{-1}; [b]Estimated from the onset oxidation peak values by using the formula E_{HOMO}= -(4.8-$E_{1/2, Fc, Fc+}$ + $E_{ox, onset}$); [c]Estimated from the onset reduction peak values by using E_{LUMO}= -(4.8-$E_{1/2, Fc, Fc+}$ + $E_{red, onset}$), $E_{1/2, Fc, Fc+}$ = 0.46 V; [d]Estimated from the formula ΔE_{CV}= E_{LUMO}-E_{HOMO}. [e]Bandgap determined from the red edge of the longest wavelength in the UV/Vis absorption spectrum.

The optical band gap E_{opt} was estimated from the red edge of the absorption spectra. Energy levels of LUMO and HOMO were determined by using the formulae ΔE_{CV} = E_{LUMO} - E_{HOMO}, E_{HOMO}= - (4.8 - $E_{1/2, Fc, Fc+}$ + $E_{ox, onset}$) eV and E_{LUMO} = - (4.8 - $E_{1/2, Fc, Fc+}$ + $E_{red, onset}$) eV. Compounds **TO1-4** exhibited LUMO levels of -3.04 to -3.21 eV and HOMO levels of -5.95 to -6.11 eV. Compounds **TT1-4** exhibited LUMO levels of -3.17 to -3.31 eV and HOMO levels of -5.90 to -5.96 eV. Oxadiazole derivatives **TO1-4** exhibited a higher bandgap of 3.07 to 3.2 eV compared with thiadiazole derivatives **TT1-4**, which showed a bandgap of 2.73 to 2.92 eV. Compounds **TT1-4** can be compared with polycatenars reported previously, in which the central benzene ring is connected to thiadiazole rings at 3,5-positions.[11b] These compounds show reduced LUMO, HOMO levels and bandgaps in comparison to their benzene analogues.

3.2.5. Gelation properties

Compounds **TO3** and **TT3** were investigated for their ability to undergo organogelation in solutions of hexane, decane, dodecane, hexadecane, chloroform, dichloromethane, ethanol, dimethylsulfoxide (DMSO), *n*-butanol, tetrahydrofuran, benzene, toluene and *m*-xylene. Both of these compounds showed gelation in hydrocarbon solvents, such as hexane, decane, dodecane and hexadecane (Table 3.8). We also checked the gelation of other compounds in decane (Table 3.9). Compound **TO2**, **TT1**, **TT2** and **TT4** precipitated after being dissolved in decane, whereas compound **TO4** dissolved in decane.

Table 3.8. Gelation behavior and CGCs of compound **TO3** and **TT3** in various solvents.

Sl. No.	Solvent	TO3			TT3		
		Properties	CGC (wt%)	T_{gel}(^{o}C)	Properties	CGC (wt%)	T_{gel}(^{o}C)
1	Hexane	G(O)	1.05	67	G(O)	0.73	45
2	Decane	G(O)	1.00	71	G(O)	0.70	47
3	Dodecane	G(O)	0.98	72	G(O)	0.67	52
4	Hexadecane	G(O)	0.93	74	G(O)	0.65	55
5	Toluene	S	----	---	S	----	---
6	Benzene	S	----	---	S	----	---
7	*m*- xylene	S	----	---	S	----	---
8	DCM	S	----	---	S	----	---
9	Chloroform	S	----	---	S	----	---
10	THF	S	----	---	S	----	---
11	*n*-butanol	P	----	---	P	----	---
12	Ethanol	P	----	---	P	----	---
13	DMSO	I	----	---	I	----	---

G = stable gel; P = precipitate; I = insoluble; O = opaque. The critical gelation concentration (wt. %) is the minimum concentration necessary for gelation. T_{gel} (^{o}C) is the thermal stability of the gels.

Table 3.9. Gelation behavior and CGCs of compound **TO1-4** and **TT1-4** in decane.

Entry	Properties	CGC (wt%)	T_{gel}(^{o}C)
TO1	G(O)	0.45	63
TO2	P	-----	-----
TO3	G(O)	1.00	71
TO4	S	-----	-----
TT1	P	-----	-----
TT2	P	-----	-----
TT3	G(O)	0.70	47
TT4	P	-----	-----

G = stable gel; P = precipitate; I = insoluble; S = soluble; O = opaque. The critical gelation concentration (wt%) is the minimum concentration necessary for gelation. T_{gel} (^{o}C) is the thermal stability of the gels.

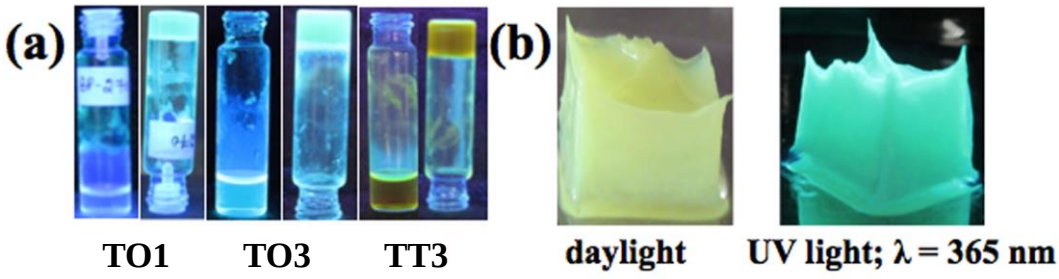

Figure 3.20. a) Photographs of **TO1**, **TO3** and **TT3** in solution and gel states under long wavelength UV light (λ = 365 nm) at CGC; b) Formation of a self-standing gel of compound **TO1** at CGC.

Of the oxadiazole derivatives, **TO1** and **TO3** showed gelation whereas for the thiadiazole derivatives none of the compounds except **TT3** showed gelation in decane. Oxadiazole-based compound **TO1**, with four alkyl tails, showed the gelation at a very low critical gel concentration (CGC) of 0.45 wt%. This compound was gelated within 6 minutes after heat-assisted dissolution. Immediately after adding the compound to decane, the suspension was heated to obtain a clear solution. The resultant solution was allowed to cool for 10 minutes to form a gel at room temperature. Gel formation was confirmed by "stable to inversion of the glass vial" method, that is, the gel was unable to flow on inversion of the container, which confirmed the formation of a stable gel. Oxadiazole-based compound **TO3**, with six alkyloxy tails, showed a CGC of 1 wt% and took longer time to gelate (approximately 3 h), whereas thiadiazole-based compound **TT3** (again with six alkyl tails) took almost 50 minutes from the point of complete dissolution with a CGC of 0.7 wt% respectively. Therefore, compounds **TO1** and **TT3** qualify as supergelators because they are able to gelate at a very low CGC, that is, well below 1 wt%.[16] All the gels were opaque and fluorescent (Fig. 3.20a). Compound **TO1** showed the ability to form self-standing and moldable gels of any given shape (Fig. 3.20b). It is apparent that the gelation depends on a very delicate balance of number and pattern of substitution of alkyl tails and the type of the heterocycle present in the polycatenar.

Because we were interested to deriving the structure-property relationships, we decided to investigate compounds **TO3** and **TT3** by using extensive photophysical studies, microscopy and XRD studies. Detailed rheological measurements were also carried out on the two representative samples, as described below. Formation of the organogel was monitored by measuring the emission spectra of the solution with respect to temperature and time. For compound **TO3** the emission intensity increased as the temperature was decreased from 70 to 20 ^{o}C with a concomitant red-shift from λ = 461 nm to 471 nm (Fig. 3.21a-b). A huge four-fold increase in the emission intensity was observed on gelation, compared with solution-state emission (5.51 mM in decane; Fig. 3.22a). Similarly, the intensity of the emission was highest at 115 min and thereafter it remained steady (Fig. 3.21d). This is a phenomenon of aggregation-induced enhanced emission (AIEE). The emission spectra showed a red-shift upon gelation (Fig. 3.21c), which was similar to the observation in Fig. 3.21b. This gel formation was reversible for many cycles of heating and cooling, as shown by the change in the emission intensity at its emission maximum (Fig. 3.22b).

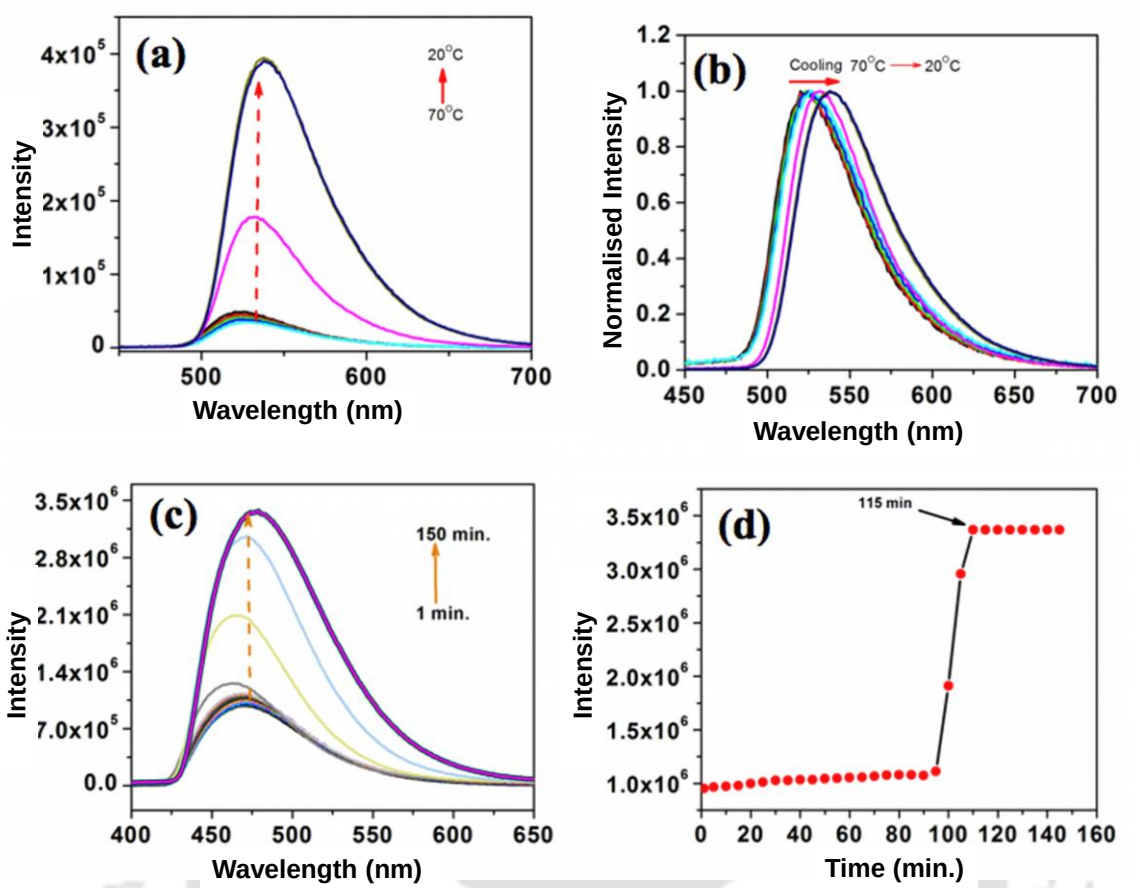

Figure 3.21. a) Emission spectra showing an increase in the emission intensity with the decrease in temperature from solution to gel state for **TO3**; b) Normalized emission spectra of **TO3**, showing a red shift on gelation; c) Emission spectra showing an increase in the emission intensity with time during transformation of solution to gel; d) Plot showing the change in the emission intensity at emission maximum (λ = 362 nm) vs. time (Concentration: 5.51 mM, decane).

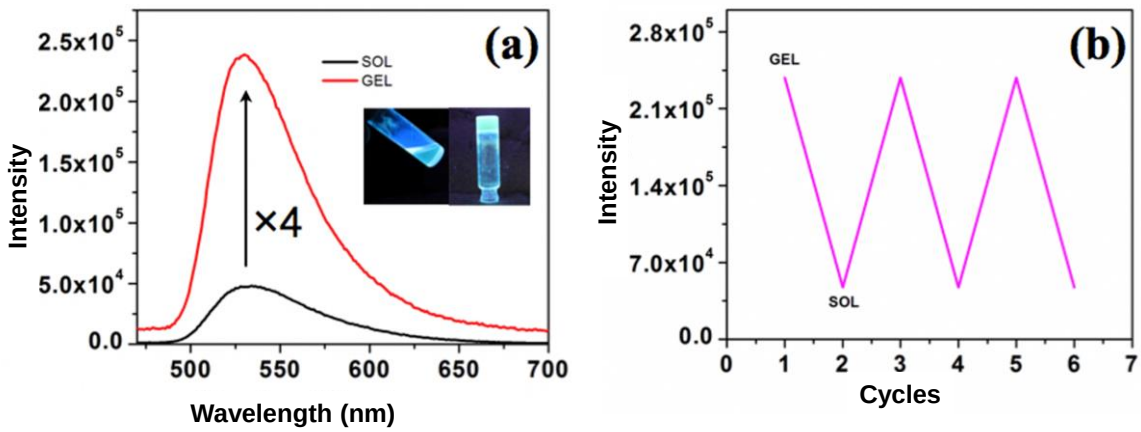

Figure 3.22. a) The increase in intensity from the solution state to gelation showing aggregation-induced emission for **TO3** at the CGC; b) Reversible change in the emission intensity at λ = 362 nm on repeated sol-gel transition (Concentration: 5.51 mM, decane).

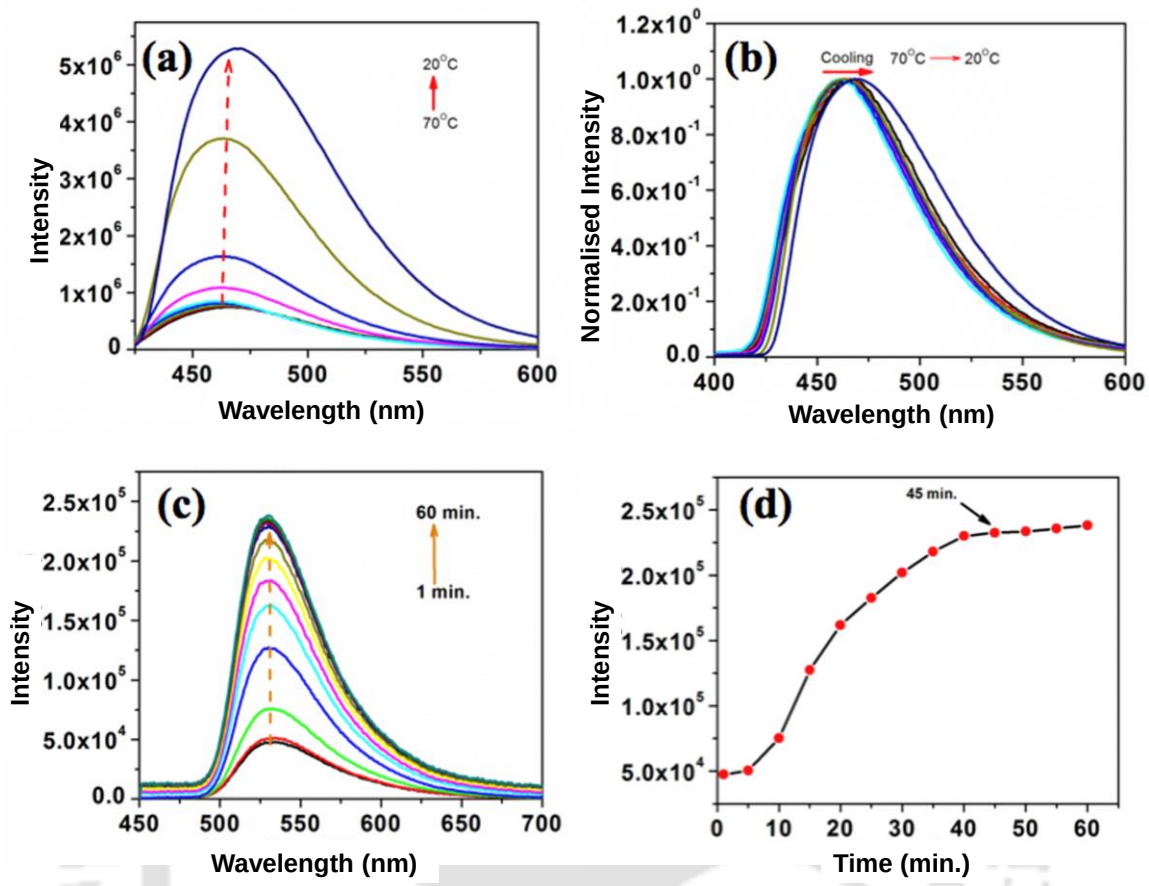

Figure 3.23. a) Emission spectra showing an increase in the emission intensity with the decrease in temperature from solution to gel state for **TT3**; b) Normalized emission spectra of **TT3**, showing a red shift on gelation; c) Emission spectra showing an increase in the emission intensity with time during transformation of solution to gel; d) Plot showing the change in the emission intensity at emission maximum (λ = 383 nm) vs. time (Concentration: 3.8 mM, decane).

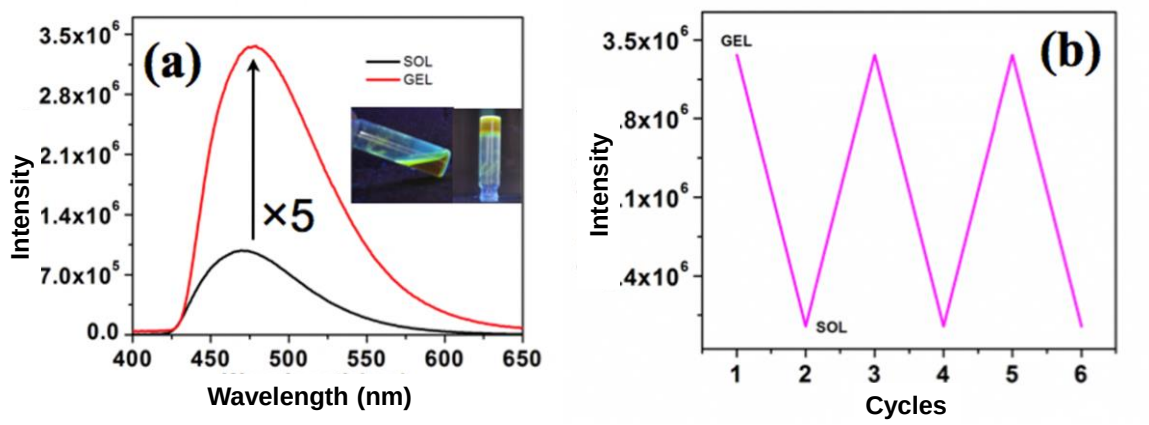

Figure 3.24. a) The increase in intensity from the solution state to gelation showing aggregation-induced emission for **TT3** at the CGC; b) Reversible change in the emission intensity at λ = 383 nm on repeated sol-gel transition (Concentration: 3.8 mM, decane).

Compound **TT3** exhibited similar behavior. An increase in the emission intensity and red-shift in the emission was observed upon gelation (Fig. 3.23a-b). The increase in the emission intensity upon gelation from solution at the CGC (3.8 mM, decane) was found to be five-fold, which confirmed the AIEE phenomenon (Fig. 3.24a). From solution to the gel state, a red-shift was observed from λ = 520 to 538 nm. The gelation process, monitored by fluorescence spectroscopy with respect to time and temperature, showed similar behavior (Fig. 3.23). The gelation was complete in 45 min and the intensity of the emission remained steady (Fig. 3.23d). Similar to **TO3**, the gel formation was reversible over many cycles of heating and cooling (Fig. 3.24b).

Fluorescence lifetimes of the excited species formed in dilute (20 μM) or concentrated (5.51 mM) solutions of **TO3** in decane (at CGC) were measured by monitoring at the emission maxima (λ = 472 & 471 nm for dilute solution & concentrated solution). The solution with lower concentration showed mono exponential decay with a single excited species [T_1 = 1.05 ns (100%)]. The solution with higher concentration showed the presence of two excited-state species, one with a higher lifetime [T_1 = 1.6 ns (49%)] and the other with a lower lifetime [T_2 = 0.93 ns (51%)] (Fig. 3.25a). Similar behavior was observed for **TT3**. The fluorescence lifetimes of the excited-species formed in the 20 μM and 5.51 mM solutions of **TT3** in decane were measured by monitoring at their emission maxima (λ = 487 & 538 nm for dilute solution & concentrated solution). The 20 μM solution showed single species [T_1 = 0.55 ns (100%)]. The solution at higher concentration exhibited biexponential decay with two species. One species showed a lower life time [T_1 = 0.57 ns (22%)], which can be attributed to solvated monomer, whereas the other showed a higher life time [T_2 = 3.79 ns (78%)], which is due to aggregation (Fig. 3.25b). We measured the excitation spectra of **TO3** and **TT3** at 20 μM and also at their CGC. The excitation spectra of **TO3** at gelation concentration showed a large blue-shift compared with the excitation spectra obtained for 20 μM solution. For **TT3**, a slight red-shift was observed with associated broadening of the excitation spectrum (Fig. 3.26). An additional band was also observed at lower wavelengths. This shows that although the aggregation takes place in compounds, the extent and nature of aggregation is different in each compound. The blue-shifted excitation spectra of **TO3** hint at the formation of H- aggregates. For **TT3**, both blue-shifted and slightly red-shifted bands are present in the excitation spectra, which correspond to the formation of both H- and J-aggregates, with the latter being the major product.[14, 22]

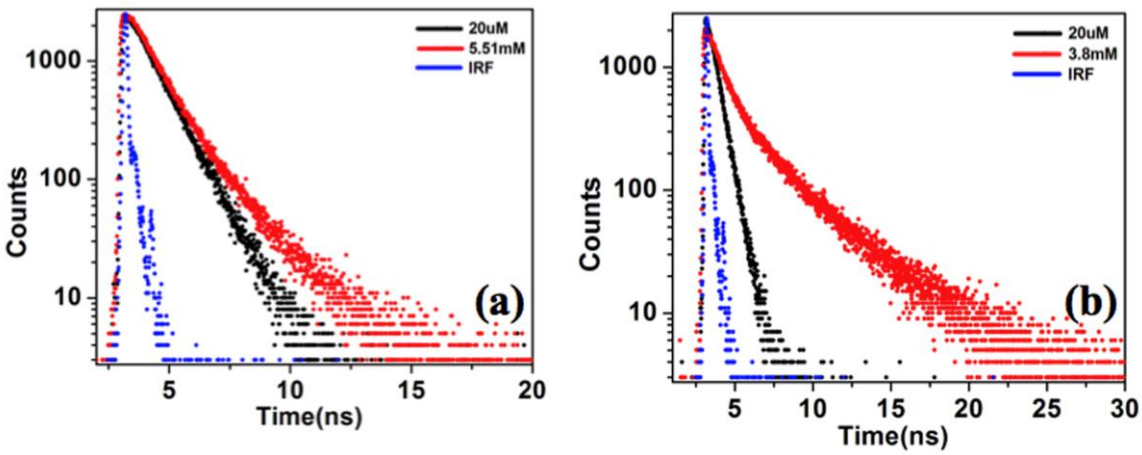

Figure 3.25. a) The fluorescence decay of **TO3** in decane; IRF is the instrument-response function, λ_{exc} = 375 nm; b) The fluorescence decay of **TT3** in decane, λ_{exc} = 375 nm.

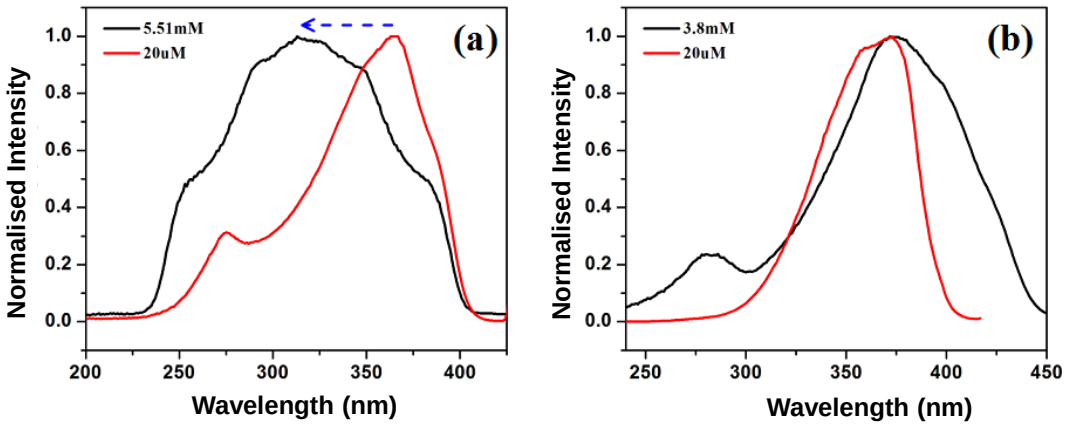

Figure 3.26. a) Excitation spectra obtained for **TO3** at 20 μM and 5.51 mM decane solution; b) for compound **TT3** at 20 μM and 3.8 mM decane solution.

At this point, we were curious to compare the emission of the LC aggregates in the thin films and gels of **TO3** and **TT3**. An overlay of the emission spectra of these compounds in the solution, gel and thin film states showed that the emission intensity of LC thin films was quite high compared with the solution and gel states (Fig. 3.27). It is surprising to see that the thin film of **TO3** exhibited five-fold enhanced emission (Fig. 3.27a), whereas **TT3** exhibited nine-fold enhanced emission with respect to the solution state (Fig. 3.27b). From an application point of view, this is of high technological importance in emissive displays.

These gels were further characterized extensively through atomic force microscopy (AFM; Fig. 3.28) and scanning electron microscopy (SEM; Fig. 3.29). The AFM microscopic images of the xerogels of **TO3** and **TT3** show entangled networks of

fibers. The fibers found in the xerogels were several micrometers in length, with an average height of 30 to 40 nm and average thickness of around 150 nm. The SEM images of the xerogels of compound **TO3** and **TT3** also show similar entangled network of fibers.

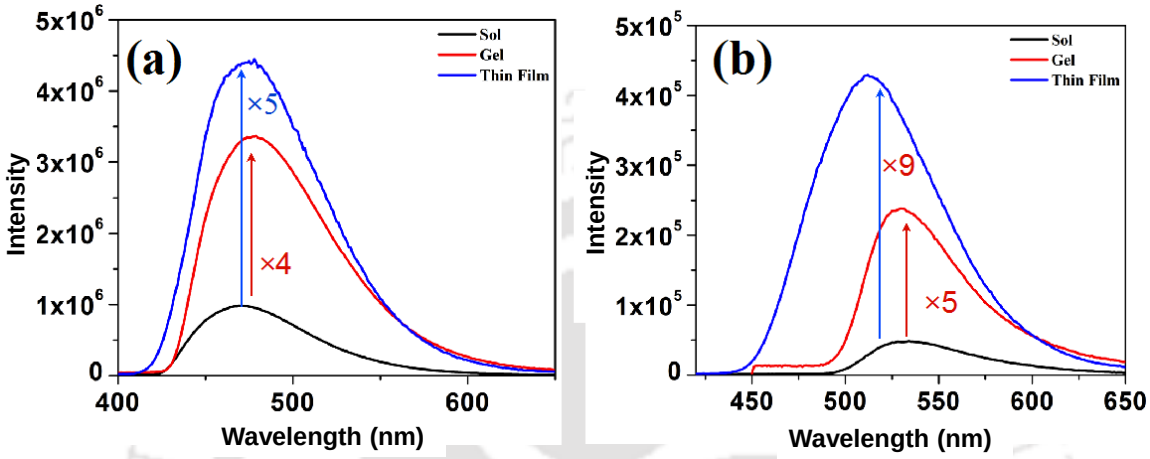

Figure 3.27. a) Emission spectra of **TO3** in solution, gel (5.51 mM, decane) and thin film state and b) emission spectra of compound **TT3** in solution, gel (3.8 mM, decane) and thin film state.

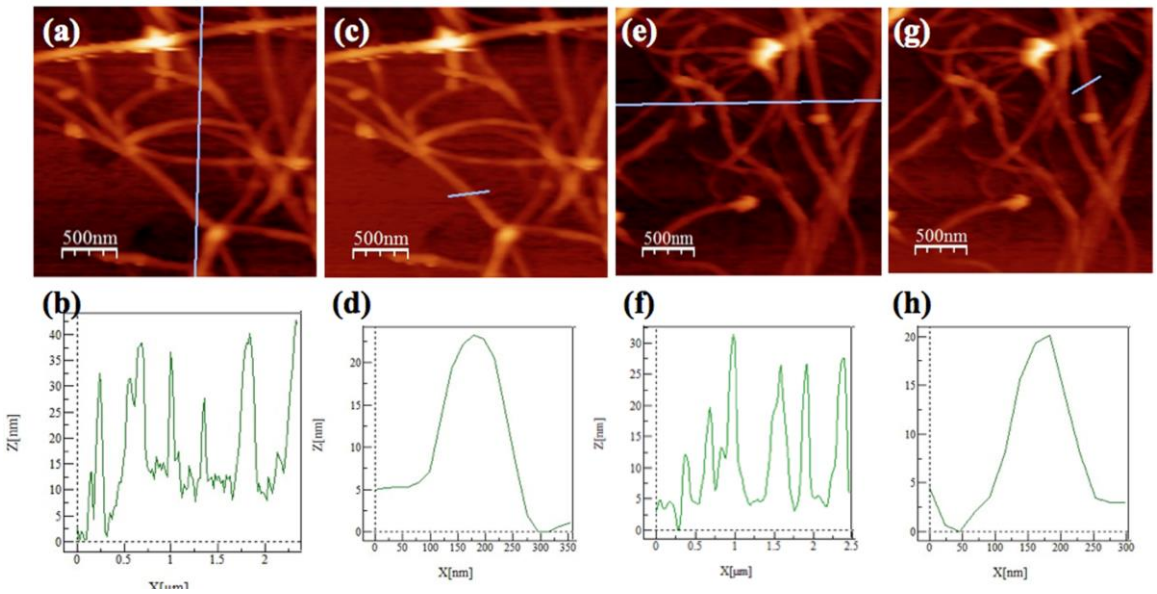

Figure 3.28. a), c) AFM images obtained for the xerogel of **TO3** obtained from a 5.51 mM decane (scale bar 0.5 μm); b) Expanded region of (a) showing the height profiles of the individual fibers and d) Expanded regions of (b) showing the thickness of an individual fiber; e), g) AFM images obtained for the xerogel of **TT3** obtained from 3.8 mM solution in decane (scale bar is 0.5 μm); f) Expanded region of (e) showing the height profiles of the individual fibers and h) Expanded regions of (g) showing the thickness of an individual fiber.

POM of the xerogels of **TO3** and **TT3** show a birefringent pattern as shown in Fig. 3.30, inset, which suggests the presence of anisotropic order. Therefore, a powder XRD study of the xerogel was carried out to investigate the structure of this self-assembly. The XRD pattern of the xerogel of compound **TO3** shows several peaks at low angles that can be indexed to the Col_r phase with lattice constants a = 26.5 and b = 36.5 Å (Fig. 3.30a, Table 3.10). The presence of several peaks at low and mid-angle region suggested higher intercolumnar order in the columnar self-assembly. Therefore, compound **TO3** forms a columnar self-assembly in LC and gel states. Similarly, the *d*-spacings obtained from the diffraction pattern (Fig. 3.30b) of the xerogel of compound **TT3** could be fitted into Col_h phase with a lattice constant a = 108.3 Å. Thus the self-assembly of the two polycatenars in LC and gel states is dependent on the type of hetero atoms present in the adjacent rings of the thiophene moiety.

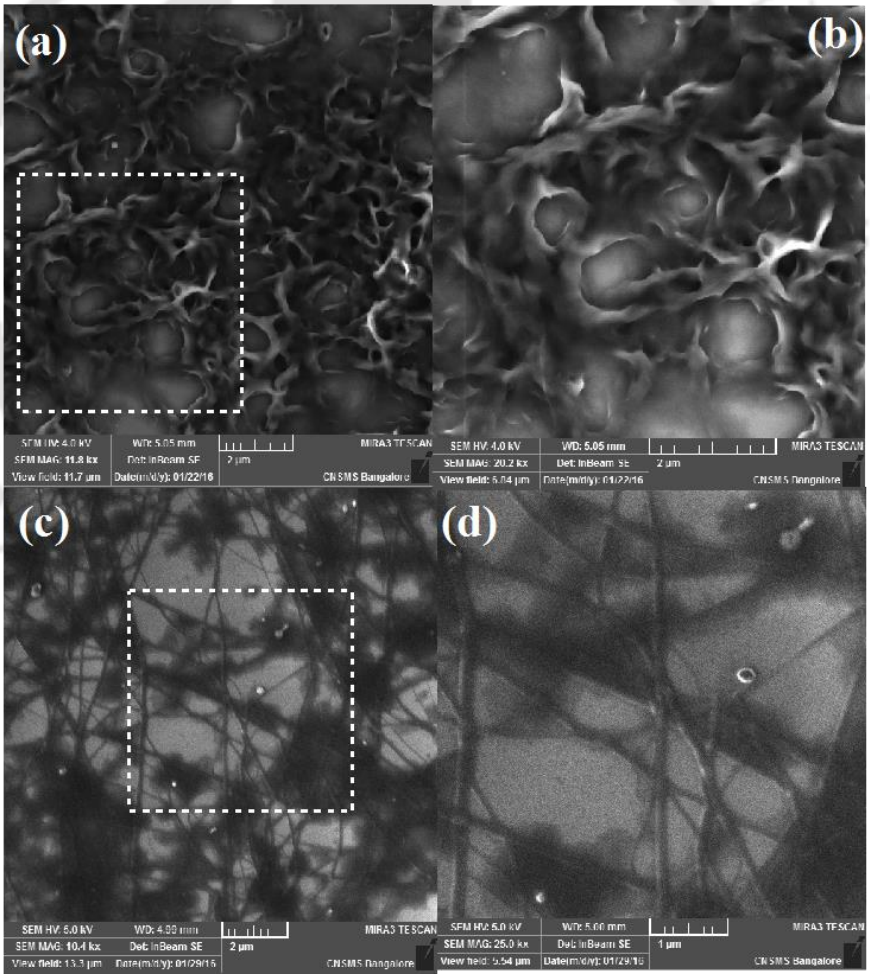

Figure 3.29. a) SEM images obtained for the xerogel of compound **TO3** obtained from 5.51 mM decane solution; b) an expanded region of the first image (scale bar is 2μm); c) SEM images obtained for the xerogel of compound **TT3** at 3.8 mM decane solution (scale bar is 2μm); d) an expanded region of the first image (scale bar is 1μm).

Table 3.10. Results of indexation of XRD profiles of the xerogels of compounds **TO3** and **TT3** at room temperature[a].

Compounds (*D*/Å)	Phase (T/°C)	d_{obs} (Å)[b]	d_{cal} (Å)[b]	Miller indices *hk*	Lattice parameters (Å)
TO3 (60.3)	Col_r	26.5 18.3 15.1 12.0 9.6 7.7 4.2 3.7 3.5	26.5 18.3 15.0 12.2 9.1 7.5 4.3 3.7 3.6	10 02 12 03 04 24 55 57 66	a = 26.5 b = 36.5
TT3 (60.4)	Col_h	54.2 21.9 16.4 13.0 4.68 3.98	54.2 21.5 16.9 13.4	11 32 51 53	a = 108.3

[a]The average diameter (D) of the polycatenars (estimated from Chem 3D Pro 8.0 molecular model software from Cambridge Soft). [b]d_{obs}: spacing observed; d_{cal}: spacing calculated (deduced from the lattice parameters; a and b for Col_h and Col_r phase.

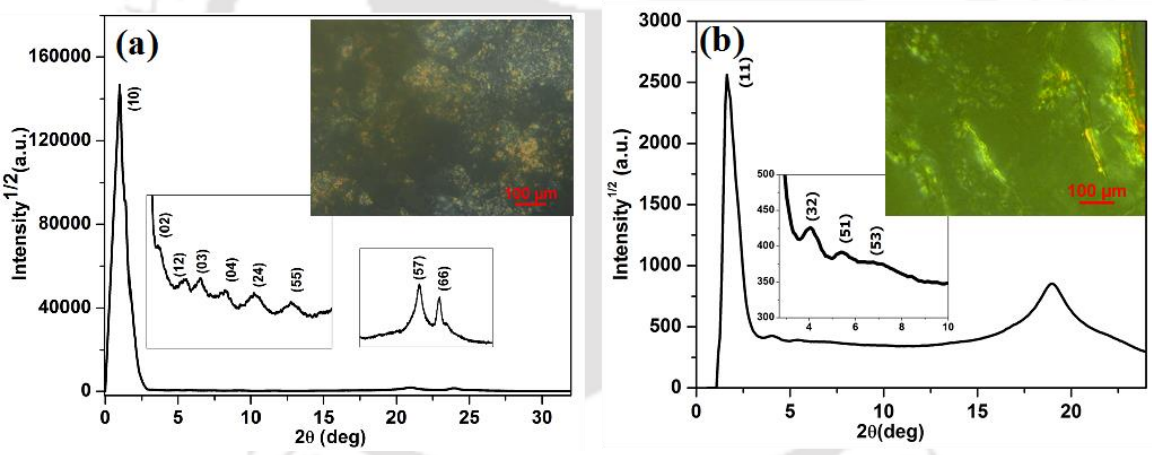

Figure 3.30. a) XRD patterns obtained for the xerogel of **TO3** (Col_r phase, inset shows the POM image of the xerogel of compound **TO3**); b) xerogel of compound **TT3** (Col_h phase, inset shows the POM image of the xerogel of compound **TT3**.

This can be schematically represented as shown in the Fig. 3.31a, b. Compound **TO3**, which is in the form of a discoid, self-assembles to form columns and these columns further self-organize into a Col_r phase that is stable at room temperature. In presence of a hydrocarbon solvent, the compound forms nanofibers of several micrometer in length, which further entangle to form a dense network of fibers that entrap a huge amount of solvent (Fig. 3.31a). In compound **TT3**, two molecules organize to form a disc that self-assembles to form columns and these columns further self-organize into a Col_h phase. On cooling, the arrangement of columns changes to a rectangular lattice that is stable at room

temperature. Interestingly, on interaction with the hydrocarbon solvent this compound forms nanofibers with the columns arranged in a hexagonal lattice, as revealed by the XRD studies (Fig. 3.31b). This shows the impact of atomic scale difference (< 2% of the molecular weight) on the self-assembly of polycatenars in the gel state. It is also important to note that the long nanofibers are mainly formed by the π-π interactions and can be termed as molecular nanowires with a central conductive core and a peripheral insulating sheath. This long-range self-assembly is helpful from the viewpoint of the application in organic electronic devices.

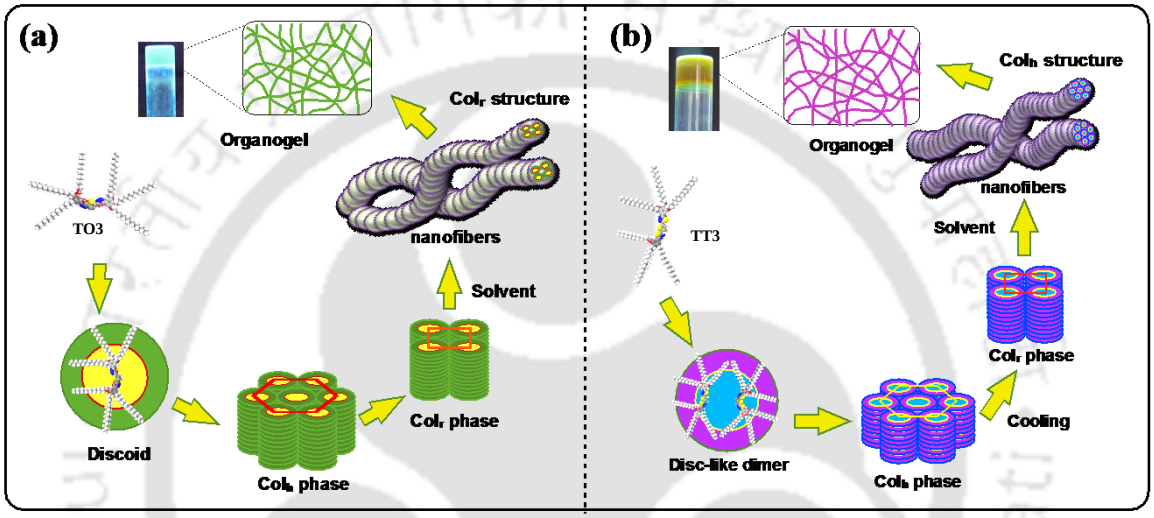

Figure 3.31. Schematics showing the self-assembly of a) **TO3** and b) **TT3** in LC and gel states.

3.2.6. Rheological properties

To establish the elastic nature of the gel samples, dynamic rheological measurements that involved strain sweep, angular frequency sweep and step-strain measurements were carried out. The dependence on the strain amplitude (γ) of the storage or elastic modulus (G') and loss or viscous modulus (G") obtained for representative gels **TO3** and **TT3** is shown in Fig. 3.32a. At low γ values, both the samples show strain-independent behavior of G' and G", with G' > G". This solid-like behavior is typical of a gel structure.[17] Above a critical strain amplitude (γ_c = 0.004 for **TT3** and 0.03 for **TO3**), which defines the upper limit of the linear viscoelastic regime (LVR), both G' and G" become strain-dependent. G' shows a monotonic decrease for both samples, whereas G" for **TT3** passes through a maximum before decreasing. The latter feature is associated with soft glassy rheological (SGR) behaviour[18] universally seen in materials such as foams, slurries, pastes.

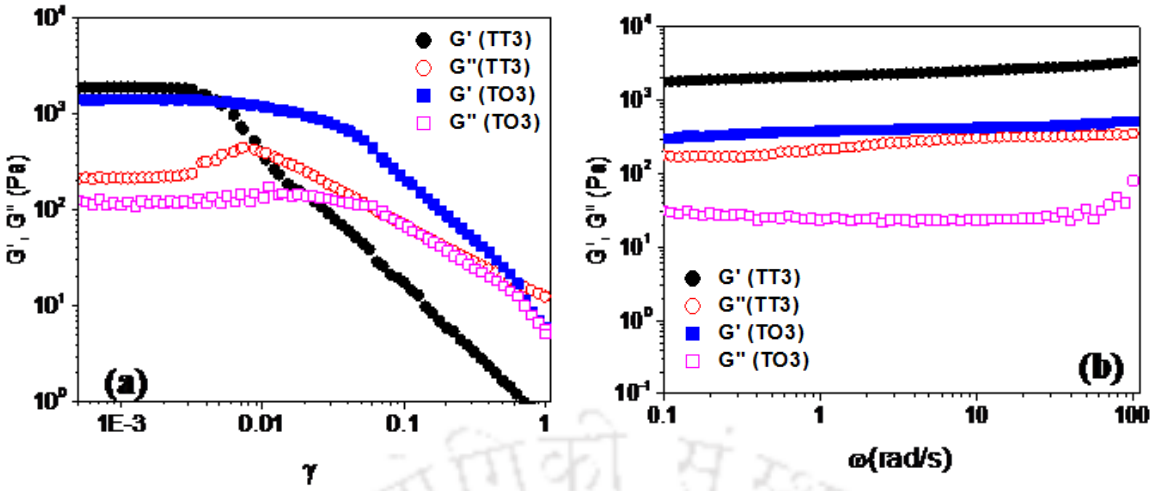

Figure 3.32. a) The dependence of storage (G') and loss (G") moduli on strain (γ) for **TO3** and **TT3**. The temperature was kept constant at 20 ^{o}C and angular frequency (ω) at 1 rad/s; b) Angular frequency (ω) vs. G' and G" for **TO3** and **TT3**. The temperature was kept constant at 20 ^{o}C. The strain amplitude (γ) for both the samples was kept constant with a value corresponding to the LVR (b).

The magnitude of G', a direct measure of the mechanical stiffness, was found to be lower and the LVR longer for **TT3**. These features indicate that although **TT3** is a stiff gel (higher G'), it is less robust compared to **TO3**. In both gels, G' crosses over G" at higher γ values (above γ_c), which signal a deformation-driven transition from a viscoelastic solid to a viscoelastic liquid.[19] In the steady state measurements the shear viscosity (η) was determined as the samples were subjected to increasing shear rate ($\dot{\gamma}$). The obtained flow curves (η *vs* $\dot{\gamma}$) are shown in Fig. 3.34a, b for **TT3** and **TO3** respectively. Although both samples show an overall shear thinning behavior, **TT3** exhibits an anomaly in the data that gives rise to three distinct regions. In region I at low shear rates, the viscosity decreased as the shear rate was increased, which is a typical shear thinning behavior. In region II, η started increasing as $\dot{\gamma}$ was increased and exhibited a shear thickening behavior. This unusual behavior is indicative that structural changes taking place in the gel and needs extensive opto-rheological measurements to explain the phenomena. Similar flow behavior has been observed in triblock-copolymer-decorated systems in which region II (termed as transition region) corresponds to the coexistence of lamellar and onion phases.[20] On further increasing the shear rate, the shear-thinning behavior reappeared (region III). Regions I and III both show a power-law behavior with an identical exponent of 0.8 ± 0.06 which is lower than the power law exponent (0.95 ± 0.01) obtained for **TO3**. The neat shear thinning behavior of **TO3** with increased shearing conditions makes it more suitable for applications that require uniform spreadability.[21]

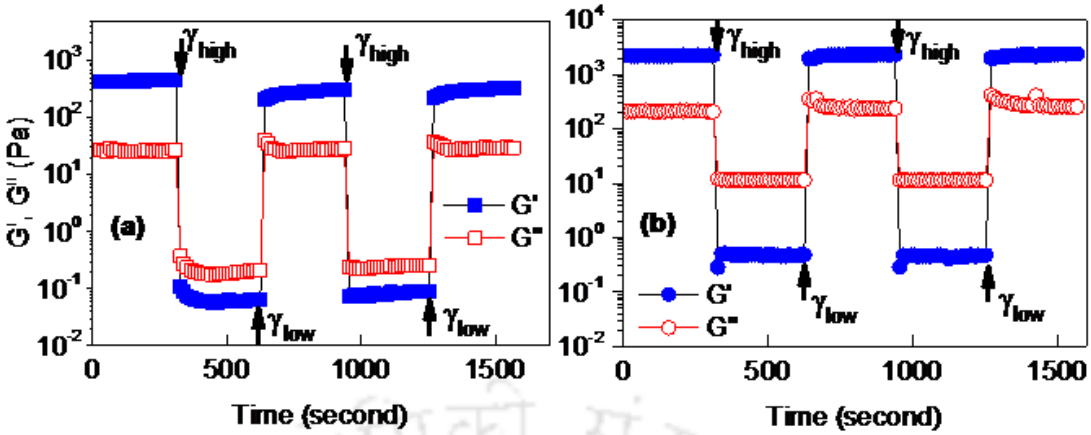

Figure 3.33. a) The step-strain with ω = 1 rad/s for a gel of **TO3** showing the collapse of gel structure when the gel was subjected to a high oscillatory strain (γ) of 5 (regions indicated as high), On application of low γ of 0.001 (regions marked low), the gel recovery took place within about 20 s and was reproduced over repeated cycles of measurement, b) The data obtained for the same experiment for compound **TT3**.

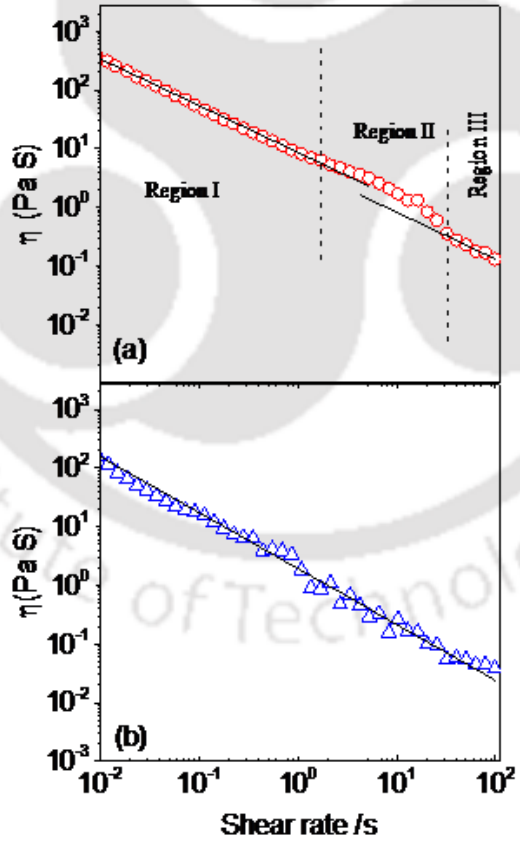

Figure 3.34. Shear rate dependence of viscosity (η) for (a) **TT3** and (b) **TO3**. Whereas **TO3** exhibits simple shear thinning behavior, **TT3** shows an anomaly in the data with regions I and III showing shear thinning and region II showing shear thickening behavior.

3.3. Conclusion

Two series of polycatenar mesogens that contain a central thiophene moiety connected to two substituted oxadiazole or thiadiazole units have been prepared. These heterocycles are connected to peripherally substituted phenyl groups. The number, length and position of substitution of the peripheral chains were varied. The oxadiazole-based polycatenars exhibited a columnar phase with rectangular and hexagonal or oblique symmetry, whereas thiadiazole-based polycatenars exhibited columnar phases with rectangular and/or hexagonal symmetry. All the compounds exhibited bright emission in the solution and thin-film states. Two oxadiazole-based molecules and one thiadiazole-based molecule exhibited good ability to undergo gelation in hydrocarbon solvents at very low concentrations, which qualifies them as supergelators. The supergelation is mainly supported by attractive π–π interactions, along with other weak forces. Of these gels, the oxadiazole- and thiadiazole-containing hexacatenars with *n*-hexadecyloxy chains were studied extensively. These gels showed aggregation-induced enhanced emission, which is of high technological importance for applications in solid-state emissive displays. X-ray diffraction studies showed that the fibers of the xerogels formed by oxadiazole-based polycatenars self-assembled in a rectangular columnar phase, whereas those of the thiadiazole-based polycatenars self-assembled in a hexagonal columnar phase. The number, length, and position of substitution of the peripheral tails and the type of heterocycle moiety adjacent to the thiophene ring greatly affected the self-assembly of the molecules in the LC and gel states. Rheological measurements carried out on the samples confirmed the formation of gels quantitatively and showed that these gels are mechanically robust. The shear-rate dependence of bulk viscosity exhibited an overall shear-thinning behavior, with the exception of an anomaly of shear thickening at a smaller range of shear rates in one of the gels studied. The impact of an atomic-scale difference (oxygen to sulfur, < 2% of the molecular weight) on the self-assembly and the macroscopic properties of these self-assembled compounds have been clearly visualized. This molecular design helps in the development of long molecular nanowires with a strong overlap of central conducting cores and an insulating peripheral sheath, which will be helpful for applications inorganic electronic devices.

3.4. Experimental Section

In this section the detailed synthetic procedures and the molecular structural characterization data have been presented for the intermediates and target compounds mentioned in the scheme.

Synthesis of ethyl 3, 4-bis(hexadecyloxy)benzoate (**3b**):

A mixture of ethyl 3,4-dihydroxybenzoate (16.5 mmol, 1 equiv.), anhydrous K_2CO_3 (72.6 mmol, 4.4 equiv.), *n*-bromohexadecane (36.3 mmol, 2.2 equiv.) were taken in dry DMF and heated at 80 ^oC for 24 h under nitrogen atmosphere. Then the reaction mixture was poured into water and extracted with ethyl acetate. The combined extract was washed with brine, dried over anhydrous Na_2SO_4 and then concentrated. The crude product was purified by column chromatography on silica. Elution with hexane followed by 2-5% ethyl acetate-hexane produced the desire product.

R_f = 0.45 (5% EtOAc-hexane); white solid; yield: 80%; IR (KBr pellet): ν_{max} in cm^{-1} 3419, 2919, 2849, 1710, 1598, 1518, 1277, 1211, 1129, 761; ^1H NMR ($CDCl_3$, 400 MHz, 298 K): δ 7.63 (d, 1H, *J* = 8Hz, H_{Ar}), 7.54 (s, 1H, H_{Ar}), 6.86 (d, 1H, *J* = 8Hz, H_{Ar}), 4.34 (q, 2H, *J* = 8Hz, $COOCH_2$), 4.02-4.05 (m, 4H, 2 × OCH_2), 1.78-1.87 (m, 4H, 2 × CH_2), 1.43-1.49 (m, 4H, 2 × CH_2), 1.38 (t, 3H, CH_3), 1.25-1.36 (m, 48H, 24 × CH_2), 0.88 (t, 6H, 2 × CH_3); ^{13}C NMR ($CDCl_3$, 100 MHz, 298 K): δ 166.75, 153.35, 148.70, 123.66, 122.99, 114.56, 112.14, 69.52, 69.21, 60.90, 32.15, 29.93, 29.89, 29.85, 29.83, 29.64, 29.61, 29.59, 29.42, 29.30, 26.24, 26.20, 22.91, 14.62, 14.33; HRMS (+ESI) exact mass calculated for $C_{41}H_{75}O_4$ ($M+H^+$): 631.5665, Found: 631.5665.

Synthesis of ethyl 3, 5-bis (hexadecyloxy)benzoate (**3c**):

A mixture of ethyl 3,5-dihydroxybenzoate (16.5 mmol, 1 equiv.), anhydrous K_2CO_3 (72.6 mmol, 4.4 equiv.), *n*-bromohexadecane (36.3 mmol, 2.2 equiv.) were taken in dry DMF and heated at 80 ^oC for 24 h under nitrogen atmosphere. Then the reaction mixture was poured into water and extracted with ethyl acetate. The combined extract was washed with brine, dried over anhydrous Na_2SO_4 and then concentrated. The crude product was purified by column chromatography on silica. Elution with hexane followed by 2-5% ethyl acetate-hexane produced the desire product.

R_f = 0.45 (5% EtOAc-hexane); white solid; yield: 80%; IR (KBr pellet): ν_{max} in cm^{-1} 3434, 1703, 1596, 1452, 1399, 1164, 1029, 1001, 851, 771; ^{1}H NMR ($CDCl_3$, 600 MHz, 298 K): δ 7.16 (s, 2H, H_{Ar}), 6.63 (s, 1H, H_{Ar}), 4.36 (q, 2H, *J* = 7.2 Hz, $COOCH_2$), 3.97 (t, 4H, 2 × OCH_2), 1.75-1.80 (m, 4H, 2 × CH_2), 1.26-1.47 (m, 55H, 26 × CH_2, CH_3), 0.87-0.89 (t, 6H, 2 × CH3); ^{13}C NMR ($CDCl_3$, 150 MHz, 298 K): δ 166.73, 160.34, 132.41, 107.85, 106.51, 68.52, 61.25, 32.15, 29.92, 29.88, 29.82, 29.79, 29.59, 29.41, 26.24, 22.91, 14.54, 14.33; HRMS (ESI) exact mass calculated for $C_{41}H_{75}O_4$ (M+1): 631.5665, Found: 631.5651.

Synthesis of ethyl 3,4,5-trihexadecyloxy benzoate (**3d**):

A mixture of ethyl gallate (15.1 mmol, 1 equiv.), anhydrous K_2CO_3 (99.9 mmol, 6.6 equiv.), *n*-bromohexadecane (49.83 mmol, 3.3 equiv.) were taken in dry DMF and heated at 80 ^{o}C for 24 h under nitrogen atmosphere. Then the reaction mixture was poured into water and extracted with ethyl acetate. The combined extract was washed with water and dried over anhydrous Na_2SO_4 and then concentrated. The crude product was purified by column chromatography on silica. Elution with hexane followed by 2-5% ethyl acetate-hexane produced the desire product.

R_f = 0.5 (5% EtOAc-hexane); white solid; yield: 75%; IR (KBr pellet): ν_{max} in cm^{-1} 2922, 2850, 1716, 1583, 1468, 1426, 1331, 1218, 1110, 1041; ^{1}H NMR ($CDCl_3$, 400 MHz, 298 K): δ 7.25 (s, 2H, H_{Ar}), 4.35 (q, 2H, *J* = 7.2 Hz, $COOCH_2$), 4.01 (t, 6H, 3 × OCH_2), 1.25-1.82 (m, 84H, 42 × CH_2), 0.87 (m, 12H, 4 × CH_3); ^{13}C NMR ($CDCl_3$, 100 MHz, 298 K): δ 166.70, 153.04, 142.61, 125.28, 108.29, 73.72, 69.44, 61.17, 33.05, 32.16, 30.56, 29.94, 29.89, 29.87, 29.80, 29.63, 29.60, 29.57, 26.32, 26.29, 22.92, 14.63, 14.33; HRMS (ESI+) exact mass calculated for $C_{57}H_{107}O_5$ (M+1): 871.8113, Found: 871.8031.

Synthesis of ethyl 3,4,5-tridecyloxy benzoate (**5d**):

A mixture of ethyl gallate (15.1 mmol, 1 equiv.), anhydrous K_2CO_3 (99.9 mmol, 6.6 equiv.), *n*-bromodecane (49.83 mmol, 3.3 equiv.) were taken in dry DMF and heated at 80 ^{o}C for 24 h under nitrogen atmosphere. Then the reaction mixture was poured into water and extracted with ethyl acetate. The combined extract was washed with water and dried over anhydrous Na_2SO_4 and then concentrated. The crude product was purified by column chromatography on silica. Elution with hexane followed by 5-10% ethyl acetate-hexane produced the desire product.

R_f = 0.6 (5% EtOAc-hexane); Low melting white solid; yield: 70%; IR (KBr pellet): ν_{max} in cm^{-1} 2920, 2850, 1710, 1597, 1516, 1466, 1424, 1347, 1213, 1103, 760, 613; ^{1}H NMR ($CDCl_3$, 600 MHz, 298 K): δ 7.26 (s, 2H, Ar), 4.35-4.36 (m, 2H, $COOCH_2$), 4.01 (s, 6H, 3 × OCH_2), 0.89-1.81 (m, 60H, 24 × CH_2, 4 × CH_3); ^{13}C NMR ($CDCl_3$, 150 MHz, 298 K): δ 166.67, 152.99, 145.31, 125.24, 108.19, 73.68, 69.37, 61.14, 32.12, 30.53, 29.93, 29.84, 29.79, 29.60, 29.56, 26.29, 22.89, 14.30; HRMS (ESI+) exact mass calculated for $C_{39}H_{71}O_5$ (M+1): 619.5302, Found: 619.5218.

Synthesis of ethyl 3,4-bis (hexadecyloxy)benzhydrazide (**4b**):

A mixture of ethyl 3,4-bis(hexadecyloxy)benzoate (10.2 mmol, 1 equiv.), excess hydrazine hydrate (20 equiv.) in butanol was refluxed for 48 h. Excess solvent was removed and water was added to it. Resulting precipitate was collected by filtration, washed with excess water, dried under vacuum and recrystallization from ethanol gave white solid product.

R_f = 0.25 (20% EtOAc-hexane); white solid; yield: 70%; IR (KBr pellet): ν_{max} in cm^{-1} 3248, 2919, 2848, 1711, 1514, 1467, 1278, 1212, 1150, 761; ^{1}H NMR ($CDCl_3$, 400 MHz, 298 K): δ 7.34 (d, 1H, *J* = 8Hz, H_{Ar}), 7.26 (b s, 1H, CONH), 7.22 (dd, 1H, *J* = 4Hz, *J* = 8Hz, H_{Ar}), 6.85 (d, 1H, *J* = 8Hz, H_{Ar}), 4.08 (b s, 2H, NH_2), 4.00-4.05 (m, 4H, 2 × OCH_2), 1.79-1.86 (m, 4H, 2 × CH_2), 1.38-1.50 (m, 4H, 2 × CH_2), 1.25-1.36 (m, 48H, 24 × CH_2), 0.88 (m, 6H, 2 × CH_3); ^{13}C NMR ($CDCl_3$, 150 MHz, 298 K): δ 168.77, 152.55, 149.33, 125.21, 119.70, 112.76, 112.65, 69.62, 69.37, 32.15, 29.94, 29.89, 29.85, 29.63, 29.59, 29.43, 29.34, 26.23, 22.90, 14.33; HRMS (+ESI) exact mass calculated for $C_{39}H_{73}N_2O_3$ ($M+H^+$): 617.5621, Found: 617.5726.

Synthesis of ethyl 3,5-bis(hexadecyloxy)benzhydrazide (**4c**):

A mixture of ethyl 3,5-bis(hexadecyloxy)benzoate (10.2 mmol, 1 equiv.), excess hydrazine hydrate (20 equiv.) in butanol was refluxed for 48 h. Excess solvent was removed and water was added to it. Resulting precipitate was collected by filtration, washed with excess water, dried under vacuum and recrystallization from ethanol gave white solid product.

R_f = 0.25 (20% EtOAc-hexane); white solid; yield: 70%; IR (KBr pellet): ν_{max} in cm^{-1} 3446, 2920, 2849, 1597, 1469, 1332, 1170, 1064, 913, 721; ^{1}H NMR ($CDCl_3$, 400 MHz, 298 K): δ 7.38 (b s, 1H, CONH), 6.83 (s, 2H, H_{Ar}), 6.58 (s, 1H, H_{Ar}), 4.08 (b s, 2H, NH_2),

3.95 (t, 4H, 2 × OCH_2), 1.74-1.79 (m, 4H, 2 × CH_2), 1.42-1.46 (m, 4H, 2 × CH_2), 1.26-1.41 (m, 48H, 24 × CH_2), 0.88 (m, 6H, 2 × CH_3); ^{13}C NMR ($CDCl_3$, 100 MHz, 298 K): δ 168.91, 160.71, 134.76, 105.34, 105.02, 68.57, 32.14, 29.92, 29.88, 29.82, 29.79, 29.58, 29.38, 26.22, 22.91, 14.34; HRMS (+ESI) exact mass calculated for $C_{39}H_{73}N_2O_3$ ($M+H^+$): 617.5621, Found: 617.5600.

Synthesis of ethyl 3, 4, 5-tris (hexadecyloxy)benzhydrazide (**4d**):

A mixture of ethyl 3,4,5-tri-*n*-hexadecyloxybenzoate (10 mmol, 1 equiv.), excess hydrazine hydrate (20 equiv.) in butanol was refluxed for 48 h. Excess solvent was removed and water was added to it. Resulting precipitate was collected by filtration, washed with excess water, dried under vacuum and recrystallization from ethanol gave white solid product.

R_f = 0.52 (20% EtOAc-hexane); white solid; yield: 75%; IR (KBr pellet): ν_{max} in cm^{-1} 3448, 3248, 2921, 2850, 1635, 1579, 1466, 1427, 1238, 1122; ^{1}H NMR ($CDCl_3$, 400 MHz, 298 K): δ 7.22 (b s, 1H, CONH), 6.92 (s, 2H, H_{Ar}), 4.07 (s, 2H, NH_2), 3.99 (m, 6H, 3 × OCH_2), 1.26-1.80 (m, 84H, 42 × CH_2), 0.88 (m, 9H, 3 × CH_3); ^{13}C NMR ($CDCl_3$, 150 MHz, 298 K): δ 168.70, 153.54, 141.92, 127.68, 105.74, 69.60, 30.53, 29.97, 29.95, 29.88, 29.60, 26.30, 22.92, 14.33; HRMS (ESI+) exact mass calculated for $C_{55}H_{105}N_2O_4$ (M+1): 857.8069, Found: 857.8151.

Synthesis of ethyl 3,4,5-tris (decyloxy)benzhydrazide (**6d**):

A mixture of ethyl 3,4,5-tri-*n*-decyloxybenzoate (10 mmol, 1 equiv.), excess hydrazine hydrate (20 equiv.) in butanol was refluxed for 48 h. Excess solvent was removed and water was added to it. Resulting precipitate was collected by filtration, washed with excess water, dried under vacuum and recrystallization from ethanol gave white solid product.

R_f = 0.45 (20% EtOAc-hexane); white solid; yield: 80%; IR (KBr pellet): ν_{max} in cm^{-1} 3475, 2923, 2852, 1746, 1640, 1019, 826, 719, 523; ^{1}H NMR ($CDCl_3$, 400 MHz, 298 K): δ 7.33 (b s, 1H, CONH), 6.92 (s, 2H, Ar), 3.99 (m, 8H, NH_2, 3 × OCH_2), 0.88-1.80 (m, 57H, 24 × CH_2, 3 × CH_3); ^{13}C NMR ($CDCl_3$, 100 MHz, 298 K): δ 168.91, 153.37, 141.60, 127.61, 105.71, 73.70, 69.50, 32.10, 30.50, 29.91, 29.59, 29.53, 22.87, 14.28; HRMS (ESI+) exact mass calculated for $C_{37}H_{69}N_2O_4$ (M+1): 605.5257, Found: 605.5171.

Synthesis of **TO1**:

2,5-Thiophenedicarboxylic acid (1 mmol) in 5 mL thionyl chloride and one drop of DMF (catalytic amount) was refluxed for around 6 h. Then excess thionyl chloride was removed through distillation and the crude product was used as such without purification in the next step. The solution of 2,5-Thiophenedicarboxylic acid chloride (0.9 mmol, 1 equiv.) in dry THF was added dropwise to a solution of 3, 4-di-*n*-hexadecyloxy benzohydrazide (1.8 mmol, 2.05 equiv.) and triethylamine (1.8 mmol, 2 equiv.) in dry THF. Then the reaction was heated to reflux for 24 h. After cooling to rt, THF was removed completely by distillation and then extracted with ethyl acetate. The extract was washed with water, dried over Na_2SO_4 and concentrated. The resulting crude product (**7a**) was directly used for next reaction.

The crude product **7a** (0.5 mmol, 1 equiv.) was dissolved in $POCl_3$ and refluxed for 24 h. The residue was slowly added to ice water and extracted with dichloromethane. The combined extract was washed with brine, dried over anhydrous Na_2SO_4 and then concentrated. Then, the crude product was further purified through column chromatography on neutral alumina. Elution with 30-40% DCM-hexane produces the desire product.

R_f = 0.55 (50% DCM-hexane); pale yellow solid; yield: 60%; λ_{max} = 365 nm; ε = 31,150 M^{-1} cm^{-1}; IR (KBr pellet): ν_{max} in cm^{-1} 3448, 2955, 2917, 2849, 1706, 1607, 1504, 1466, 1284, 1015; ^{1}H NMR ($CDCl_3$, 600 MHz, 298 K): δ 7.87 (s, 2H, H_{Ar}), 7.64 (d, 2H, *J* = 6Hz, H_{Ar}), 7.62 (s, 2H, H_{Ar}), 6.98 (d, 2H, *J* = 6Hz, H_{Ar}), 4.11-4.07 (m, 8H, 4 × OCH_2), 1.89-1.85 (m, 8H, 4 × CH_2), 1.62-1.60 (m, 16H, 8 × CH_2),), 1.52-1.50 (m, 8H, 4 × CH_2), 1.49-1.47 (m, 8H, 4 × CH_2), 1.38-1.26 (m, 72H, 36 × CH_2), 0.87 (t, 12H, 4 × CH_3); ^{13}C NMR ($CDCl_3$, 150 MHz, 298 K): δ 165.00, 159.75, 152.85, 149.63, 130.00, 129.05, 120.89, 115.78, 113.12, 111.90, 69.70, 69.39, 32.14, 29.94, 29.88, 29.84, 29.65, 29.62, 29.59, 29.42, 29.31, 26.25, 26.21, 22.91, 14.32; MALDI TOF MS: *m/z* for $C_{84}H_{141}N_4O_6S[M+H^+]$, calculated: 1334.0572, Found: 1334.7080.

Synthesis of **TO2**:

2,5-Thiophenedicarboxylic acid (1 mmol) in 5 mL thionyl chloride and one drop of DMF (catalytic amount) was refluxed for around 6 h. Then excess thionyl chloride was removed through distillation and the crude product was used as such without purification

in the next step. The solution of 2, 5-Thiophenedicarboxylic acid chloride (0.9 mmol, 1 equiv.) in dry THF was added dropwise to a solution of 3, 5-di-*n*-hexadecyloxy benzohydrazide (1.8 mmol, 2.05 equiv.) and triethylamine (1.8 mmol, 2 equiv.) in dry THF. Then the reaction was heated to reflux for 24 h. After cooling to rt, THF was removed completely by distillation and then extracted with ethyl acetate. The extract was washed with water, dried over Na_2SO_4 and concentrated. The resulting crude product (**7b**) was directly used for next reaction.

The crude product **7b** (0.5 mmol, 1 equiv.) was dissolved in $POCl_3$ and refluxed for 24 h. The residue was slowly added to ice water and extracted with dichloromethane. The combined extract was washed with brine, dried over anhydrous Na_2SO_4 and then concentrated. Then, the crude product was further purified through column chromatography on neutral alumina. Elution with 30-40% DCM-hexane produces the desire product.

R_f = 0.5 (50% DCM-hexane); white solid; yield: 60%; λ_{max} = 353 nm; ε = 29,550 M^{-1} cm^{-1}; IR (KBr pellet): ν_{max} in cm^{-1} 3445, 2920, 2851, 1730, 1597, 1548, 1466, 1441, 1342, 1172; ^{1}H NMR ($CDCl_3$, 600 MHz, 298 K): δ 7.59 (s, 2H, H_{Ar}), 7.12 (s, 2H, H_{Ar}), 6.59 (s, 2H, H_{Ar}), 4.01 (t, 8H, 4 × OCH_2), 1.83-1.78 (m, 8H, 4 × CH_2), 1.47-1.44 (m, 8H, 4 × CH_2), 1.36-1.35 (m, 8H, 4 × CH_2), 1.32-1.26 (m, 88H, 44 × CH_2), 0.88 (t, 12H, 4 × CH_3); ^{13}C NMR ($CDCl_3$, 150 MHz, 298 K): δ 164.92, 160.97, 160.05, 130.30, 129.06, 124.73, 105.46, 68.68, 32.14, 29.92, 29.83, 29.81, 29.61, 29.59, 29.40, 26.23, 22.91, 14.33; MALDI TOF MS: *m/z* for $C_{84}H_{141}N_4O_6S[M+H^+]$, calculated: 1334.0572, Found: 1334.5090.

Synthesis of **TO3**:

2,5-Thiophenedicarboxylic acid (1 mmol) in 5 mL thionyl chloride and one drop of DMF (catalytic amount) was refluxed for around 6 h. Then excess thionyl chloride was removed through distillation and the crude product was used as such without purification in the next step. The solution of 2, 5-Thiophenedicarboxylic acid chloride (0.9 mmol, 1 equiv.) in dry THF was added dropwise to a solution of 3, 4, 5-tri-*n*-hexadecyloxy benzohydrazide (1.8 mmol, 2.05 equiv.) and triethylamine (1.8 mmol, 2 equiv.) in dry THF. Then the reaction was heated to reflux for 24 h. After cooling to rt, THF was removed completely by distillation and then extracted with ethyl acetate. The extract was

washed with water, dried over Na_2SO_4 and concentrated. The resulting crude product (**7c**) was directly used for next reaction.

The crude product **7c** (0.5 mmol, 1equiv.) was dissolved in $POCl_3$ and refluxed for 24 h. The residue was slowly added to ice water and extracted with dichloromethane. The combined extract was washed with brine, dried over anhydrous Na_2SO_4 and then concentrated. Then, the crude product was further purified through column chromatography on neutral alumina. Elution with 20-30% DCM-hexane produces the desire product.

R_f = 0.45 (40% DCM-hexane); pale yellow solid; yield: 70%; λ_{max} = 362 nm; ε = 28,800 M^{-1} cm^{-1}; IR (KBr pellet): ν_{max} in cm^{-1} 3442, 2919, 2850, 1636, 1591, 1492, 1468, 1385, 1239, 1122; ^{1}H NMR ($CDCl_3$, 600 MHz, 298 K): δ 7.89 (s, 2H, H_{Ar}), 7.30 (s, 4H, H_{Ar}), 4.08 (t, 8H, 4 × OCH_2), 4.05 (t, 4H, 2 × OCH_2), 1.88-1.83 (m, 8H, 4 × CH_2), 1.79-1.74 (m, 4H, 2 × CH_2), 1.53-1.47 (m, 12H, 6 × CH_2), 1.38-1.26 (m, 144H, 72 × CH_2), 0.87 (t, 18H, 6 × CH_3); ^{13}C NMR ($CDCl_3$, 150 MHz, 298 K): δ 165.05, 159.93, 153.89, 141.97, 130.15, 129.03, 118.00, 105.77, 73.90, 69.66, 32.15, 30.56, 29.94, 29.88, 29.81, 29.64, 29.59, 29.56, 26.32, 26.30, 22.91, 14.33; MALDI TOF MS: *m/z* for $C_{116}H_{204}N_4O_8S[M^+]$, calculated: 1814.5433, Found: 1814.998.

Synthesis of **TO4**:

2,5-Thiophenedicarboxylic acid (1 mmol) in 5 mL thionyl chloride and one drop of DMF (catalytic amount) was refluxed for around 6 h. Then excess thionyl chloride was removed through distillation and the crude product was used as such without purification in the next step. The solution of 2, 5-Thiophenedicarboxylic acid chloride (0.9 mmol, 1 equiv.) in dry THF was added dropwise to a solution of 3, 4, 5-tri-*n*-decyloxy benzohydrazide (1.8 mmol, 2.05 equiv.) and triethylamine (1.8 mmol, 2 equiv.) in dry THF. Then the reaction was heated to reflux for 24 h. After cooling to rt, THF was removed completely by distillation and then extracted with ethyl acetate. The extract was washed with water, dried over Na_2SO_4 and concentrated. The resulting crude product (**7d**) was directly used for next reaction.

The crude product **7d** (0.5 mmol, 1 equiv.) was dissolved in $POCl_3$ and refluxed for 24 h. The residue was slowly added to ice water and extracted with dichloromethane. The combined extract was washed with brine, dried over anhydrous Na_2SO_4 and then

concentrated. Then, the crude product was further purified through column chromatography on neutral alumina. Elution with 20-30% DCM-hexane produces the desire product.

R_f = 0.45 (40% DCM-hexane); pale yellow solid; yield: 70%; λ_{max} = 362 nm; ε = 30,670 M^{-1} cm^{-1}; IR (KBr pellet): ν_{max} in cm^{-1} 3198, 2919, 2851, 1639, 1509, 1468, 1444, 1423, 1238, 1126; ^{1}H NMR ($CDCl_3$, 600 MHz, 298 K): δ 7.89 (s, 2H, H_{Ar}), 7.30 (s, 4H, H_{Ar}), 4.08 (t, 8H, 4 × OCH_2), 4.05 (t, 4H, 2 × OCH_2), 1.88-1.83 (m, 8H, 4 × CH_2), 1.77-1.66 (m, 4H, 2 × CH_2), 1.53-1.47 (m, 12H, 6 × CH_2), 1.38-1.35 (m, 12H, 6 × CH_2), 1.33-1.28 (m, 60H, 30 × CH_2), 0.88 (t, 18H, 6 × CH_3); ^{13}C NMR ($CDCl_3$, 150 MHz, 298 K): δ 165.04, 159.93, 153.89, 141.96, 130.13, 129.02, 118.00, 105.75, 73.88, 69.65, 32.13, 30.56, 29.95, 29.89, 29.86, 29.81, 29.62, 29.57, 29.54, 26.29, 22.90, 14.33; MALDI TOF MS: *m/z* for $C_{80}H_{134}N_4O_8S[M+2H^+]$, calculated: 1310.9922, Found: 1310.3160.

Synthesis of **TT1**:

2,5-Thiophenedicarboxylic acid (1 mmol) in 5 mL thionyl chloride and one drop of DMF (catalytic amount) was refluxed for around 6 h. Then excess thionyl chloride was removed through distillation and the crude product was used as such without purification in the next step. The solution of 2, 5-Thiophenedicarboxylic acid chloride (0.9 mmol, 1 equiv.) in dry THF was added dropwise to a solution of 3, 4-di-*n*-hexadecyloxy benzohydrazide (1.8 mmol, 2.05 equiv.) and triethylamine (1.8 mmol, 2 equiv.) in dry THF. Then the reaction was heated to reflux for 24 h. After cooling to rt, THF was removed completely by distillation and then extracted with ethyl acetate. The extract was washed with water, dried over Na_2SO_4 and concentrated. The resulting crude product (**7a**) was directly used for next reaction.

The crude product **7a** (0.5 mmol, 1 equiv.) was dissolved in dry toluene and added to lawesson's reagent (2.2 equiv.) at room temperature. Then the reaction mixture was refluxed for 24 h. After completion of the reaction, toluene was removed by distillation and the residue was extracted with dichloromethane. The combined extract was washed with brine, dried over anhydrous Na_2SO_4 and then concentrated. Then, the crude product was further purified through column chromatography on neutral alumina. Elution with 40-50% DCM-hexane produces the desire product.

R_f = 0.45 (70% DCM-hexane); yellow solid; yield: 40%; λ_{max} = 368 nm; ε = 21,850 M^{-1} cm^{-1}; IR (KBr pellet): ν_{max} in cm^{-1} 3445, 2920, 2850, 1594, 1520, 1465, 1388, 1273, 1138, 1016; ^{1}H NMR ($CDCl_3$, 600 MHz, 298 K): δ 7.62 (s, 2H, H_{Ar}), 7.42 (d, 2H, *J* = 6Hz, H_{Ar}), 7.26 (s, 2H, H_{Ar}), 6.92 (d, 2H, *J* = 6Hz, H_{Ar}), 4.09 (t, 4H, 2 × OCH_2), 4.05 (t, 4H, 2 × OCH_2), 1.86-1.85 (m, 8H, 4 × CH_2), 1.49-1.48 (m, 8H, 4 × CH_2), 1.36-1.29 (m, 8H, 4 × CH_2), 1.29-1.25 (m, 88H, 44 × CH_2), 0.87 (t, 12H, 4 × CH_3); ^{13}C NMR ($CDCl_3$, 150 MHz, 298 K): δ 165.00, 159.75, 152.85, 149.63, 130.00, 129.05, 120.89, 115.78, 113.12, 111.90, 69.70, 69.39, 32.14, 29.94, 29.88, 29.84, 29.65, 29.62, 29.59, 29.42, 29.31, 26.25, 26.21, 22.91, 14.32; MALDI TOF MS: *m/z* for $C_{84}H_{141}N_4O_4S_3[M+H^+]$, calculated: 1366.0115, Found: 1366.575.

Synthesis of **TT2**:

2,5-Thiophenedicarboxylic acid (1 mmol) in 5 mL thionyl chloride and one drop of DMF (catalytic amount) was refluxed for around 6 h. Then excess thionyl chloride was removed through distillation and the crude product was used as such without purification in the next step. The solution of 2, 5-Thiophenedicarboxylic acid chloride (0.9 mmol, 1 equiv.) in dry THF was added dropwise to a solution of 3, 5-di-*n*-hexadecyloxy benzohydrazide (1.8 mmol, 2.05 equiv.) and triethylamine (1.8 mmol, 2 equiv.) in dry THF. Then the reaction was heated to reflux for 24 h. After cooling to rt, THF was removed completely by distillation and then extracted with ethyl acetate. The extract was washed with water, dried over Na_2SO_4 and concentrated. The resulting crude product (**7b**) was directly used for next reaction.

The crude product **7b** (0.5 mmol, 1 equiv.) was dissolved in dry toluene and added to lawesson's reagent (2.2 equiv.) at room temperature. Then the reaction mixture was refluxed for 24 h. After completion of the reaction, toluene was removed by distillation and the residue was extracted with dichloromethane. The combined extract was washed with brine, dried over anhydrous Na_2SO_4 and then concentrated. Then, the crude product was further purified through column chromatography on neutral alumina. Elution with 40-50% DCM-hexane produces the desire product

R_f = 0.45 (70% DCM-hexane); yellow solid; yield: 40%; λ_{max} = 374 nm; ε = 20,650 M^{-1} cm^{-1}; IR (KBr pellet): ν_{max} in cm^{-1} 3445, 2918, 2850, 1603, 1464, 1422, 1346, 1172, 1060; ^{1}H NMR ($CDCl_3$, 600 MHz, 298 K): δ 7.91 (s, 2H, H_{Ar}), 7.28 (s, 2H, H_{Ar}), 6.66 (s, 2H,

H_{Ar}), 4.03 (t, 8H, 4 × OCH_2), 1.83-1.79 (m, 8H, 4 × CH_2), 1.49-1.44 (m, 8H, 4 × CH_2), 1.36-1.32 (m, 8H, 4 × CH_2), 1.29-1.26 (m, 88H, 44 × CH_2), 0.88 (t, 12H, 4 × CH_3); ^{13}C NMR ($CDCl_3$, 150 MHz, 298 K): δ 168.57, 160.47, 135.68, 131.29, 129.85, 106.53, 104.74, 68.65, 32.15, 29.93, 29.85, 29.82, 29.63, 29.59, 29.41, 26.25, 22.91, 14.33; MALDI TOF MS: *m/z* for $C_{84}H_{142}N_4O_4S_3[M+2H^+]$, calculated: 1367.0193, Found: 1367.526.

Synthesis of **TT3**:

2,5-Thiophenedicarboxylic acid (1 mmol) in 5 mL thionyl chloride and one drop of DMF (catalytic amount) was refluxed for around 6 h. Then excess thionyl chloride was removed through distillation and the crude product was used as such without purification in the next step. The solution of 2, 5-Thiophenedicarboxylic acid chloride (0.9 mmol, 1 equiv.) in dry THF was added dropwise to a solution of 3, 4, 5-tri-*n*-hexadecyloxy benzohydrazide (1.8 mmol, 2.05 equiv.) and triethylamine (1.8 mmol, 2 equiv.) in dry THF. Then the reaction was heated to reflux for 24 h. After cooling to rt, THF was removed completely by distillation and then extracted with ethyl acetate. The extract was washed with water, dried over Na_2SO_4 and concentrated. The resulting crude product (**7c**) was directly used for next reaction.

The crude product **7c** (0.5 mmol, 1 equiv.) was dissolved in dry toluene and added to lawesson's reagent (2.2 equiv.) at room temperature. Then the reaction mixture was refluxed for 24 h. After completion of the reaction, toluene was removed by distillation and the residue was extracted with dichloromethane. The combined extract was washed with brine, dried over anhydrous Na_2SO_4 and then concentrated. Then, the crude product was further purified through column chromatography on neutral alumina. Elution with 50-60% DCM-hexane produces the desire product

R_f = 0.6 (70% DCM-hexane); yellow solid; yield: 50%; λ_{max} = 383 nm; ε = 21,800 M^{-1} cm^{-1}; IR (KBr pellet): ν_{max} in cm^{-1} 3444, 2919, 2850, 1582, 1466, 1382, 1239, 1122, 1010; ^1H NMR ($CDCl_3$, 600 MHz, 298 K): δ 7.58 (s, 2H, H_{Ar}), 7.18 (s, 4H, H_{Ar}), 4.06 (t, 8H, 4 × OCH_2), 4.03 (t, 4H, 2 × OCH_2), 1.85-1.83 (m, 8H, 4 × CH_2), 1.77-1.75 (m, 4H, 2 × CH_2), 1.49-1.41 (m, 12H, 6 × CH_2), 1.36-1.35 (m, 12H, 6 × CH_2), 1.35-1.34 (m, 136H, 68 × CH_2), 0.87 (t, 18H, 6 × CH_3); ^{13}C NMR ($CDCl_3$, 150 MHz, 298 K): δ 168.60, 160.60, 153.82, 141.43, 135.66, 129.63, 124.66, 106.76, 73.89, 69.63, 32.15, 30.56, 29.95, 29.88,

29.81, 29.64, 29.60, 29.56, 26.31, 22.92, 14.33; MALDI TOF MS: *m/z* for $C_{116}H_{205}N_4O_6S_3[M+H^+]$, calculated: 1847.5055, Found: 1847.061.

Synthesis of **TT4**:

2, 5-Thiophenedicarboxylic acid (1 mmol) in 5 mL thionyl chloride and one drop of DMF (catalytic amount) was refluxed for around 6 h. Then excess thionyl chloride was removed through distillation and the crude product was used as such without purification in the next step. The solution of 2, 5-Thiophenedicarboxylic acid chloride (0.9 mmol, 1 equiv.) in dry THF was added dropwise to a solution of 3, 4, 5-tri-*n*-decyloxy benzohydrazide (1.8 mmol, 2.05 equiv.) and triethylamine (1.8 mmol, 2 equiv.) in dry THF. Then the reaction was heated to reflux for 24 h. After cooling to rt, THF was removed completely by distillation and then extracted with ethyl acetate. The extract was washed with water, dried over Na_2SO_4 and concentrated. The resulting crude product (**7d**) was directly used for next reaction.

The crude product **7d** (0.5 mmol, 1 equiv.) was dissolved in dry toluene and added to lawesson's reagent (2.2 equiv.) at room temperature. Then the reaction mixture was refluxed for 24 h. After completion of the reaction, toluene was removed by distillation and the residue was extracted with dichloromethane. The combined extract was washed with brine, dried over anhydrous Na_2SO_4 and then concentrated. Then, the crude product was further purified through column chromatography on neutral alumina. Elution with 50-60% DCM-hexane produces the desire product

R_f = 0.6 (70% DCM-hexane); yellow solid; yield: 50%; λ_{max} = 394 nm; ε = 22,900 M^{-1} cm^{-1}; IR (KBr pellet): ν_{max} in cm^{-1} 3444, 2919, 2851, 1583, 1444, 1422, 1382, 1238, 1126, 1065; ^{1}H NMR ($CDCl_3$, 600 MHz, 298 K): δ 7.59 (s, 2H, H_{Ar}), 7.19 (s, 4H, H_{Ar}), 4.06 (t, 8H, 4 × OCH_2), 4.03 (t, 4H, 2 × OCH_2), 1.87-1.82 (m, 8H, 4 × CH_2), 1.79-1.74 (m, 4H, 2 × CH_2), 1.49-1.48 (m, 12H, 6 × CH_2), 1.37-1.36 (m, 12H, 6 × CH_2), 1.34-1.28 (m, 60H, 30 × CH_2), 0.88 (t, 18H, 6 × CH_3); ^{13}C NMR ($CDCl_3$, 150 MHz, 298 K): δ 168.61, 160.63, 153.84, 141.45, 135.67, 129.63, 124.68, 106.79, 73.90, 69.65, 32.15, 30.56, 29.96, 29.90, 29.87, 29.81, 29.63, 29.57, 29.55, 26.30, 22.92, 14.34; MALDI TOF MS: *m/z* for $C_{80}H_{132}N_4O_6S_3[M+2H^+]$, calculated: 1342.9466, Found: 1342.116.

3.5. References

1. (a) A. Mishra, C. Q. Ma and P. Bäuerle, *Chem. Rev*., 2009, **109**, 1141-1276; (b) M. Melucci, L. Favaretto, A. Zanelli, M. Cavallini, A. Bongini, P. Maccagnani, P. Ostoja, G. Derue, R. Lazzaroni and G. Barbarella, *Adv. Func. Mat.*, 2010, **20**, 445-452; (c) K. Takimiya, S. Shinamura, I. Osaka and E. Miyazaki, *Adv. Mater.*, 2011, **23**, 4347-4370; (d) I. F. Perepichka and D. F. Perepichka, *Handbook of Thiophene-Based Materials*, Ed.Wiley-VCH, 2009.
2. (a) J. Zaumseil and H. Sirringhaus, *Chem. Rev.*, 2007, **107**, 1296-1323; (b) J. L. Brusso, O. D. Hirst, A. Dadvand, S. Ganesan, F. Cicoira, C. M. Robertson, R. T. Oakley, F. Rosei and D. F. Perepichka, *Chem. Mater.*, 2008, **20**, 2484-2494; (c) J. Shi, Y. Li, M. Jia, L. Xu and H. Wang, *J. Mater. Chem.*, 2011, **21**, 17612-17614.
3. (a) I. F. Perepichka, D. F. Perepichka, H. Meng and F. Wudl, *Adv. Mater.*, 2005, **17**, 2281-2305; (b) X. Jiang, Z. Zheng, Y. Harima, J. Ohshita and P. Sun, *J. Mater. Chem.*, 2011, **21**, 1902-1906.
4. (a) S. Roquet, R. M. De Bettignies, P. Leriche, A. Cravino and J. Roncali, *J. Mater. Chem.*, 2006, **16**, 3040-3045; (b) Y. Li and Y. Zou, *Adv. Mater.*, 2008, **20**, 2952-2958; (c) T. H. Kwon, V. Armel, A. Nattestad, D. R. Macfarlane, U. Bach, S. J. Lind, K. C. Gordon, W. Tang, D. J. Jones and A. B. Holmes, *J. Org. Chem.*, 2011, **76**, 4088-4093; (d) P. L. T. Boudreault, A. Najari and M. Leclerc, *Chem. Mater.*, 2011, **23**, 456-469.
5. (a) D. Byron, A. Matharu, R. Wilson and G. Wright, *Mol. Cryst. Liq. Cryst.*, 1995, **265**, 61-76; (b) R. Azumi, G. Go¨tz and P. Bäuerle, *Synth. Met.*, 1999, **101**, 544-545; (c) M. Funahashi, F. Zhang and N. Tamaoki, *Adv. Mater.*, 2007, **19**, 353-358.
6. (a) T. Yasuda, K. Kishimoto and T. Kato, *Chem. Commun.*, 2006, 3399-3401; (b) T. Yasuda, T. Shimizu, F. Liu, G. Ungar and T. Kato, *J. Am. Chem. Soc.*, 2011, **133**, 13437-13444.
7. Q. Li, *Self-Organized Organic Semiconductors: From Materials to Device Applications*; John Wiley & Sons: New York, 2011.
8. (a) X. Li, A. Liu, S. Xun, W. Qiao, X. Wan and Z. Y. Wang, *Org. Lett.*, 2008, **10**, 3785-3787; (b) K. B. Woody, B. J. Leever, M. F. Durstock and D. M. Collard, *Macromolecules*, 2011, **44**, 4690-4698; (c) Y. Zhou, Y. Xiao, S. Chi and X. Qian, *Org. Lett.*, 2008, **10**, 633-636.
9. (a) Y. Shirota, *J. Mater. Chem.* 2000, **10**, 1-25; (b) D. Apreutesei and G. H. Mehl, *J. Mater. Chem.*, 2007, **17**, 4711-4715.
10. (a) J. Han, *J. Mater. Chem. C*, 2013, **1**, 7779-7797; (b) B. Roy, N. De and K. C. Majumdar, *Chem. Eur. J.*, 2012, **18**, 14560-14588; (c) J. Tang, R. Huang, H. Gao, X. Cheng, M. Prehm and C. Tschierske, *RSC Adv.*, 2012, **2**, 2842-2847; (d) X. Yang, H. Dai, Q. He, J. Tang, X. Cheng, M. Prehm and C. Tschierske, *Liquid Crystals*, 2013, **40**, 1028-1034.
11. (a) S. K. Pathak, R. K. Gupta, S. Nath, D. S. S. Rao, S. K. Prasad and A. S. Achalkumar, *J. Mater. Chem. C*, 2015, **3**, 2940-2952; (b) S. K. Pathak, S. Nath, R. K. Gupta, D. S. S. Rao, S. K. Prasad and A. S. Achalkumar, *J. Mater. Chem. C*, 2015, **3**, 8166-8182.
12. (a) V. Coropceanu, J. Cornil, D. A. da Silva Filho, Y. Olivier, R. Silbey and J. L. Bredás, *Chem. Rev.*, 2007, **107**, 926-952; (b) I. F. Perepichka, D. F. Perepichka, H. Meng and F. Wudl, *Adv. Mater.*, 2005, **17**, 2281-2305; (c) S. Prasanthkumar, A. Gopal and A. Ajayaghosh, *J. Am. Chem. Soc.*, 2010, **132**, 13206-13207; (d) S. S. Babu, V. K. Praveen and A. Ajayaghosh, *Chem. Rev*., 2014, **114**, 1973-2129.
13. (a) P. Sivadas, N. S. S. Kumar, D. D. Prabhu, S. Varghese, S. K. Prasad, D. S. S. Rao and S. Das, *J. Am. Chem. Soc.*, 2014, **136**, 5416-5423.

14. (a) F. Würthner, T. E. Kaiser and C. R. Saha-Moller, *Angew. Chem. Int. Ed*., 2011, **50**, 3376-3410; (b) F. Würthner, C. Bauer, V. Stepanenko and S. A. Yagai, *Adv. Mater*., 2008, **20**, 1695-1698; (c) F. Würthner, C. Thalacker, S. Diele and C. Tschierske, *Chem. Eur. J*., 2001, **7**, 2245-2253.
15. (a) D. D. Prabhu, N. S. S. Kumar, A. P. Sivadas, S. Varghese and S. Das, *J. Phys. Chem. B*, 2012, **116**, 13071-13080; (b) M. Kasha, H. R. Rawls and M. A. El-Bayoumi, *Pure Appl. Chem*., 1965, **11**, 371-392; (c) F. C. Spano, *Acc. Chem. Res*., 2010, **43**, 429-439.
16. (a) R. Yoshida, *Adv. Mater.*, 2010, **22**, 3463-3483; (b) A. Harada, R. Kobayashi, Y. Takashima, A. Hashidzume and H. Yamaguchi, *Nat. Chem.*, 2011, **3**, 34-37; (c) T. Yamamoto and M. Yoshida, *Langmuir*, 2012, **28**, 8463-8469; (d) M. Zhang, D. Xu, X. Yan, J. Chen, S. Dong, B. Zheng and F. Huang, *Angew. Chem. Int. Ed*., 2012, **51**, 7011-7015; (e) K. Yuichiro, T. Yoshinori, H. Akihito, Y. Hiroyasu and H. Akira, *Sci. Rep.*, 2013, **3**, 1243.
17. S. B. Ross Murphy, *J. Rheol*., 1995, **39**, 1451-1463.
18. (a) P. Sollich, *Molecular gels, Materials with Self-assembled Fibrillar Networks*', Ed: R. G. Weiss and P. Terech, Springer the Netherlands 2006; (b) H. M. Wyss, K. Miyazaki, J. Mattsson, Z. Hu, D. R. Reichman and D. A. Weitz, *Phys. Rev. Lett.*, 2007, **98**, 238303.
19. G. G. Nair, S. K. Prasad, R. Bhargavi, V. Jayalakshmi, G. Shanker and C. V. Yelamaggad, *J. Phys. Chem. B*, 2010, **114**, 697-704.
20. S. Fujii, D. Mitusmasu, Y. Isono and W. Richtering, *Soft Matter*, 2012, **8**, 5381-5390.
21. B.W. Barry and M. C. Meyer, *Int. Journal of Pharmaceutics*, 1979, **2**, 1-25.
22. (a) Y. Deng, W. Yuan, Z. Jia and G. Liu, *J. Phys. Chem. B*, 2014, **118**, 14536-14545; (b) D. D. Prabhu, A. P. Sivadas and S. Das, *J. Mater. Chem. C*, 2014, **2**, 7039-7046.
23. (a) K. T. Lin, G. H. Lee and C. K. Lai, *Tetrahedron*, 2015, **71**, 4352-4361; (b) C. Selvarasu and P. Kannan, *J. Chem. Sci.*, 2015, **127**, 1831-1838; (c) G. Shanker, M. Prehm, M. Nagaraj, J. K. Vij, M. Weyland, A. Eremin and C. Tschierske, *ChemPhysChem*, 2014, **15**, 1323-1335.

Chapter 4

Columnar self-assembly of luminescent bent-shaped hexacatenars with a central pyridine core connected with substituted 1,3,4-oxadiazole and thiadiazoles

Results have been published in *J. Mater. Chem. C*, 2016, **4**, 9669-9673; *New J. Chem.*, 2018, **42**, 3781-3798.

4.1. Introduction

The molecules possessing an anisotropic shape along with incompatible molecular segments exhibit the ability to self-assemble into different liquid crystalline (LC) phases. This self-assembly is mainly driven by the nano-segregation of incompatible molecular subunits and the tendency of the molecules to align with long-range orientational order or/and positional order.[1] This exceptional amalgamation of order and mobility present in LC materials gives rise to a plethora of properties that is being exploited in several applications.[2] Several non-conventional molecular designs that deviate from the conventional rod (calamitic) and disc-like (discotic) systems have been prepared over the years in quest of novel mesophases and to understand the impact of different anisometric shapes and noncovalent interactions on the self-assembly.[1,3] Polycatenar liquid crystals (LCs), are one such nonconventional LCs, which have a combination of central elongated rod like and terminal hemi disc shaped units.[4] The hemi discs may contain four to six flexible alkyl chains that provide the necessary fluidity. As they possess the structural characters of both calamitic and discotic LCs, they display various mesophases that are common to these classes of LCs. This depends on the number of outer flexible tails. The columnar self-assembly of such molecules resulting in the one-dimensional (1D) columnar (Col) phases with a large π-overlap are interesting, as they resemble 'molecular wires' with an nonconductive external casing of alkyl tails.[5] This self-assembly shows anisotropic conductivity and optical properties and thus holds promise in the development of several optoelectronic devices.[6] Polycatenar molecular design provides a seamless synthetic flexibility in tuning the transition temperatures as well as the optical and charge transport behavior through proper molecular design, which is a definite advantage in comparison to traditional discotics. Most of the polycatenars reported are known to have a central linear rod-like structure, while very few are known to have a bent structure.[7] The polycatenars with central bent structure have shown lower transition temperature and an enhanced mesophase range.[8] There is a growing interest in the research community, in the incorporation of heterocycles in the LC design, as they help in varying the overall lateral and/or longitudinal dipole moment of the molecule, along with the variations in their molecular shape.[9,10] These changes affect the molecular self-assembly and the macroscopic properties of such molecules, and therefore can be effectively utilized to modify the material properties. 1,3,4-oxadiazole and thiadiazoles are preferential candidates among the heterocycles because of their high luminescence and high thermal

and photochemical stability.[10] Incorporation of the heterocyclic moieties has shown enhanced mesophase stability due to the increased intermolecular interactions. Col LCs that exhibit high luminescence are of significant importance as this combination features 1D conductivity and luminescence in a single material, which has the potential to be utilized as an emissive layer of OLEDs along with good conductivity.[11g] Such molecular materials will be promising in comparison to inorganic semiconductors (which are hazardous and expensive) and polymers (which have got processability and conductivity issues). Col LCs are known to have high intermolecular order, solution processability and self-healing ability of structural defects. Some of our and other group's recent works on luminescent Col LCs based on heterocyclic moieties showed their potential as active emissive layers in OLEDs.[12] Efficient π-conjugated and coplanar molecular structure is a major requirement to achieve reduced band gaps in organic semiconductors with high charge carrier mobility and an electro-optical response. Recently, donor-acceptor (D-A) molecular structures have been investigated to attain low-band gap characteristics.[13] 1,3,4-Oxadiazole and thiadiazole moieties can be good electron acceptor molecular components, because of the presence of electronegative atoms. Their presence creates stronger polar induction and reduced molecular symmetry that affects the optical and electronic behaviors.[9] Such molecular structures also promote the ordered self-assembly in bulk as well as in the presence of solvents.[14] Recently we have reported such D-A-D structures that stabilized liquid crystal phases over a long range and also showed supergelation in hydrocarbon solvents due to the enhanced π-π interactions.[8c-e,10f] It is always interesting to see if such organogelators show aggregation induced enhanced emission (AIEE) effect, especially in the case of π-gelators. This is because the molecules are prepared with a view to utilize them in organic light emitting diodes (OLEDs), where both charge carrier mobility and emission in aggregated state is equally important. In most of the cases, such aggregated systems exhibit low luminescence due to the aggregation induced quenching (ACQ). Thus columnar self-assembly and AIEE contradict each other. However, over the years, several polycatenars including bent ones, showed AIEE behavior.[14b,8d,e,10f] Further, utilization of 2,6-substituted pyridine will provide an additional functionality for acid sensing due to the presence of an sp^2 hybridized nitrogen atom.[8e] In addition, only a few number of pyridine based bent polycatenars were reported in the literature, prompted us to work on this area.[7c,d,g,h,8e]

As a part of our efforts to synthesize luminescent liquid crystals toward the application in OLEDs, we have synthesized and characterized two series of bent-shaped polycatenars with a central pyridine unit flanked with unsymmetrically substituted oxadiazole or thiadiazole unit (Fig. 4.1). We were curious to compare the optical, photophysical and gelation properties of polycatenars based on 1,3,4-oxadiazole derivatives to their thiadiazole counterparts considering the alternate arrangement of donor and acceptor moieties in the molecular system. We visualized that the incorporation of oxadiazole or thiadiazole in the polycatenar structure had an impact on the self-assembly and related macroscopic properties. The number of flexible chains and their length were modified to understand the impact on the LC behavior and gelation. These molecules exhibit low temperature Col_r and/or high temperature Col_h phases over a wide thermal range. Most importantly five of the polycatenars were able to gelate in different hydrocarbon solvents. Some of these compounds exhibited aggregation-induced enhancement in emission (AIEE) in thin film and gel state.

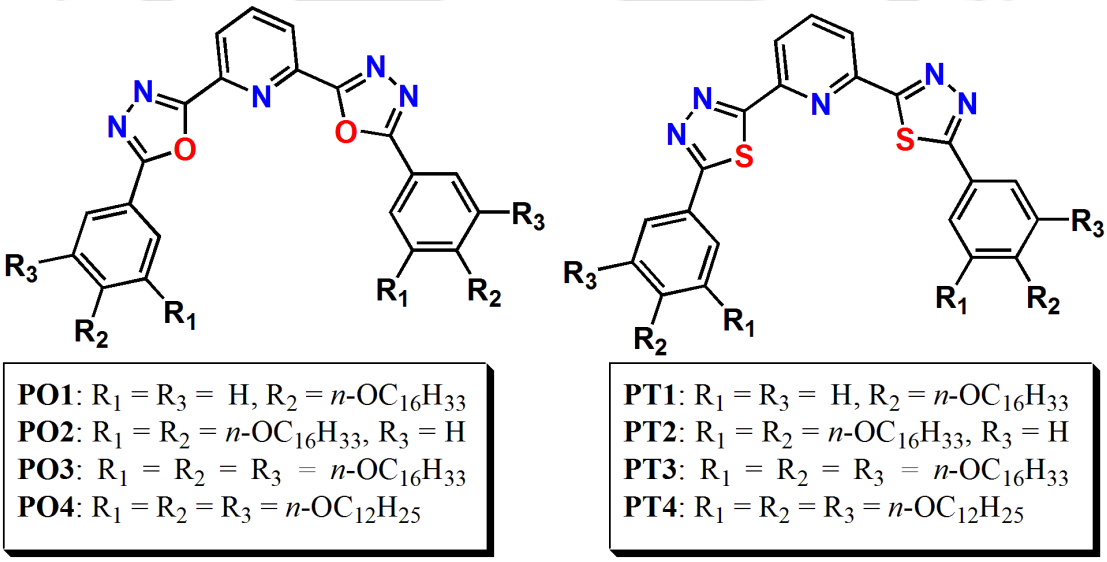

Figure 4.1. The molecular structures of pyridine based 1,3,4-oxadiazole and 1,3,4-thiadiazole derivatives.

4.2. Results and discussion

4.2.1. Synthesis and Characterization

The synthetic route is elucidated in Scheme 4.1. The target molecules **PO1-4** and **PT1-4** (Fig. 4.1) and their precursors were synthesized as presented in scheme 4.1. Syntheses of ethyl mono/di/trihydroxy benzoates (**8, 10-11**) are carried out as reported earlier.[10e] Compounds **3a, 3b, 3d, 3h** were prepared from corresponding ethyl hydroxyl benzoates following williamson's ether synthesis protocol. These alkoxy esters (**3a, 3b, 3d, 3h**)

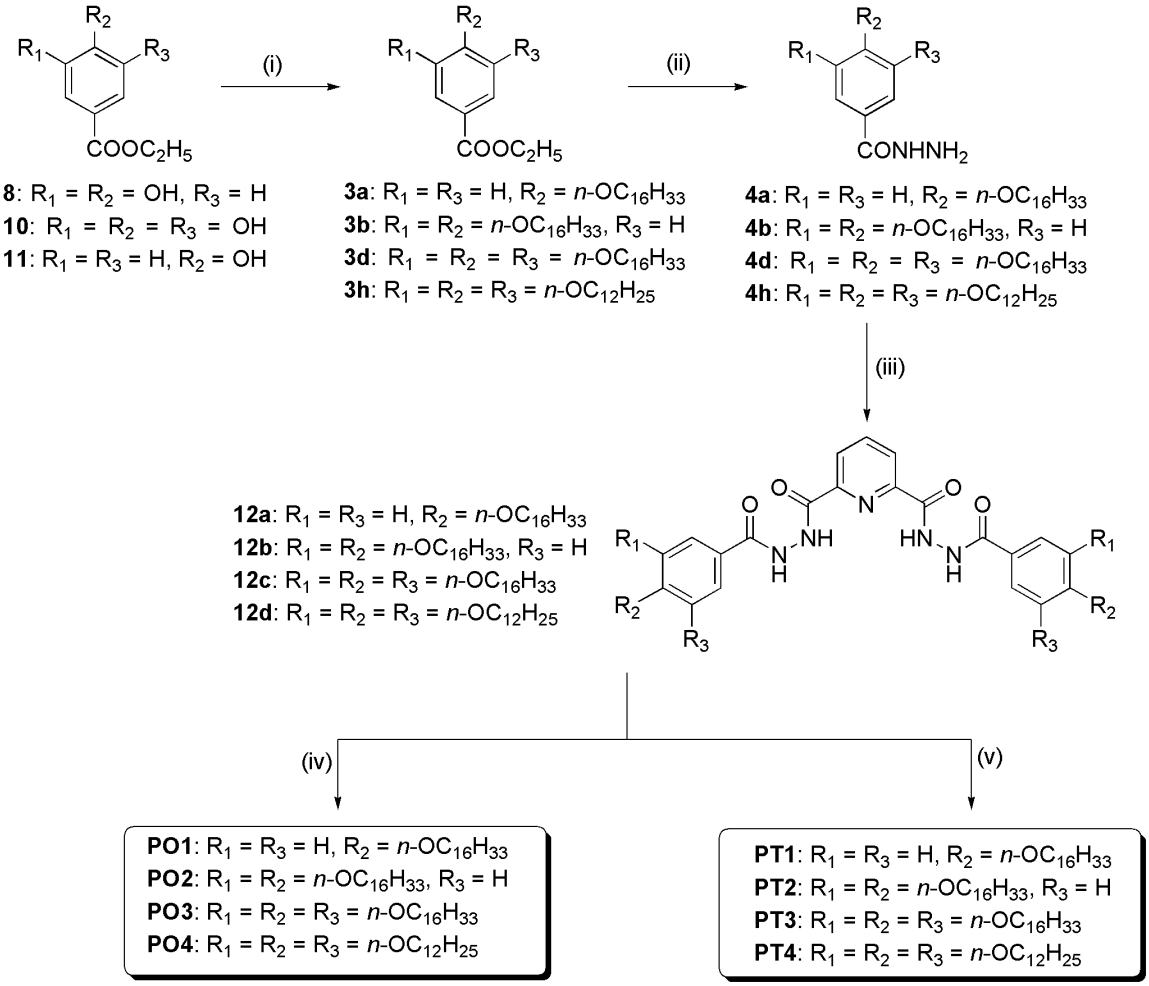

Scheme 4.1. Synthesis of pyridine based 1,3,4-oxadiazole and 1,3,4-thiadiazole derivatives. (i) *n*-bromoalkane, anhydrous K_2CO_3, DMF, 80 ^oC, 24 h (70-80%); (ii) $NH_2NH_2.H_2O$, Ethanol or butanol, reflux, 48 h (70-80%); (iii) Pyridine-2,6-diacid chloride, THF, Et_3N, 12 h, reflux; (iv) $POCl_3$, reflux, 17 h (60-72%); (v) Lawesson's reagent, toluene, reflux, 17 h (55-60%).

were utilized to prepare the corresponding hydrazides (**4a, 4b, 4d, 4h**).[10e] These hydrazides on refluxing with 2,6-pyridine dicarboxyllic acid chloride in the presence of triethylamine base provided 2,6-di-*N*-pyridinebenzohydrazides **(12a-d)**.[8e] $POCl_3$ mediated dehydrocyclization provided dioxadiazole derivatives (**PO1-4**). The corresponding dithiadiazole derivatives (**PT1-4**) were prepared by refluxing the compounds **12a-d** in presence of Lawesson's reagent in toluene.

The molecular structures of the final compounds and their precursors were confirmed by various analytical techniques such as ^1H NMR, ^{13}C NMR, IR spectroscopy and HRMS or MALDI-TOF. (See experimental part presented in section 4.4 for the details). The electron withdrawing nature of oxadiazole ring is more in comparison to its thiadiazole counterpart due to more electronegative nature of oxygen than sulphur, which

is reflected by the ^{1}H NMR signals. For illustration, ^{1}H NMR of compound **PO3** with two oxadiazole units showed the down field signal for proton H_b (δ = 8.46 ppm) and in comparison to the proton H_b of compound **PT3** (δ = 8.42 ppm) with two thiadiazole units (Fig. 4.2). Similarly the proton H_a of compound **PT3** (δ = 8.13 ppm) appeared at low field in comparison, to that of compound **PO3** (δ = 8.04 ppm). On the other hand, ^{13}C NMR of compound **PO3** exhibited low field signals for the heterocyclic ring carbons of the 1,3,4-oxadiazole at 171 ppm and 169 ppm in comparison to the heterocyclic ring carbons of the 1,3,4-thiadiazole (signals at 169 ppm and 167 ppm) of compound **PT3**. (See experimental part presented in section 4.4 for the details).

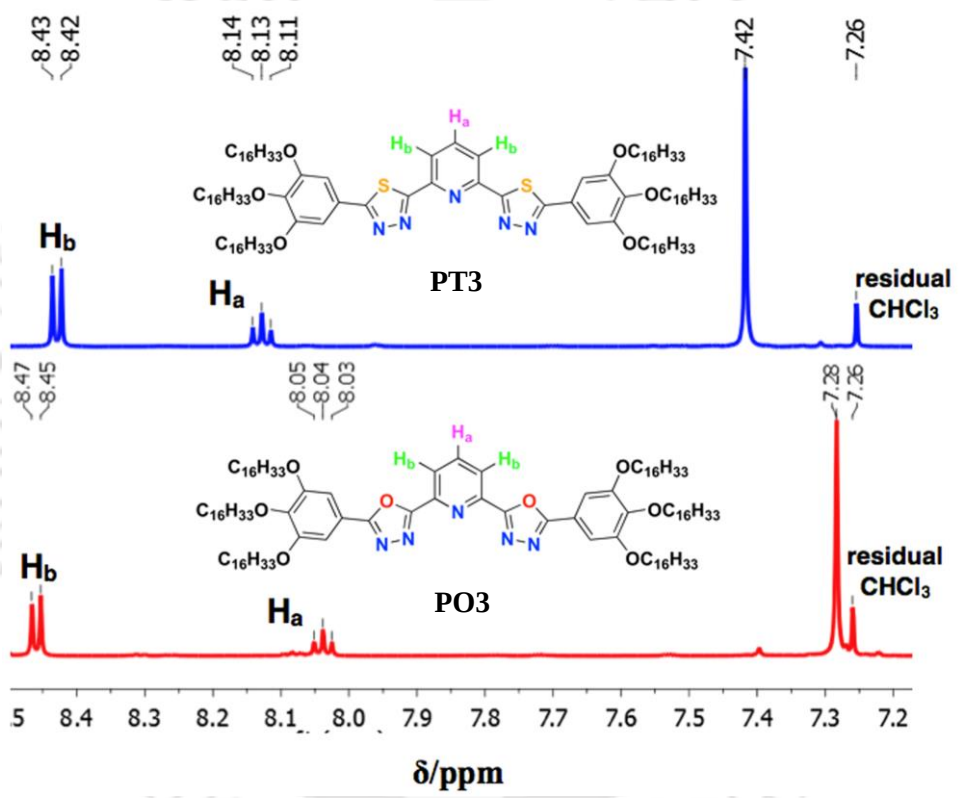

Figure 4.2. Overlay of the expanded portion of the ^{1}H NMR spectra ($CDCl_3$, 600 MHz) of **PO3** and **PT3**.

4.2.2. Thermal behavior

The preliminary confirmation for the occurrence of thermotropic liquid crystallinity was the appearance of strong birefringence along with the fluidity on gradual heating of the sample, under the polarizing optical microscopy (POM) observations. Transition temperatures and the enthalpy changes corresponding to these phase transitions were obtained by differential scanning calorimetry (DSC) thermograms. Further, the mesophase assignment was carried out by performing X-ray diffraction (XRD) measurements at different temperature intervals. The phase transitions and the

corresponding enthalpy changes are tabulated in table 4.1 and represented in fig. 4.3. In comparison to normal carbocyclic LCs, heterocyclic derivatives are expected to show higher enthalpy changes associated with phase transitions, which may be due to the attractive hetero atom interactions and intermolecular H-bonding interactions.[8,10,15]

Compound **PO1** and **PT1** with the two terminal *n*-hexadecyloxy tails and compound **PO2** with the four terminal *n*-hexadecyloxy tails attached to the 3 and 4 positions of the terminal benzene rings turned out to be crystalline (Fig. 4.4). The POM images and XRD patterns confirmed their crystalline nature. Hexacatenar **PO3** with six *n*-hexadecyloxy tails observed as a birefringent fluidic mass under POM observation, which at 66 ^{o}C showed a transition in the DSC thermogram with an enthalpy change of 107.8 kJ/mol. This mesophase was converted into an isotropic liquid at around 82 ^{o}C (ΔH = 2.8 kJ/mol) (Fig. 4.5c). In the cooling cycle, the isotropic liquid showed the growth of mosaic

Table 4.1. Phase transition temperatures [a] (^{o}C) and corresponding enthalpies (kJ/mol) of the oxadiazole and thiadiazole derivatives.

Entry	Phase sequence	
	2nd Heating	**1st Cooling**
PO1	Cr_1 131.1 (24.6) Cr_2 196.6 (54) I	I 191.5 (55.7) Cr_2 128.7 (23.5) Cr_1
PO2	Cr_1 48.4 (9) Cr_2 133.1 (15.5) I	I 122 (20.1) Cr_2 44.1 (5.9) Cr_1
PO3	Col_{r1} 66 (107.8) Col_{r2} 82.1 (2.8) I	I 75.8 (3) Col_{r2} 45.3 (103.8) Col_{r1} [b]
PO4	Cr 60.8 (18.1) Col_h 96.2 (0.9) I	I 92.2 (0.2) Col_h 42.1 (14.5) Cr
PT1	Cr_1 127.9 (14.3) Cr_2 213.9 (22.8) I	I 208.2 (27.4) Cr_2 124.7 (16.6) Cr_1
PT2	Cr 119.8 (27.2) Col_r 129.2 (2) I	I 126.7 (2.5) Col_r 99.1 (32.7) Cr
PT3	Col_{r2} 52.4 (2.2) Col_{r1} 87 (9.7) Col_h 101 (11.1) I	I 95.6 (1.3) Col_h 70 (8.84) Col_{r1} 43.6 (0.6) Col_{r2} [b]
PT4	Col_r 61.6 (9) Col_r 95.2 (16.6) Col_r 121.6 (3.1) I	I 119.7 (3.1) Col_r 73 (13.2) Col_{r1} 57.3 (6) Col_r [b]

[a]Peak temperatures in the DSC thermograms obtained during the first heating and cooling cycles at 5 ^{o}C/min. [b]Crystallization was not observed till -20 ^{o}C; Cr = crystal; Col_h = columnar hexagonal phase; Col_r = columnar rectangular phase; I = isotropic liquid.

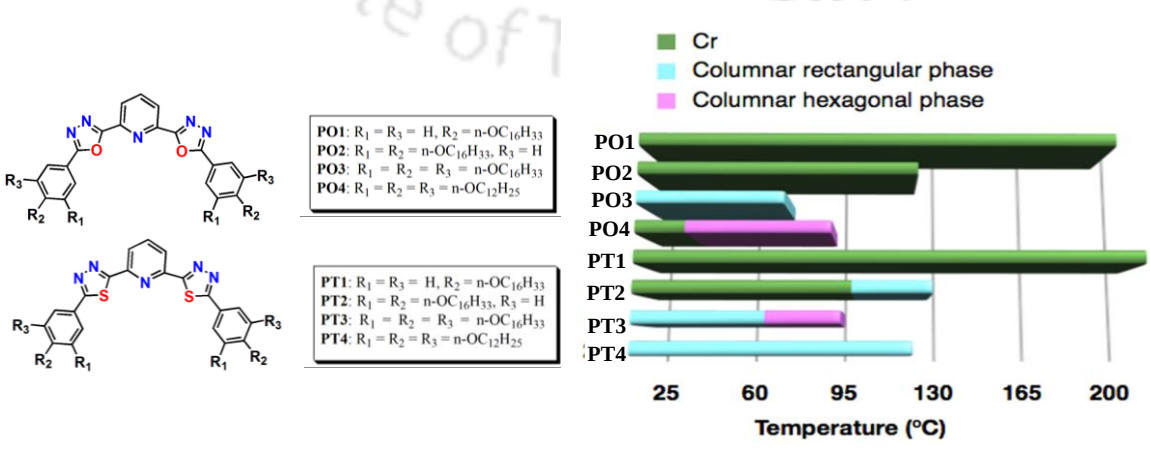

Figure 4.3. Bar graph summarizing the thermal behavior of **PO1-4** and **PT1-4** (first cooling cycle).

pattern at around 76 ^{o}C (Fig. 4.5a). Further cooling showed a transition in DSC at 45 ^{o}C (ΔH = 103.8 kJ/mol), but the texture did not show much difference (Fig. 4.5b). The X-ray diffractogram obtained at 65 ^{o}C showed a sharp low angle peak along with two diffused wide angle peaks. The first diffused peak with a *d*-spacing of 4.96 Å corresponds to the packing of alkyl tails, while the second one at a *d*-spacing of 4.19 Å corresponds to the core-core stacking. As it was difficult to identify the organization of columns in a 2D-lattice with a single peak at low angle, we decided to investigate through small angle X-ray scattering (SAXS) studies. The intensity *vs* 2θ profiles obtained from the SAXS patterns for compound **PO3** at 65 ^{o}C (Fig. 4.5d), showed peaks corresponding to *d*-spacings of 36.11, 19.2 and 14.48 Å which can be indexed to Miller indices 01, 11, 12 of a rectangular lattice. From these values, the lattice parameters were calculated and found to be *a* = 22.67 Å, *b* = 36.11 Å. The unit cell area (*S*) was found to be 818.6 Å^2 and cell volume (V) was found to be 3430 Å^3. The number of molecules (*Z*) in the unit rectangular cell was found to be 1.1.

The XRD pattern obtained at lower temperatures (*i.e.* at 40 ^{o}C and room temperature), were well below the transition temperature 45 ^{o}C in cooling cycle (Fig. 4.5e-f). The XRD pattern obtained at 40 ^{o}C showed five peaks at low angle corresponding to the *d*-spacings of 45.62, 21.05, 15.73, 12.73 and 7.69 Å along with a relatively sharp peak at 4.55 Å (in comparison to the XRD pattern at 65 ^{o}C). The peaks at low angle can be indexed into miller indices 01, 10, 12, 13 and 24 of a rectangular lattice. Thus the transition observed at 45 ^{o}C is from one Col_r to another Col_r phase. For the sake of identification we have named the higher temperature Col phase as Col_{r2} and the low temperature one as Col_{r1} phase. The rectangular lattice parameters were calculated and from that the total number of molecules (*Z*) present in a unit cell was found to be 1.5. The relatively sharp peak at the wide angle corresponds to the enhanced columnar order. Since the texture remained the same even at room temperature we were curious to know whether the phase structure remains same or different. The XRD pattern obtained at room temperature showed several peaks in the low to mid angle region along with a relatively sharp peak in the wide-angle region, which can be fit into a rectangular lattice. Thus the Col_r phase remains unchanged at room temperature. Compound **PO4**, the dodecyloxy version of compound **PO3** exhibited a Col_h phase, which was confirmed by POM images, DSC and XRD studies (Fig. 4.6 and table 4.2).

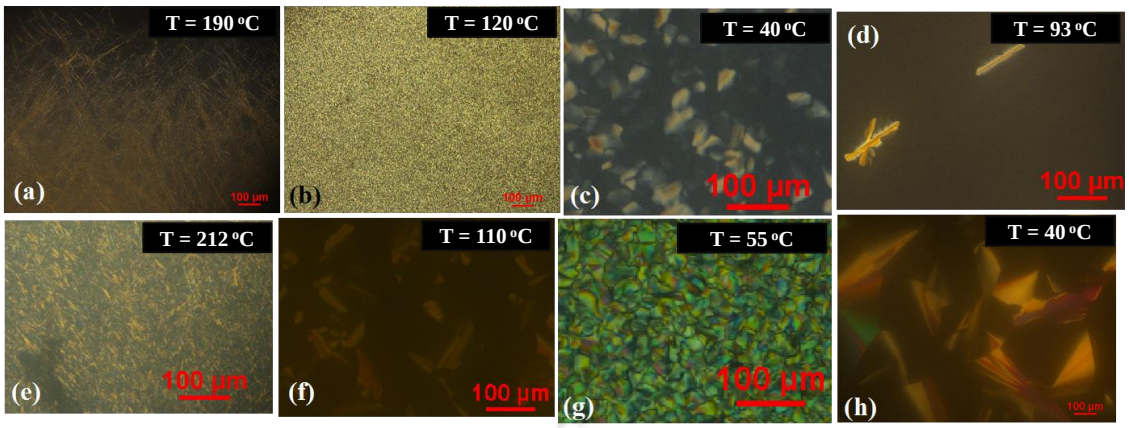

Figure 4.4. POM images obtained for the Cr phase of **PO1** (a); Cr phase of **PO2** (b); Col_r phase of **PO3** (c); Col_h phase of **PO4** (d); Cr phase of **PT1** (e); Col_h phase of **PT2** (f); Col_r phase of **PT3** (g) and Col_r phase of **PT4** (h).

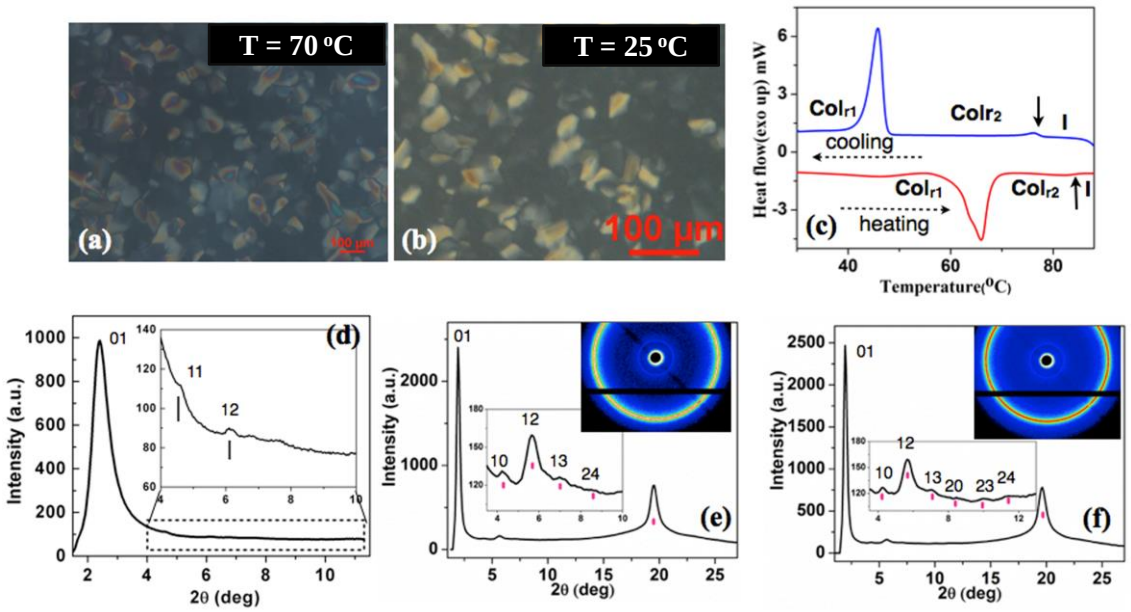

Figure 4.5. POM images obtained for **PO3** at 70 °C (a); at RT (b); DSC thermogram of **PO3** in the second heating (red trace) and first cooling (blue trace) at a scan rate of 5 °C/min (c); Intensity *vs* 2θ profiles obtained from the SAXS patterns for **PO3** at 65 °C for Col_{r2} phase (d); 40 °C for Col_{r1} phase (e) and 25 °C (f) for Col_{r1} phase, inset shows the expanded portion in the middle angle region and the image pattern.

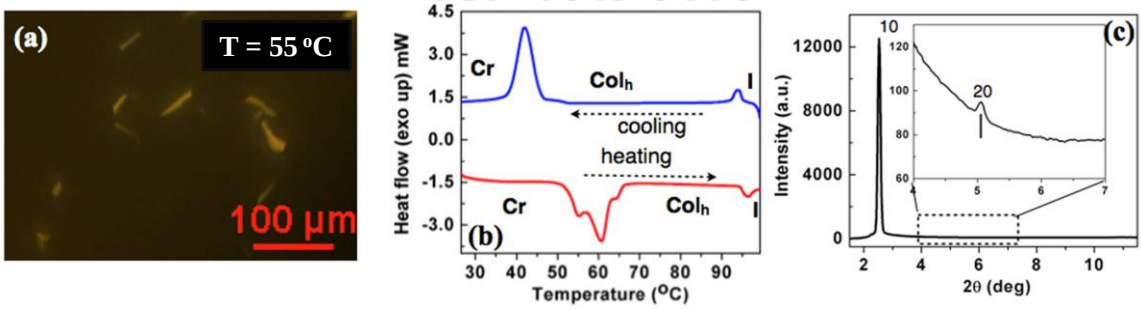

Figure 4.6. POM image obtained for the Col_h phase of **PO4** at 55 °C (a); DSC thermogram of **PO4** in the second heating (red trace) and first cooling (blue trace) at a scan rate of 5 °C/min (b); Intensity *vs* 2θ profiles obtained from the SAXS pattern for **PO4** at 65 °C for Col_h phase (c), inset shows the expanded portion in the middle angle region.

Table 4.2. Results of indexation of XRD profiles of compounds **PO3** & **PO4** at a given temperature (T) of the mesophases[a].

Compounds (*D*/Å)	Phase (T/°C)	d_{obs}(Å)[b]	d_{cal}(Å)[b]	Miller indices *hkl*	Lattice parameter [c]
PO3 (59.95)	Col_{r2} (65)	36.11	36.11	01	a = 22.67, b = 36.11, S = 818.6, V = 3430, Z = 1.1
		19.2	19.20	11	
		14.48	14.12	12	
		4.96 (h_a)			
		4.19 (h_c)			
	Col_{r1} (40)	45.62	45.62	01	a = 21.05, b = 45.62, S = 960.3, V = 4369.37, Z = 1.45
		21.05	21.05	10	
		15.73	15.47	12	
		12.73	12.33	13	
		7.69	7.73	24	
		4.55 (h_a)			
	Col_{r1} (25)	45.55	45.55	01	a = 20.96, b = 45.55, S = 954.73, V = 4315.37, Z = 1.44
		20.96	20.96	10	
		15.69	15.42	12	
		12.59	12.30	13	
		10.45	10.48	20	
		8.85	8.62	23	
		7.75	7.71	24	
		4.52(h_a)			
PO4 (49.77)	Col_h (65)	35.03	35.03	10	a = 40.45, S = 1417, V = 5653.8, Z = 2.3
		17.47	17.52	20	
		4.86(h_a)			
		3.99(h_c)			

[a]The diameter (D) of the disc (estimated from Chem 3D Pro 8.0 molecular model software from Cambridge Soft). [b]d_{obs}: spacing observed; d_{cal}: spacing calculated (deduced from the lattice parameters; a for Col_h phase; c is height of the unit cell). The spacings marked h_a and h_c correspond to diffuse reflections in the wide-angle region arising from correlations between the alkyl chains and core regions, respectively. Z indicates the number of molecules per columnar slice of thickness h_c estimated from the lattice area S and the volume V.

Here again the low angle showed a single peak, which prevented us from the unambiguous assignment to a particular mesophase. Thus the SAXS measurements were carried out at this temperature and the *d*-spacings obtained at low angle were closely fitting into a hexagonal lattice (Table 4.2 and Fig. 4.6c). The POM texture (Fig. 4.6a) with large homeotropic domains supports the uniaxial nature of the Col_h phase.

Thiadiazole based tetracatenar compound **PT2** exhibited enantiotropic Col_r phase as evidenced from SAXS studies (Fig. 4.7). Preliminary investigation with polarizing optical microscopy (POM) and differential scanning calorimetry (DSC) proved that the compound **PT3** was enantiotropic and bimesomorphic (Fig. 4.8c-f). The compound showed a high temperature columnar hexagonal (Col_h) phase and low temperature columnar rectangular (Col_r) phase. Interestingly the Col_r phase lost its shearability at around 50 °C, with an unaltered optical texture, which remains as such upto –20 °C

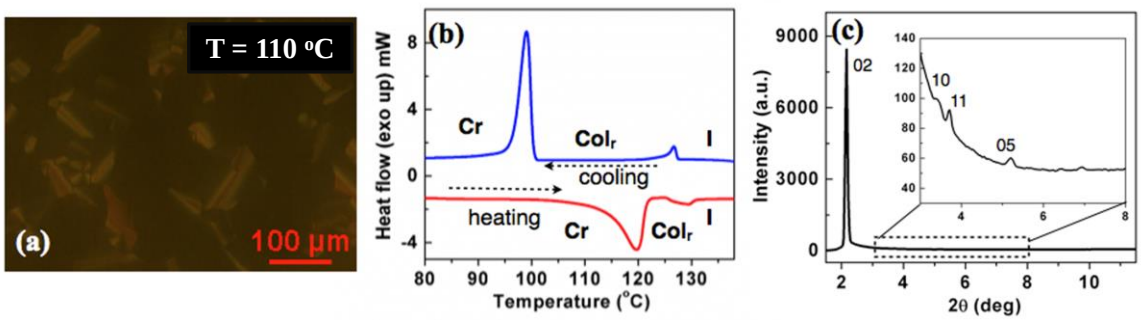

Figure 4.7. POM image obtained for the Col$_r$ phase of compound **PT2** at 110 °C (a); DSC thermogram of compound **PT2** in the second heating (red trace) and first cooling (blue trace) at a scan rate of 5 °C/min (b); Intensity *vs* 2θ profiles obtained from the SAXS pattern for compound **PT2** at 110 °C for Col$_r$ phase (c), inset shows the expanded portion in the middle angle region.

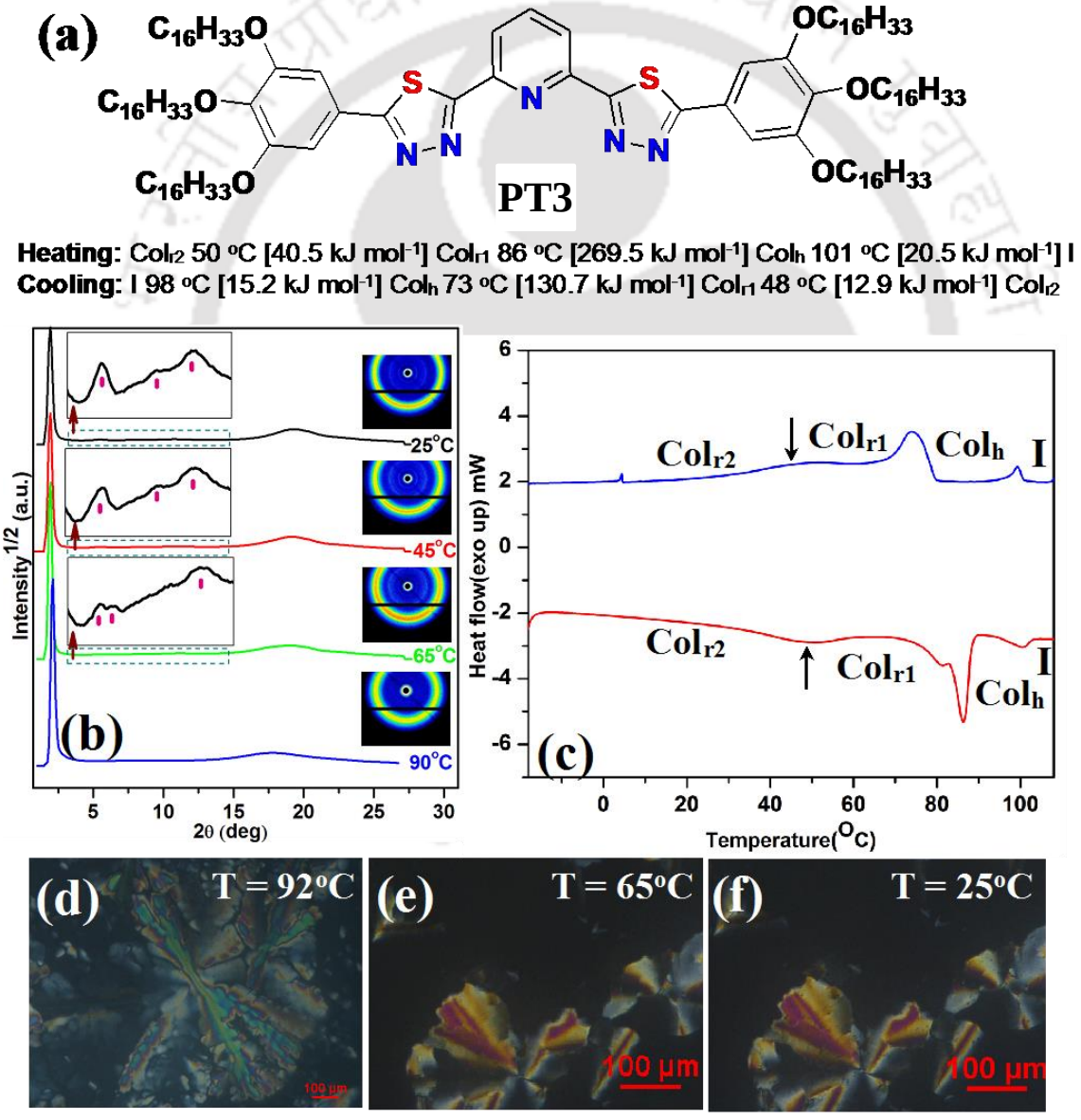

Figure 4.8. Structure and phase transition of **PT3** in first cooling and second heating (a); XRD patterns obtained at 90, 65, 45 and 25 °C (b); DSC traces obtained for second heating (red trace) and first cooling (blue trace) (c); POM image obtained for Col$_h$ phase (d); Col$_{r1}$ phase (e) and Col$_{r2}$ phase (f).

without any signs of crystallization. X-ray diffraction of compound **PT3** carried out at 90 ^{o}C showed a sharp peak centered at 41.48 Å at the low-angle region, followed by a diffused peak at 4.99 Å (Fig. 4.8b & table 4.3). The sharp peak at the low angle specifies the distance between the adjacent (100) planes, i.e. d_{100} and from this value the hexagonal cell parameter '*a*' was calculated, which provides the intercolumnar distance of 48 Å. This value was almost 20% less than the molecular length of compound **PT3** in all *trans* conformation suggesting interdigitation of peripheral alkyl chains in the mesophase due to the chain melting. The number of molecules present within a hypothetical unit cell (*Z*) with a 4.99 Å height was found to be approximately 3. We can expect that the association of three molecules may form a disc, which further self-assembles to form the column, and these columns organize in the hexagonal lattice to form the Col_h phase. The small textural change (Fig. 4.8d, e) along with an exothermic peak (ΔH = 131 kJ/mol) at 73 ^{o}C prompted us to carry out XRD studies well below this transition *i.e.* at 65 ^{o}C. The XRD pattern showed peaks at low angle region centered at 45.52, 16.52, 14.25, 7.95 Å corresponding to Miller indices 03, 11, 15 and 25 respectively, which fit well with the rectangular lattice with lattice parameters *a* = 16.6 and *b* = 136.6 Å. The value of *Z* for this rectangular unit cell comes to be 3 again. During the POM studies, it was seen that at around 50 ^{o}C the sample under investigation was not shearable and there was second order transition detected in DSC traces (Fig. 4.8c, f) and remained as such up to -20 ^{o}C. This was attributed to the freezing of the columnar structure in glassy state. Generally glassy liquid crystalline state is rigid with distorted alignment. However, in this case the molecular alignments remain unaltered and they retain the Col_r structure as confirmed from XRD analysis (Fig. 4.8b). Glassy columns allow unidirectional charge migration with simultaneous restriction on the movement of ionic impurities, which is very important from the viewpoint of optoelectronics. In addition, glassy columnar state assures long-term morphological stability that provides an easy way to produce defect free films due to their self-healing nature.[12]

Interestingly hexacatenar **PT4** with six dodecyloxy chains exhibited several phase transitions as evidenced from DSC thermograms (Fig. 4.9). POM images showed a mosaic texture (Fig. 4.10a-c) and the XRD patterns obtained at different temperature intervals showed that there are three different Col_r phases (Fig. 4.10d-f, Table 4.3). The low temperature Col_r phase stayed upto RT without any signs of crystallization. Such transitions between different Col_r phases have been reported earlier.[15b]

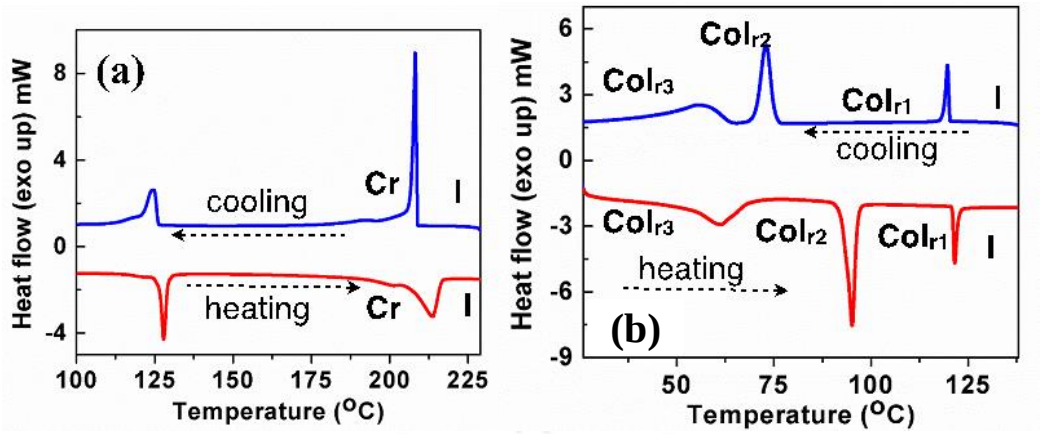

Figure 4.9. DSC scans obtained for the first cooling (blue trace) and second heating (red trace) cycle of compound **PT1** (a) and **PT4** (b).

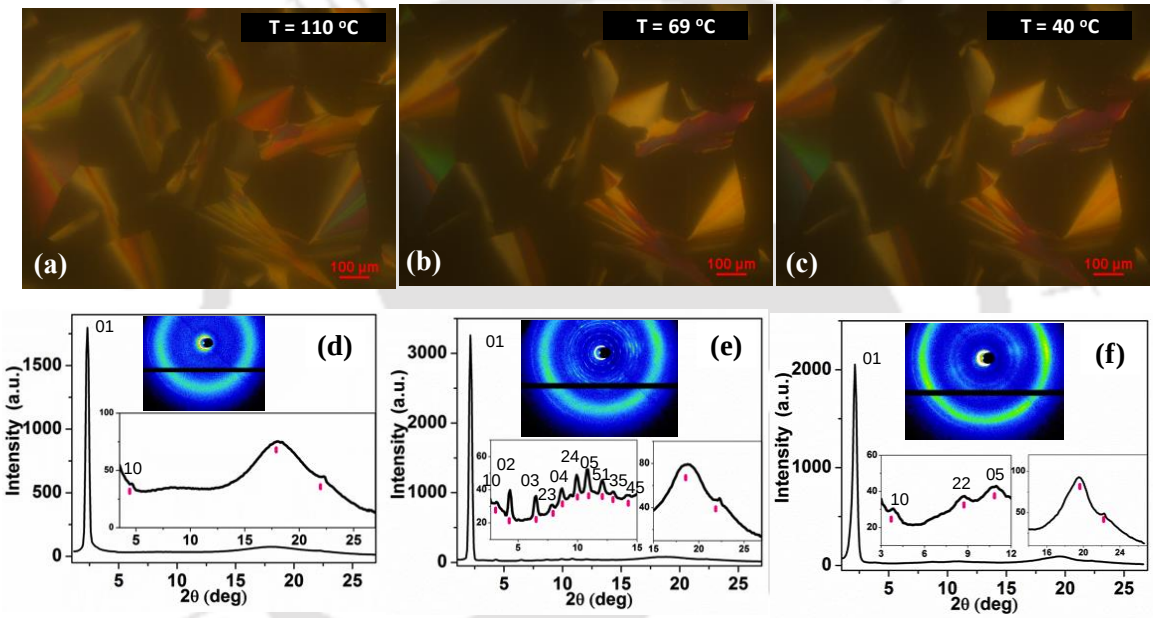

Figure 4.10. POM image obtained for the Col$_{r1}$ phase of compound **PT4** at 110 °C (a); Col$_{r2}$ phase of compound **PT4** at 69 °C (b); Col$_{r3}$ phase of compound **PT4** at 40 °C (c); Intensity *vs* 2θ profiles obtained from the XRD patterns for the Col$_{r1}$ phase of compound **PT4** at 110 °C (d); Col$_{r2}$ phase of compound **PT4** at 69 °C (b); Col$_{r3}$ phase of compound **PT4** at 40 °C (c).

It was interesting to compare the thermal behavior of pyridine based bent-shaped molecules **PO3-4** and **PT3-4** with corresponding benzene based bent-shaped molecules reported earlier (Fig. 4.11). Hexacatenar **PO3** with hexadecyloxy chains exhibited Col$_r$ phase over a wide range including room temperature, while the corresponding benzene based hexacatenar **16O** was crystalline at room temperature and exhibited a short-range Col$_h$ phase.[8a] Similarly, compound **PT3** exhibited enhanced mesophase stability by exhibiting Col$_r$ and Col$_h$ phases in comparison to the monomesomorphic **16T** which exhibited Col$_{ob}$ phase.[10b] Hexacatenar **PT4** having shorter alkyl chains exhibited solely Col$_r$ phase, while the corresponding benzene based hexacatenar **12T** exhibited Col$_{ob}$

Table 4.3. Results of the (*hkl*) indexation of the XRD profiles of the compounds **PT2-4** at a given temperature (T) of the mesophases[a].

Compounds (*D*/Å)	**Phase (T/°C)**	**d_{obs}(Å)[b]**	**d_{cal}(Å)[b]**	**Miller indices *hkl***	**Lattice parameter (Å)**
PT2 (60.0)	Col_r (110)	40.83 25.60 23.79 16.97 4.98 (h_a) 4.02 (h_c)	40.83 25.60 24.43 16.33	02 10 11 05	a = 25.6, b = 81.7, c = 4.02, S = 2091.5, V = 8407.9, Z = 3.7
PT3 (61.06)	Col_h (90)	41.48 4.99 (h_c)	41.48	10	a = 47.87, S = 1984.47, V = 9902.51, Z = 3.2
	Col_{r1} (65)	45.52 16.52 14.25 7.95 4.63(h_a) 4.33(h_c)	45.52 16.52 14.21 7.96	03 11 15 25	a = 16.64, b = 136.56, c = 4.33, S = 2272.36, V = 9839.32, Z = 3.2
	Col_{r2} (45)	45.52 15.69 9.88 8.09 4.63 (h_a) 4.31 (h_c)	45.52 15.69 9.78 8.10	01 22 42 52	a = 43.32, b = 45.52, c = 4.31, S = 1971.93, V = 8499.02, Z = 2.78
	Col_{r2} (25)	45.52 16.24 10.21 8.09 4.61 (h_a) 4.35 (h_c)	45.52 16.24 10.20 8.09	02 20 33 41	a = 32.48, b = 91.04, c = 4.35, S = 2957, V = 12863, Z = 4.2
PT4 (50.85)	Col_{r1} (100)	37.99 19.39 4.89 (h_a) 4.00 (h_c)	37.99 19.39	01 10	a = 19.39, b = 37.99, c = 4.00, S = 736.63, V = 2946.5, Z = 1.2
	Col_{r2} (68.5)	41.35 27.88 20.47 13.65 11.33 10.20 8.91 8.20 7.32 6.83 6.23 4.74 (h_a) 3.99 (h_c)	41.35 27.88 20.68 13.78 11.13 10.34 9.07 8.27 7.43 6.91 6.22	01 10 02 03 23 04 24 05 51 35 45	a = 37.75, b = 41.35, c = 3.99, S = 1560.96, V = 6228.24, Z = 2.5
	Col_{r3} (40)	41.35 23.09 10.11 8.11 4.55 (h_a) 4.00 (h_c)	41.35 23.09 10.08 8.27	01 10 22 05	a = 23.09, b = 41.35, c = 4.00, S = 954.77, V = 3819.09, Z = 1.5

[a]The diameter (D) of the disc (estimated from Chem 3D Pro 8.0 molecular model software from Cambridge Soft). [b]d_{obs}: spacing observed; d_{cal}: spacing calculated (deduced from the lattice parameters; a and b for Col_h and Col_r phase; c is height of the unit cell).

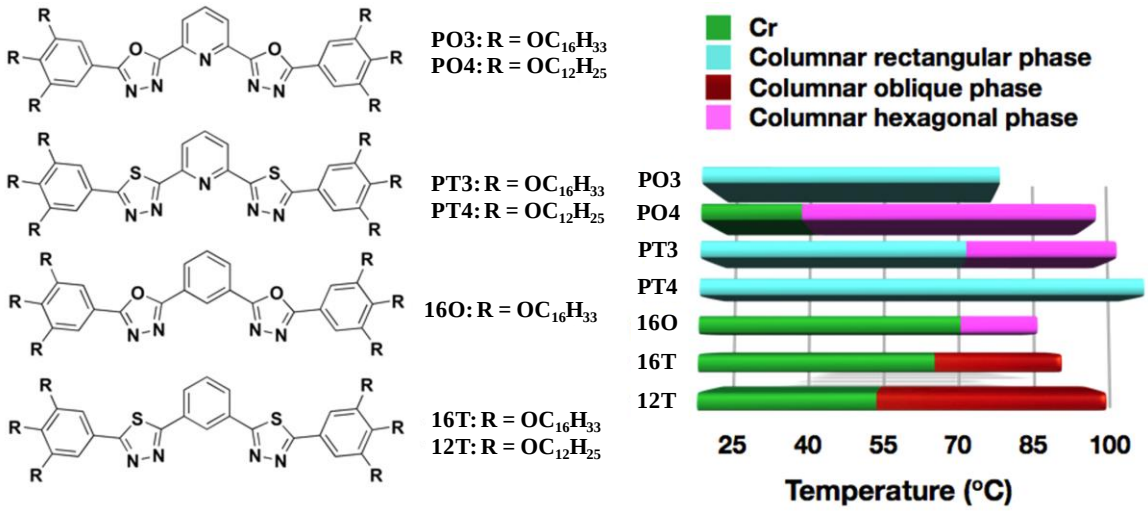

Figure 4.11. Comparison of the thermal behavior of pyridine based bent-shaped molecules **PO3-4** and **PT3-4** with benzene based bent-shaped molecules reported earlier (**16O**,[8a] **16T** and **12T**[10b]) considering the first cooling cycle.

phase. In general, the introduction of pyridine as a central core enhanced the mesophase stability, by lowering the melting temperature. In both cases, whether it is pyridine or benzene; the thiadiazole based hexacatenars exhibited wider mesophase range and higher stability, which was in line with earlier reports.[8c-e,10a-f]

4.2.3. Photophysical properties

Photophysical properties of oxadiazole and thiadiazole based compounds **PO1-4** and **PT1-4** in THF (20 micromolar) solution and in annealed thin film state were investigated and the data are summarized in table 4.4. It is expected that the presence of two different heterocycles (substituted 1,3,4-oxadiazole and 1,3,4-thiadiazole) may have a distinguishable impact on the photophysical properties.[10] Absorption and emission spectra of the compounds **PO1-4** and **PT1-4** were measured in micromolar THF solution (Fig. 4.12a and 4.13a). These compounds exhibited a red-shifted absorption and emission spectra, in comparison to the benzene-based polycatenars reported earlier.[8a,10b] The solution absorption spectra of compounds **PO1-4** exhibited a single absorption band at a wavelength of 314 nm whereas compound **PT1-4** showed red-shifted absorption band in range of 337-347 nm. Both the series of compounds **PO1-4** and **PT1-4** showed a large value of molar extinction coefficients, which is the inherent property of highly conjugated systems. The single absorption band for these compounds can be attributed to spin allowed π-π^* transition of the aromatic system. The values of molar extinction coefficients of oxadiazole derivatives **PO1-4** (ε = 13,000-22,500 $M^{-1}cm^{-1}$) were found to be more in comparison to thiadiazole derivatives **PT1-4** (ε = 4,000-11,000 $M^{-1}cm^{-1}$).

Optical bandgaps of these systems obtained from the absorption onset values showed that the oxadiazoles derivatives **PO1-4** (3.39-3.46 eV) showed higher band gap in comparison to their thiadiazole counterpart **PT1-4** (3.10-3.22 eV). Likewise, emission spectra obtained by exciting the solutions of these compounds at their absorption maxima exhibited a single emission maximum in the range of 385-465 nm for **PO1-4** and a red-shifted emission maximum in the range of 421-473 nm for **PT1-4** (Table 4.4, Fig. 4.12 & 4.13) with large stokes shift. Relative quantum yields of these compounds were measured with respect to standard quinine sulphate solution (0.1 M in H_2SO_4), exhibited almost similar quantum yields in the range of 0.48-0.58. Quantum yield was measured according to established procedure by using quinine sulfate in 0.1 M H_2SO_4 solution as the standard. Absolute values were calculated according to the following equation: $Q_S = Q_R \times (m_S / m_R) \times (n_S / n_R)^2$ Where, Q: Quantum yield, m: Slope of the plot of integrated fluorescence intensity *vs* absorbance; n: refractive index (1.407 for THF and 1.33 for distilled water); the subscript R refers to the reference fluorophore *i.e*. quinine sulphate solution in 0.1 M H_2SO_4 and subscript S refers to the sample under investigation.

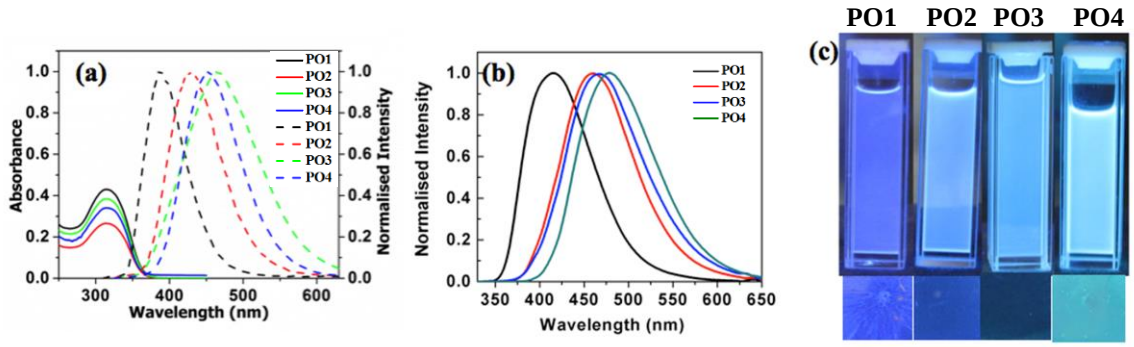

Figure 4.12. Absorption (solid trace) and normalized emission (dotted trace) spectra of compounds **PO1-4** (a); Normalized emission spectra of spin coated thin films (b); photographs taken under the UV light (λ_{exc} = 365 nm) in micromolar THF solution and thin films (c).

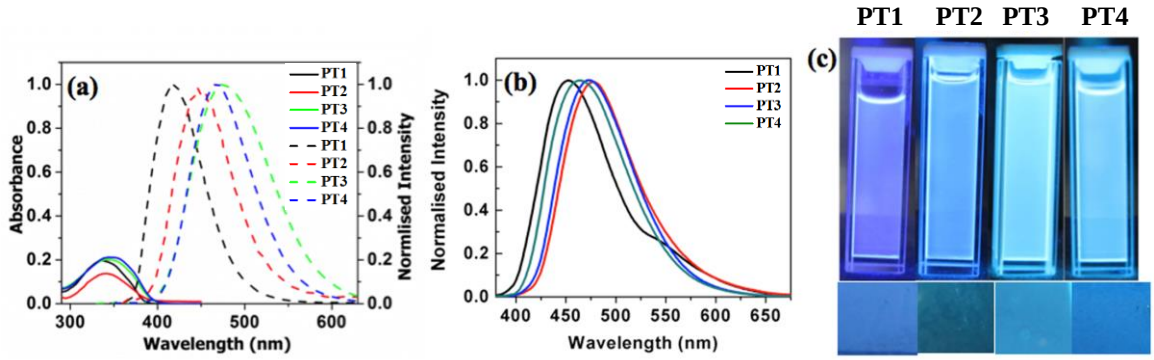

Figure 4.13. Absorption (solid trace) and normalized emission (dotted trace) spectra of compounds **PT1-4** (a); Normalized emission spectra of spin-coated thin films (b); photographs taken under the UV light (λ_{exc} = 365 nm) in micromolar THF solution and thin films (c).

Table 4.4. Photophysical properties of compounds **PO1-4** and **PT1-4** in solution[a] and film state.

Entry	Solution State						Thin film State		
	Absorption(nm)	**Emission[b](nm)**	**Stokes shift(cm^{-1})**	**λ_{onset} (nm)**	**$\Delta E^{c,d}_{opt}$**	**Relative Q. Y.**	**Absorption (nm)**	**Emission[b](nm)**	**Stokes shift(cm^{-1})**
PO1	314	385	5873	366	3.39	0.58	315	416	7708
PO2	314	428	8483	367	3.39	0.48	316	461	9954
PO3	314	465	10342	363	3.42	0.50	311	467	10741
PO4	314	452	9723	359	3.46	0.48	318	479	10570
PT1	337	421	5921	386	3.22	0.55	343	453	7080
PT2	341	446	6904	389	3.19	0.56	345	478	8065
PT3	343	473	8013	398	3.12	0.53	345	473	7844
PT4	347	466	7359	401	3.10	0.48	345	464	7434

[a]micromolar solutions in THF; [b]excited at the respective absorption maxima; [c]Band gap determined from the red edge of the longest wave length (λ_{onset}) in the UV-vis absorption spectra; [d] In volts (eV).

In order to minimize re-absorption effects, absorbance was kept below 0.15 at the excitation wavelength of 347 nm. Quantum Yield of quinine sulphate is 0.54. Simplified equation for the calculation after substituting the appropriate values is given as: $Q_S = 0.54 \times (m_S/2.71) \times (1.407/1.33)^2 = 0.223 \times m_S$ and values obtained are given in the table 4.5.

The thin films of the compounds on quartz plates were made by the spin coating of the solutions of these compounds in chloroform. As expected, the absorption and emission bands of these compounds were found to be broad in comparison to their solution spectra. The absorption spectra of the thin films of most of the oxadiazole based compounds **PO1-4** as well as thiadiazole based compounds **PT1-4** showed a red-shift in comparison to the solution spectra, pointing towards the formation of J-type aggregates.[14c] Compound **PO3** and **PT4** showed a slight blue-shift in the absorption maximum, which may be due to the formation of H-aggregates.[20] Considering the possibility of the several conformational isomers, it is difficult to conclude the type of the aggregates. As the room temperature Col_r phase of compound **PO3** and **PT3** we examined the thin films of the compounds, which were found to be transparent in visible light and remained stable over a long period. The irradiation of these films with UV light of long wavelength provided blue emission, which masked the pattern placed behind (Fig. 4.15a-d). The thin film of compound **PO3** exhibited higher emission intensity (2 folds) in comparison to their micromolar solution in THF, while the emission intensity for compound **PT3** was reduced by half (Fig. 4.15e-f). Both the solutions and thin films of oxadiazole and thiadiazole based compounds exhibited a visually perceivable blue emission under the UV light of long wavelength (Fig. 4.12c & 4.13c).

Table 4.5. Results of the quantum yield of the compounds **PO3** and **PT3** in THF solution.

Entry	m_S	m_R	$Q_s^{a,b,c}$
PO3	2.24	2.71	0.50
PT3	2.38	2.71	0.53
[a]Measured in THF; [b]Excited at absorption maxima; [c]Standard quinine sulphate (Q_f = 0.54) in 0.1M H_2SO_4.			

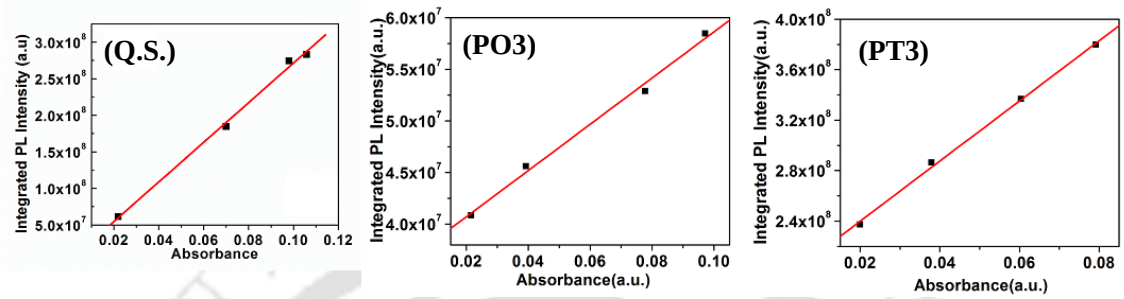

Figure 4.14. Plots of integrated photoluminescence intensity vs absorbance of Quinine sulphate (0.1M H_2SO_4 solution), compounds **PO3** and **PT3** (micromolar THF solution).

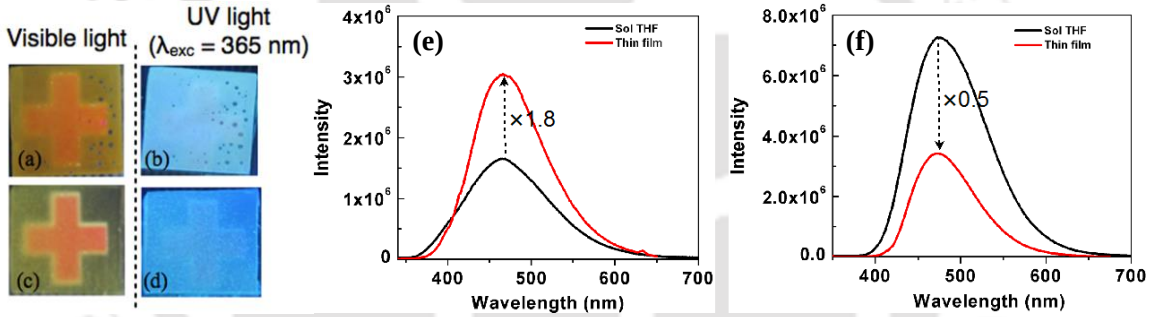

Figure 4.15. Thin film of compound **PO3** annealed in Col_r phase placed above a pattern under visible light (a); the same under the UV light (λ_{ex} = 365 nm) (b); Thin film of compound **PT3** annealed in Col_r phase placed above a pattern under visible light (c); the same under the UV light (λ_{ex} = 365 nm) (d). Comparison of the emission spectra of compounds **PO3** (e) and **PT3** (f) in micromolar THF solution and thin film state.

4.2.4. Solvatochromism and acidochromism

We investigated the effect of solvent polarity on the absorption and emission properties of the compounds. The absorption and fluorescence spectra of representative compounds **PO3** and **PT3** in different solvents like decane, hexane, tetrachloromethane (CCl_4), dichloromethane (DCM), chloroform ($CHCl_3$), tetrahydrofuran (THF) and toluene were recorded and the corresponding photophysical details are summarized in table 4.6. The pictures of micromolar solution of compounds **PO3** and **PT3** in different solvents were depicted in figure 4.17 & 4.18. As we know, solvent polarity influences the energy levels of the absorption or emission bands. [16] From the absorption spectra we found that the

energy levels of the absorption remain almost unaffected indicating non-polar ground state. In contrast to the absorption band, the emission was red-shifted on increasing the solvent polarity from decane to polar solvents like THF (Fig. 4.16). This corresponds to the polar nature of the excited state.[16]

Table 4.6. Photophysical properties of compound **PO3** and **PT3** in different solvents[a].

Solvent	PO3			PT3		
	Absorption (nm)	Emission[b] (nm)	Stokes shift (nm)	Absorption (nm)	Emission[b] (nm)	Stokes shift(nm)
Hexane	310	433	123	343	453	110
Decane	310	428	118	343	449	106
DCM	310	460	150	343	484	141
CCl_4	311	427	116	343	457	114
Toluene	311	435	124	343	471	128
$CHCl_3$	313	457	144	343	472	129
THF	314	465	151	343	473	130

[a] micromolar solutions in Decane, Toluene, Chloroform, THF; [b] excited at the respective absorption maxima.

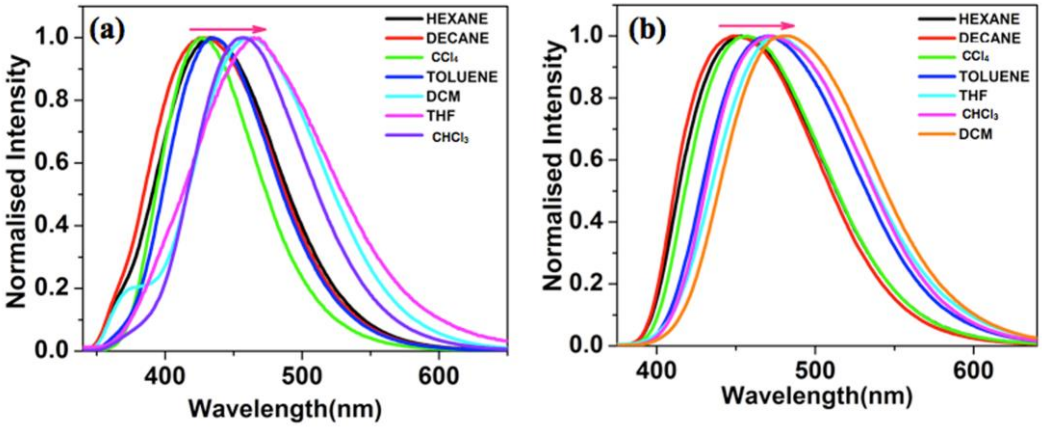

Figure 4.16. Normalized emission spectra of compounds **PO3** (a) and **PT3** (b) in micromolar concentrations of different solvents.

Considering the presence of a sp^2 hybridized N atom of the pyridine ring, we envisaged that these compounds might act as good proton acceptors. The protonation may change the extent of delocalization and thus affect the optical properties of these compounds, which can be beneficial in the detection of acids. As seen from the fig. 4.19a and b, the emission intensities of compounds **PO3** and **PT3** were reduced by the addition of trifluoroacetic acid (TFA). In the case of compound **PO3** the gradual addition of TFA led to a blue-shifted emission spectra, and thus the solution under UV light showed blue

light emission, where the difference was not very much detectable visually. However, in the case of compound **PT3**, the gradual addition of TFA led to red-shifted emission spectra, with a visually perceivable green emission under UV light of long wavelength (Fig. 4.20). In both cases the original blue emission was recovered to a certain extent by the addition of an equivalent amount of triethylamine (TEA) (Fig. 4.21 bottom panel).

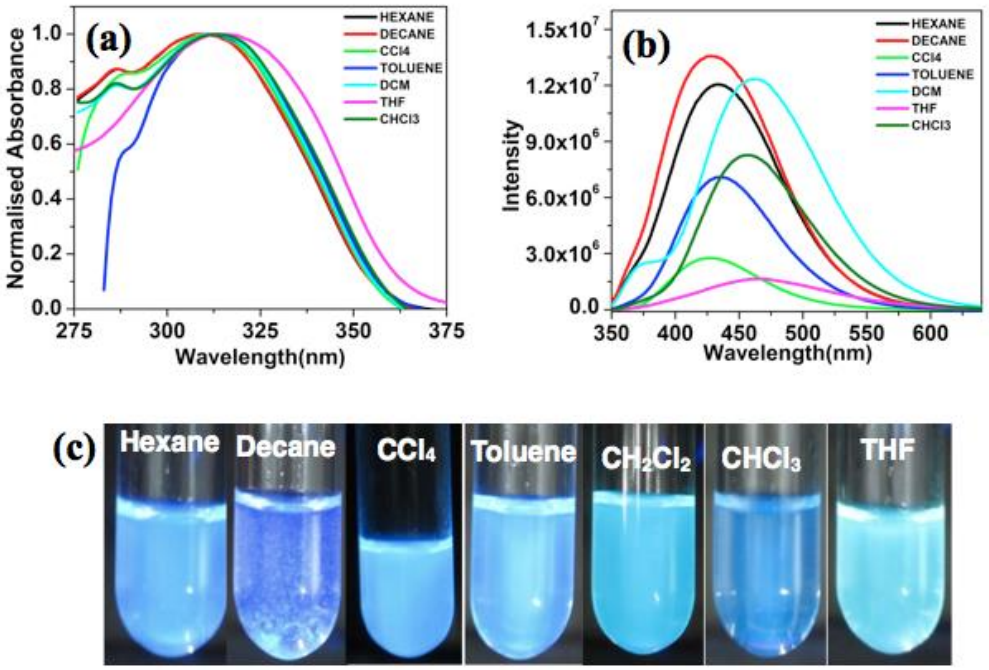

Figure 4.17. Normalized absorption (a) and emission spectra (b) of **PO3** in micromolar concentration in different solvents; Images of the same solutions under the light of long wavelength (365 nm) (c).

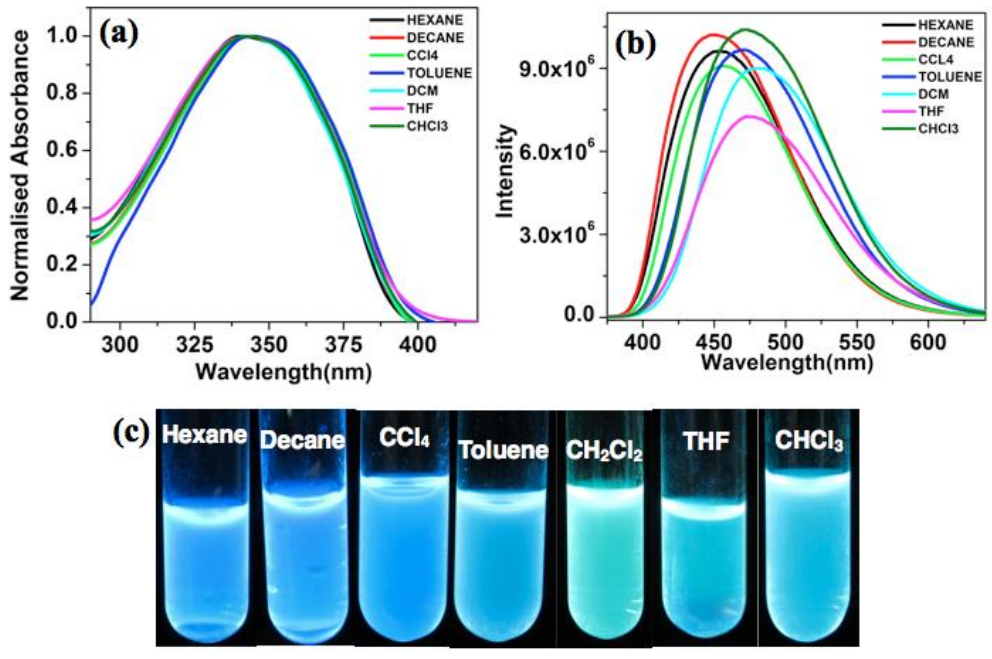

Figure 4.18. Normalized absorption (a) and emission spectra (b) of **PT3** in micromolar concentration in different solvents; Images of the same solutions under the light of long wavelength (365 nm) (c).

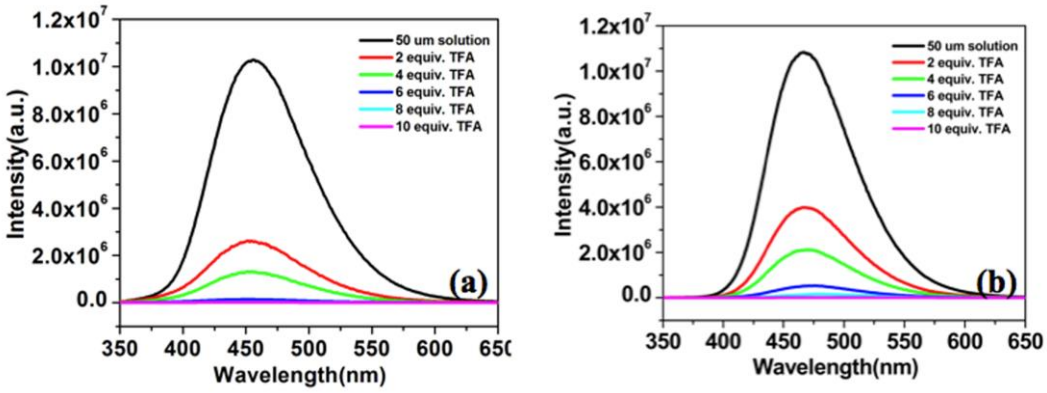

Figure 4.19. Emission spectra obtained for the **PO3** on gradual addition of TFA to the in same (50 μM in $CHCl_3$) (a); the same obtained for the **PT3** on gradual addition of TFA to the in same (50 μM in $CHCl_3$) (b).

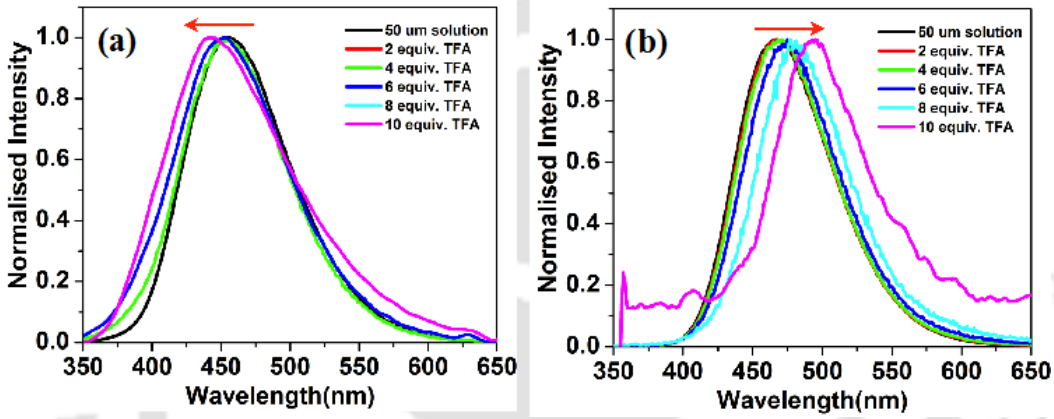

Figure 4.20. Comparison of the normalized emission spectra of compounds **PO3** (a) and **PT3** (b) in micromolar THF solution on gradual addition of TFA.

From the ^{1}H NMR spectra, it was visualized that the protonation of the compounds led to a large downfield shift of the protons on pyridine ring, whereas the neutralization with the triethylamine recovered the signals back to the original in the case of compound **PO3** or near to the original position in the case of compound **PT3** (Fig. 4.21 upper panel).

We were curious to analyze the proton sensing ability of compound **PT3** considering red-shifted emission spectra, with a visually perceivable green emission under UV light of long wave length and may be beneficial in detecting volatile acids like trifluoro-acetic acid (TFA). TFA was used as an analyte due to its strong acidic and volatile properties. Upon gradual addition of TFA to solution of compound **PT3** (20 μmol), the color of the solution changes from colorless to light yellow, producing a new red-shifted shoulder in the absorption spectrum along with lowering of absorbance value (Fig. 4.22b). On excess addition of TFA (500 μL), a new broad red-shifted (34 nm) absorption band centered at around 368 nm was appeared. This suggests that the protonation of **PT3** strongly affects the electronic energy levels of the molecule.

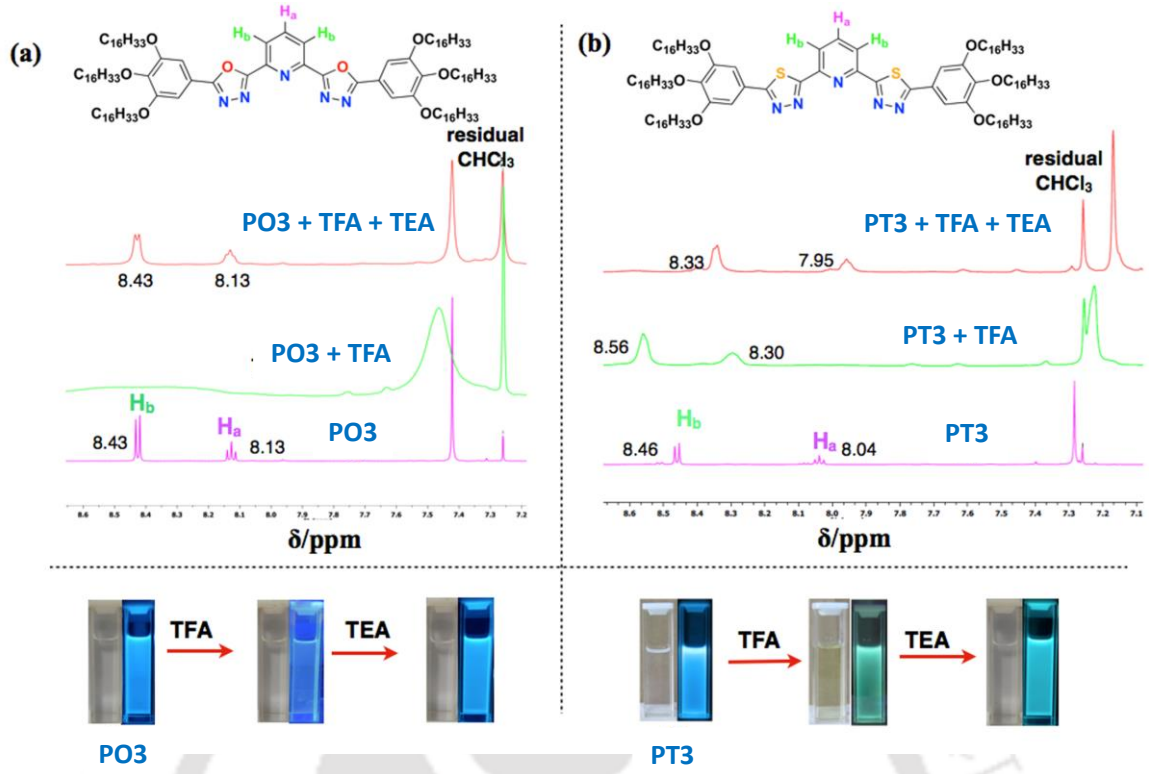

Figure 4.21. Expanded region of ^{1}H NMR spectra of **PO3** (a) and **PT3** (b) on subsequent addition of TFA and TEA in $CDCl_3$ (The bottom panel shows the changes happen on the subsequent addition of TFA and TEA, as seen under daylight and UV light of long wavelength).

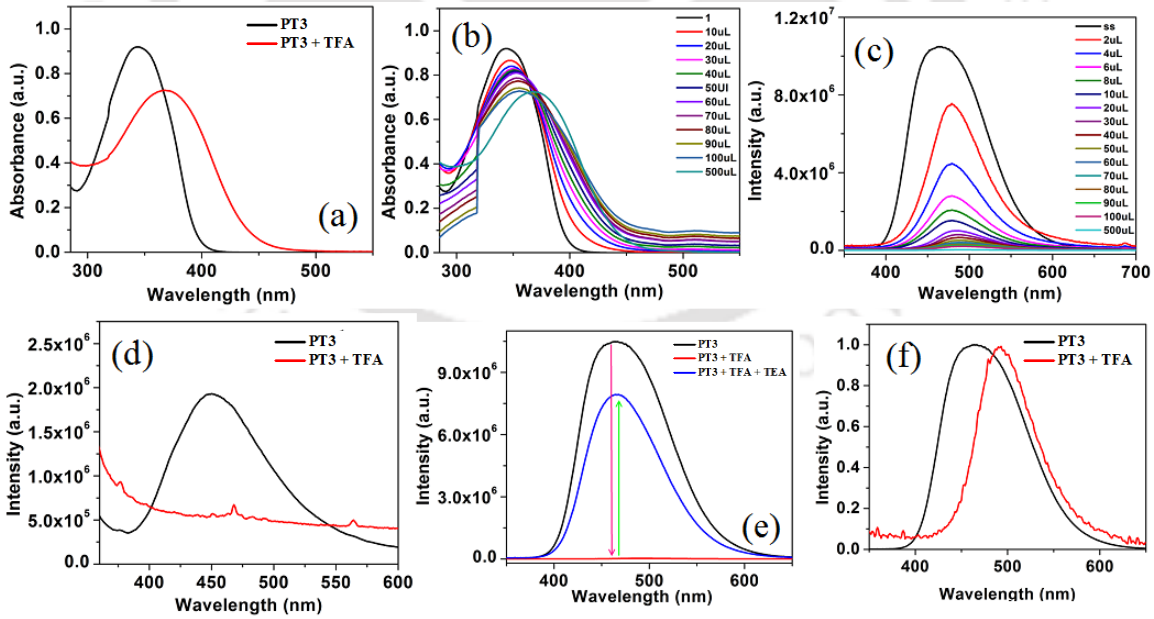

Figure 4.22. Absorbance spectra of compound **PT3** in chloroform before and after addition of TFA (a); Absorbance spectra (b); Emission spectra of compound **PT3** in chloroform upon gradual addition of TFA (c); Emission spectra of thin film of compound **PT3** before and after addition of TFA (d); Emission spectra of compound **PT3** in chloroform before and after addition of TFA and TEA (e); Normalized emission spectra of compound **PT3** in chloroform before and after addition of TFA (f).

The emission intensity of compound **PT3** gradually decreases with the addition of TFA (Fig. 4.22c). On excess addition of TFA (500 μL), along with a decrease in emission intensity there was a red-shift in emission maximum from 464 nm to 493 nm. Visually it was a blue to green emission under the UV light (λ = 365 nm) (Fig. 4.23d, 4.22f). The emission intensity of compound **PT3** reverts back to certain extent with the addition of triethyl amine (TEA) to this solution (Fig. 4.23b). Hence, a noticeable change in the absorbance and faster luminescence quenching along with a red-shifted emission suggests the strong interaction of compound **PT3** with TFA.[11] From the luminescence quenching the detection limit for the TFA solution was calculated and found to be 85 parts per billion. The interaction of compound **PT3** with TFA was further confirmed by the analysis of ^{1}H NMR spectra of **PT3** in the absence and presence of TFA. All the protons on the pyridine ring observed a large downfield shift, which indicated the protonation of the pyridine ring. Again, the deprotonation of compound **PT3** via addition of TEA leads to the upfield shift of the pyridine ring protons (Fig. 4.23a). We also tested the application of acidochromic behavior of compound **PT3** for making rewritable media by coating the solution of **PT3** on filter paper. The word written on the filter paper ('IIT') using the solution of compound **PT3**, turned yellow on treating with TFA vapors, which can be erased only upon treating with TEA (Fig. 4.23f). This illustrates that compound **PT3** can be used as stable rewritable media. This also implies that the protonated species of compound **PT3** was stable. Qualitatively, we have studied the volatile acid sensing or proton sensing ability of **PT3** in thin film and gel state. The annealed thin film (in Col_r phase) of **PT3** showed blue emission under UV light (365 nm), on exposure to TFA exhibited a quenching (Fig. 4.23e) and color of thin film also changed from light yellow to deep yellow. Similar behavior was observed in the case of the word "IIT" written on the filter paper under the light of long wavelength. Similarly, the organogel, which showed aggregation induced blue emission, upon exposure to TFA became unstable, and the colorless opaque gel collapsed into a yellow colored solution. Upon keeping the solution for a day the solution is again converted to gel (Fig. 4.24). However, immediate reconversion to gel state is attained on addition of TEA to the yellow solution with TFA (Fig. 4.23c). Similar bent shaped gelator with two pyridine units is reported that showed sensing for TFA vapors, but needs a longer synthetic route and does not show any ordered arrangement of molecules in bulk or gel state.[11d]

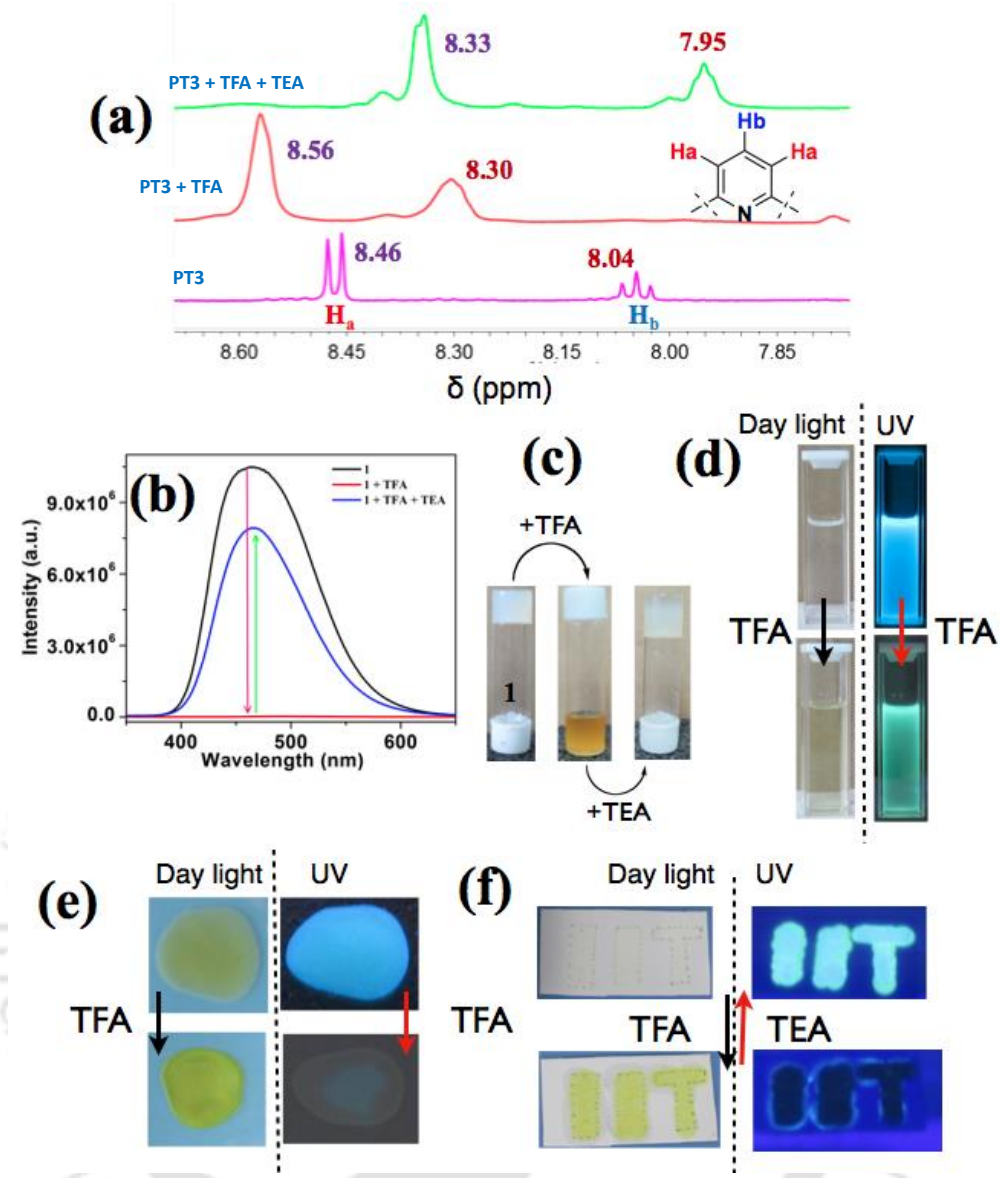

Figure 4.23. Expanded region of ^{1}H NMR spectra of **PT3** on subsequent addition of TFA and TEA in $CDCl_3$ (a); Emission spectra obtained for the same (20 μM in $CHCl_3$) (b); Response of the gel towards TFA and TEA (c); response of the solution (d); and annealed thin film towards TFA (e); application of acidochromism for a rewritable medium (f).

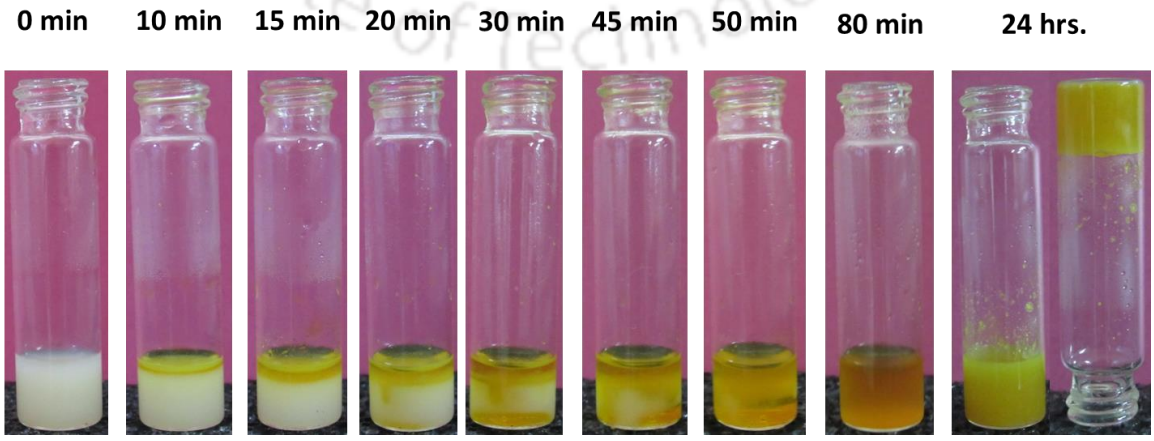

Figure 4.24. Photographs of **PT3** in gel state after exposing to TFA vapour as a function of time.

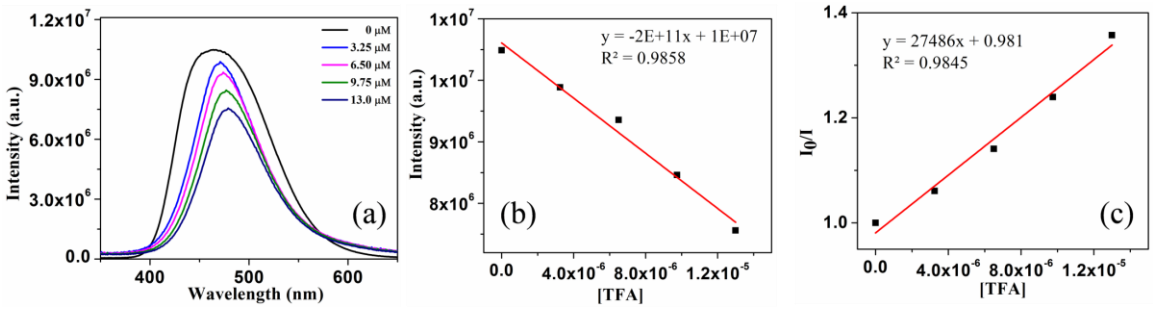

Figure 4.25. Fluorescence response of compound **PT3** (20 μM) in chloroform toward TFA solution (a); Fluorescence intensity of compound **PT3** (20 μM) taken in chloroform as a function of TFA concentration (b); Stern-Volmer plot for TFA (c).

Table 4.7. A brief comparison of probe **PT3** with other reported sensors of TFA.

Publication	Properties of the materials	Force of interaction / specific functional group for gelation	State of matter used for sensing	Reversibility of state of matter shown	Supporting data for sensing
Present work	Liquid crystal, Organogel	π-π interaction	Wet gel, Xerogel, Thin LC film, Solution	In all cases (TFA and TEA)	^{1}H NMR, Absorbance, Fluorescence.
Soft Matter, 2015, **11**, 9179-9187	Organogel	π-π interaction	Thin film	In thin film (TFA and TEA)	Fluorescence
J. Mater. Chem. C, 2015, **3**, 8888-8894	Organogel	π-π interaction	Wet gel, Thin film	Not available	Fluorescence
Chem. Eur. J., 2015, **21**, 4712-4720	Organogel	H-bonding/amide group	Wet gel, Thin film	In thin film (TFA and TEA)	Fluorescence
Chem. Eur. J., 2015, **21**, 17508-17515	Organogel	H-bonding/amide group	Wet gel, Thin film, Solution	Not available	Fluorescence
J. Mater. Chem. C, 2015, **3**, 10225−10231	Chromophore	Protonation of heteroatom	Solution	Solution (TFA and NH_3)	Fluorescence
J. Mater. Chem. A, 2015, **3**, 22441–22447	Photochromic molecule	Not available	Solution and thin film on PDMS	Heating and UV irradiation	Absorbance
Dyes and Pigments, 2016, **130**, 233-244	Chromophores	Dipole-dipole interactions, intermolecular π-π stacking	Solution	Solution (TFA and TEA)	Fluorescence

This shows that the present molecular design shows stronger intermolecular interactions to form the self-assembled structures over a long range. A brief comparison of probe **PT3** with other reported sensors of TFA has been analyzed from literature (Table 4.7). For calculating detection limit, different samples of compound **PT3** (20 μM) each containing TFA solution (0, 3.25, 6.5, 9.75 and 13 μM) in 2 mL $CHCl_3$ were prepared separately and fluorescence spectrum was then

recorded for each sample by exciting at 343 nm. The detection limit plot for TFA was obtained by plotting change in the fluorescence intensity vs. the concentration of TFA. The curve demonstrates a linear relationship and the correlation coefficient (R^2) via linear regression analysis were calculated to be 0.9845. The limit of detection (LOD) was then calculated using the equation 3σ/K, where σ signifies the standard deviation for the intensity of compound **PT3** in the absence of TFA and K denotes slope of the equation.

$$LOD = 3 \times \sigma / k$$

$$= 3 \times 25087.88 / 2 \times 10^{11}$$

$$= 37.63 \times 10^{-8} M \text{ (85ppb)}$$

4.2.5. Gelation properties

We were interested in the gelation behavior of these different series of compounds and wanted to study the effect of different heterocycles and the number of peripheral alkoxy tails. Further the hexacatenars **PO3** and **PT3** stabilized Col phases in bulk, and thus it is interesting to compare their aggregation behavior in presence of solvents (Fig. 4.26). Compounds **PO3** and **PT3** were mixed separately in different solvents of varying polarity and proticity. Polar aprotic solvents like chloroform, dichloromethane, tetrahydrofuran (THF), dimethylsulfoxide (DMSO), dimethylformamide (DMF); polar protic solvents like ethanol, *n*-butanol; nonpolar aromatic solvents like benzene, toluene, *m*-xylene, nonpolar aliphatic solvents like hexane, decane, dodecane and hexadecane were utilized to probe the gelation behavior of these compounds (Table 4.8). Immediately after mixing, the suspensions were heated to obtain a clear solution. Then, the solutions were allowed to cool to room temperature to form gels. Both the compounds **PO3** and **PT3** were found to be soluble in most of the solvents like chloroform, dichloromethane, tetrahydrofuran, toluene, benzene and *m*-xylene. These compounds were insoluble in DMSO and DMF, and found to precipitate in ethanol and *n*-butanol. In the case of all aliphatic nonpolar solvents, the clear solutions of these compounds became turbid, finally forming a translucent gel. Finally, the formation of the gel was confirmed by "stable to inversion of the glass vial" method (Fig. 4.26a-d). Further we checked the gelation behavior of other compounds **PO1, PO2, PO4, PT1, PT2** and **PT4** in decane (Table 4.9, Fig. 4.27). Compounds **PO1**, **PT1** and **PT2** precipitated in decane after dissolving in decane. Among the oxadiazole derivatives **PO2-4** showed gelation, while in the case of thiadiazole

derivatives, only compounds **PO3** and **PO4** have shown gelation. Since we were interested to derive the structure-property relationships we decided to investigate the compounds **PO3** and **PT3** by extensive photophysical studies, microscopy and XRD studies. Detailed rheological measurements were also carried out on these two representative samples, which are described in a later section. The critical gelation concentration (CGC) and T_{gel} of all the gelators were studied in different gelating solvents by 'dropping ball method'[17] and are tabulated in table 4.9. Compounds **PO3-4** and **PT3-4** can be classified as supergelators as their CGC was found to be lesser than 10 mg/mL or 1 wt%.[18] Again, thermal stability of compounds **PO3** and **PT3** with respect to concentration (Fig. 4.26e-f) was estimated for both derivatives in decane. The plots showed a steady increase in the thermal stability on increasing concentration. It may be noted that at higher concentration, the gel formed could be casted into any given shape of self-standing gel (Fig. 4.26g-j), with higher mechanical strength. It is interesting to note that, even with the lack of any specific hydrogen bonding moieties, the compounds **PO3** and **PT3** were able to form strong gels. The formation of stable gels can be attributed mainly to aromatic π-π interaction, dipole-dipole interaction and van der Waals interaction of hydrophobic alkyl chains with long chain hydrocarbon solvents.

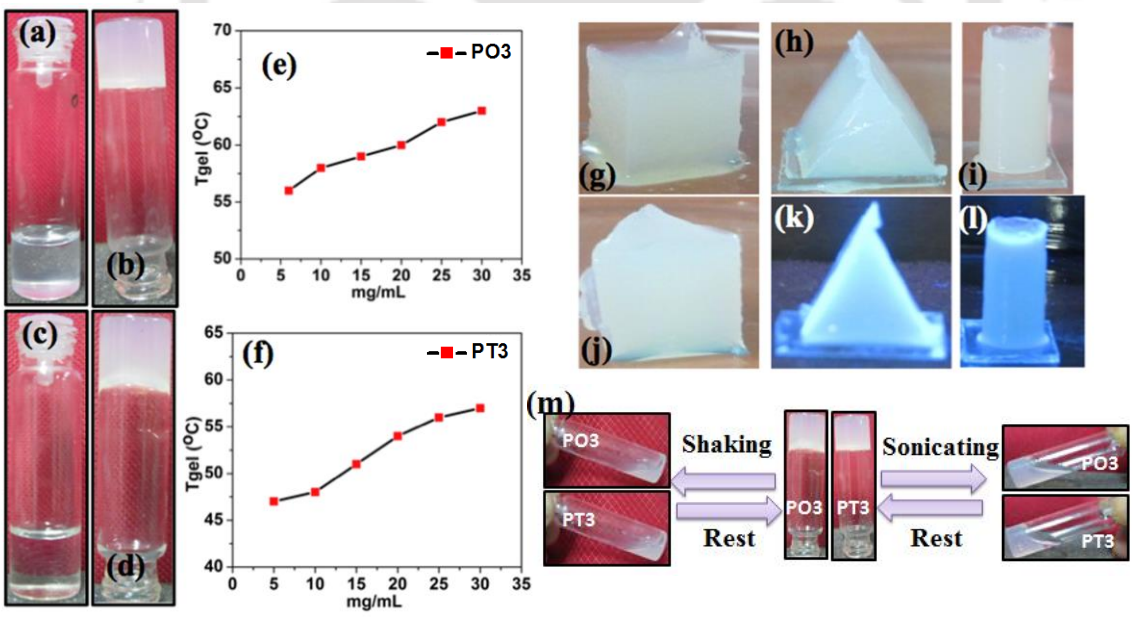

Figure 4.26. Solution (a) and gel (b) form of **PO3** and the same for **PT3** (c, d); Plots of T_{gel} *vs* concentration for **PO3** (e) and for **PT3** (f) in decane; Images showing the moldability of both the organogels in decane (Concentrations: 1.2 wt% for **PO3** and 0.8 wt% for **PT3**) into shapes like cube for **PO3** (g); trigonal prism for **PO3** (h); trigonal prism for **PT3** (j); the same under UV light (365 nm) (k); 2.5 cm long cylinder shaped gel of **PT3** (i); the same under UV light (365 nm) (l); Images showing response to mechanical forces by **PO3** and **PT3** and their recovery (m).

Table 4.8. Gelation behavior and CGCs of compound **PO3** and **PT3** in various solvents

Sl. No.	Solvent	PO3			PT3		
		Properties	CGC (wt%)	T_{gel}(^{o}C)	Properties	CGC (wt%)	T_{gel}(^{o}C)
1	Hexane	G(O)	0.78	48	G(O)	0.56	43
2	Decane	G(O)	0.60	56	G(O)	0.50	47
3	Dodecane	G(O)	0.60	57	G(O)	0.48	52
4	Hexadecane	G(O)	0.58	59	G(O)	0.41	56
5	Toluene	S	----	---	S	----	---
6	Benzene	S	----	---	S	----	---
7	*m*-xylene	S	----	---	S	----	---
8	DCM	S	----	---	S	----	---
9	Chloroform	S	----	---	S	----	---
10	CCl_4	S	----	---	S	----	---
11	THF	S	----	---	S	----	---
12	*n*-butanol	P	----	---	P	----	---
13	Ethanol	P	----	---	P	----	---
14	DMSO	I	----	---	I	----	---

G = stable gel; P = precipitate; I = insoluble; O = opaque. The critical gelation concentration (wt%) is the minimum concentration necessary for gelation. T_{gel} (^{o}C) is the thermal stability of the gels.

Table 4.9. Gelation behavior and CGCs of compound **PO1-4** and **PT1-4** in decane

Entry	Properties	CGC (wt%)	T_{gel}(^{o}C)
PO1	P	-----	-----
PO2	G(O)	1.5	53
PO3	G(O)	0.6	56
PO4	G(O)	0.9	52
PT1	P	-----	-----
PT2	P	-----	-----
PT3	G(O)	0.5	47
PT4	G(O)	0.7	45

G = stable gel; P = precipitate; I = insoluble; S = soluble; O = opaque. The critical gelation concentration (wt%) is the minimum concentration necessary for gelation. T_{gel} (^{o}C) is the thermal stability of the gels.

The gel-sol transformation can also be achieved by the appliance of mechanical force (Fig. 4.26m) such as vigorous shaking or sonication, while the solutions reverted back to the original gel state on standing. Interestingly, these organogels have also shown significant self-healing property and can be recovered from any damage imposed on them, on standing (Fig. 4.28).

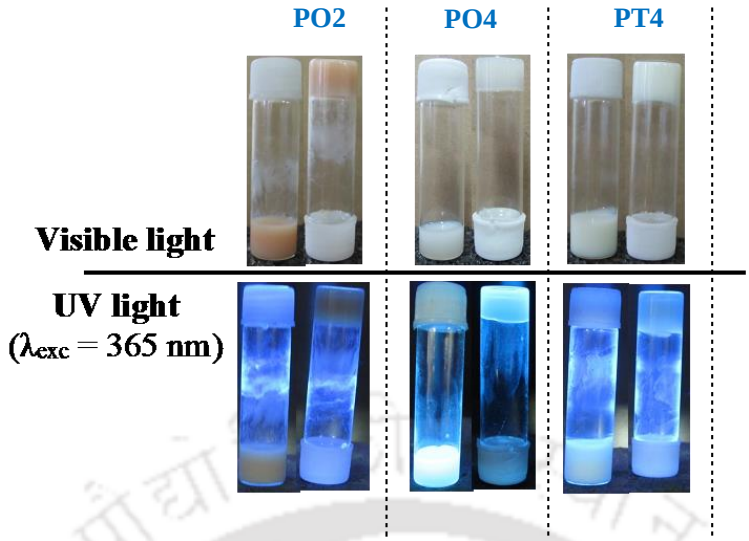

Figure 4.27. Images of solutions (left side) and gels (right side) seen under visible light and UV light of long wavelength.

The microstructures of the representative organogels formed from the compounds **PO3** and **PT3** in decane were investigated with field emission scanning microscopy (FESEM) and atomic force microscopy (AFM). The xerogel films of compounds **PO3** and **PT3** were prepared by evaporating the spin-coated films of decane solutions (5×10^{-6} M), followed by their vacuum evaporation for 2-3 h. The AFM images of the xerogels (Fig. 4.29a, b), exhibited dense interwoven network of fibers measuring several micrometers length. For compound **PO3**, the height of the fiber is around 30-35 nm with a thickness of 0.8 μm. In case of compound **PT3**, the average length of fibers was 40-60 nm, with a thickness of around 130 nm. These results were again supported through SEM micrographs obtained for the xerogels of **PO3** and **PT3** (Fig. 4.29c, d).

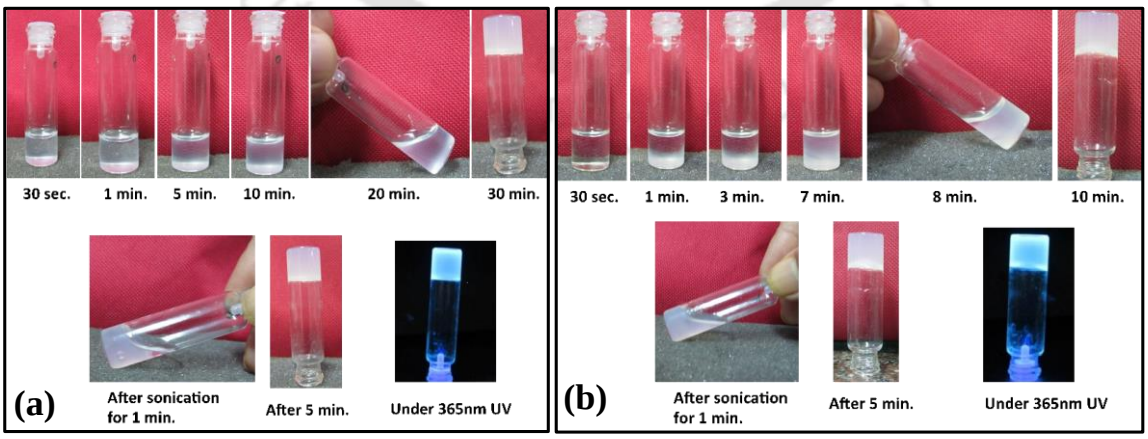

Figure 4.28. Images showing the transformation of solution to gel for compound **PO3** (a) and **PT3** (b).

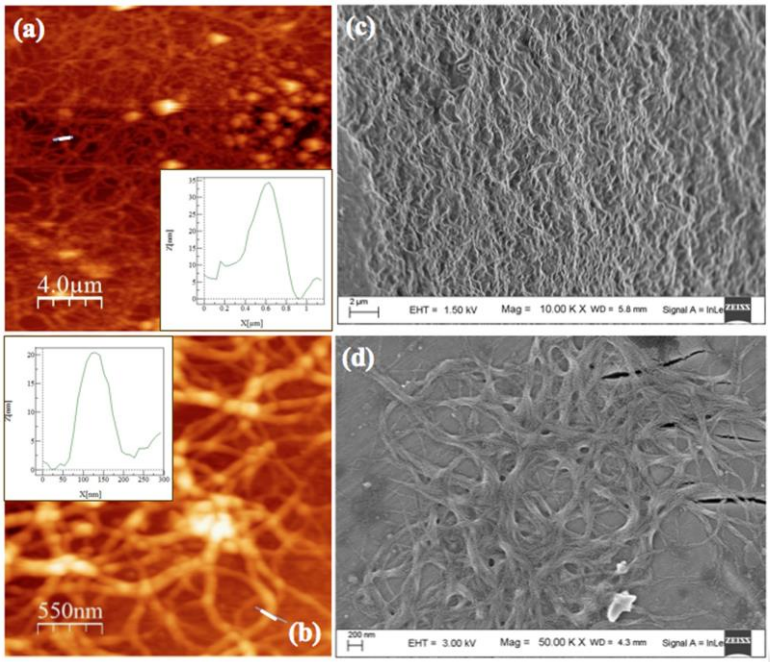

Figure 4.29.AFM image obtained for the xerogel of compound **PO3** obtained from 3.33 mM decane solution (scale bar is 4.0 µm) (a); xerogel of compound **PT3** (scale bar is 550 nm) (b) (Inset shows the thickness of an individual fiber); SEM images obtained for the xerogel of compound **PO3** (scale bar is 2 µm) (c); for the xerogel of compound **PT3** (scale bar is 200 nm) (d).

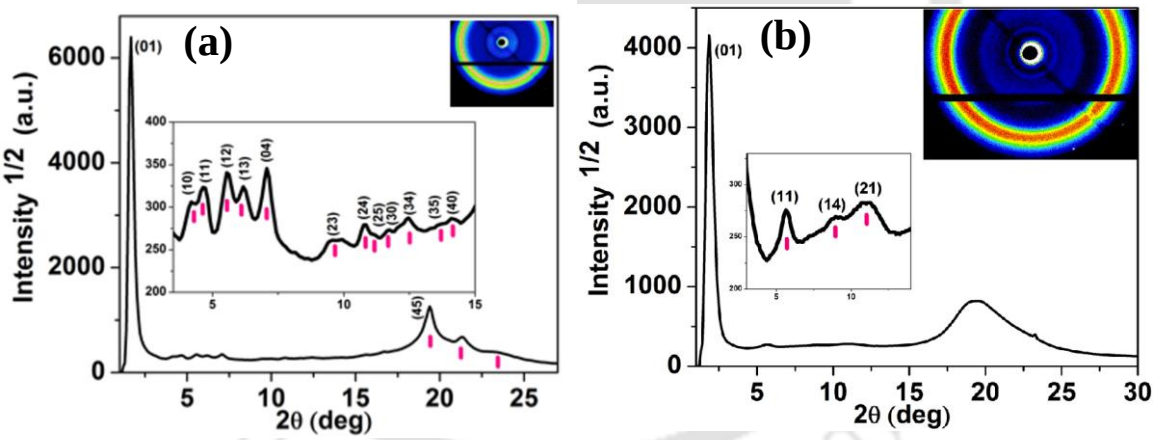

Figure 4.30. Intensity *vs* 2θ profiles obtained from the XRD pattern for the Col_r phase of the xerogel of compound **PO3** (a); Colr phase of the xerogel of compound **PT3** (b).

Further the arrangement of the molecules in the xerogel state was extensively probed with the help of small angle X-ray diffraction studies. The XRD pattern for xerogel **PO3** at room temperature showed several peaks centered at 53.05, 21.11, 19.04, 15.95, 14.33, 12.51, 9.18, 8.19, 7.57, 7.10, 6.26, 5.66, 5.31 and 4.57 Å. These *d*-spacings were quite ideally fitting into a rectangular (Col_r) lattice structure (Fig. 4.30a and table 4.10). In the wide-angle region we have found two diffused reflections centered at 4.16 and 3.77 Å, could be ascribed to the packing of flexible alkyl chains and to the packing of aromatic cores. Similar rectangular arrangement was found in case of compound **PT3**

where the XRD pattern for xerogel at room temperature showed several peaks centered at 47.95, 15.69, 9.89 and 8.04 Å. (Fig. 4.30b and table 4.10). [8e] From the lattice parameters we calculated the number of molecules forming a columnar slice in the case of **PO3** and **PT3**, which was found to be almost 1. It is interesting to note that these molecules exhibit liquid crystalline behavior and organogelation, while maintaining the same order (Columnar assembly with a rectangular symmetry) over a long range, which is beneficial from the viewpoint of organic electronic devices. [23]

Table 4.10. Results of (*hk*) indexation of XRD profiles of the compounds **PO3** and **PT3** in the xerogel state at room temperature (RT).

Compounds (state)	Phase (T/°C)	d_{obs} (Å)	d_{cal}(Å)	Miller indices *hk*	Lattice parameters (Å), Lattice area S (Å^2), Molecular volume V (Å^3)
PO3 Xerogel	Col_r (RT)	53.05 21.11 19.04 15.95 14.33 12.51 9.18 8.19 7.57 7.10 6.26 5.66 5.31 4.57 4.16(h_a) 3.77(h_c)	53.05 21.11 19.61 16.52 13.56 13.26 9.06 8.26 7.48 7.04 6.22 5.86 5.28 4.73	01 10 11 12 13 04 23 24 25 30 34 35 40 45	a = 21.11, b = 53.05, c = 3.77, S = 1119.9, V = 4212, Z = 1.4
PT3 Xerogel	Col_r (RT)	47.95 15.69 9.89 8.04 4.58(h_a) 3.82(h_c)	47.95 15.69 9.72 8.18	01 11 14 21	a = 16.60, b = 47.95, c = 3.82, S = 796, V = 3040.6, Z = 1

d_{obs}: spacing observed; d_{cal}: spacing calculated (deduced from the lattice parameters; a for Col_h phase; c is height of the unit cell). The spacings marked h_a and h_c correspond to diffuse reflections in the wide-angle region arising from correlations between the alkyl chains and core regions, respectively. Z indicates the number of molecules per columnar slice of thickness h_c estimated from the lattice area S and the volume V.

4.2.6. Aggregation induced enhanced emission (AIEE) behavior

The gelation of compounds **PO3** and **PT3** in decane was followed with the help of fluorescence spectroscopy. They showed a blue-shifted excitation spectrum in gel state in comparison to the excitation spectra of solution state (Fig. 4.31a, c). There was a slight red-shifted emission observed in the case of compound **PO3**, while the emission was not shifted in the case compound **PT3** (Fig. 4.31b, d). We were curious to know the photophysical properties of compound **PO3** and **PT3** in thin film state. The spin coated

thin films on quartz plates showed a blue-shifted absorption bands in comparison to the solution state excitation spectra (Fig. 4.31a, c). This points to the formation of aggregates in the case of thin films and gels in comparison to solution state. The blue-shift in the absorption usually corresponds to the formation of H-aggregates, where the molecules are stacked one above the other in a cofacial or parallel manner. The aggregated states (in thin film and gel) showed several fold enhanced luminescence in comparison to the solution state (Fig. 4.31b, d). Notably, the luminescence was higher in gel state for compound **PO3** than in thin film state, while it is higher in thin film state for compound **PT3** than in gel state.

To determine the effect of aggregate formation on the luminescence properties as well as organogel formation, decane gels of **PO3** and **PT3** were measured at different temperatures and times. In both cases, the intensity of emission increases with the decrease in temperature (Fig. 4.32a, 4.33a). A bathochromic shift in the emission of

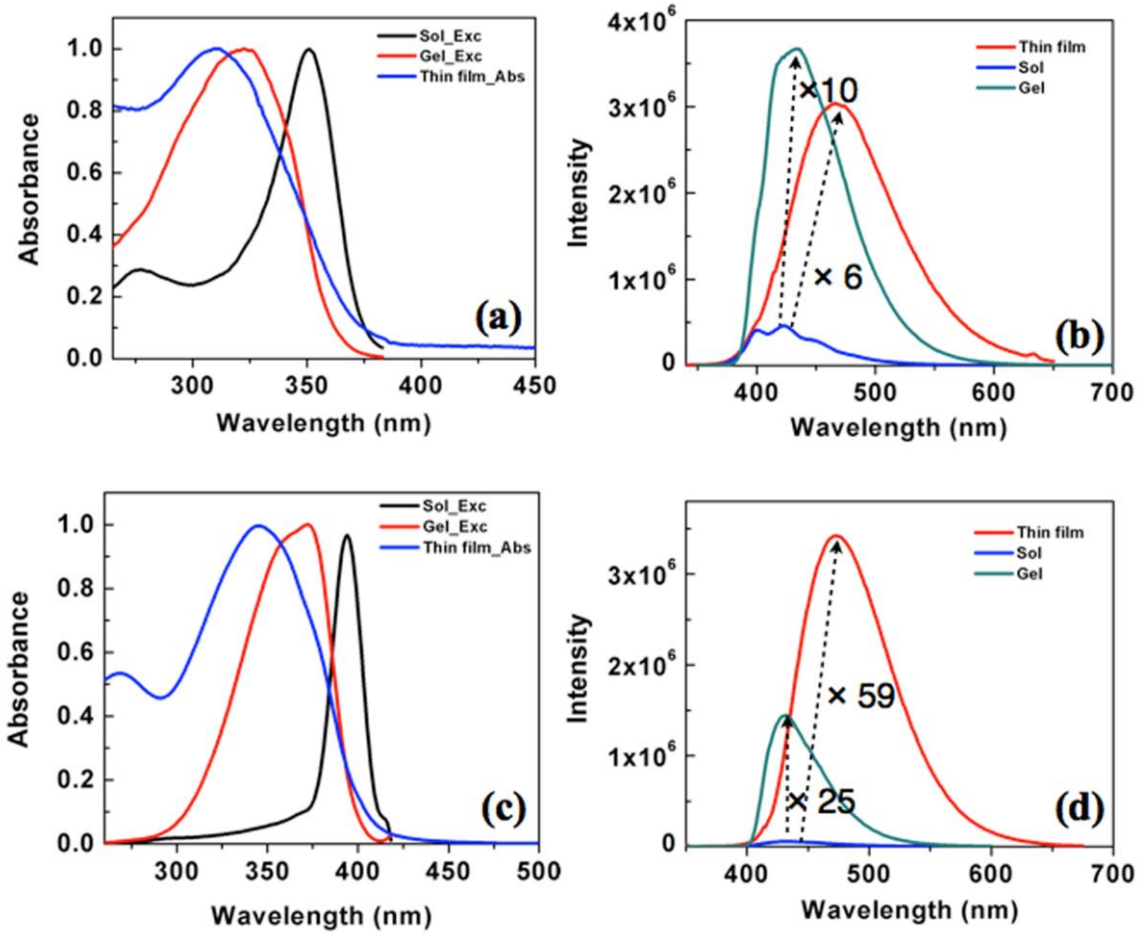

Figure 4.31. Excitation and absorption spectra of compound **PO3** (a); **PT3** (c) in solution, gel (at CGC) and thin film state; Emission spectra of compound **PO3** (b); **PT3** (d) in solution, gel (at CGC) and thin film state.

25 nm was observed in the case of **PO3** in comparison to that of compound **PT3** (12 nm red-shift) (Fig. 4.32b, 4.33b). In comparison to solution state, a huge increase in the fluorescence intensity in the gel state *i.e.* 10 fold in case of **PO3** (which is higher than the emission intensity of the thin film), whereas 25 fold in the case of **PT3** (which is lower than the emission intensity of the thin film) was noted (Fig. 4.32c, 4.33c). Thus even though both the compounds points to the formation of H-aggregates in thin films and gel state, the molecular arrangement is not same in these two different states, which results in different emission behavior.

Formation of organogel was also confirmed by measuring the emission spectra of the solution as a function of increasing time (Fig. 4.32d, 4.33d). The organogel was formed within 35 minutes in the case of **PO3** (Fig. 4.32e, 4.33e), which is little longer in comparison to that of **PT3** (10 minutes in **PT3**). The reproducibility of gel formation was confirmed after heating and cooling for many cycles as presented in Fig. 4.32f and 4.33f. The increase in the emission intensity upon aggregation, rather than the emission quenching is due to the ability to overcome aggregation caused quenching (ACQ).[20] In other words the favorable molecular packing in the gel state results in the restricted intramolecular rotations. Thus both bent-shaped oxadiazole and thiadiazole based bent polycatenars **PO3** and **PT3** exhibited aggregation-induced enhanced emission (AIEE) effect in the organogel state.

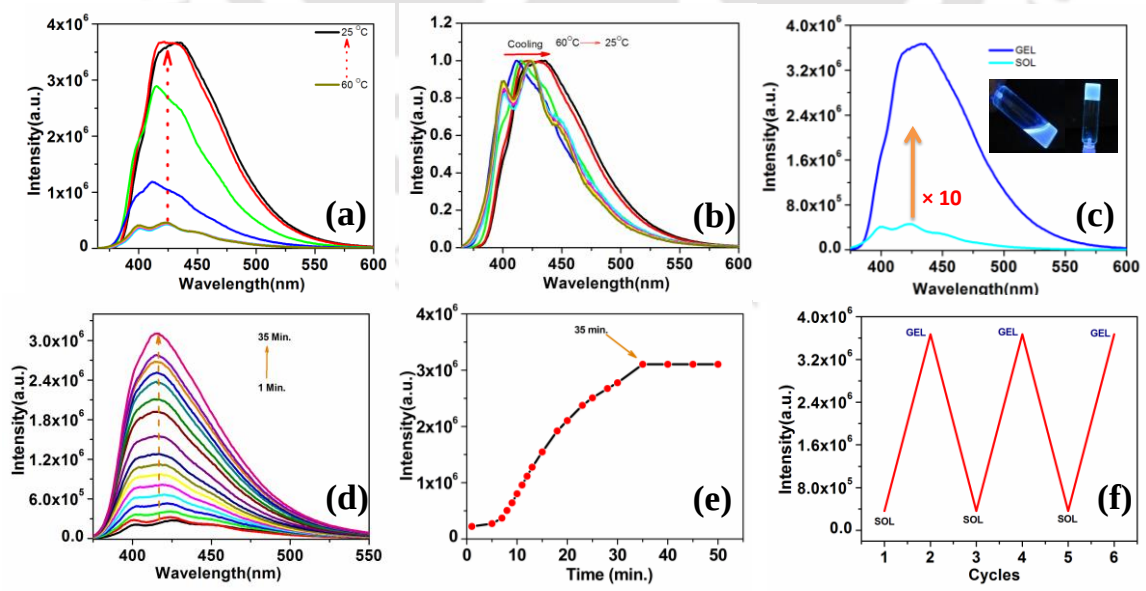

Figure 4.32. Emission spectra of **PO3** in decane (3.33 mM) on cooling from 60 °C to 25 °C (a); Normalized emission spectra on cooling from 60 °C to 25 °C (b); Comparison of emission spectra of sol-gel transition (c); Emission spectra obtained as a function of time (d); Plot showing the emission intensity at 415 nm as a function of time (e); Reversible change in the emission intensity at 415 nm by repeated sol-gel transition (f).

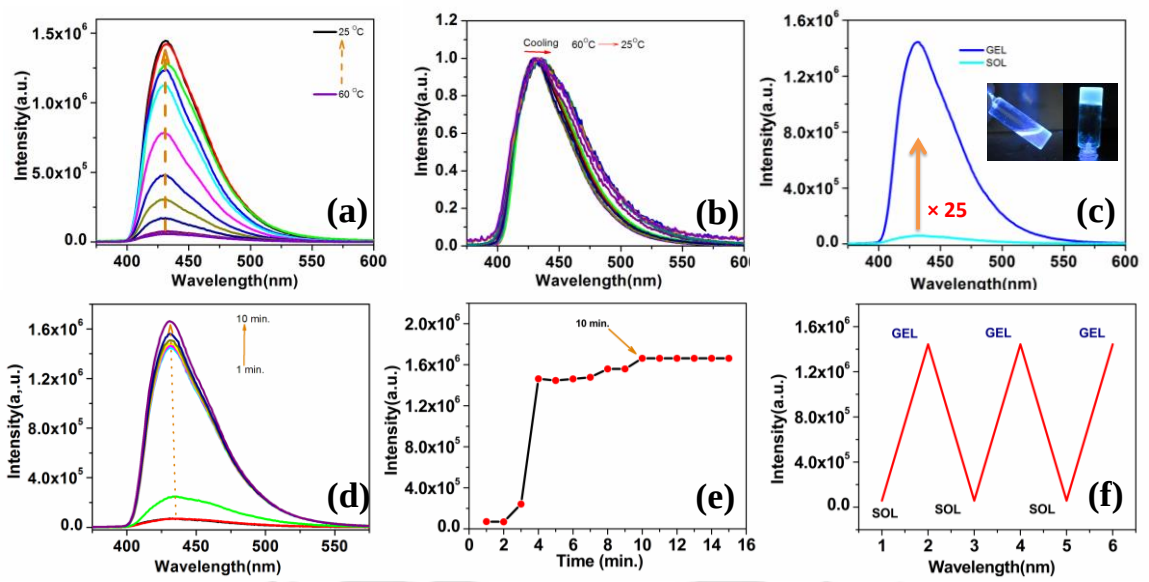

Figure 4.33. Emission spectra of **PT3** in decane (0.27 mM) on cooling from 60 °C to 25 °C (a); Normalized emission spectra on cooling from 60 °C to 25 °C (b); Comparison of emission spectra of sol-gel transition (c); Emission spectra obtained as a function of time (d); Plot showing the emission intensity at 431 nm as a function of time (e); Reversible change in the emission intensity at 431 nm by repeated sol-gel transition (f).

Fluorescence life-time measurements carried out for **PO3** and **PT3** in decane at 20 μM and at their CGC showed the biexponential emission decay with the increase in the life-time of the excited species (Fig. 4.34 and table 4.11). Even though H-aggregates are known to exhibit aggregation caused quenching (ACQ) of luminescence compared to the monomer emission in solution, here completely reverse behavior of the expected was observed.[19] There are very few reports on luminescent H-aggregates,[21] where the luminescence is attributed for the excimer species or due to a small displacement of the two exciton-coupled molecules in the excited state.

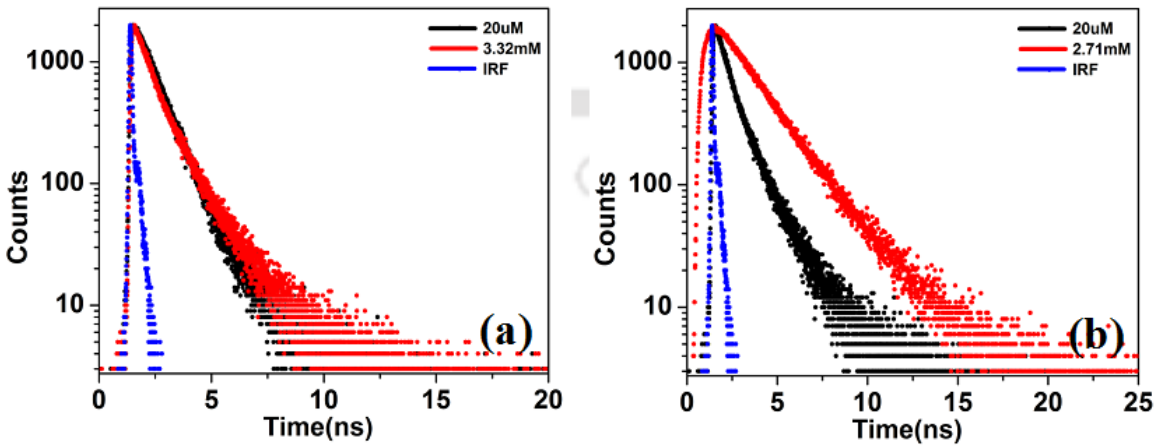

Figure 4.34. The fluorescence decay profiles of compound **PO3** in decane at 20 μM (black trace) and 3.32 mM (red trace) concentrations (blue trace is instrument response function: IRF; λ_{exc} = 375 nm) (a); The fluorescence decay profiles of compound **PT3** in decane at 20 μM (black trace) and 2.71 mM (red trace) concentrations (blue trace is instrument response function: IRF; λ_{exc} = 375 nm).

Table 4.11. Data obtained from time resolved photoluminescence studies for **PO3** and **PT3**.

Compound	State of matter	Fraction of molecule	Life time (ns)
PO3	Sol	55%	0.6
		45%	1.5
	Gel	88%	0.8
		12%	1.8
PT3	Sol	83%	1.9
		17%	3.1
	Gel	45%	1.8
		55%	6.1

4.2.7. Rheological properties

The viscoelastic properties of the gels formed from compound **PO3** and **PT3** at concentrations of 0.6 wt% and 0.5 wt% were measured with the help of rheological measurements. This involved strain sweep, angular frequency sweep and step strain measurements. For the measurement of rheological responses, a dynamic frequency sweep experiment at constant stress (0.2 kPa) was performed, which can be described by the equation G* (ω) = G' (ω) + iG" (ω), where ω is the angular frequency, G' is the storage modulus and G" is the loss modulus.[22] The value of G' slightly increase and the value of G" decrease with the frequency from 0.01 to 100 Hz and the value of G' is always higher than that of G" in the whole range (0.01-100 Hz), signifying that the gels **PO3** and **PT3** are fairly tolerant to the external force. From Fig. 4.35a and 4.35d, it is quite obvious that both **PO3** and **PT3** gels behave like a solid or viscoelastic like material (i.e. G' > G"). Both G', G" are feebly dependent on angular frequency at 25 ^{o}C using 0.2 mPa stress (Fig. 4.35b and e). As can be observed, these are the two requirements for a sample to be considered as a gel that is approximately satisfied by both gels **PO3** and **PT3**. In order to establish the non-linear viscoelastic regime, which is the characteristic features for dynamics of the sol-gel system, we performed stress dependent nonlinear measurements for compound **PO3** (0.6 wt%) and **PT3** (0.5 wt%). From fig. 4.35b and 4.35e, we make two observations in case for **PO3** and **PT3** separately. Firstly, at low strain amplitudes both G' and G" are nearly constant and G' > G" is steady confirming the solid like behavior and a linear viscoelastic regime. Secondly, both storage modulus and loss modulus became strain dependent above a stress value of 3.27 kPa and 0.8 kPa for **PO3** and **PT3** gels respectively. This observation leads to the formation of viscoelastic liquid behavior (G" > G') for both cases at high stress. In order to examine the thixotropic nature of the gels, we have studied the retrieval process of the damaged

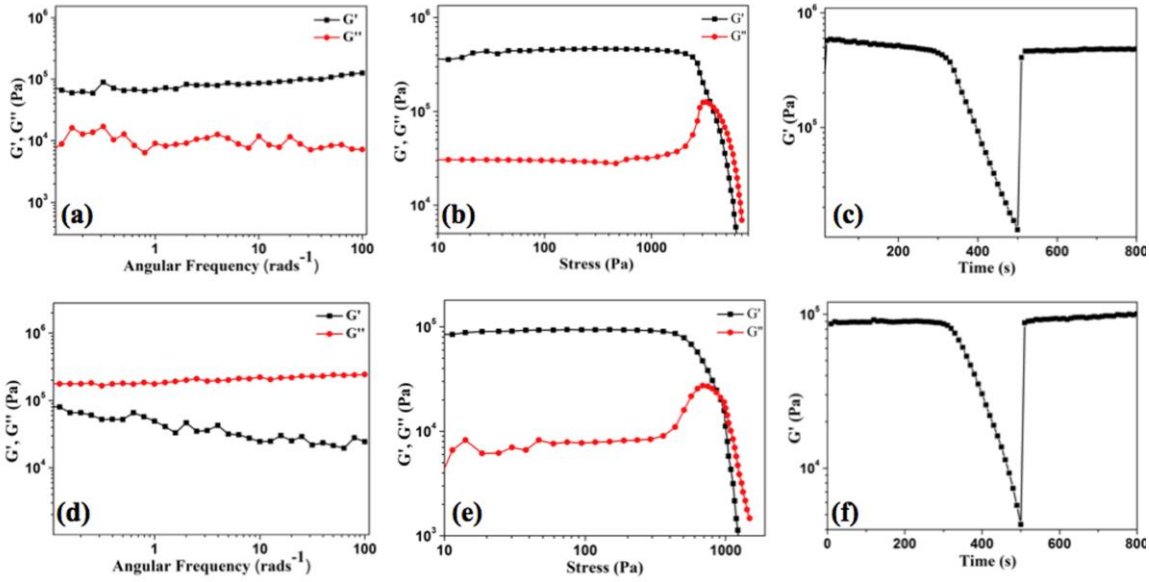

Figure 4.35. Angular frequency (rad s^{-1}) dependence of G' and G" obtained with small stress amplitudes: (a) 0.6 wt% of compound **PO3** in decane at 25 °C using 0.2 kPa stress; (b) Stress dependence of G' and G" of the same gel **PO3** measured at constant frequency (at 25 °C, and frequency at 10 Hz); (c) Thixotropic nature of organogel of **PO3** (3.32 mM) in decane at 25 °C (Deformation; stress: 0.2 to 4 kPa, time: 300 s, angular frequency: 10 Hz; Recovery; Stress: 0.2 kPa, time: 300 s; angular frequency: 10 Hz.); Angular frequency (rad s^{-1}) dependence of G' and G" obtained with small stress amplitudes: (d) 0.5 wt% of compound **PT3** in decane at 25 °C using 0.2 kPa stress; (e) Stress dependence of G' and G" of the same gel **PT3** measured at constant frequency (at 25 °C, and frequency at 10 Hz); (f) Thixotropic nature of organogel of **PT3** (2.71 mM) in decane at 25 °C (Deformation; stress: 0.2 to 4 kPa, time: 300 s, angular frequency: 10 Hz; Recovery; Stress: 0.2 kPa, time: 300 s; angular frequency: 10 Hz.)

gels via two continuous processes of deformation and recovery for several times. As observed from fig. 4.35c for **PO3** and fig. 4.35f for **PT3**, at a particular angular frequency of 10 Hz for 300 seconds a variable stress of 0.2 to 4 kPa was applied for the deformation process and the value of G' *vs* time was recorded. It was found that the value of G' decrease in deformation process leading to the formation of viscoelastic liquid at 300 seconds. The same graph was continued in the recovery process where the value of G' starts increasing with time leading to solid like properties at the same angular frequency for a shear stress of 0.2 kPa in both gels. This set of experiment was done five times for the reproducibility of the gel. It can also be concluded that we are dealing with high elastic modulus of consistent physical gels that can be recovered instantly, once eliminating the applied stress.

4.3. Conclusion

In this chapter, we have synthesized several bent-shaped molecules with a central pyridine unit flanked by two unsymmetrically substituted 1,3,4-oxadiazole and thiadiazole moieties. The number and position of the terminal tails were varied. The type of the heterocycle and the number of peripheral tails had a significant impact on the

stabilization of the liquid crystalline and organogel self-assembly as well as photophysical properties. Thiadiazole based compounds exhibited higher mesophase stability in comparison to oxadiazole derivatives, while oxadiazole based compounds exhibited higher gelation tendency. In the case of oxadiazole derivatives, tetracatenar and hexacatenars exhibited gelation behavior, while in the case of thiadiazole derivatives only hexacatenars exhibited gelation. The number of peripheral tails also plays an important role in stabilizing the gelation in hydrocarbon solvents, which is evident from the fact that all the hexacatenars stabilized supergelation irrespective of the type of heterocycle. The gelation is mainly promoted by attractive π-π interactions, which is in contrast to other supergelators that require strong intermolecular hydrogen bonding. The supergelators showed the capability to form self-standing, moldable gel at higher concentration. Thiadiazole based compounds exhibited bathochromically shifted absorption and emission in comparison to oxadiazole derivatives but with a lower quantum yield. In addition these compounds showed the ability to sense the acid with a quenching/shifting in the emission spectrum, which makes it possible to detect acids by naked eye at low concentration. Two of the hexacatenar supergelators investigated, exhibited aggregation induced enhanced emission with a several fold increase in luminescence intensity in the gel state. The variation in the gelation capability of these molecules shows that although the π-π interactions plays a major role in self-assembly, the nanoseggregation of incompatible molecular segments like peripheral flexible tails also contribute in organogelation and LC self-assembly. Scanning probe microscopic studies of the xerogels revealed a fibrillar network of several micrometers corroborating the long range supramolecular self-assembly. Extensive rheological studies proved the viscoelastic and thixotropic nature of the gels. Similar AIEE effect was observed in thin film state too. Stabilization of columnar self-assembly over a long range, along with AIEE behavior is significant from the perspective of emissive solid-state displays. In a nutshell, this study accounts the effect of molecular structural variations on the nature of supramolecular self-assembly and the resultant macroscopic properties, that is of substantial significance to the scientific community working in the broad area of supramolecular chemistry.

4.4. Experimental Section

In this section the detailed synthetic procedures and the molecular structural characterization data have been presented for the intermediates and target compounds mentioned in the scheme.

Synthesis of ethyl 4-(*n*-hexadecyloxy)benzoate (**3a**):

A mixture of ethyl 4-hydroxybenzoate (18.1 mmol, 1 equiv.), anhydrous K_2CO_3 (39.82 mmol, 2.2 equiv.), *n*-bromohexadecane (19.91 mmol, 1.1 equiv.) were taken in dry DMF (15 mL) and heated at 80 ^oC for 24 h under nitrogen atmosphere. After the reaction time was over, the reaction mixture was poured into ice water and extracted with ethyl acetate. The extract was washed with brine, dried over anhydrous Na_2SO_4 and then concentrated. The crude product was purified by column chromatography on silica. Elution with hexane followed by 2-5% ethyl acetate-hexane yielded the desired product.

R_f = 0.4 (5% EtOAc-hexane); white solid; yield: 85%; IR (KBr pellet): ν_{max} in cm^{-1} 2921, 2847, 1714, 1606, 1511, 1470, 1367, 1287, 1243, 1105, 695; ^1H NMR ($CDCl_3$, 400 MHz, 298K): δ 7.98 (d, 2H, *J* = 9.2Hz, H_{Ar}), 6.89 (d, 2H, *J* = 8.4Hz, H_{Ar}), 4.34 (q, 2H, *J* = 7.2Hz, $COOCH_2$), 3.99 (t, 2H, *J* = 6.4Hz, OCH_2), 1.75-1.83 (m, 2H, CH_2), 1.39-1.47 (m, 2H, CH_2), 1.36 (t, 3H, CH_3), 1.25-1.32 (m, 24H, 12 × CH_2), 0.88 (t, 3H, CH_3); ^{13}C NMR ($CDCl_3$, 100 MHz, 298K): δ 166.65, 163.09, 131.70, 122.87, 114.21, 68.40, 60.78, 32.14, 29.91, 29.88, 29.80, 29.77, 29.58, 29.34, 26.20, 22.91, 14.60, 14.33; HRMS (+APCI) exact mass calculated for $C_{25}H_{43}O_3$ ($M+H^+$): 391.3207, Found: 391.3100.

Synthesis of ethyl 3, 4-bis(hexadecyloxy)benzoate (**3b**):

A mixture of ethyl 3,4-dihydroxybenzoate (16.5 mmol, 1 equiv.), anhydrous K_2CO_3 (72.6 mmol, 4.4 equiv.), *n*-bromohexadecane (36.3 mmol, 2.2 equiv.) were taken in dry DMF and heated at 80 ^oC for 24 h under nitrogen atmosphere. Then the reaction mixture was poured into water and extracted with ethyl acetate. The combined extract was washed with brine, dried over anhydrous Na_2SO_4 and then concentrated. The crude product was purified by column chromatography on silica. Elution with hexane followed by 2-5% ethyl acetate-hexane produced the desire product.

R_f = 0.45 (5% EtOAc-hexane); white solid; yield: 80%; IR (KBr pellet): ν_{max} in cm^{-1} 3419, 2919, 2849, 1710, 1598, 1518, 1277, 1211, 1129, 761; ^1H NMR ($CDCl_3$, 400 MHz, 298

K): δ 7.63 (d, 1H, *J* = 8Hz, H_{Ar}), 7.54 (s, 1H, H_{Ar}), 6.86 (d, 1H, *J* = 8Hz, H_{Ar}), 4.34 (q, 2H, *J* = 8Hz, $COOCH_2$), 4.02-4.05 (m, 4H, 2 × OCH_2), 1.78-1.87 (m, 4H, 2 × CH_2), 1.43-1.49 (m, 4H, 2 × CH_2), 1.38 (t, 3H, CH_3), 1.25-1.36 (m, 48H, 24 × CH_2), 0.88 (t, 6H, 2 × CH_3); ^{13}C NMR ($CDCl_3$, 100 MHz, 298 K): δ 166.75, 153.35, 148.70, 123.66, 122.99, 114.56, 112.14, 69.52, 69.21, 60.90, 32.15, 29.93, 29.89, 29.85, 29.83, 29.64, 29.61, 29.59, 29.42, 29.30, 26.24, 26.20, 22.91, 14.62, 14.33; HRMS (+ESI) exact mass calculated for $C_{41}H_{75}O_4$ ($M+H^+$): 631.5665, Found: 631.5665.

Synthesis of ethyl 3,4,5-trihexadecyloxy benzoate (**3d**):

A mixture of ethyl gallate (15.1 mmol, 1 equiv.), anhydrous K_2CO_3 (99.9 mmol, 6.6 equiv.), *n*-bromohexadecane (49.83 mmol, 3.3 equiv.) were taken in dry DMF and heated at 80 ^oC for 24 h under nitrogen atmosphere. Then the reaction mixture was poured into water and extracted with ethyl acetate. The combined extract was washed with water and dried over anhydrous Na_2SO_4 and then concentrated. The crude product was purified by column chromatography on silica. Elution with hexane followed by 2-5% ethyl acetate-hexane produced the desire product.

R_f = 0.5 (5% EtOAc-hexane); white solid; yield: 75%; IR (KBr pellet): ν_{max} in cm^{-1} 2922, 2850, 1716, 1583, 1468, 1426, 1331, 1218, 1110, 1041; ^{1}H NMR ($CDCl_3$, 400 MHz, 298K): δ 7.25 (s, 2H, H_{Ar}), 4.35 (q, 2H, *J* = 7.2 Hz, $COOCH_2$), 4.01 (t, 6H, 3 × OCH_2), 1.25-1.82 (m, 84H, 42 × CH_2), 0.87 (m, 12H, 4 × CH_3); ^{13}C NMR ($CDCl_3$, 100 MHz, 298K): δ 166.70, 153.04, 142.61, 125.28, 108.29, 73.72, 69.44, 61.17, 33.05, 32.16, 30.56, 29.94, 29.89, 29.87, 29.80, 29.63, 29.60, 29.57, 26.32, 26.29, 22.92, 14.63, 14.33; HRMS (ESI+) exact mass calculated for $C_{57}H_{107}O_5$ (M+1): 871.8113, Found: 871.8031.

Synthesis of ethyl 3,4,5-tridodecyloxy benzoate (**3h**):

A mixture of ethyl gallate (15.1 mmol, 1 equiv.), anhydrous K_2CO_3 (99.9 mmol, 6.6 equiv.), *n*-bromododecane (49.83 mmol, 3.3 equiv.) were taken in dry DMF (15 mL) and heated at 80 ^oC for 24 h under nitrogen atmosphere. Then the reaction mixture was poured into ice water and extracted with ethyl acetate. The extract was washed with water, dried over anhydrous Na_2SO_4 and then concentrated. The crude product was purified by column chromatography on silica. Elution with hexane followed by 2-5% ethyl acetate-hexane yielded the desired product.

R_f = 0.45 (5% EtOAc-hexane); white solid; yield: 82%; IR (KBr pellet): ν_{max} in cm^{-1} 2922, 2850, 1716, 1583, 1468, 1426, 1331, 1218, 1110, 1029, 985, 820; ^1H NMR ($CDCl_3$, 600 MHz, 298K): δ 7.25 (s, 2H, H_{Ar}), 4.35 (q, 2H, *J* = 7.2Hz, $COOCH_2$), 4.01 (t, 6H, 3 × OCH_2), 1.79-1.83 (m, 4H, 2 × CH_2), 1.72-1.75 (m, 2H, CH_2), 1.44-1.49 (m, 6H, 3 × CH_2), 1.30 (t, 3H, CH_3), 1.26-1.35 (m, 48H, 24 × CH_2), 0.88 (m, 9H, 3 × CH_3); ^{13}C NMR ($CDCl_3$, 150 MHz, 298K): δ 166.67, 152.98, 142.45, 125.23, 108.17, 108.12, 73.68, 69.34, 61.16, 32.16, 32.14, 30.53, 30.08, 30.05, 29.97, 29.95, 29.94, 29.92, 29.88, 29.85, 29.79, 29.61, 29.59, 29.52, 26.30, 26.71, 22.91, 14.61, 14.33; HRMS (+ESI) exact mass calculated for $C_{45}H_{83}O_5(M+H^+)$: 703.6241, Found: 703.6240.

Synthesis of ethyl 4-(hexadecyloxy)benzhydrazide (**4a**):

A mixture of ethyl 4-(hexadecyloxy)benzoate (19 mmol, 1 equiv.), excess hydrazine hydrate (20 equiv.) in ethanol were refluxed for 48 h. Excess solvent was removed and water was added to it. Resulting precipitate was collected by filtration, washed with excess water, dried under vacuum and recrystallization from ethanol gave white solid product.

R_f = 0.25 (30% EtOAc-hexane); white solid; yield: 75%; IR (KBr pellet): ν_{max} in cm^{-1} 3429, 2919, 2850, 1648, 1617, 1508, 1472, 1252, 1180, 836; ^1H NMR ($CDCl_3$, 400 MHz, 298K): δ 7.69 (d, 2H, *J* = 8Hz, H_{Ar}), 7.33 (b s, 1H, CONH), 6.91 (d, 2H, *J* = 8Hz, H_{Ar}), 4.07 (b s, 2H, NH_2), 3.98 (s, 2H, OCH_2), 1.75-1.82 (m, 2H, CH_2), 1.41-1.45 (m, 2H, CH_2), 1.25-1.31 (m, 24H, 12 × CH_2), 0.87 (m, 3H, 1× CH_3); ^{13}C NMR ($CDCl_3$, 100 MHz, 298K): δ 168.61, 162.31, 128.81, 124.77, 114.62, 68.43, 32.12, 29.88, 29.85, 29.78, 29.75, 29.56, 29.31, 29.18, 22.88, 14.31; HRMS (+APCI) exact mass calculated for $C_{23}H_{41}N_2O_2$ $(M+H^+)$: 377.3168, Found: 377.3082.

Synthesis of ethyl 3,4-bis (hexadecyloxy)benzhydrazide (**4b**):

A mixture of ethyl 3,4-bis(hexadecyloxy)benzoate (10.2 mmol, 1 equiv.), excess hydrazine hydrate (20 equiv.) in butanol was refluxed for 48 h. Excess solvent was removed and water was added to it. Resulting precipitate was collected by filtration, washed with excess water, dried under vacuum and recrystallization from ethanol gave white solid product.

R_f = 0.25 (20% EtOAc-hexane); white solid; yield: 70%; IR (KBr pellet): ν_{max} in cm^{-1} 3248, 2919, 2848, 1711, 1514, 1467, 1278, 1212, 1150, 761; ^1H NMR ($CDCl_3$, 400 MHz,

298 K): δ 7.34 (d, 1H, *J* = 8Hz, H_{Ar}), 7.26 (b s, 1H, CONH), 7.22 (dd, 1H, *J* = 4Hz, *J* = 8Hz, H_{Ar}), 6.85 (d, 1H, *J* = 8Hz, H_{Ar}), 4.08 (b s, 2H, NH_2), 4.00-4.05 (m, 4H, 2 × OCH_2), 1.79-1.86 (m, 4H, 2 × CH_2), 1.38-1.50 (m, 4H, 2 × CH_2), 1.25-1.36 (m, 48H, 24 × CH_2), 0.88 (m, 6H, 2 × CH_3); ^{13}C NMR ($CDCl_3$, 150 MHz, 298 K): δ 168.77, 152.55, 149.33, 125.21, 119.70, 112.76, 112.65, 69.62, 69.37, 32.15, 29.94, 29.89, 29.85, 29.63, 29.59, 29.43, 29.34, 26.23, 22.90, 14.33; HRMS (+ESI) exact mass calculated for $C_{39}H_{73}N_2O_3$ ($M+H^+$): 617.5621, Found: 617.5726.

Synthesis of ethyl 3, 4, 5-tris (hexadecyloxy)benzhydrazide (**4d**):

A mixture of ethyl 3,4,5-tri-*n*-hexadecyloxybenzoate (10 mmol, 1 equiv.), excess hydrazine hydrate (20 equiv.) in butanol was refluxed for 48 h. Excess solvent was removed and water was added to it. Resulting precipitate was collected by filtration, washed with excess water, dried under vacuum and recrystallization from ethanol gave white solid product.

R_f = 0.52 (20% EtOAc-hexane); white solid; yield: 75%; IR (KBr pellet): ν_{max} in cm^{-1} 3448, 3248, 2921, 2850, 1635, 1579, 1466, 1427, 1238, 1122; ^{1}H NMR ($CDCl_3$, 400 MHz, 298K): δ 7.22 (b s, 1H, CONH), 6.92 (s, 2H, H_{Ar}), 4.07 (s, 2H, NH_2), 3.99 (m, 6H, 3 × OCH_2), 1.26-1.80 (m, 84H, 42 × CH_2), 0.88 (m, 9H, 3 × CH_3); ^{13}C NMR ($CDCl_3$, 150 MHz, 298K): δ 168.70, 153.54, 141.92, 127.68, 105.74, 69.60, 30.53, 29.97, 29.95, 29.88, 29.60, 26.30, 22.92, 14.33; HRMS (ESI+) exact mass calculated for $C_{55}H_{105}N_2O_4$ (M+1): 857.8069, Found: 857.8151.

Synthesis of ethyl 3, 4, 5-tris (dodecyloxy)benzhydrazide (**4h**):

A mixture of ethyl 3,4,5-tri-*n*-dodecyloxybenzoate (10 mmol, 1 equiv.), excess hydrazine hydrate (20 equiv.) in ethanol were refluxed for 48 h. Excess solvent was removed and water was added to it. Resulting precipitate was collected by filtration, washed with excess water, dried under vacuum. The solid was recrystallized from ethanol to yield a white solid product.

R_f = 0.4 (20% EtOAc-hexane); white solid; yield: 80%; IR (KBr pellet): ν_{max} in cm^{-1} 3448, 3248, 2921, 2850, 1635, 1579, 1466, 1427, 1238, 1122; ^{1}H NMR ($CDCl_3$, 600 MHz, 298K): δ 7.31 (b s, 1H, CONH), 6.92 (s, 2H, H_{Ar}), 4.98 (s, 2H, NH_2), 3.99 (t, 6H, 3 × OCH_2), 1.79-1.82 (m, 4H, 2 × CH_2), 1.70-1.75 (m, 2H, 2 × CH_2), 1.44-1.45 (m, 6H, 3 × CH_2), 1.25 (m, 48H, 24 × CH_2), 0.87 (m, 9H, 3 × CH_3); ^{13}C NMR ($CDCl_3$, 150 MHz,

298K): δ 168.95, 153.38, 141.52, 127.63, 106.61, 73.71, 69.47, 32.13, 30.49, 29.90, 29.84, 29.59, 29.57, 29.51, 26.27, 22.89, 14.31; HRMS (+ESI) exact mass calculated for $C_{43}H_{81}N_2O_4$ ($M+H^+$): 689.6196, Found: 689.5764.

Synthesis of 2,6-bis(5-(4-(hexadecyloxy)phenyl)-1,3,4-oxadiazol-2-yl)pyridine (**PO1**):

Pyridine dicarboxyllic acid (0.7 mmol) in 4 mL of thionyl chloride and DMF (2-3 drops) was heated under reflux for 8 h. The excess of thionyl chloride was removed by distillation and the crude product (pyridine di acid chloride) was dried in vacuo and used for the next reaction without further purification and characterization. The solution of pyridine diacid chloride (0.6 mmol, 1 equiv.) in THF was added dropwise to a solution of 4-(hexadecyloxy) benzohydrazide (1.2 mmol, 2.05 equiv.) and triethylamine (1.2 mmol, 2 equiv.) in THF (15 mL). The reaction mixture was stirred at 55 ^oC for 12 h. After cooling, THF was removed through distillation and the residue was extracted with EtOAc. The extract was washed with water and brine, dried over Na_2SO_4 and concentrated. The resulting crude product (**12a**) was directly used for next reaction.

The solution of crude product **12a** (1.2 mmol, 1 equiv.) in $POCl_3$ (10 mL) was refluxed for 24 h. After the reaction, the crude mixture was added dropwise to ice water. Then, it was extracted with DCM. After removal of solvent *in vacuo*, the crude product was further purified through column chromatography on neutral alumina. Elution with DCM yielded the desired product. Again, the product was recrystallized with DCM-ethanol system (2:1).

R_f = 0.6 (80% DCM-hexane); white solid; yield: 72%; IR (KBr pellet): ν_{max} in cm^{-1} 3443, 2919, 2849, 1617, 1497, 1430, 1298, 1253, 1180, 835; ^1H NMR ($CDCl_3$, 600 MHz, 298 K): δ 8.45 (d, 2H, *J* = 9Hz, H_{Ar}), 8.20 (d, 4H, *J* = 9Hz, H_{Ar}), 8.10 (t, 1H, *J* = 8.4Hz, H_{Ar}), 7.06 (d, 4H, *J* = 8.4Hz, H_{Ar}), 4.05 (t, 4H, 2 × OCH_2), 1.81-1.85 (m, 4H, 2 × CH_2), 1.47-1.48 (m, 4H, 2 × CH_2), 1.26-1.45 (m, 48H, 24 × CH_2), 0.87 (t, 6H, 2 × CH_3); ^{13}C NMR ($CDCl_3$, 150 MHz, 298 K): δ 166.25, 163.10, 162.63, 144.62, 138.67, 129.20, 125.04, 115.94, 115.25, 68.58, 32.14, 29.91, 29.80, 29.57, 29.36, 26.23, 22.90, 14.34; MALDI TOF MS: m/z for $C_{53}H_{78}N_5O_4$ [$M+H^+$], calculated: 848.6050, Found: 848.9870.

Synthesis of 2,6-bis(5-(3,4-bis(hexadecyloxy)phenyl)-1,3,4-oxadiazol-2-yl)pyridine (**PO2**):

Pyridine dicarboxyllic acid (0.7 mmol) in 4 mL of thionyl chloride and DMF (2-3 drops) was heated under reflux for 8 h. The excess of thionyl chloride was removed by

distillation and the crude product (pyridine di acid chloride) was dried in vacuo and used for the next reaction without further purification and characterization. The solution of pyridine diacid chloride (0.6 mmol, 1 equiv.) in THF was added dropwise to a solution of solution of 3,4-bis(hexadecyloxy)benzohydrazide (1.2 mmol, 2.05 equiv.) and triethylamine (1.2 mmol, 2 equiv.) in THF (15 mL). The reaction mixture was stirred at 55 ^{o}C for 12 h. After cooling, THF was removed through distillation and the residue was extracted with EtOAc. The extract was washed with water and brine, dried over Na_2SO_4 and concentrated. The resulting crude product (**12b**) was directly used for next reaction.

The solution of crude product **12b** (1.2 mmol, 1 equiv.) in $POCl_3$ (10 mL) was refluxed for 24 h. After the reaction, the crude mixture was dropwise added to ice water. Then, it was extracted with DCM. After removal of solvent *in vacuo*, the crude product was further purified through column chromatography on neutral alumina. Elution with DCM yielded the desired product. Again, the product was recrystallized with DCM-ethanol system (2:1).

R_f = 0.63 (80% DCM-hexane); white solid; yield: 68%; IR (KBr pellet): ν_{max} in cm^{-1} 3444, 2918, 2850, 1606, 1498, 1465, 1281, 1145, 1034, 821; ^{1}H NMR ($CDCl_3$, 600 MHz, 298 K): δ 8.44 (d, 2H, *J* = 9Hz, H_{Ar}), 8.11 (s, 1H, H_{Ar}), 7.80 (d, 2H, *J* = 8.4Hz, H_{Ar}), 7.75 (s, 2H, H_{Ar}), 6.99 (d, 2H, *J* = 8.4Hz, H_{Ar}), 4.09-4.13 (m, 8H, 4 × OCH_2), 1.87 (m, 8H, 4 × CH_2), 1.50 (m, 8H, 4 × CH_2), 1.26-1.38 (m, 96H, 48 × CH_2), 0.88 (s, 12H, 4 × CH_3); ^{13}C NMR ($CDCl_3$, 150 MHz, 298 K): δ 166.31, 163.04, 152.91, 149.58, 144.60, 138.69, 125.04, 121.35, 115.99, 112.98, 112.14, 69.67, 69.36, 32.15, 29.94, 29.89, 29.64, 29.59, 29.45, 29.34, 26.27, 22.91, 14.33; MALDI TOF MS: m/z for $C_{85}H_{142}N_5O_6$ [M+H$^+$], calculated: 1329.0950, Found: 1329.5650.

Synthesis of 2,6-bis(5-(3,4,5-tris(hexadecyloxy)phenyl)-1,3,4-oxadiazol-2-yl)pyridine (**PO3**):

Pyridine dicarboxyllic acid (0.7 mmol) in 4 mL of thionyl chloride and DMF (2-3 drops) was heated under reflux for 8 h. The excess of thionyl chloride was removed by distillation and the crude product (pyridine di acid chloride) was dried in vacuo and used for the next reaction without further purification and characterization. The solution of pyridine diacid chloride (0.6 mmol, 1 equiv.) in THF was added dropwise to a solution of solution of 3,4,5-tris(hexadecyloxy)benzohydrazide (1.2 mmol, 2.05 equiv.) and triethylamine (1.2 mmol, 2 equiv.) in THF (15 mL). The reaction mixture was stirred at

55 ^{o}C for 12 h. After cooling, THF was removed through distillation and the residue was extracted with EtOAc. The extract was washed with water and brine, dried over Na_2SO_4 and concentrated. The resulting crude product (**12c**) was directly used for next reaction.

The solution of crude product **12c** (1.2 mmol, 1 equiv.) in $POCl_3$ (10 mL) was refluxed for 24 h. After the reaction, the crude mixture was dropwise added to ice water. Then, it was extracted with DCM. After removal of solvent *in vacuo*, the crude product was further purified through column chromatography on neutral alumina. Elution with DCM yielded the desired product. Again, the product was recrystallized with DCM-ethanol system (2:1).

R_f = 0.68 (80% DCM-hexane); white solid; yield: 65%; IR (KBr pellet): ν_{max} in cm^{-1} 3438, 2961, 2917, 2849, 1640, 1593, 1467, 1123, 837, 720; ^{1}H NMR ($CDCl_3$, 600 MHz, 298 K): δ 8.43 (d, 2H, *J* = 6Hz, H_{Ar}), 8.13 (t, 1H, H_{Ar}), 7.42 (s, 4H, H_{Ar}), 4.08 (t, 8H, 4 × OCH_2), 4.05 (t, 4H, 2 × OCH_2) 1.75-1.86 (m, 12H, 6 × CH_2), 1.46-1.50 (m, 12H, 6 × CH_2), 1.25-1.36 (m, 144H, 72 × CH_2), 0.87 (t, 18H, 6 × CH_3); ^{13}C NMR ($CDCl_3$, 150 MHz, 298 K): δ 170.82, 168.56, 153.86, 149.63, 138.68, 125.12, 122.46, 106.98, 73.92, 69.75, 32.16, 30.59, 29.96, 29.82, 29.67, 29.60, 26.34, 22.91, 14.33; MALDI TOF MS: m/z for $C_{117}H_{206}N_5O_8$ [M+H$^+$], calculated: 1810.5900, Found: 1810.1970.

Synthesis of 2,6-bis(5-(3,4,5-tris(dodecyloxy)phenyl)-1,3,4-oxadiazol-2-yl)pyridine (**PO4**):

Pyridine dicarboxyllic acid (0.7 mmol) in 4 mL of thionyl chloride and DMF (2-3 drops) was heated under reflux for 8 h. The excess of thionyl chloride was removed by distillation and the crude product (pyridine di acid chloride) was dried in vacuo and used for the next reaction without further purification and characterization. The solution of pyridine diacid chloride (0.6 mmol, 1 equiv.) in THF was added dropwise to a solution of solution of 3,4,5-tris(dodecyloxy)benzohydrazide (1.2 mmol, 2.05 equiv.) and triethylamine (1.2 mmol, 2 equiv.) in THF (15 mL). The reaction mixture was stirred at 55 ^{o}C for 12 h. After cooling, THF was removed through distillation and the residue was extracted with EtOAc. The extract was washed with water and brine, dried over Na_2SO_4 and concentrated. The resulting crude product (**12d**) was directly used for next reaction.

The solution of crude product **12d** (1.2 mmol, 1 equiv.) in $POCl_3$ (10 mL) was refluxed for 24 h. After the reaction, the crude mixture was dropwise added to ice water. Then, it was extracted with DCM. After removal of solvent *in vacuo*, the crude product was

further purified through column chromatography on neutral alumina. Elution with DCM yielded the desired product. Again, the product was recrystallized with DCM-ethanol system (2:1).

R_f = 0.66 (80% DCM-hexane); white solid; yield: 65%; IR (KBr pellet): ν_{max} in cm^{-1} 3445, 2918, 2849, 1589, 1520, 1467, 1420, 1277, 1149, 808; ^{1}H NMR ($CDCl_3$, 600 MHz, 298 K): δ 8.43 (d, 2H, *J* = 6Hz, H_{Ar}), 8.13 (t, 1H, *J* = 6Hz, H_{Ar}), 7.42 (s, 4H, H_{Ar}), 4.08 (t, 8H, *J* = 6Hz, 4 × OCH_2), 4.05 (t, 4H, *J* = 6Hz, 2 × OCH_2) 1.76-1.85 (m, 8H, 4 × CH_2), 1.46-1.50 (m, 4H, 2 × CH_2), 1.35-1.36 (m, 12H, 6 × CH_2), 1.25-1.33 (m, 96H, 48 × CH_2), 0.87 (t, 18H, *J* = 6Hz, 6 × CH_3); ^{13}C NMR ($CDCl_3$, 150 MHz, 298 K): δ 166.36, 163.14, 153.86, 144.56, 142.07, 138.79, 125.21, 118.10, 106.12, 73.87, 69.68, 32.13, 29.95, 29.90, 29.86, 29.80, 29.63, 29.56, 26.32, 26.29, 22.89, 14.31; MALDI TOF MS: m/z for $C_{93}H_{158}N_5O_8$ [M^+], calculated: 1473.2105, Found: 1473.7620.

Synthesis of 2,6-bis(5-(4-(hexadecyloxy)phenyl)-1,3,4-thiadiazol-2-yl)pyridine (**PT1**):

Pyridine dicarboxyllic acid (0.7 mmol) in 4 mL of thionyl chloride and DMF (2-3 drops) was heated under reflux for 8 h. The excess of thionyl chloride was removed by distillation and the crude product (pyridine di acid chloride) was dried in vacuo and used for the next reaction without further purification and characterization. The solution of pyridine diacid chloride (0.6 mmol, 1 equiv.) in THF was added dropwise to a solution of solution of 4-(hexadecyloxy) benzohydrazide (1.2 mmol, 2.05 equiv.) and triethylamine (1.2 mmol, 2 equiv.) in THF (15 mL). The reaction mixture was stirred at 55 ^oC for 12 h. After cooling, THF was removed through distillation and the residue was extracted with EtOAc. The extract was washed with water and brine, dried over Na_2SO_4 and concentrated. The resulting crude product (**12a**) was directly used for next reaction.

The solution of crude product **12a** (1.2 mmol, 1 equiv.) in dry toluene (8 mL) was added dropwise to a solution of Lawesson's reagent (3 mmol, 2.4 equiv.) in toluene at room temperature under argon atmosphere and refluxed for 24 h. After the reaction, toluene was evaporated under reduced pressure. After removal of solvent *in vacuo*, the crude product was further purified through column chromatography on neutral alumina. Elution with DCM followed by 5-10% EtOAc-hexane yielded the desired product. Again, the product was recrystallized with DCM-ethanol system (2:1).

R_f = 0.5 (50% DCM-hexane); white solid; yield: 58%; IR (KBr pellet): ν_{max} in cm^{-1} 3417, 2919, 2849, 1606, 1516, 1432, 1407, 1310, 1256, 836; ^{1}H NMR ($CDCl_3$, 600 MHz, 298

K): δ 8.43 (d, 2H, *J* = 7.8Hz, H_{Ar}), 8.02 (t, 1H, *J* = 6Hz, H_{Ar}), 8.01 (d, 4H, *J* = 6Hz, H_{Ar}), 7.00 (d, 4H, *J* = 7.8Hz, H_{Ar}), 4.03 (t, 4H, 2 × OCH_2), 1.79-1.86 (m, 4H, 2 × CH_2), 1.44-1.48 (m, 4H, 2 × CH_2), 1.26-1.34 (m, 48H, 24 × CH_2), 0.88 (t, 6H, 2 × CH_3); ^{13}C NMR ($CDCl_3$, 150 MHz, 298 K): δ 170.50, 168.19, 162.00, 149.53, 138.60, 129.80, 122.73, 122.12, 115.26, 68.51, 32.51, 29.93, 29.91, 29.88, 29.82, 29.79, 29.61, 29.59, 29.36, 26.22, 22.92, 14.36; MALDI TOF MS: m/z for $C_{53}H_{78}N_5O_2S_2$ [$M+H^+$], calculated: 880.5600, Found: 880.9410.

Synthesis of 2,6-bis(5-(3,4-bis(hexadecyloxy)phenyl)-1,3,4-thiadiazol-2-yl)pyridine (**PT2**):

Pyridine dicarboxyllic acid (0.7 mmol) in 4 mL of thionyl chloride and DMF (2-3 drops) was heated under reflux for 8 h. The excess of thionyl chloride was removed by distillation and the crude product (pyridine di acid chloride) was dried in vacuo and used for the next reaction without further purification and characterization. The solution of pyridine diacid chloride (0.6 mmol, 1 equiv.) in THF was added dropwise to a solution of solution of 3,4-bis(hexadecyloxy)benzohydrazide (1.2 mmol, 2.05 equiv.) and triethylamine (1.2 mmol, 2 equiv.) in THF (15 mL). The reaction mixture was stirred at 55 ^oC for 12 h. After cooling, THF was removed through distillation and the residue was extracted with EtOAc. The extract was washed with water and brine, dried over Na_2SO_4 and concentrated. The resulting crude product (**12b**) was directly used for next reaction.

The solution of crude product **12b** (1.2 mmol, 1 equiv.) in dry toluene (8 mL) was added dropwise to a solution of Lawesson's reagent (3 mmol, 2.4 equiv.) in toluene at room temperature under argon atmosphere and refluxed for 24 h. After the reaction, toluene was evaporated under reduced pressure. After removal of solvent *in vacuo*, the crude product was further purified through column chromatography on neutral alumina. Elution with DCM followed by 5-10% EtOAc-hexane yielded the desired product. Again, the product was recrystallized with DCM-ethanol system (2:1).

R_f = 0.55 (50% DCM-hexane); white solid; yield: 55%; IR (KBr pellet): ν_{max} in cm^{-1} 3417, 2918, 2848, 1637, 1520, 1420, 1387, 1277, 1149, 808; ^{1}H NMR ($CDCl_3$, 600 MHz, 298 K): δ 8.45 (d, 2H, *J* = 9Hz, H_{Ar}), 8.03 (s, 1H, H_{Ar}), 7.71 (d, 2H, *J* = 9Hz, H_{Ar}), 7.54 (d, 2H, *J* = 8.4Hz, H_{Ar}), 6.95 (d, 2H, *J* = 8.4Hz, H_{Ar}), 4.13 (t, 4H, 2 × OCH_2), 4.08 (t, 4H, 2 × OCH_2), 1.85-1.90 (m, 8H, 4 × CH_2), 1.51 (m, 8H, 4 × CH_2), 1.25-1.49 (m, 96H, 48 × CH_2), 0.87 (t, 12H, 4 × CH_3); ^{13}C NMR ($CDCl_3$, 150 MHz, 298 K): δ 170.69, 168.20,

152.31, 149.67, 149.62, 138.62, 123.03, 122.21, 122.08, 113.31, 112.46, 69.65, 69.43, 32.11, 29.90, 29.85, 29.60, 29.55, 29.42, 29.33, 26.23, 26.20, 22.87, 14.29; MALDI TOF MS: m/z for $C_{85}H_{142}N_5O_4S_2$ [M+H^+], calculated: 1361.0500, Found: 1361.8440.

Synthesis of 2,6-bis(5-(3,4,5-tris(hexadecyloxy)phenyl)-1,3,4-thiadiazol-2-yl)pyridine (**PT3**):

Pyridine dicarboxyllic acid (0.7 mmol) in 4 mL of thionyl chloride and DMF (2-3 drops) was heated under reflux for 8 h. The excess of thionyl chloride was removed by distillation and the crude product (pyridine di acid chloride) was dried in vacuo and used for the next reaction without further purification and characterization. The solution of pyridine diacid chloride (0.6 mmol, 1 equiv.) in THF was added dropwise to a solution of solution of 3,4,5-tris(hexadecyloxy)benzohydrazide (1.2 mmol, 2.05 equiv.) and triethylamine (1.2 mmol, 2 equiv.) in THF (15 mL). The reaction mixture was stirred at 55 ^oC for 12 h. After cooling, THF was removed through distillation and the residue was extracted with EtOAc. The extract was washed with water and brine, dried over Na_2SO_4 and concentrated. The resulting crude product (**12c**) was directly used for next reaction.

The solution of crude product **12c** (1.2 mmol, 1 equiv.) in dry toluene (8 mL) was added dropwise to a solution of Lawesson's reagent (3 mmol, 2.4 equiv.) in toluene at room temperature under argon atmosphere and refluxed for 24 h. After the reaction, toluene was evaporated under reduced pressure. After removal of solvent *in vacuo*, the crude product was further purified through column chromatography on neutral alumina. Elution with DCM followed by 5-10% EtOAc-hexane yielded the desired product. Again, the product was recrystallized with DCM-ethanol system (2:1).

R_f = 0.58 (50% DCM-hexane); white solid; yield: 55%; IR (KBr pellet): ν_{max} in cm^{-1} 3438, 2950, 2917, 2849, 1585, 1432, 1331, 1124, 813, 773; ^1H NMR ($CDCl_3$, 600 MHz, 298 K): δ 8.46 (d, 2H, *J* = 9Hz, H_{Ar}), 8.04 (t, 1H, H_{Ar}), 7.28 (s, 4H, H_{Ar}), 4.10 (t, 8H, 4 × OCH_2), 4.05 (t, 4H, 2 × OCH_2), 1.75-1.88 (m, 12H, 6 × CH_2), 1.35-1.53 (m, 12H, 6 × CH_2), 1.25-1.29 (m, 144H, 72 × CH_2), 0.87 (m, 18H, 6 × CH_3); ^{13}C NMR ($CDCl_3$, 150 MHz, 298 K): δ 169.11, 166.76, 153.83, 141.37, 131.55, 130.29, 130.12, 127.27, 124.93, 106.80, 73.89, 69.65, 32.15, 30.56, 29.94, 29.88, 29.81, 29.64, 29.59, 26.32, 22.91, 14.32; MALDI TOF MS: m/z for $C_{117}H_{206}N_5O_6S_2$ [M+H^+], calculated: 1841.5404, Found: 1841.835.

Synthesis of 2,6-bis(5-(3,4,5-tris(dodecyloxy)phenyl)-1,3,4-thiadiazol-2-yl)pyridine (**PT4**):

Pyridine dicarboxyllic acid (0.7 mmol) in 4 mL of thionyl chloride and DMF (2-3 drops) was heated under reflux for 8 h. The excess of thionyl chloride was removed by distillation and the crude product (pyridine di acid chloride) was dried in vacuo and used for the next reaction without further purification and characterization. The solution of pyridine diacid chloride (0.6 mmol, 1 equiv.) in THF was added dropwise to a solution of solution of 3,4,5-tris(dodecyloxy)benzohydrazide (1.2 mmol, 2.05 equiv.) and triethylamine (1.2 mmol, 2 equiv.) in THF (15 mL). The reaction mixture was stirred at 55 ^{o}C for 12 h. After cooling, THF was removed through distillation and the residue was extracted with EtOAc. The extract was washed with water and brine, dried over Na_2SO_4 and concentrated. The resulting crude product (**12d**) was directly used for next reaction.

The solution of crude product **12d** (1.2 mmol, 1 equiv.) in dry toluene (8 mL) was added dropwise to a solution of Lawesson's reagent (3 mmol, 2.4 equiv.) in toluene at room temperature under argon atmosphere and refluxed for 24 h. After the reaction, toluene was evaporated under reduced pressure. After removal of solvent *in vacuo*, the crude product was further purified through column chromatography on neutral alumina. Elution with DCM followed by 5-10% EtOAc-hexane yielded the desired product. Again, the product was recrystallized with DCM-ethanol system (2:1).

R_f = 0.58 (50% DCM-hexane); white solid; yield: 60%; IR (KBr pellet): ν_{max} in cm^{-1} 3444, 2919, 2849, 1606, 1516, 1432, 1407, 1310, 1256, 1024; ^{1}H NMR ($CDCl_3$, 600 MHz, 298 K): δ 8.46 (d, 2H, *J* = 9Hz, H_{Ar}), 8.04 (t, 1H, *J* = 9Hz, H_{Ar}), 7.29 (s, 4H, H_{Ar}), 4.10 (t, 8H, *J* = 6Hz, 4 × OCH_2), 4.05 (t, 4H, *J* = 6Hz, 2 × OCH_2) 1.86-1.87 (m, 8H, 4 × CH_2), 1.78-1.85 (m, 4H, 2 × CH_2), 1.36-1.52 (m, 12H, 6 × CH_2), 1.27-1.31 (m, 96H, 48 × CH_2), 0.88 (t, 18H, *J* = 6Hz, 6 × CH_3); ^{13}C NMR ($CDCl_3$, 150 MHz, 298 K): δ 170.78, 168.54, 153.82, 149.56, 141.45, 138.64, 125.08, 122.42, 106.86, 73.87, 69.67, 32.13, 30.56, 29.88, 29.58, 26.31, 22.89, 14.31; MALDI TOF MS: m/z for $C_{93}H_{158}N_5O_6S_2$ [$M+H^+$], calculated: 1505.1650, Found: 1505.8340.

4.5. References

1. (a) C. Tschierske, *Angew. Chem. Int. Ed.*, 2013, **52**, 8828-8878; (b) T. Kato, M. Yoshio, T. Ichikawa, B. Soberats, H. Ohno and M. Funahashi, *Nature Reviews*, 2017, **2**, 17001, 1-20.
2. (a) E. K. Fleischmann and R. Zentel, *Angew. Chem. Int. Ed.*, 2013, **52**, 8810-8827; (b) M. Bremer, P. Kirsch, M. Klasen-Memmer and K. Tarumi, *Angew. Chem. Int. Ed.*, 2013, **52**, 8880-8896; (c) J. P. F. Laggerwall and G. Scalia, *Current Applied Physics*, 2012, **12**, 1387-1412; (d) S. Kumar, *Isr. J. Chem.*, 2012, **52**, 820-829; (e) Q. Li, *Liquid Crystals Beyond Displays*, John Wiley & Sons, Inc., 2012; (f) R. J. Bushby and O. R. Lozman, *Curr. Opin. Colloid Interface Sci.*, 2002, **7**, 343-354.
3. (a) C. Tschierske, *Handbook of Liquid Crystals: Fundamentals*, Wiley-VCH, 2014; (b) S. Kumar, *Chemistry of Discotic Liquid Crystals: From Monomers to Polymers*, CRC Press, Boca Raton, FL, 2010.
4. (a) J. Malthete, A. M. Levelut and N. H. Tinh, *J. Phys. Lett*., 1985, **46**, 875-880; (b) J. Malthete, H. T. Nguyen and C. Destrade, *Liq. Cryst.*, 1993, **13**, 171-187; (c) H. T. Nguyen, C. Destrade and J. Malthete, *Adv. Mater*., 1997, **9**, 375-388.
5. (a) W. Pisula, M. Zorn, J. Y. Chang, K. Müllen and R. Zentel, *Macromol Rapid Comm*, 2009, **30**, 1179-1202; (b) T. Wöhrle, I. Wurzbach, J. Kirres, A. Kostidou, N. Kapernaum, J. Litterscheidt, J. C. Haenle, P. Staffeld, A. Baro, F. Giesselmann and S. Laschat, *Chem Rev.*, 2016, **116**, 1139-1241.
6. Q. Li, *Self-Organized Organic Semiconductors*, John Wiley & Sons, Inc., 2011.
7. (a) M. Gharbia, A. Gharbia, H.T. Nguyen and J. Malthete, *Current Opinion in Colloid and Interface Science*, 2002, **7**, 312-325; (b) H. Cheng, R. Zhang, T. Li, X. Peng, M. Xia, Y. Xiao and X. Cheng, *New J. Chem.*, 2017, **41**, 8443-8450; (c) E. Gorecka, D. Pociecha, J. Mieczkowski, J. Matraszek, D. Guillon and B. Donnio, *J. Am. Chem. Soc*., 2004, **126**, 15946-15947; (d) E. Gorecka, D. Pociecha, J. Matraszek, J. Mieczkowski, Y. Shimbo, Y. Takanishi and H. Takezoe, *Physical Review E*, 2006, **73**, 031704(1-5); (e) E. Beltran, B. Robles-Hernandez, N. Sebastian, J. L. Serrano, R. Gimenez and T. Sierra, *RSC Adv.*, 2014, **4**, 23554-23561; (f) H. Gallardo, M. Ferreira, A. A. Vieira, E. Westphal, F. Molin, J. Eccher and I. H. Bechtold, *Tetrahedron*, 2011, **67**, 9491-9499; (g) D. M. Huck, H. L. Nguyen, B. Donnio and D. W. Bruce, *Liquid Crystals*, 2004, **31**(4), 503-507; (h) R. L. Coelho, E. Westphal, D. Z. Mezalira and H. Gallardo, *Liquid Crystals*, 2017, **44**(2), 405-416; (i) M. Ferreira, E. Westphal, M. V. Ballottin, I. H. Bechtold, A. J. Bortoluzzi, D. Z. Mezaliraa and H. Gallardo, *New J. Chem*., 2017, **41**, 11766-11777; (j) H. Cheng, R. Zhang, T. Li, X. Peng, M. Xia, Y. Xiao and X. Cheng, *New J. Chem.*, 2017, **41**, 8443-8450.
8. (a) J. Tang, R. Huang, H. Gao, X. Cheng, M. Prehm and C. Tschierske, *RSC Adv.*, 2012, **2**, 2842-2847; (b) X. Yang, H. Dai, Q. He, J. Tang, X. Cheng, M. Prehm and C. Tschierske, *Liq. Cryst.*, 2013, **40**(8), 1028-1034; (c) S. K. Pathak, B. Pradhan, R. K. Gupta, M. Gupta, S. K. Pal and A. S. Achalkumar, *J. Mater. Chem. C*, 2016, **4**, 6546-6561; (d) S. K. Pathak, Monika Gupta, Santanu K. Pal, and A. S. Achalkumar, *ChemistrySelect*, 2016, **1**, 5107-5120; (e) B. Pradhan, M. Gupta, S. K. Pal and A. S. Achalkumar, *J. Mater. Chem. C*, 2016, **4**, 9669-9673.
9. B. Roy, N. De and K. C. Majumdar, *Chem. Eur. J.*, 2012, **18**, 14560-14588.
10. (a) S. K. Pathak, R. K. Gupta, S. Nath, D. S. S. Rao, S. K. Prasad and A. S. Achalkumar, *J. Mater. Chem. C*, 2015, **3**, 2940-2952; (b) S. K. Pathak, S. Nath, R. K. Gupta, D. S. S. Rao, S. K. Prasad and A. S. Achalkumar, *J. Mater. Chem. C*, 2015, **3**, 8166-8182; (e) B. Pradhan, S. K. Pathak, R. K. Gupta, M. Gupta, S. K. Pal and A. S. Achalkumar, *J. Mater. Chem. C*, 2016, **4**, 6117-6130; (f) B. Pradhan, V. M. Vaisakh,

G. G. Nair, D. S. S. Rao, S. K. Prasad and A. S. Achalkumar, *Chem. Eur. J.*, 2016, **22**, 17843-17856; (g) A. A. Vieira, E. Cavero, P. Romero, H. Gallardo, J. L. Serrano and T. Sierra, *J. Mater. Chem. C*, 2014, **2**, 7029-7038; (h) E. Girotto, J. Eccher, A. A. Vieira, I. H. Bechtold and H. Gallardo, *Tetrahedron*, 2014, **70**, 3355-3360; (i) R. Cristiano, H. Gallardo, A. J. Bortoluzzi, I. H. Bechtold, C. E. M. Campos and R. L. Longo, *Chem. Commun.*, 2008, 5134.

11. (a) K. C. Naeem, A. Subhakumari, S. Varughesec and V. C. Nair, *J. Mater. Chem. C*, 2015, **3**, 10225-10231; (b) K. Wang, S. Huang, Y. Zhang, S. Zhao, H. Zhang and Y. Wang, *Chem. Sci*., 2013, **4**, 3288-3293; (c) M. E. Genovese, A. Athanassiou and D. Fragouli, *J. Mater. Chem. A*, 2015, **3**, 22441-22447; (d) X. Qian, W. Gong, M. K. Dhinakaran, P. Gao, D. Na and G. Ning, *Soft Matter*, 2015, **11**, 9179-9187; (e) J. Sun, P. Xue, J. Sun, P. Gong, P. Wang and R. Lu, *J. Mater.Chem. C*, 2015, **3**, 8888-8894; (f) P. Xue, B. Yao, P. Wang, P. Gong, Z. Zhang and R. Lu, *Chem. Eur. J.*, 2015, **21**, 17508-17515; (g) A. C. Grimsdale, K. L. Chan, R. E. Martin, P. G. Jokisz and A. B. Holmes, *Chem. Rev*., 2009, **109**, 897-1091.
12. (a) R. K. Gupta, D. Das, M. Gupta, S. K. Pal, P. K. Iyer and A. S. Achalkumar, *J. Mater. Chem. C*, 2017, **5**, 1767-1781; (b) A. K. Yadav, B. Pradhan, H. Ulla, S. Nath, J. De, S. K. Pal, M. N. Satyanarayan and A. S. Achalkumar, *J. Mater. Chem. C*, 2017, **5**, 9345-9358; (c) K. Kotwica, A. S. Kostyuchenko, P. Data, T. Marszalek, L. Skorka, T. Jaroch, S. Kacka, M. Zagorska, R. Nowakowski, A. P. Monkman, A. S. Fisyuk, W. Pisula and A. Pron, *Chem. Eur. J.*, 2016, **22**, 11795-11806.
13. (a) K. B. Woody, B. J. Leever, M. F. Durstock and D. M. Collard, *Macromolecules*, 2011, **44**, 4690-4698; (b) K. Mullen and W. Pisula, *J. Am. Chem. Soc.*, 2015, **137**, 9503-9505.
14. (a) R. M. Ongungal, A. P. Sivadas, N. S. S. Kumar, S. Menon and S. Das, *J. Mater. Chem. C*, 2016, **4**, 9588-9597; (b) A. P. Sivadas, N. S. S. Kumar, D. D. Prabhu, S. Varghese, S. K. Prasad, D. S. S. Rao and S. Das, *J. Am. Chem. Soc.*, 2014, **136**, 5416-5423; (c) D. D. Prabhu, N. S. S. Kumar, A. P. Sivadas, S. Varghese and S. Das, *J. Phys. Chem. B*, 2012, **116**, 13071-13080.
15. (a) S. K. Pathak, S. Nath, R. K. Gupta, D. S. S. Rao, S. K. Prasad and A. S. Achalkumar, *J. Mater. Chem. C*, 2015, **3**, 8166-8182; (b) B. Pradhan, S. K. Pathak, R. K. Gupta, M. Gupta, S. K. Pal and A. S. Achalkumar, *J. Mater. Chem. C*, 2016, **4**, 6117-6130.
16. Y. Zhang, H. Li, G. Zhang, X. Xu, L. Kong, X. Tao, Y. Tian and J. Yang, *J. Mater. Chem. C*, 2016, **4**, 2971-2978.
17. (a) A. Takahashi, M. Sakai and T. Kato, *Polym. J.*, 1980, **12**, 335; (b) K. Murata, M. Aoki, T. Suzuki, T. Harada, H. Kawabata, T. Komri, F. Olrseto, K. Ueda and S. Shinkai, *J. Am. Chem. Soc.*,1994, **116**(15), 6664-6676.
18. (a) M. Zhang, D. Xu, X. Yan, J. Chen, S. Dong, B. Zheng and F. Huang, *Angew. Chem., Int. Ed.*, 2012, **51**, 7011; (b) R. Yoshida, *Adv. Mater.*, 2010, **22**, 3463-3483.
19. (a) B. W. Messmore, J. F. Hulvat, E. D. Sone and S. I. Stupp, *J. Am. Chem. Soc.*, 2004, **126**, 14452-14458; (b) M. Kasha, H. R. Rawls and M. A. E. Bayoumi, *Pure Appl. Chem.*, 1965, **11**, 371-392; (c) D. G. Whitten, *Acc. Chem. Res.*, 1993, **26**, 502-509; (d) K. C. Hannah and B. A. Armitage, *Acc. Chem. Res.*, 2004, **37**, 845-853; (e) S. Y. Ryu, S. Kim, J. Seo, Y. W. Kim, O. H. Kwon, D. J. Jang and S. Y. Park, *Chem. Commun*., 2004, 70-71; (f) H. H. Yao, K. Domoto, T. Isohashi and K. Kimura, *Langmuir*, 2005, **21**, 1067-1073.
20. Y. Hong, J. W. Y. Lam and B. Z. Tang, *Chem. Commun.*, 2009, 4332-4353.
21. (a) S. Basak, S. Bhattacharya, A. Datta and A. Banerjee, *Chem. Eur. J.*, 2014, **20**, 5721-5726; (b) F. Alexandre, D. J. Marc, G. D. Todor, I. G. Nikolai, A. V. Aleksey

and V. Eric, *J. Am. Chem. Soc*., 2006, **128**, 7661-7669; (c) M. Cigan, J. Donovalova, V. Szocs, J. Gaspar, K. Jakusova and A. Gaplovsky, *J. Phys. Chem. A*, 2013, **117**, 4870-4883; (d) Q. Fang, F. Wang, H. Zhao, X. Liu, R. Tu, D. Wang and Z. Zhang, *J. Phys. Chem. B*, 2008, **112**, 2837-2841; (e) V. Lau and B. Heyne, *Chem. Commun.*, 2010, **46**, 3595-3597; (f) U. Rosch, S. Yao, R. Wortmann and F. Wurthner, *Angew. Chem., Int. Ed*., 2006, **45**, 7026-7030; (g) L. Liangde, J. L. Rene, L. P. Thomas, P. Jerry and G. W. David, *J. Am. Chem. Soc*., 1999, **121**, 8146-8156; (h) Y. S. Jun, C. J. Won, G. Johannes, K. K. Suk, C. M. Gun, K. Dongho and P. S. Young, *J. Am. Chem. Soc*., 2010, **132**, 13675-13683; (i) Y. S. Jun and P. S. Young, *J. Mater. Chem*., 2011, **21**, 8338-8346; (j) C. Jiajia, L. Yan, H. Song, L. Chang, Z. Liancheng and Z. Xianshun, *Chem. Commun*., 2013, **49**, 6259-6261.

22. (a) C. G. Robertson and X. Wang, *Phys. Rev. Lett*., 2005, **95**(7), 075703; (b) P. Sollich, F. Lequeux, P. Hebraud and M. E. Cates, *Phys. Rev. Lett*., 1997, **78**(10), 2020; (c) H. M. Wyss, K. Miyazaki, J. Mattsson, Z. Hu, D. R. Reichman and D. A. Weitz, *Phys. Rev. Lett.*, 2007, **98**(23), 238303.
23. (a) F. Camerel, R. Ziessel, B. Donnio, C. Bourgogne, D. Guillon, M. Schmutz, C. Iacovita and J. P. Bucher, *Angew. Chem. Int. Ed*., 2007, **46**, 2659-2662; (b) S. S. Babu, V. K. Praveen, K. K. Kartha, S. Mahesh and A. Ajayaghosh, *Chem. Asian J.*, 2014, **9**, 1830-1840; (c) S. K. Pathak, B. Pradhan, M. Gupta, S. K. Pal and A. S. Achalkumar, *Langmuir*, 2016, **32**, 9301-9312.

Appendix

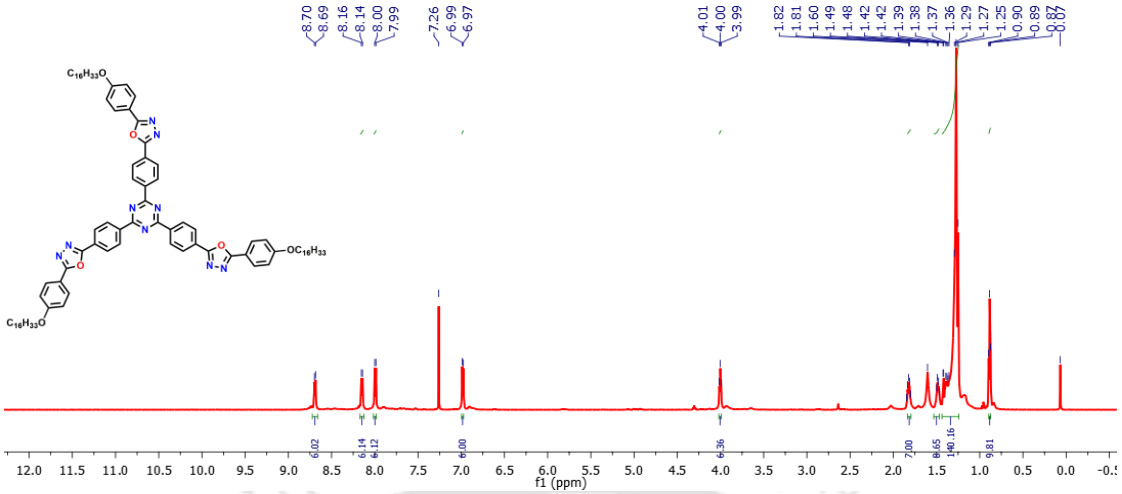

Figure 5.1. ^{1}H NMR (600MHz) spectra of **TZ1** in $CDCl_3$.

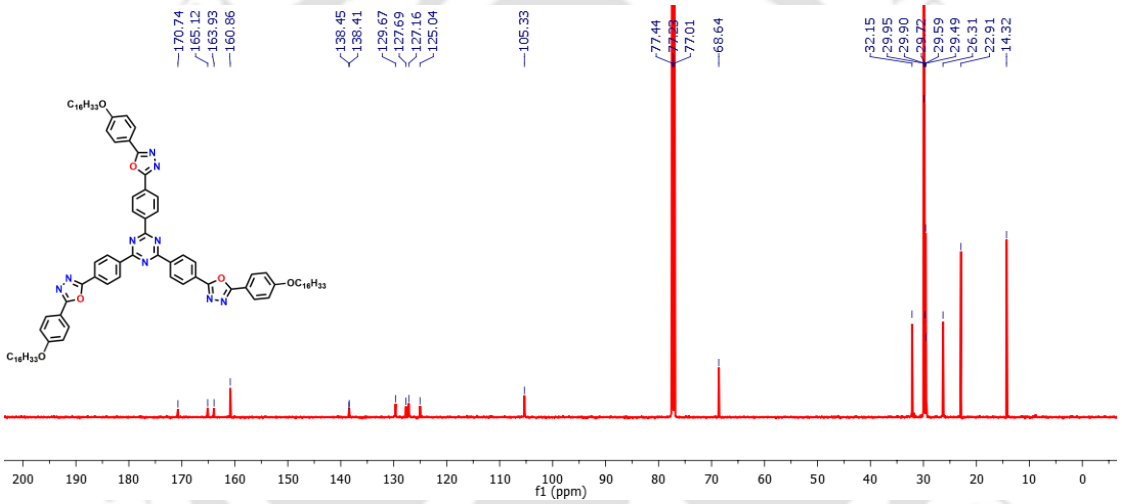

Figure 5.2. ^{13}C NMR (150MHz) spectra of **TZ1** in $CDCl_3$.

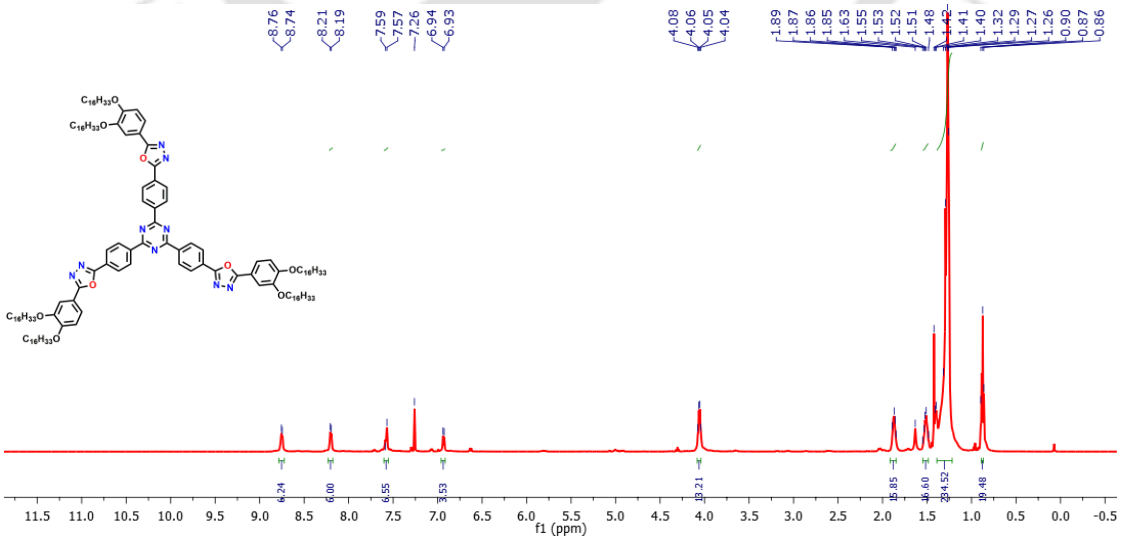

Figure 5.3. ^{1}H NMR (600MHz) spectra of **TZ2** in $CDCl_3$.

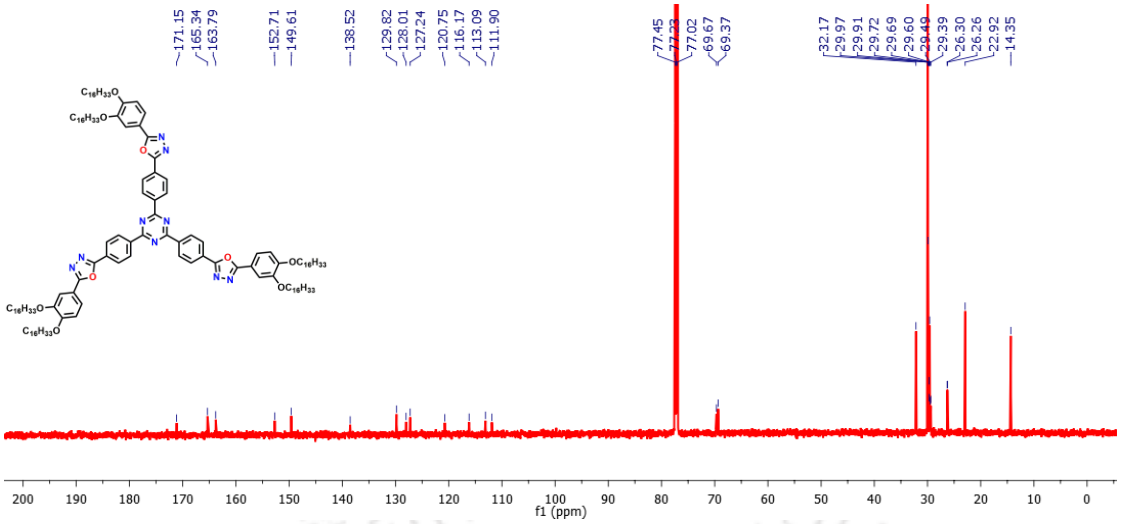

Figure 5.4. ^{13}C NMR (150MHz) spectra of **TZ2** in $CDCl_3$.

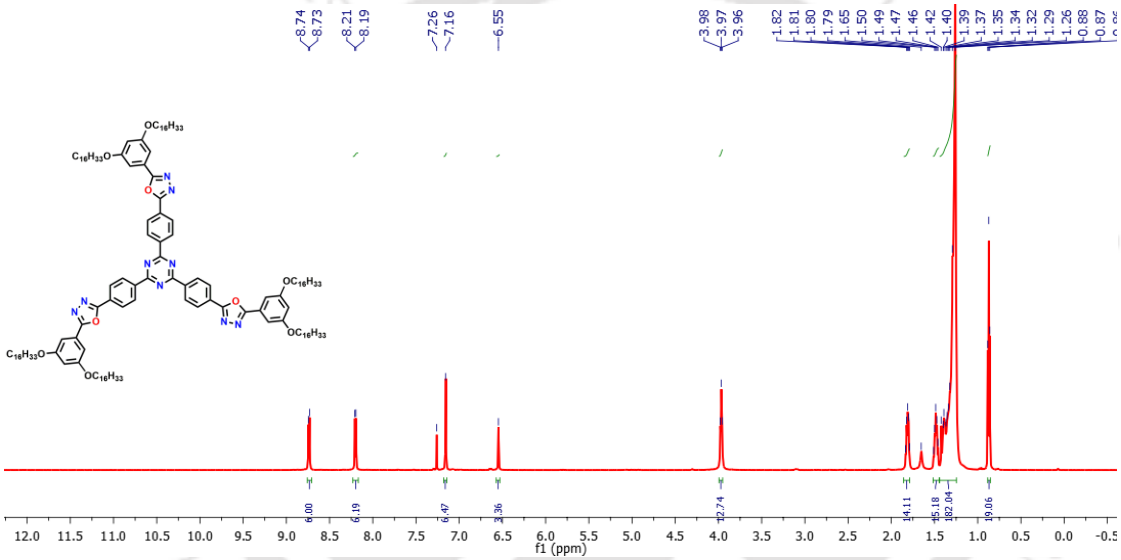

Figure 5.5. ^{1}H NMR (600MHz) spectra of **TZ3** in $CDCl_3$.

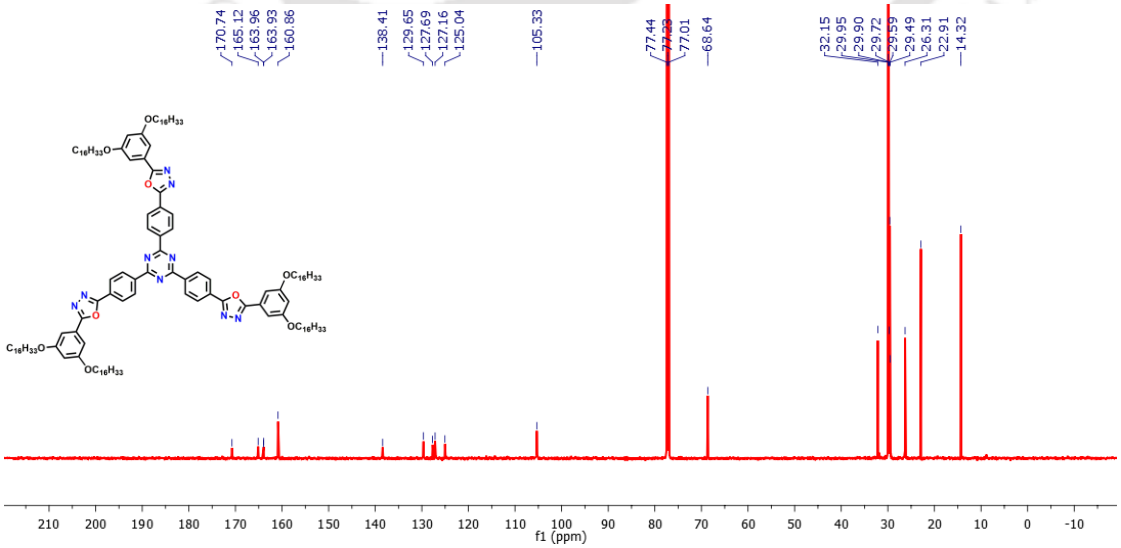

Figure 5.6. ^{13}C NMR (150MHz) spectra of **TZ3** in $CDCl_3$.

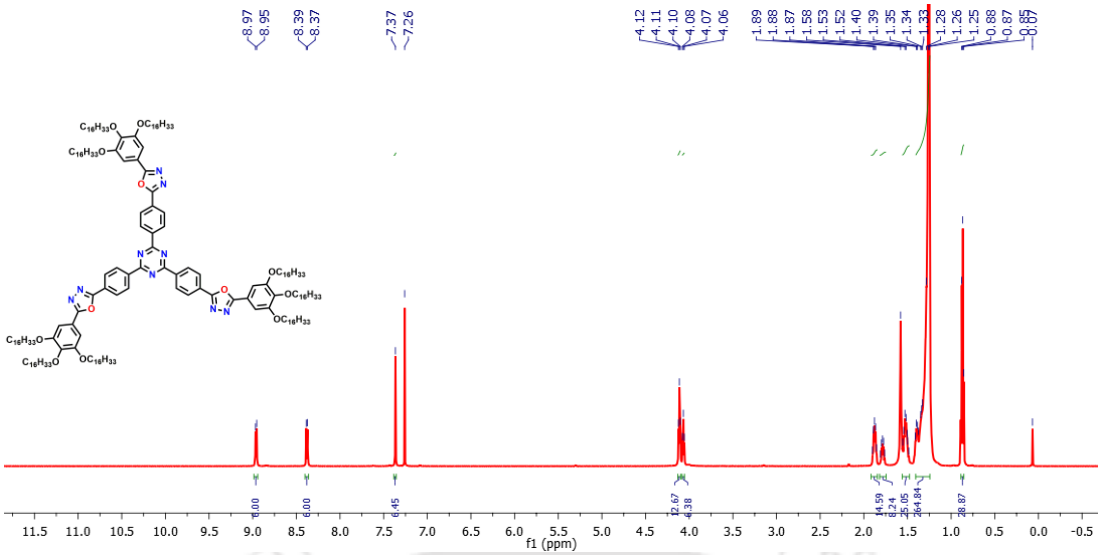

Figure 5.7. ^{1}H NMR (600MHz) spectra of **TZ4** in $CDCl_3$.

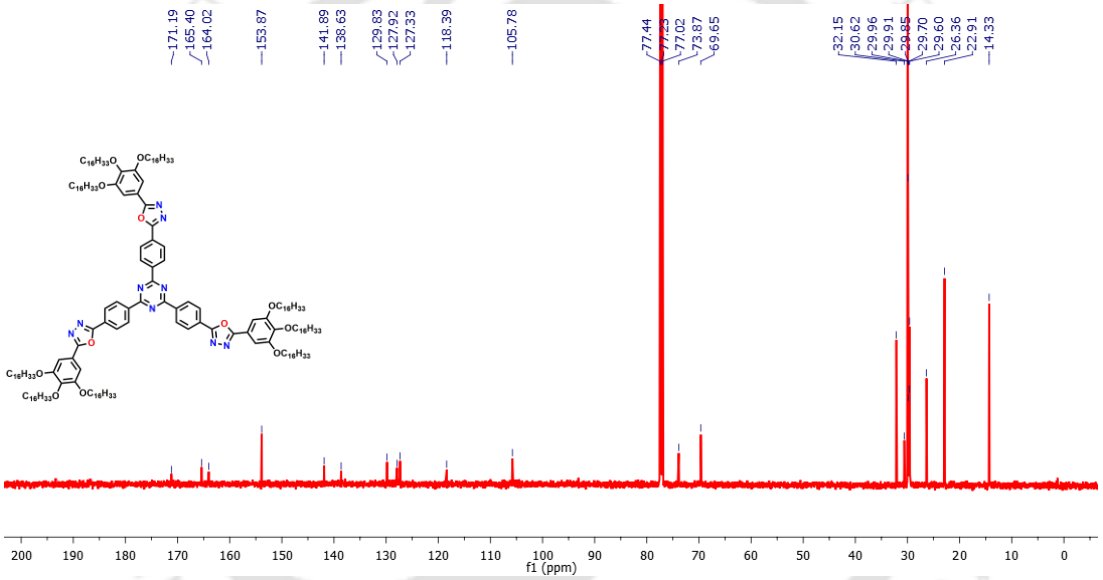

Figure 5.8. ^{13}C NMR (150MHz) spectra of **TZ4** in $CDCl_3$.

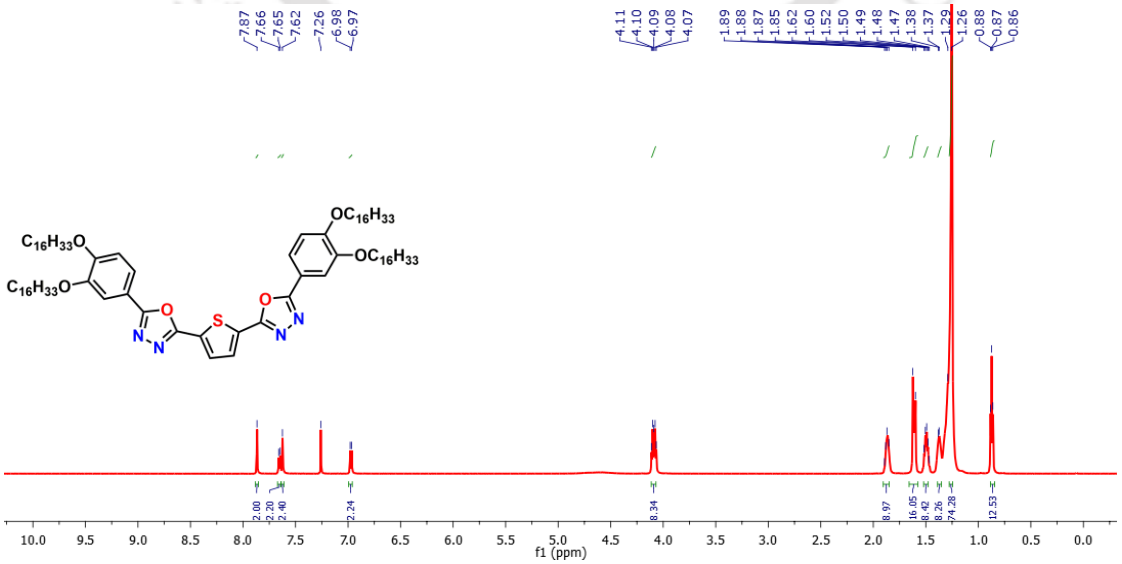

Figure 5.9. ^{1}H NMR (600MHz) spectra of **TO1** in $CDCl_3$.

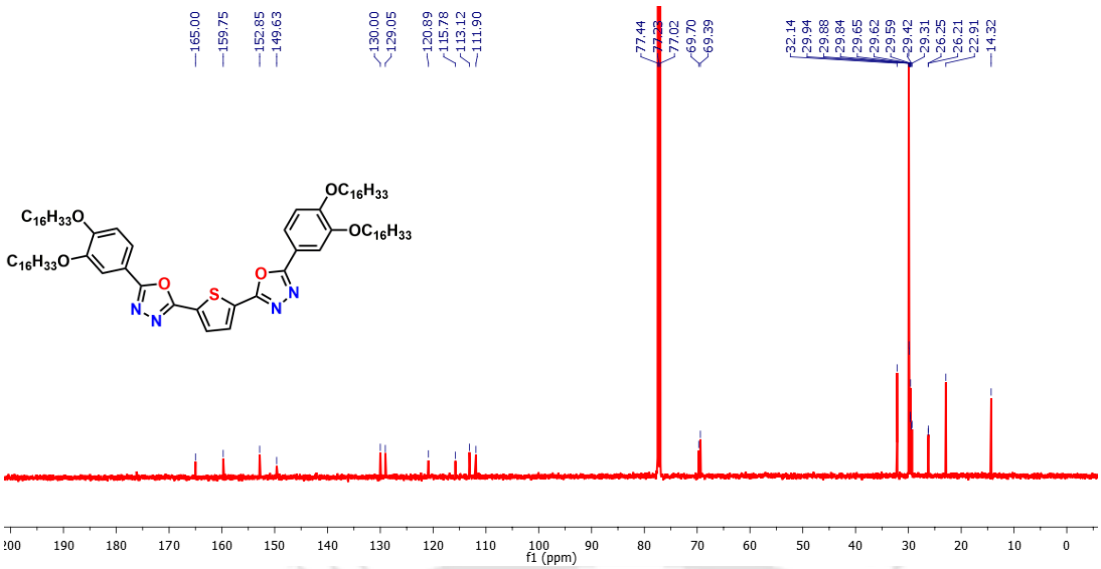

Figure 5.10. ^{13}C NMR (150MHz) spectra of **TO1** in $CDCl_3$.

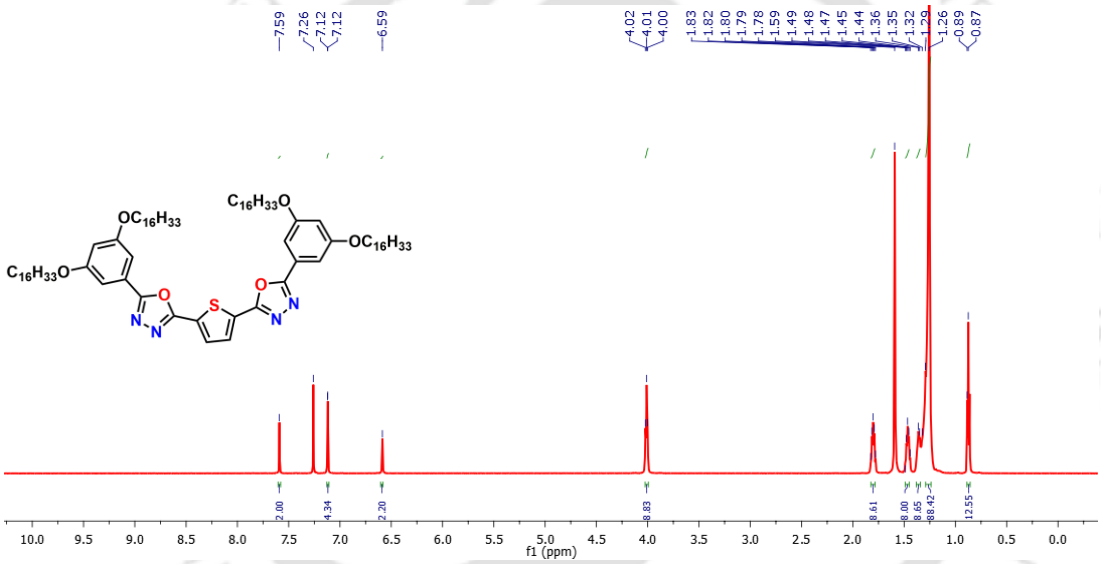

Figure 5.11. ^{1}H NMR (600MHz) spectra of **TO2** in $CDCl_3$.

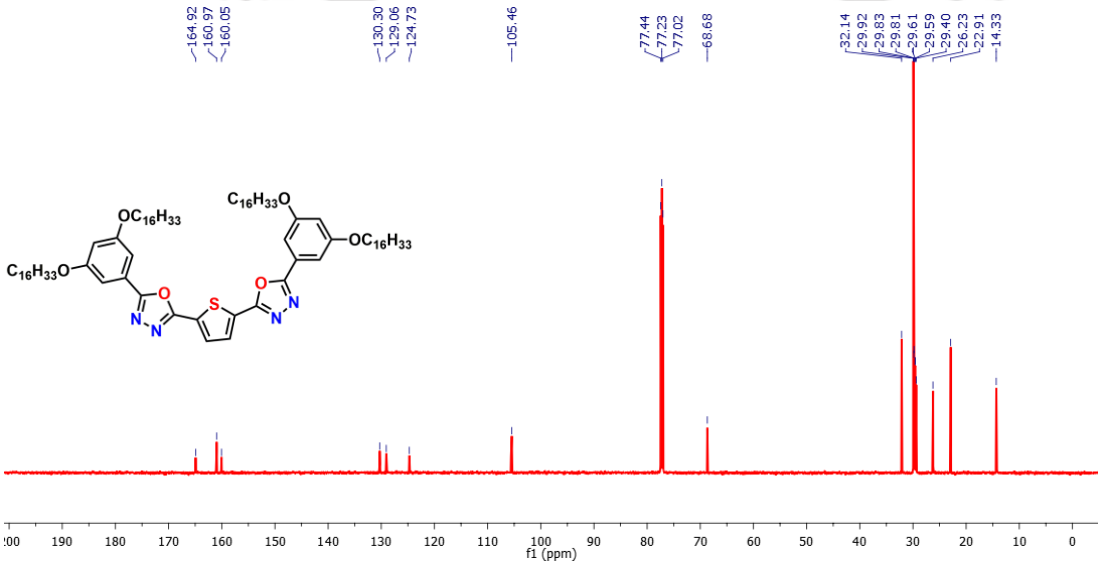

Figure 5.12. ^{13}C NMR (150MHz) spectra of **TO2** in $CDCl_3$.

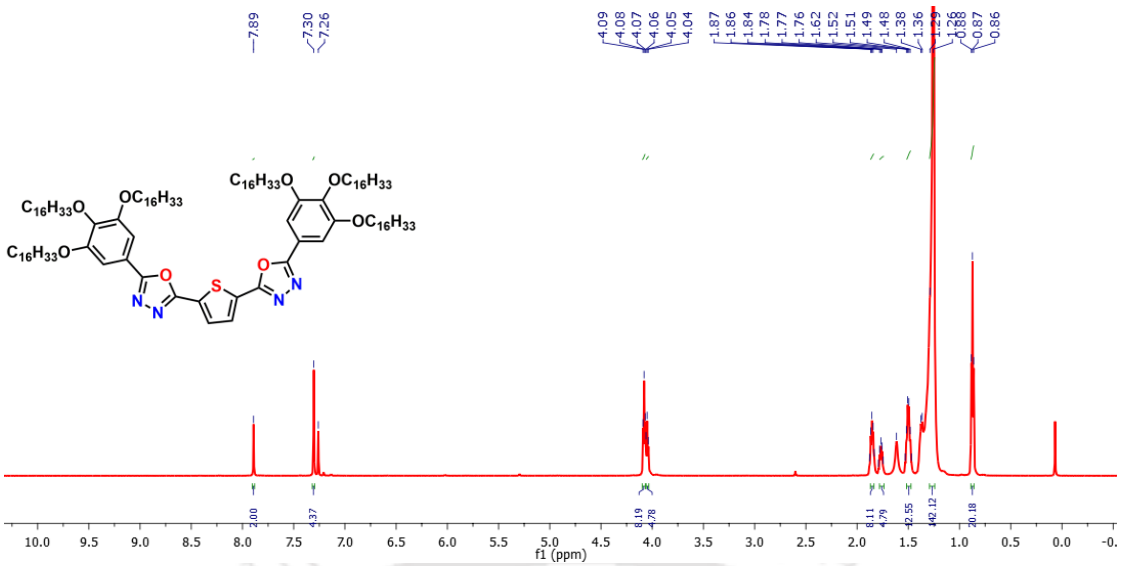

Figure 5.13. ^{1}H NMR (600MHz) spectra of **TO3** in $CDCl_3$.

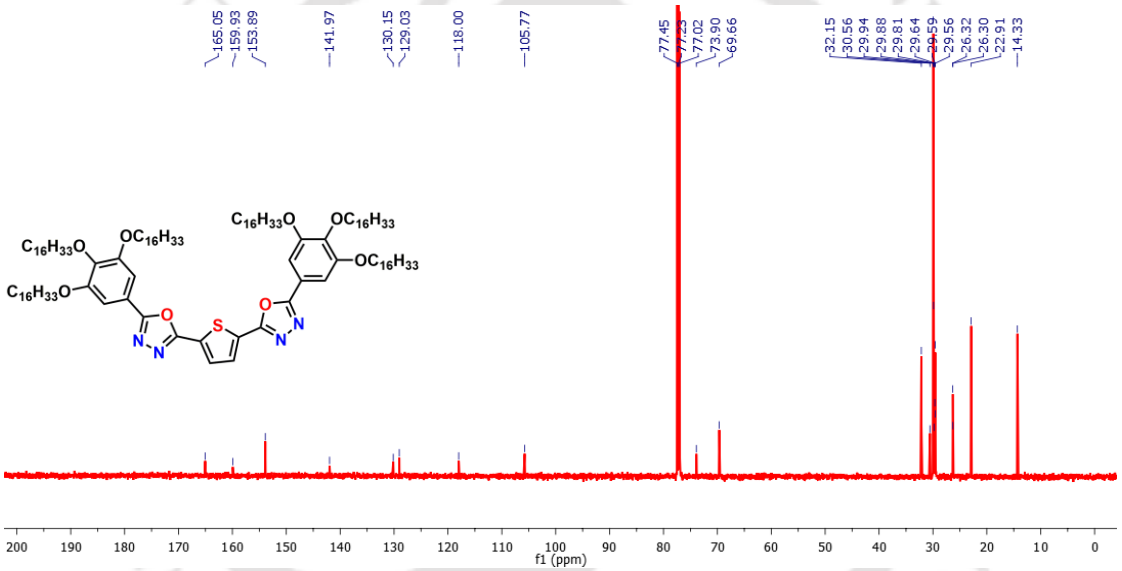

Figure 5.14. ^{13}C NMR (150MHz) spectra of **TO3** in $CDCl_3$.

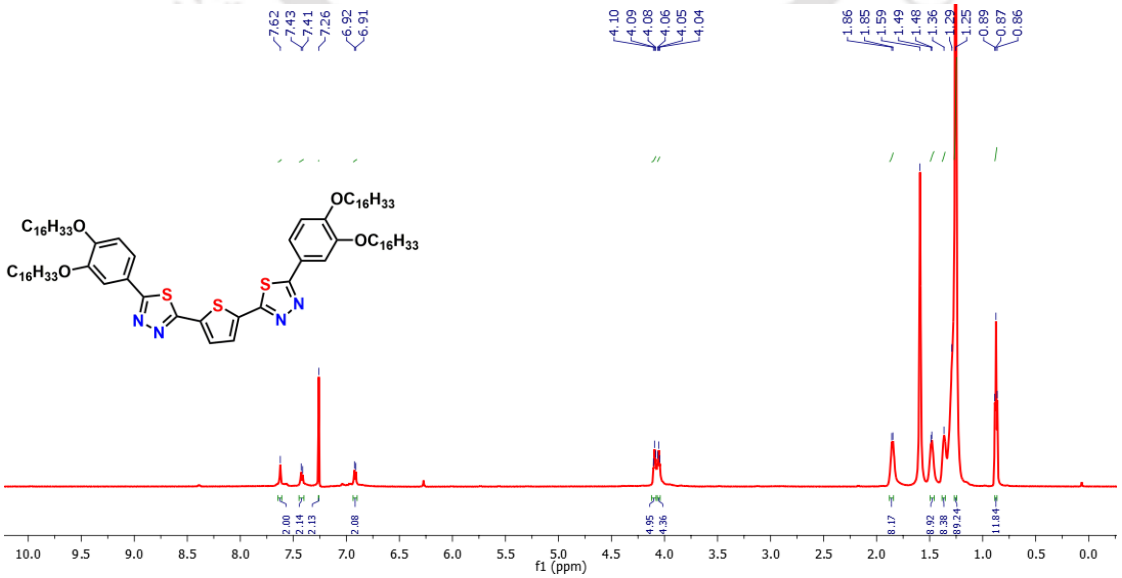

Figure 5.15. ^{1}H NMR (600MHz) spectra of **TT1** in $CDCl_3$.

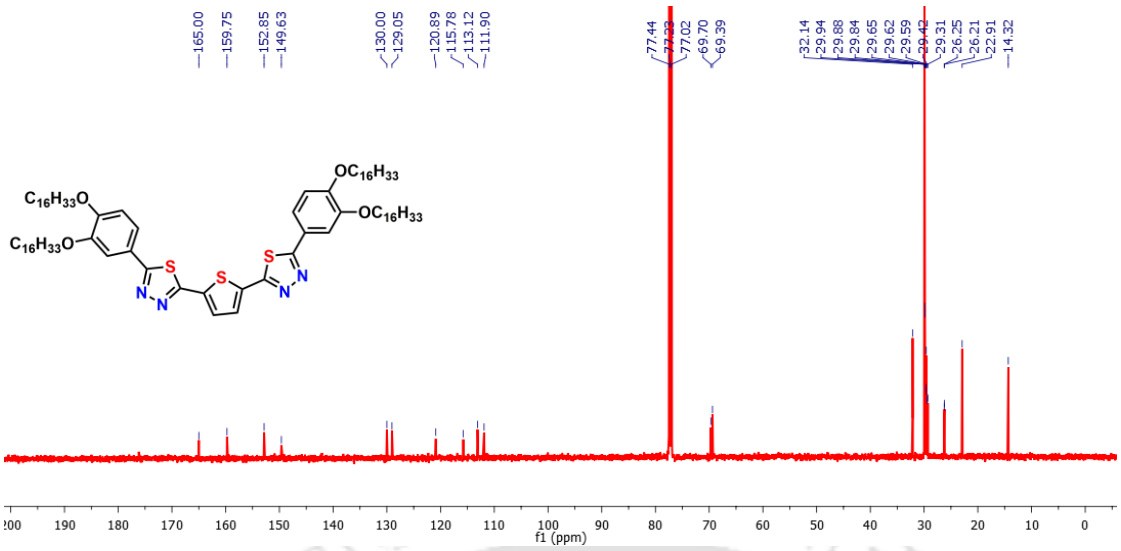

Figure 5.16. ^{13}C NMR (150MHz) spectra of **TT1** in $CDCl_3$.

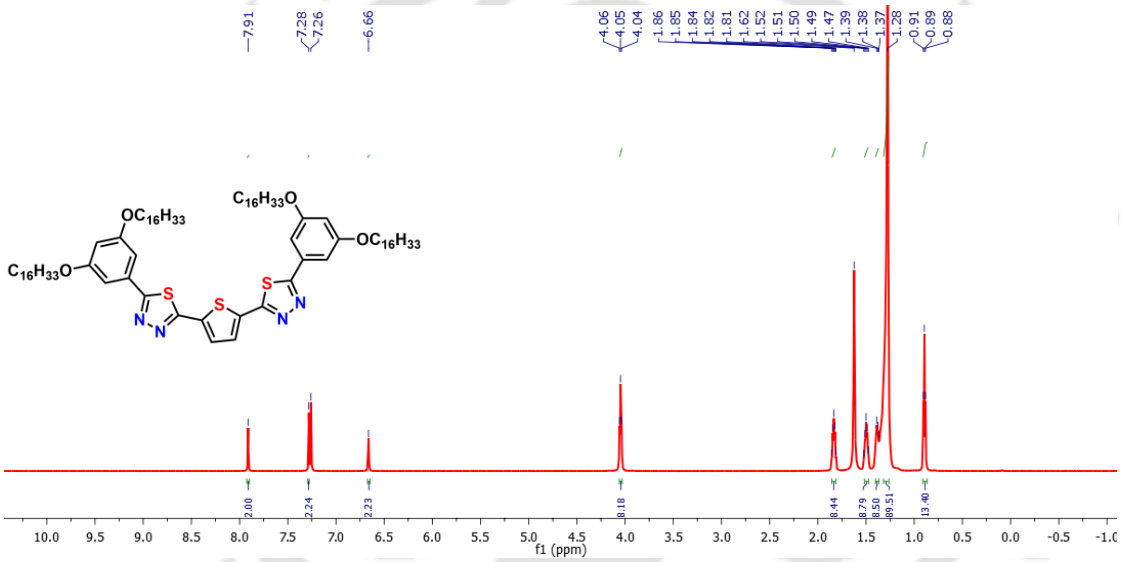

Figure 5.17. ^{1}H NMR (600MHz) spectra of **TT2** in $CDCl_3$.

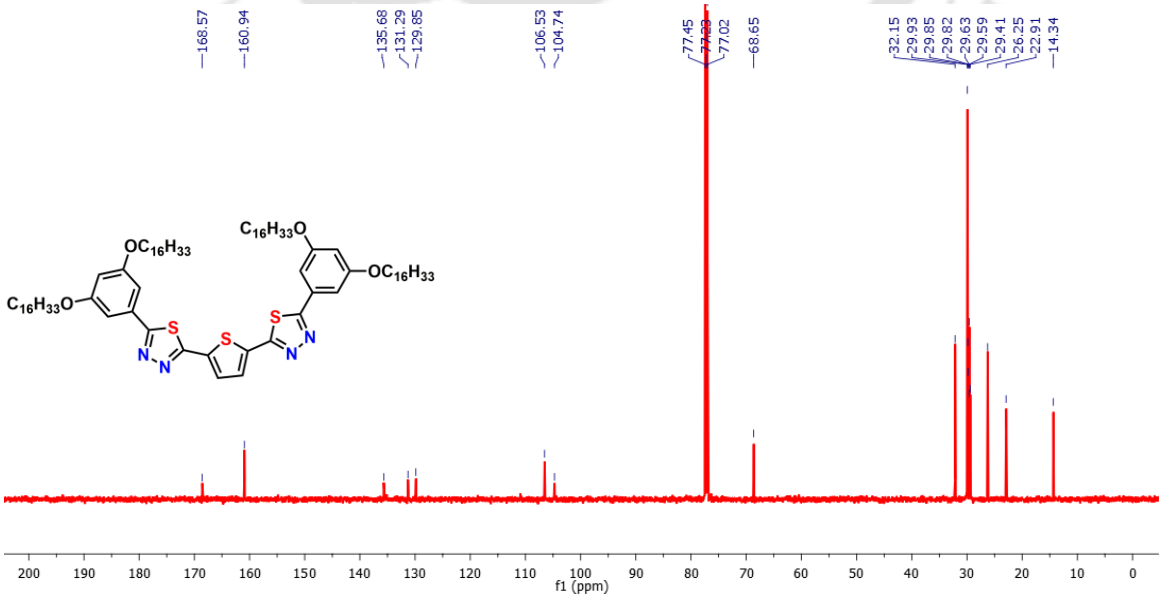

Figure 5.18. ^{13}C NMR (150MHz) spectra of **TT2** in $CDCl_3$.

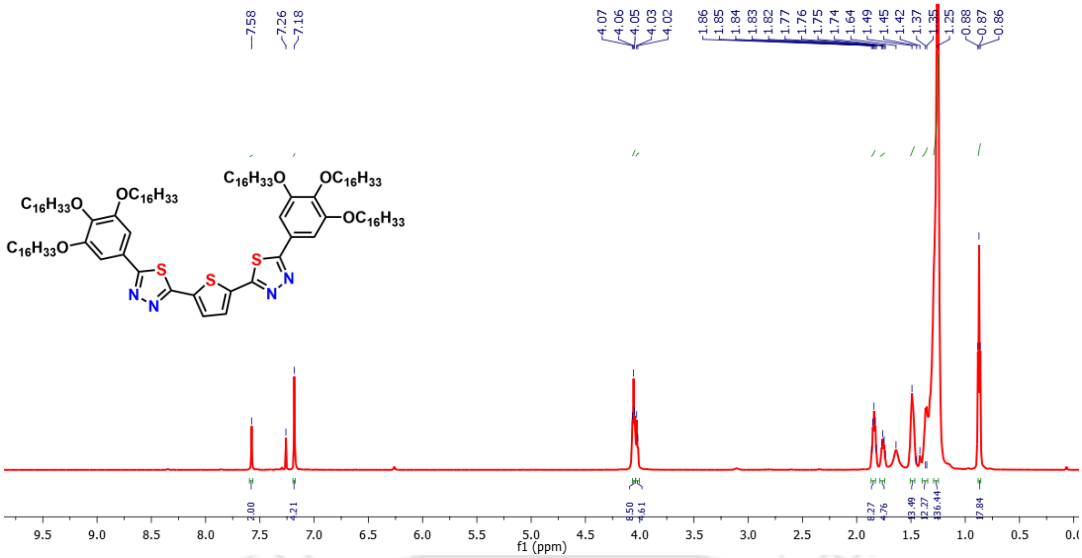

Figure 5.19. ^{1}H NMR (600MHz) spectra of **TT3** in $CDCl_3$.

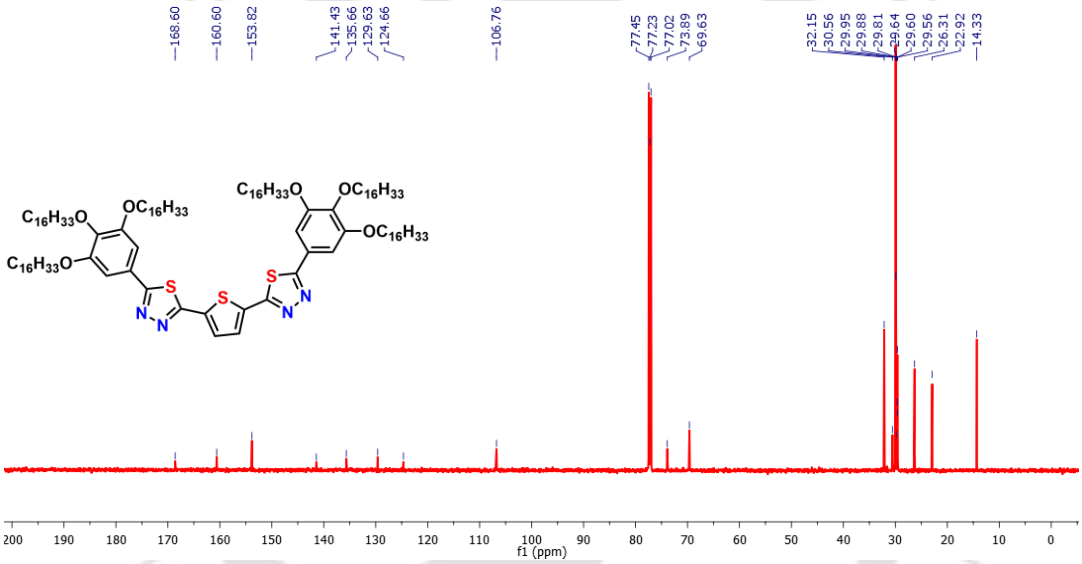

Figure 5.20. ^{13}C NMR (150MHz) spectra of **TT3** in $CDCl_3$.

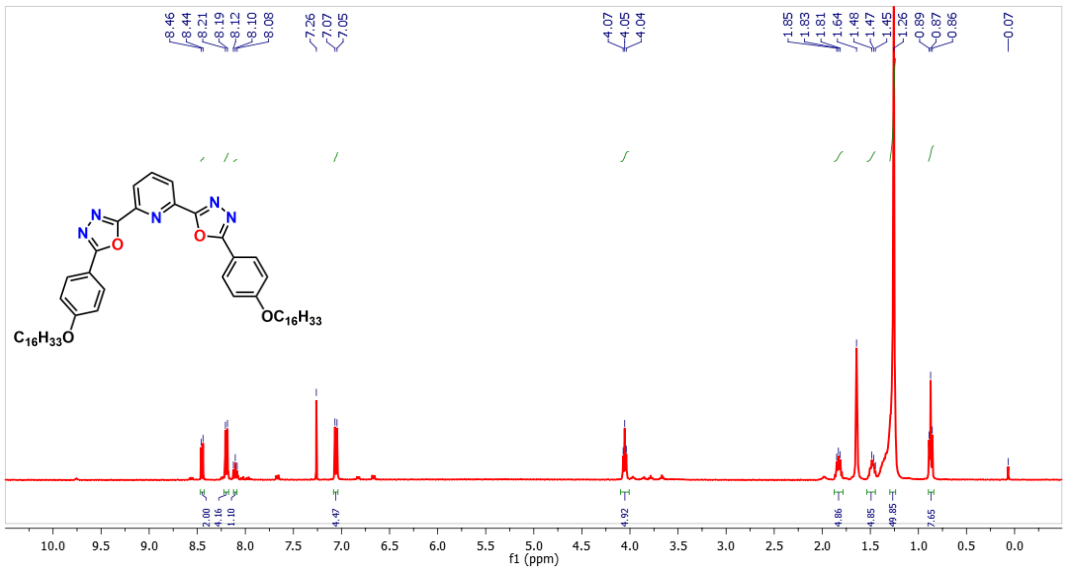

Figure 5.21. ^{1}H NMR (600MHz) spectra of **PO1** in $CDCl_3$.

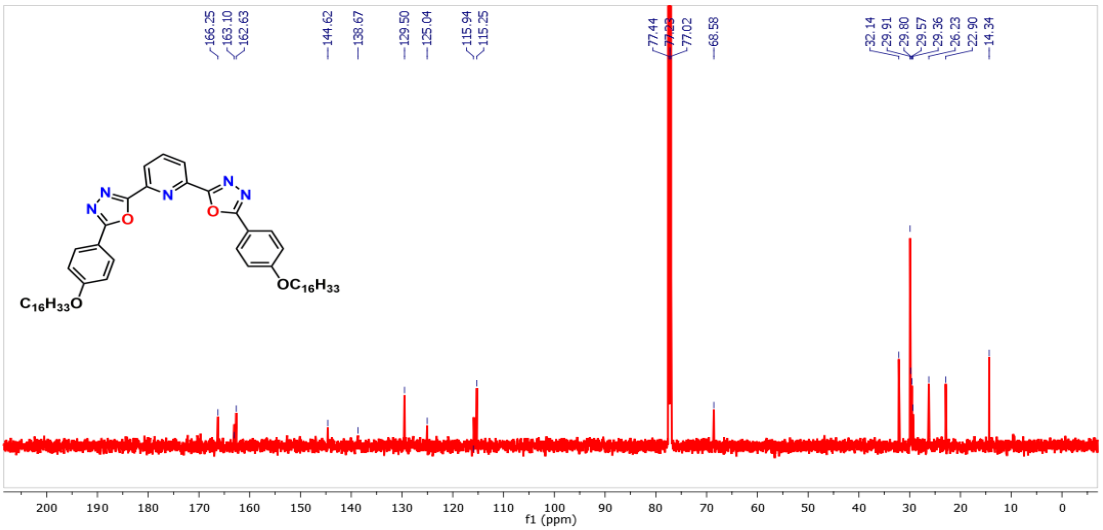

Figure 5.22. ^{13}C NMR (150MHz) spectra of **PO1** in $CDCl_3$.

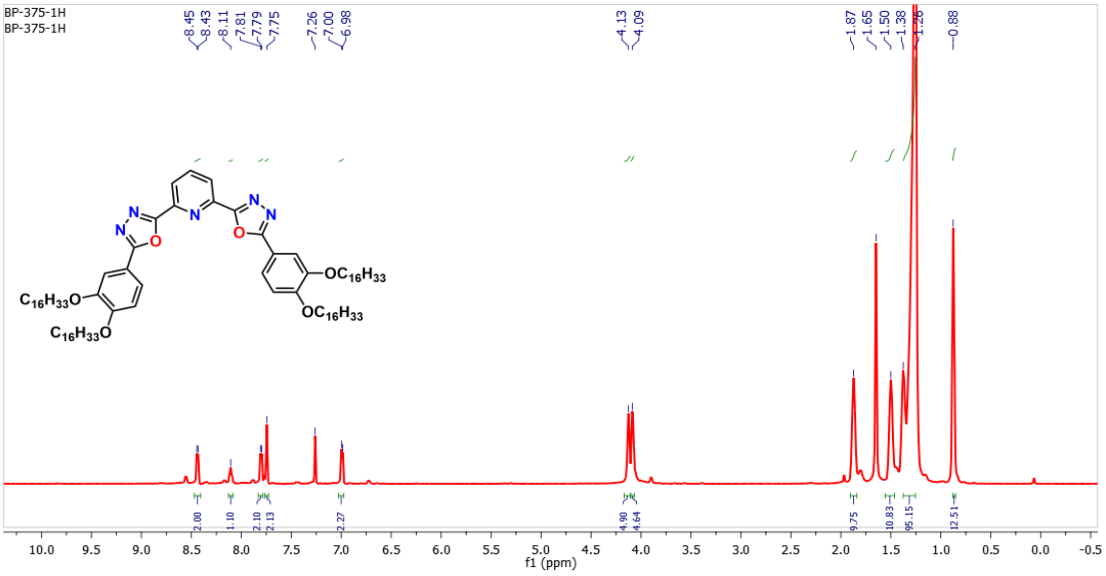

Figure 5.23. ^{1}H NMR (600MHz) spectra of **PO2** in $CDCl_3$.

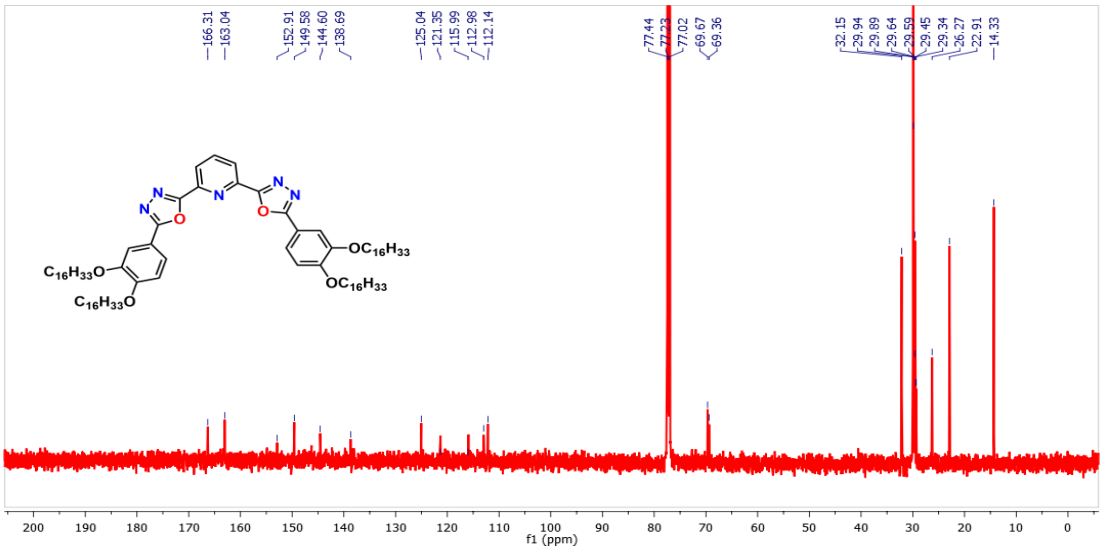

Figure 5.24. ^{13}C NMR (150MHz) spectra of **PO2** in $CDCl_3$.

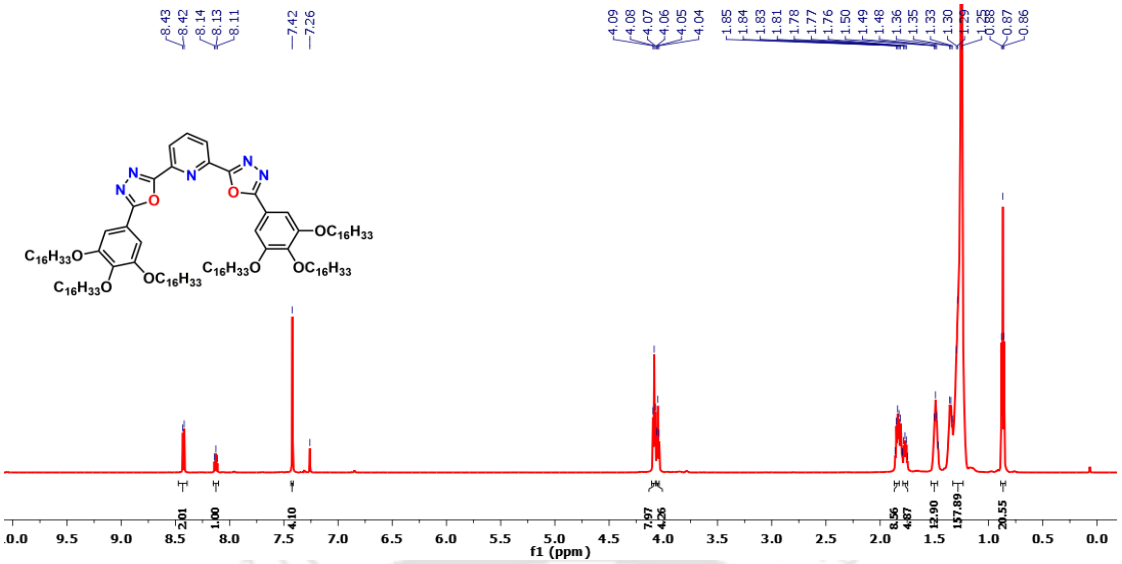

Figure 5.25. ^{1}H NMR (600MHz) spectra of **PO3** in $CDCl_3$.

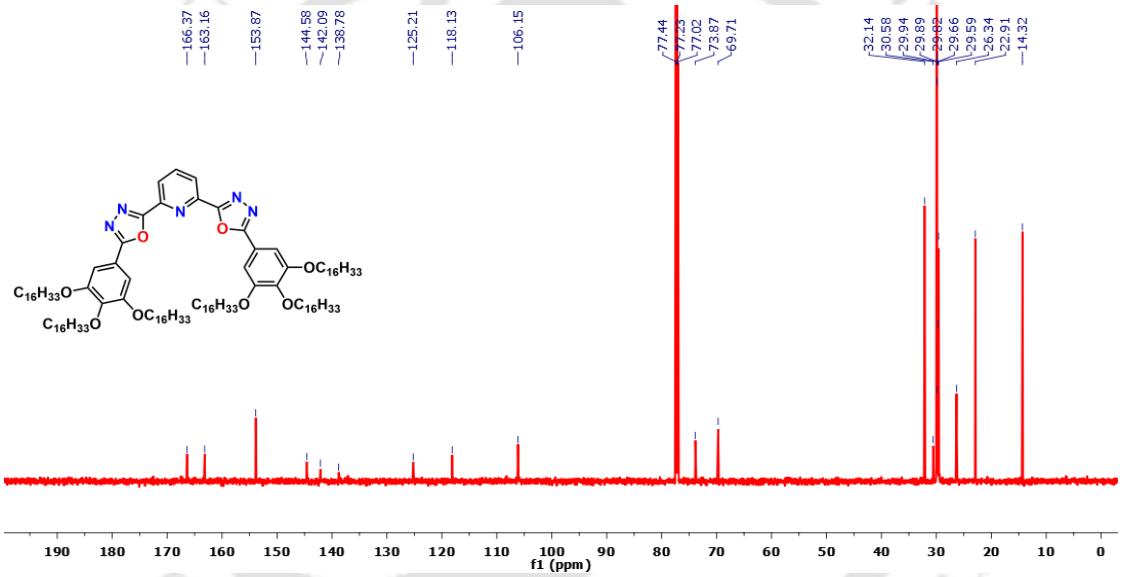

Figure 5.26. ^{13}C NMR (150MHz) spectra of **PO3** in $CDCl_3$.

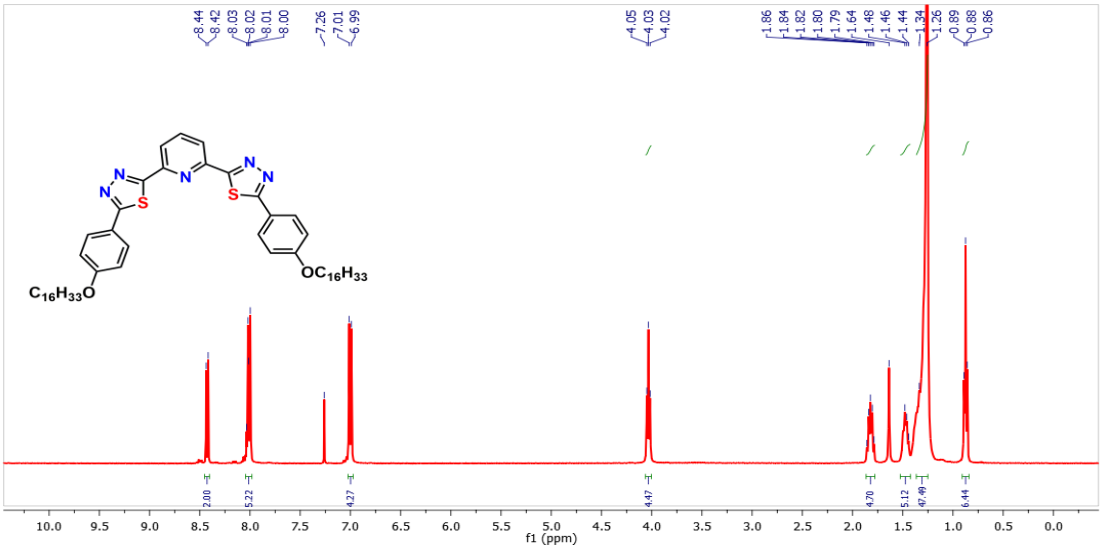

Figure 5.27. ^{1}H NMR (600MHz) spectra of **PT1** in $CDCl_3$.

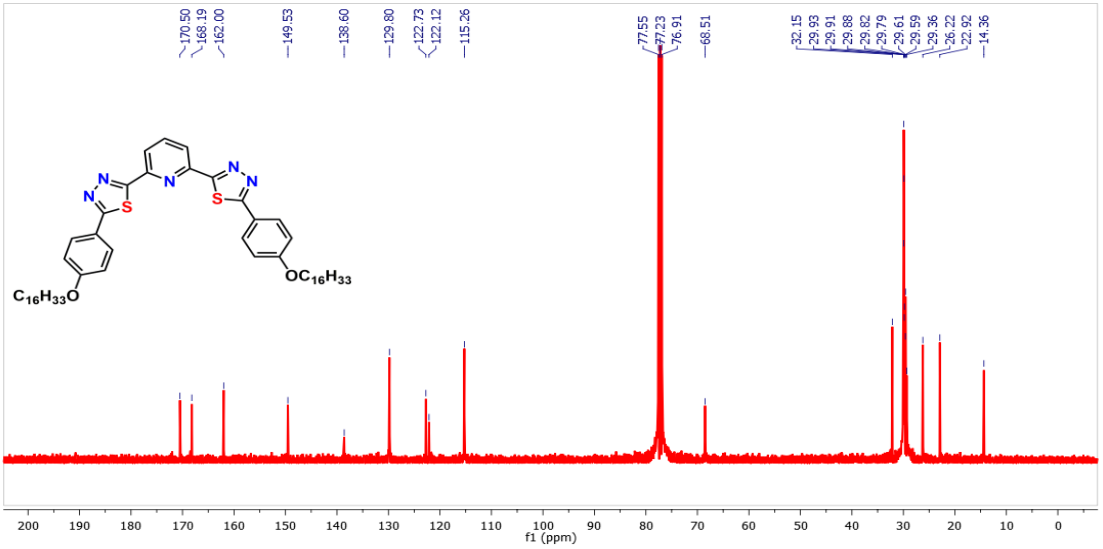

Figure 5.28. ^{13}C NMR (150MHz) spectra of **PT1** in $CDCl_3$.

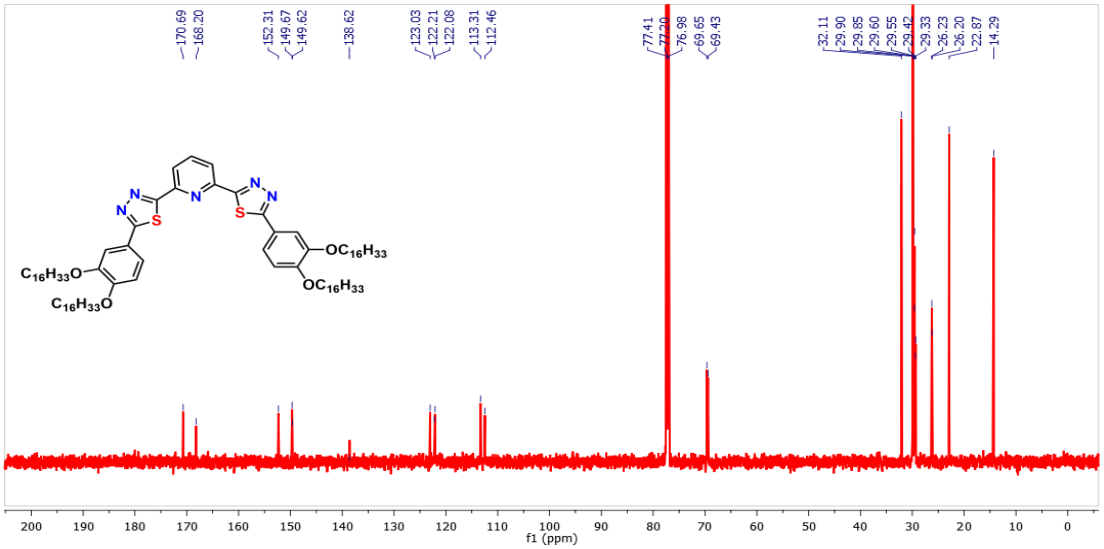

Figure 5.29. ^{1}H NMR (600MHz) spectra of **PT2** in $CDCl_3$.

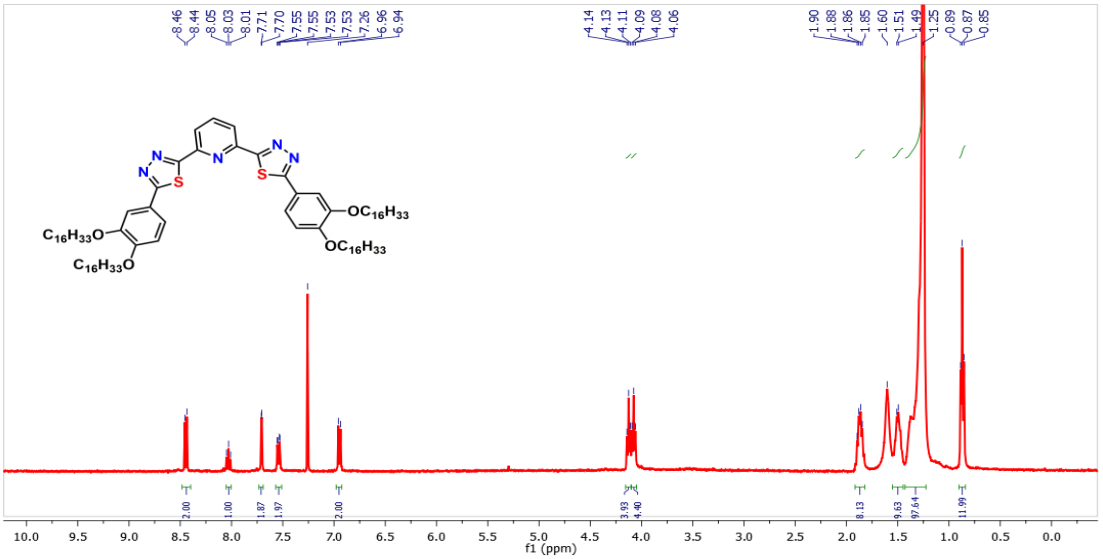

Figure 5.30. ^{13}C NMR (150MHz) spectra of **PT2** in $CDCl_3$.

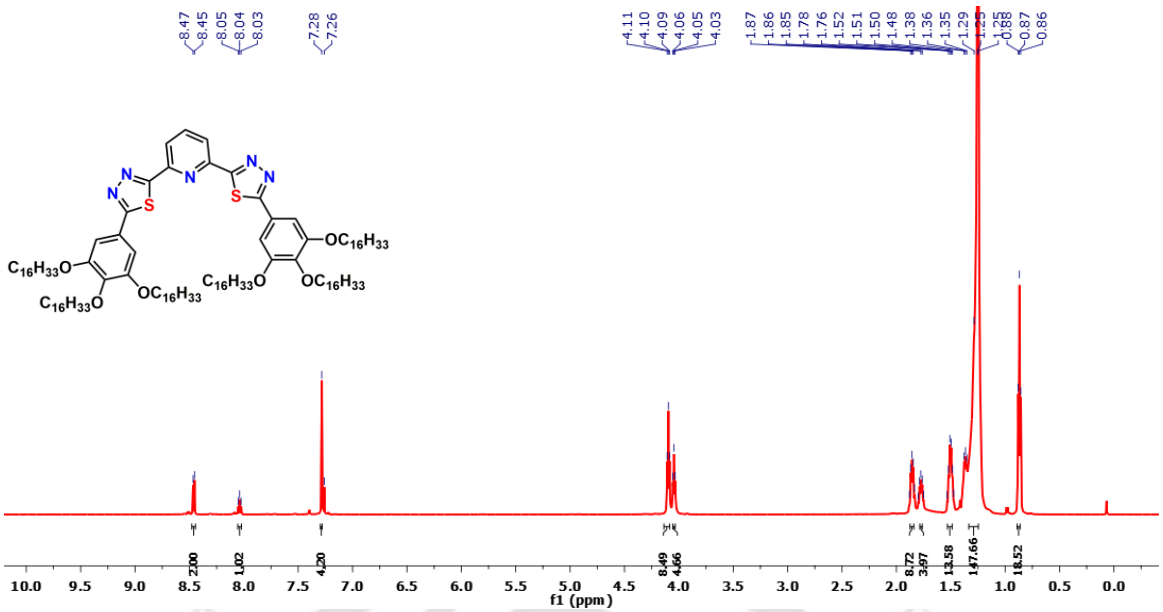

Figure 5.31. ^{1}H NMR (600MHz) spectra of **PT3** in $CDCl_3$.

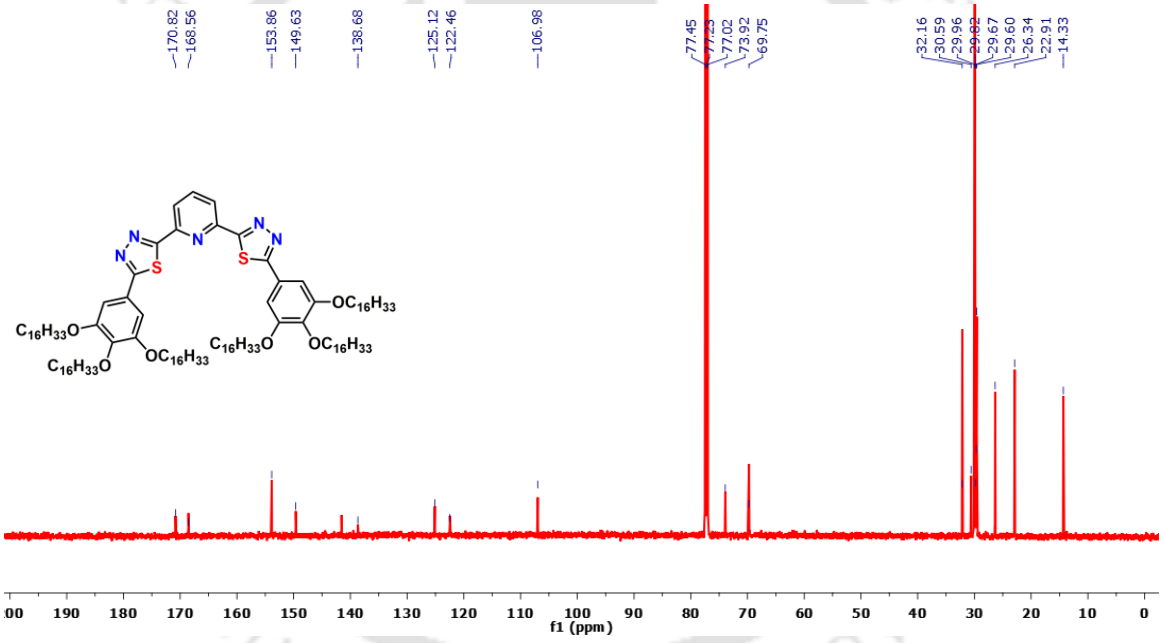

Figure 5.32. ^{13}C NMR (150MHz) spectra of **PT3** in $CDCl_3$.